2012

Selective Multivariate Applications In Forensic Science

Caitlin Rinke
University of Central Florida

SELECTIVE MULTIVARIATE APPLICATIONS IN FORENSIC SCIENCE

by

CAITLIN NOELLE RINKE
B.S. University of Central Florida, 2008

A dissertation submitted in partial fulfillment of the requirements
for the degree of Doctor of Philosophy
in the Department of Chemistry
in the College of Sciences
at the University of Central Florida
Orlando, Fl

Summer Term
2012

Major Advisor: Michael E. Sigman

ABSTRACT

A 2009 report published by the National Research Council addressed the need for improvements in the field of forensic science. In the report emphasis was placed on the need for more rigorous scientific analysis within many forensic science disciplines and for established limitations and determination of error rates from statistical analysis. This research focused on multivariate statistical techniques for the analysis of spectral data obtained for multiple forensic applications which include samples from: automobile float glasses and paints, bones, metal transfers, ignitable liquids and fire debris, and organic compounds including explosives. The statistical techniques were used for two types of data analysis: classification and discrimination.

Statistical methods including linear discriminant analysis and a novel soft classification method were used to provide classification of forensic samples based on a compiled library. The novel soft classification method combined three statistical steps: Principal Component Analysis (PCA), Target Factor Analysis (TFA), and Bayesian Decision Theory (BDT) to provide classification based on posterior probabilities of class membership. The posterior probabilities provide a statistical probability of classification which can aid a forensic analyst in reaching a conclusion. The second analytical approach applied nonparametric methods to provide the means for discrimination between samples. Nonparametric methods are performed as hypothesis test and do not assume normal distribution of the analytical figures of merit. The nonparametric

permutation test was applied to forensic applications to determine the similarity between two samples and provide discrimination rates.

Both the classification method and discrimination method were applied to data acquired from multiple instrumental methods. The instrumental methods included: Laser Induced-Breakdown Spectroscopy (LIBS), Fourier Transform Infrared Spectroscopy (FTIR), Raman spectroscopy, and Gas Chromatography-Mass Spectrometry (GC-MS). Some of these instrumental methods are currently applied to forensic applications, such as GC-MS for the analysis of ignitable liquid and fire debris samples; while others provide new instrumental methods to areas within forensic science which currently lack instrumental analysis techniques, such as LIBS for the analysis of metal transfers.

The combination of the instrumental techniques and multivariate statistical techniques is investigated in new approaches to forensic applications in this research to assist in improving the field of forensic science.

For my loving family

ACKNOWLEDGMENTS

I would like to thank Dr. Sigman for his excellent advising and support as my advisor; Dr. Campiglia, Dr. Yesterbsky, Dr. Kuebler, and Dr. Richardson for their willingness to serve on my dissertation committee; Dr. Ni for sharing his vast knowledge of statistics; Erin McIntee for introducing me to the world of LIBS; Dr. Matthieu Baudelet for expanding my understanding of the LIBS; Jessica Frisch for surviving the insanity often associated with early mornings and late nights of studying, in addition to running a marathon the day before my candidacy with me; Erin Waddell for not letting me set the computer on fire during fire debris data analysis; Dana Marie Dennis and Bala Lingam for their comedic relief on extra stressful days, “Two words for you!”; Emma Song for her random ‘Emmaisms’; Allison Killam for acting like a kid with me on extra stressful days; Ryan Kneapler for breaks from reality and unconditional love-especially during my most stressful moments; last and most importantly my family; Mom, Dad and Kirsten for teaching and encouraging me to work hard and achieve my goals and for their belief in me during the struggles involved in the journey to reach those goals.

TABLE OF CONTENTS

LISTS OF FIGURES

LISTS OF TABLES

LIST OF EQUATIONS

LIST OF ABBREVIATIONS

1,5-DMN	1,5-Dimethylnaphthalene
2,3-DNT	2,3-Dinitrotoluene
2,4-DNT	2,4-Dinitrotoluene
3,4-DNT	3,4-Dinitrotoluene
ASTM	American Society for Testing Material
ANOVA	Analysis of Variance
AR	Aromatic
ANN	Artificial Neural Networks
ATR	Attenuated Total Reflectance
CREOL	Center for Research and Education in Optics and Lasers
CCD	Charged Coupled Devices
TWGFEX	Committee of the Technical Working Group for Fire and Explosions
CJ	Copper Jacket
DRMAD	Determination of Rank by Median Absolute Deviation
DW	Different window
DW	Different Window
DA	Discriminant Analysis
EIC	Extracted Ion Chromatogram
FTIR	Fourier Transform Infrared Spectroscopy
GC-MS	Gas Chromatography-Mass Spectrometry
HPD	Heavy Petroleum Distillates

HCA	Hierarchical Cluster Analysis
HQI	Hit Quality Index
IL	Ignitable Liquid
ILRC	Ignitable Liquid Reference Collection
ISO	Isoparaffinic
LA-ICP-MS	Laser Ablation Inductively Coupled Plasma Mass Spectrometry
LIBS	Laser Induced Breakdown Spectroscopy
LPD	Light Petroleum Distillates
LDA	Linear Discriminant Analysis
MAD	Median Absolute Value
MPD	Medium Petroleum Distillates
MJ	Metal Jacket
MISC	Miscellaneous
MANOVA	Multivariate Analysis of Variance
NP	Naphthenic Paraffinic
Nd:YAG	Neodymium:Yttrium Aluminum Garnet
NJ	Non-jacketed
NA	Normal Alkane
OXY	Oxygenates
PLSDA	Partial least square discriminant analysis
PCA	Principal Component Analysis
QDA	Quadratic Discriminant Analysis

ROC	Receiver Operating Characteristics
RSD	Residual Standard Deviation
SW	Same window
SWDA	Same window-different area
SWSA	Same window-same area
SEM-EDX	Scanning Electron Microscopy-Energy Dispersive X-Ray Spectroscopy
SIMCA	Soft Independent Modeling of Class Analogy
SUB	Substrate
TFA	Target Factor Analysis
TIC	Total Ion Chromatogram
TIS	Total Ion Spectrum
TATP	Triacetone Triperoxide

CHAPTER 1: INTRODUCTION

1.1 Multivariate Statistical Techniques in Forensic Science

In 2009 a report by the National Research Council titled “Strengthening Forensic Science in the United States: A Path Forward” was published which addressed areas in need of improvement within the forensic community [1]. The major issues addressed in the report touched on the lack of error rates and scientific backing in analysis of evidence in specific disciplines of forensic science. It called for additional research into methods which could provide error rates to offer further backing to the conclusions reached by instrumental analysis or interpretation analysis. Since the introduction of DNA evidence there have been doubts cast on the accuracy of current forensic practices due to the increased number of exonerations which resulted from DNA analysis. The precise results obtained from DNA have revealed the other forensic disciplines that do not have such strong backing to conclusions. Focus has been centered on the disciplines in forensic science which have been defined as less-rigorous sciences, such as impressions, questioned documents, and tool marks. These disciplines base conclusions on expert interpretation of observed pattern characteristics based on standards and methods developed from previous cases. These disciplines are not backed by instrumental results as the disciplines defined as the rigorous sciences, such as DNA, toxicology, and controlled substances.

The research to be presented focuses on the application of multivariate statistical techniques in forensic science disciplines to provide the error rates desired in the 2009 report. Multivariate statistical techniques allow for analysis of data using multiple random variables and incorporating information about the relationship between all of the variables [2]. These statistical techniques are successfully applied to issues in forensic science such as: classification of unknown sample, determination of concentration of a compound in a complex mixture, prediction of property of a chemical compound, and evaluation of the analytical process. In this research two multivariate statistical techniques will be focused on: a combined soft classification method and the nonparametric permutation test. These two methods differ significantly in the approach of data analysis with the combined soft classification method requiring the use of a library for the classification of test data while the nonparametric permutation test compares two samples to determine whether they can be statistically discriminated from one another. These two methods will be discussed in further detail in the following chapters for their applications to forensic science disciplines which include the analysis of: fire debris, organic compounds (with a focus in explosive detection application), automobile paint and float glass, bone, and metal transfers.

1.2 Forensic Applications

The field of forensic science has many disciplines with each discipline focusing on analysis of a specific type of samples as evidence. The forensic disciplines can be

grouped into two types of disciplines as discussed above: the rigorous science disciplines and less rigorous science disciplines. Multiple types of forensic samples were investigated in the research to be presented with some from both types of disciplines being analyzed. The following pages will give a brief background of the forensic samples investigated in the course of this research.

1.2.1 Automobile Float Glass

Glass is a common piece of evidence found in cases such as automobile accidents and burglaries. Physical matching and chemical analysis are often used to determine whether two pieces of glass are similar in an attempt to connect a person to a crime. The research presented will look into automobile float glass samples to define an instrumental analysis technique and multivariate statistical data analysis method to provide statistical backing to a conclusion regarding whether pieces of glass can be differentiated at a given significance level.

Glass is characterized as “The inorganic product of fusion which has cooled to a rigid condition without crystallizing [3].” Its internal chemical structure lacks any long range structure of the network of atoms. The raw materials used for making glass are: quartz sand (SiO_2) which is a source of silicon; limestone ($CaCO_3$) and dolomite [$CaMg(CO_3)_2$] which are sources of calcium and magnesium; and trona ($Na_2CO_3 \cdot NaHCO_3 \cdot 2H_2O$) which is a source of sodium [4, 5]. The calcium and magnesium sources give the

durability to the glass and helps control the viscosity of the metal during the manufacturering process while the sodium source acts as a fining agent. The silicon component is the major constituent and can be fused to form glass.

Glass is manufactured to be highly similar in nature with a small number of large volume manufacturers producing the majority of glass with tight control over the manufacturing process [5]. Float glass is manufactured by spreading molten glass over a bath of molten tin. The molten tin is smooth and flat if the environment is free of vibration which results in the layer of glass forming on top of the tin to be nearly flat. The upper portion of the glass that is exposed to air is also going to be very flat. The glass is held at a high temperature (~1000 °C) for the surfaces to become flat and irregularities to be removed. The thickness is controlled by the stretching or constraining of the molten glass. The glass is then passed through an annealing lehr where it is cooled prior to cutting. Float glass is identified by using a short-wave ultraviolet lamp; when the lamp is used the side of the glass in contact with the molten tin will fluoresce [5].

Glass evidence is currently analyzed by both physical and chemical methods in forensic laboratories [3, 4, 6, 7]. One of the first steps of glass analysis is to determine if there is a physical fit between the unknown and known sources of glass. If the unknown piece of glass physically fits the known source than the analyst can provide a positive identification. If a physical fit is not possible between the known and unknown then additional steps are taken to identify the unknown piece of glass. Physical

examinations of color, surface characteristics, flatness, thickness and fluorescence are first performed to ensure samples could originate from the same source. Once initial examinations are performed, microscopic examination (refractive index and dispersion) and elemental analysis (scanning electron microscopy and x-ray fluorescence, neutron activation analysis, spark-source mass spectrometry, flameless atomic absorption spectrometry, inductively coupled plasma methods) are performed.

Previous research has looked into techniques for the analysis of forensic glass samples which include glass refractive index measurement (GRIM) [8-11], scanning electron microscopy-energy dispersive x-ray spectroscopy (SEM-EDX) [8, 12], laser ablation inductively coupled plasma mass spectrometry (LA-ICP-MS) [13-15], micro x-ray fluorescence (μXRF) [13], laser induced breakdown spectroscopy (LIBS) [14, 16, 17] and time of flight secondary ion mass spectrometry (TOF-SIMS) [11]. In addition to investigation of the appropriate instrumental technique, multiple statistical methods have been investigated for discrimination of forensic glass samples. These methods include: statistical t-test [11, 13, 15], Tukey's Honestly Significant Difference Test [9, 14, 17], Analysis of Variance (ANOVA) [9, 13, 14, 17], likelihood ratio based on Bayes' Theorem [17, 18], and nonparametric permutation test [17, 18].

In 2005, LA-ICP-MS was applied for the analysis of forensic evidence from multiple sources of glass including containers, architectural windows and windshields [19, 20]. LA-ICP-MS spectral data was analyzed using ANOVA and Tukey's honestly significant

different test to demonstrate discrimination of glass samples. LIBS and LA-ICP-MS were both applied to forensic glass samples in 2006 and 2007 [14, 17]. Both methods in combination with the refractive index measurements showed high discrimination percentages based on elemental ratios with the application of Tukey honestly significant difference test, ANOVA, and nonparametric permutation test methods.

Recent studies have demonstrated variation of elemental concentration within a single float glass window pane [10, 11, 15]. These variations were observed using LA-ICP-MS, refractive index and time of flight secondary ion mass spectrometry. Each analysis looked at multiple pieces of glass from the same window pane and observed discrimination within the window pane using student t-test [11] and standard deviation of the concentrations of specified elements[15].

The research presented will address the application of LIBS for the analysis of automobile float glass samples for forensic applications. The nonparametric permutation hypothesis test will be used to investigate the ability to discriminate between different window panes. In addition, the research will investigate the spatial variation being observed in the above research for within a single window pane and look to provide a method which can still be used for forensic analysis of questioned versus known comparisons despite variation within a single window pane. A method to incorporate the variance within a single window pane is necessary for forensic science as current methods assume homogeneity within a single window pane.

1.2.2 Automobile Paint

Automobile paint is prevalent in evidentiary value in forensic cases that involve any form of automobile accident. Many articles have addressed its use as evidence through different analysis methods [18, 21-36] and a standard guide [37] has been created for its analysis for forensic evidence. The research to be presented will focus on the analysis of automobile paint samples using LIBS and Fourier Transform Infrared Spectroscopy (FTIR) for the discrimination based on the nonparametric permutation test.

Automobile paint consists of many physical and chemical features which allow for macroscopic, microscopic, chemical and instrumental analyses to be performed to characterize the sample [36-38]. The physical characteristics consist of color, shape, number of layers, and presence/absence of effect pigments which can be determined macroscopically and microscopically to allow for initial separation of the samples. Chemical components consist of pigments, polymers, additives and solvents which are analyzed for after the initial separation by chemical and instrumental methods [37, 38].

Paints consist of three major components: binder, pigment and solvent. The binder provides the adhesion and cohesion which keeps the pigment within the coating and keeps the paint attached to the substrate [38]. The binders consist of the majority of the solids within the paint and typically consist of high weight polymers or lower weight monomers [30, 38]. Synthetic polymers are usually used and include epoxies,

polyesters, alkyds, acrylics and melamine. The pigments provide color while also providing protective properties, glossiness and durability [30, 38, 39]. The pigments are finely powdered solids that can be colored, black, or white and are dispersed in the binder. Colored pigments are normally organic as they provide brighter colors but both organic and inorganic components can be combined to produce a desired color. In addition to the colored pigments, effect pigments are increasingly found in the majority of automobile paint samples. Effect pigments are flakes or platelets which reflect light based on the angle of observation and are composed of a variety of substrates such as: mica platelets, silicate, and alumina flakes [30, 38, 39]. The final component is the solvent which is used to aid in the application and manufacturing by dissolving or diluting the pigments and binders. These are often organic compounds which evaporate to leave only the binder and pigment once the paint has been applied [30, 38, 39]. These are beginning to be replaced with waterborne and emulsion coatings.

Multiple layers of paint are used on an automobile to comprise the overall finish which results in a layered chip of paint. Each layer of paint consists of some or all of the components discussed above. The layers present when the car is initially manufactured are considered the original equipment manufacturer paints or OEM. The OEM paint chip usually has three to four layers which consist of primer, surface, basecoat and clear coat [18, 30, 35, 37, 39, 40]. The primer is used for adhesion to the car body and consists of a binder, basic pigmentation, an anti-rust pigmentation and extenders. The primer surface consists of basic pigmentation, extenders and a binder to provide

strength to the coating and resistance to degradation. The basecoat contains the pigments which are embedded in a binder to give the color of the paint. The final layer, the clear coat, is composed of a binder layer which protects the basecoat from degradation. In addition to these layers, after-market paint is applied sometimes to a car for repair or appeal which changes the physical characteristics therefore making it a more unique paint sample.

Previous research of automobile paint has used Raman and FTIR spectroscopy techniques. In 1999 and 2001 both techniques were used to identify organic pigments in topcoats and basecoat layers [31]. Work was published in 2000 by Kuptsov which discussed the compilation of a database of FT-Raman spectra for the analysis of the polymeric materials common in paint samples [41]. It had 900 spectra corresponding to homopolymers from 20 chemical classes, copolymers, resins, blends and related compounds. This database presented a useful tool in forensic science for the comparison of unknown samples.

In 2006, cross sections of automobile paint samples were prepared to provide Raman analysis of the four layers of paint: first primer, primer surface, basecoat, and binder [35]. This analysis demonstrated unique characteristics in the organic pigments of the basecoat which allowed for identification when compared to a reference database. Also in 2006, Raman spectroscopy was used to analyze paint samples in six forensic cases including a hit-and-run accident and an accident of undetermined driver at fault [42]. In

each case the Raman analysis was successful in providing results which allowed for solution of the crime.

In 2011, chemometrics were applied to FTIR and Raman spectra to assist in the analysis of paint data [27]. Principal component analysis and hierarchical clusters analysis was performed on 34 red paint samples to demonstrate the clustering of the paint samples into six groups. These six groups corresponded to different pigment compositions and demonstrated the ability to provide a decision-making tool and classification errors.

The research presented will combine LIBS spectral data and a nonparametric method to analyze paint samples originating from different automobile paint. The goal will be to present a method which will provide the ability to statistically discriminant between paints from different automobiles.

1.2.3 Bone

In forensic anthropology one of the primary tasks is to identify the forensic significance of skeletal material [43]. The first step of this process is to separate bone and teeth from non-bone samples. This step is normally performed by forensic anthropologist, with complications occurring when highly weathered, eroded, bleached, stained or burnt samples are encountered. Once non-bone samples have been removed it is necessary

to distinguish between human and non-human bones. The simplest method for distinguishing between these two types of bone is based on morphology and shape of the bone based on microscopic and bimolecular methods. The final step once human bones have been separated is to determine whether the skeletal remains are of forensic significance. When whole bones or large fragments of bones are present these steps are easily performed, the complexity is seen when fragments of bones are present. The research presented will address the second step of this process, distinguishing between human and non-human bones, using LIBS analysis. LIBS analysis will provide a method for analysis of bones which is minimally destructive and applicable for fast analysis for standard casework samples.

The main chemical components of bone are hydroxyapatite (50-60%), water (15-20%), carbonates (5%), phosphates (1%), collagen (20%), and proteins (1%) [44-46]. Trace elements that range from very small amounts to relatively significant contributions include: Al, Ba, K, Li, Mg, Mn, Na, Pb, Sr. These trace elements can be seen at varying concentrations in different regions of a skeleton with a single bone having higher concentrations than other bones in the same skeleton. For example higher concentrations of Co, La, Fe, Sc, Br, and Zr are seen in the epiphyseal areas of a long bone compared to the shaft of the same bone [46]. The area of the bone and elements present can give information on exposure or dietary habits. Several factors can affect the concentration of trace elements in bone and teeth; these include diet, bone disease, exposure to contaminated materials, and environmental exposure [46].

Previous research has investigated multiple elemental techniques for the analysis of bones to determine human, non-human or non-bone samples. In 2001, LIBS was used for quantitative detection and mapping of Al, Pb, and Sr elements in bones to investigate the importance of these potentially toxic elements in calcified tissue. These particular elements provide important medical, biological and environmental exposure information about the bones [45]. In 2002 and 2012, elemental analysis using scanning SEM-EDX [47]and X-ray fluorescence spectrometry [48] were used in research to determine whether an evidence fragment was bone or not. The research looked at the ratio of calcium and phosphorus elements, in addition to trace elements, for differentiating bone and tooth from other materials. Protein radioimmunoassay was used in 2004 to differentiate human from nonhuman bones and correctly identify species of bone based on antisera standards of the species [49]. LA-ICP-SF-MS with non-matrix matched standard calibration was used in 2010 to investigate quantitative analysis of trace metals in bone remains and discriminate between individuals [46]. Twelve isotopes were analyzed by LA-ICP-SF-MS and the calcium and phosphorus ratio were analyzed by SEM-EDX. Canonical discriminant analysis and principal component analysis were used to demonstrate promise for discrimination of bones with the identification of a need to focus on heterogeneity within bones.

Additional research has looked at more complex issues related to forensic bone analysis. In 2007, biochemical and x-ray diffraction analysis demonstrated a promising approach for the investigation of the postmortem interval [50]. This research looked at

the two methods for determination of postmortem interval: contributions of potassium, sulfur, nitrogen, urea, total protein, and phosphorus and degree of crystallinity of the mineral component in the medullar and cortical bone zones. Pearson correlation coefficients and student's t-test were used to test for differences between time intervals. In 2011 and 2012, presence of specific elements were investigated to provide information on preservation, dietary, and environmental effects on archaeological bones using LIBS [44, 51, 52].

As shown in previous work, many factors will contribute to the discrimination of bone samples. These factors can all provide additional information about the bone rather than human versus nonhuman but result in complexity of the analysis. The research to be presented will look at initial applications of LIBS for collection of spectral data from human and nonhuman bones. Multiple statistical approaches will be applied in an attempt to determine the most appropriate for discrimination or classification of human versus nonhuman and species the bone originated from.

1.2.4 Fire Debris and Ignitable Liquids

A fire scene presents one of the most difficult crime scenes in forensic science. The first step is to determine whether a crime has occurred or an accident. If a crime has been determined to occur a new difficultly is created with the scene consisting of destruction of the majority of the evidence. Due to these difficulties very few fire cases

are ever brought to trial. To improve analysis of a fire scene, understanding of the fires including the fuels used in arson is a necessity. By understanding the properties of ignition, density, thermal conductivity, heat capacity of the fuel, and ignitability and flame spread characteristics of the fuel the investigator may be able to more accurately investigate the scene [53]. Debris collected from a fire scene is analyzed for ignitable liquids which may have fueled the fire by separation techniques to attempt to identify the ignitable liquid present [54].

Ignitable liquids can be grouped into classes based on spectral data obtain from analysis by gas chromatography-mass spectrometry. The classes are described in detail in the American Society for Testing Material (ASTM) standard 1618 [55]. There are eight defined classes: gasoline, petroleum distillates, isoparaffinic, aromatics, naphthenic paraffinic, normal alkanes, oxygenated, and miscellaneous. Ignitable liquids are classified into these major classes based on the major ions present in the mass spectra. These classes can be further subdivided into heavy (C_9-C_{20+}), medium (C_8-C_{13}) and light (C_4-C_9) products based on the number of carbons. The ASTM 1618 standards set forth criteria for classification into each class.

The gasoline class will have a pattern characterized by abundant aromatics, with some alkanes. Compounds present in the characteristic spectral pattern of gasolines include: benzene, toluene, ethylbenzene, xylenes, cumenes, ethyltoluenes, and naphthalenes. The presence of alkylbenzenes does not guarantee a classification of gasoline as they

may be present in pyrolysis products of substrates [55]. To ensure gasoline, the spectral pattern should be compared to a known gasoline sample. The distillates class normally has a Gaussian distribution of the peaks with or without aromatic compounds present. Alkanes will be the predominant contributions, with some cycloalkanes and aromatics present in smaller amounts [55]. The isoparaffinic class is characterized by the branched chain aliphatic compounds, with aromatics and cycloalkanes not present [55]. The naphthenic paraffinic class is comprised of branched chain and cyclic alkanes, with normal alkanes and aromatics absent [55]. For classification in the normal alkane class the spectral pattern should be comprised of n-alkanes with no cycloalkanes or aromatics present [55].

Two classes are less defined then the classes discussed in the previous paragraph: oxygenate and miscellaneous [55]. The oxygenated class is comprised of any product that contains a major oxygenated compound; this includes mixtures of oxygenated compounds and other classes. The major oxygenated compounds are normally present before C8 and include: alcohols, esters, and ketones. Additional compounds may be present which include toluene, xylene, and distillate formulations. These compounds should be present in excess, with at least one order of magnitude above the matrix peaks in the chromatogram, to identify an oxygenated compound [55]. The second class is the miscellaneous, or other, class. This class has no set classification criteria like the previous classes and is more of a “catch-all” class. The compounds classified

into miscellaneous are ignitable compounds that fall into more than one of the previously defined classes or do not fall into any of the previously defined classes.

Current research uses the method set forth by ASTM E1412-00 standard method to analyze ignitable liquid residues by GC-MS [56]. The total ion chromatogram (TIC), extracted ion chromatograms (EIC), and target compound analysis (TCA) have all been used to identify an ignitable liquid [57-62]. This method is useful for neat samples of ignitable liquids, but present complications when fire debris samples of substrate pyrolysis products and evaporation of volatile compounds has occurred. This method also requires the use of visual pattern recognition which is time consuming and results in subjective analysis of an already difficult field. The research presented will apply multivariate statistical methods to ignitable liquids to provide statistical backing to classifications of unknown samples.

Previous work has looked at the application of multivariate methods for classification of post-burn ignitable liquid data, such as combined principal component analysis [58] and linear discriminant analysis [59, 63, 64], artificial neural networks [59], and soft independent model of class analogy [57].

Previous work looked at head-space analysis of fire debris. In 2003, thermal desorption-gas chromatography-mass spectrometry with PCA and a likelihood ratio approach was used to analyze the mixture of organic compounds resulting from fire

debris [65]. This research investigated the changes from unburned ignitable liquids to ignitable liquid residues within fire debris. In 2005, headspace sampling was used to investigate the distortion of the chromatographic profile of hydrocarbons based on the adsorption onto activated charcoal and methods to reduce distortion [66].

In 2007, covariance mapping of GC-MS data was tested for discrimination between gasoline samples. The method used distance metrics and covariance matrices to provide results on whether two gasoline samples were statistically distinguishable or not [67]. Previous work has also looked at summing the intensities of each mass over the full chromatographic time to give a summed ion spectra and then classifying based on the summed ion spectra using unique pairwise comparisons, cluster analysis and receiver operator characteristic curves[68]. This method provided sufficient information content to accurately identify pure ignitable liquids in a database or library. In 2003, solid phase micro extraction and GC-MS were used to investigate the analysis of two or more samples of gasoline, according to the authors, “to establish common origin” of the samples. PCA and linear discriminant analysis (LDA) were performed to identify the majority of the samples that could be classified into different groups represented by origin of the gasoline [63]. This work was continued with analysis of the C_0-C_2 substituted naphthalene compounds present in gasoline by GC-MS with selected ion monitoring and PCA to discriminate between the different gasolines [64].

The research presented here will continue with GC-MS analysis of ignitable liquids and fire debris samples. Statistical methods will be examined to provide additional support for the visual method of classification of the ignitable liquid classes and a method for classifying unknown ignitable liquid samples. In addition, a method for application of analysis and classification of not only ignitable liquids but also complex fire debris samples which include pyrolysis products from substrates and evaporation of volatile compounds will be investigated.

1.2.5 Explosive Organic Compounds

Detection of trace amounts of explosives is an active field of research due to the need imposed by civilian and military security. The need for safety in the analysis of these samples in the field requires the eventual application of a stand-off method capable of the sensitivity needed for trace amounts. These needs set out requirements that are necessary for a detection system for application to explosive compounds: identification of small amounts, rapid measurements and response, and low percentage of false positive and negatives [69]. The goal of the research will be the classification of organic compounds using LIBS spectral data and multivariate statistical techniques.

A simple definition of explosives is:

"a substance, which on initiation by friction impact, shock, spark, flame, heating, or any simple application of an energy pulse, undergoes a rapid chemical reaction evolving a large amount of heat and so exerting a high pressure on its surroundings [70]."

Many explosives are organic based with a carbon core with covalent bonds to oxidizer groups such as: nitro, nitramine, and nitrate esters [70, 71]. As most explosives are organic based they are predominantly composed of carbon, nitrogen, hydrogen and oxygen.

Explosives can be grouped multiple ways based on different parameters. First, explosives can be classified as either low or high [54, 70, 71]. Low explosives require confinement to be effective, with some examples being gunpowder and smokeless powders. High explosives on the other hand do not need to be confined to function and these consist of compounds such as trinitrotoluene (TNT), cyclotrimethylenetrinitramine (RDX), nitroglycerin (NG), and cyclotetramethylene-tetranitramine (HMX). Another method for grouping explosives is by how sensitive they are to mechanical or thermal stimuli [70, 71]. Primary explosives are those that explode from light to moderate mechanical stimuli and secondary explosives are those that explode with a shock or high energy impulse. Primary explosives include triacetone triperoxide (TATP) and

hexamethylene triperoxide diamine (HMTD), while secondary explosives include TNT and RDX.

In forensic explosives cases the main objectives of the analyst is to identify and characterize the explosives and components from a suspected explosive device. Explosives are often found on complex backgrounds such as soils, car panels, and clothes. The explosives are often found on unexploded devices, post blast debris, or in trace quantitates on the external surface of an item that has been handled by someone who has been handling explosives. Post blast samples will contain trace amounts of explosive therefore requiring a sensitive technique for analysis. Current research focuses on the detection and discrimination of trace residues of explosives using multiple analytical techniques as will be shown.

Laser techniques have shown potential for real-time analysis of the complex materials with high sensitivity and selectivity. These methods are also capable of stand-off detection of trace amounts of material. Difficulty is seen when elemental emission methods such as LIBS are applied within air for organic compounds. When collected in air, the emitters seen for organic compounds (C, N, H, O, C_2, CN) could have resulted from the sample of interest or the air due to interaction between the air and the plasma from the sample. To overcome this issue chemometric analysis is used to optimize the information and create models to discriminate between samples.

Current research has investigated multiple approaches for detection of explosive compounds which are addressed in recently published review articles [72-75]. Recent articles have addressed the issue of explosive residue detection on backgrounds that range in complexity using LIBS spectral data [74, 76-82]. Partial least squares discriminant analysis (PLDA) [76, 79, 80], PCA [74, 76-78], receiver operating characteristics curves (ROC) [77], and other multivariate statistical techniques [79] have been used to analyze the full spectral, specified elemental emissions, and element ratios for detection and discrimination of explosive residues. Specified elemental emissions investigated corresponded to the C, O, H, N, CN, C_2 emissions. In addition to the background issues, other complications of LIBS collection of organic compounds were also addressed in some of this research with investigation into sampling in different atmospheres [81], standoff detection, and shot-to-shot behavior [82].

Standoff methods have also contributed a great deal to research in explosive detection, with goals to find methods with the sensitivity for trace residue detection at long ranges. Standoff Raman spectroscopy for qualitative and quantitative analysis was demonstrated for 9 meters for pure and mixtures of inorganic and organic compounds including explosives in 2010 [83]. In 2011 standoff single-beam coherent anti-Stokes Raman scattering, 12 meters, was used to detect trace chemicals, as low as 2 $\mu g/cm^2$, in the presence of complex backgrounds [84]. Additional instrumental techniques have also been initially addressed for standoff detections [85, 86], with goals to identify an ideal standoff detection method for trace residue detection.

The research to be presented will address the detection of pure and mixture samples of organic compounds on complex backgrounds. LIBS, FTIR, and Raman will be used for the collection of spectral data and multivariate statistical techniques will be applied for the detection and classification of the organic compounds. This research will also address the issue of LIBS collection in air and fluorescence of some compounds in Raman.

1.3 Instrumental Analysis in Forensic Science

The samples discussed in the previous section are analyzed in many different ways within forensic laboratories, as was seen in the previous research discussions. Again, some require more rigorous techniques such as extractions and instrumental analysis while some are more pattern recognition based with minimal instrumental analysis. The research to be presented focuses on the application of instrumental techniques to forensic samples to either improve the current techniques or provide a new instrumental technique to the analysis of the samples. The following pages give an introduction to the instrumental techniques which will be used in the presented research in addition to addressing previous work performed in forensic science using these instrumental methods.

1.3.1 Laser Induced Breakdown Spectroscopy (LIBS)

LIBS is a technique which has been around for many decades but has just begun to be used in forensic science with the introduction of commercial LIBS instrumentation. LIBS is capable of simultaneous multi-element collection while still providing good sensitivity for many elements [75, 87, 88]. It can also be used for gas, liquid and solid samples with minimal sample preparation and minimal damage to the sample. Similarly to Raman, LIBS has the capability to be applied as a standoff technique for analysis [75, 87, 88].

While LIBS is one of the most versatile methods of elemental analysis it still experiences setbacks by its precision limitations [87]. The precision issues result from poor shot-to-shot reproducibility which could result from many aspects such as: pulse instability, laser pulse, laser-sample interactions, characteristics of the sample, and environmental factors [75, 87, 88]. This limitation results in issues in its application in forensic science as it affects quantitation of elemental concentration and shows a dependence on instrumental, sample and environmental factors for LIBS spectra. To overcome this limitation, methods have been investigated which include: calibration free and controlled calibration LIBS, femtosecond or double-pulse LIBS, and chemometric techniques. The chemometric techniques which have been investigated for LIBS data include: principal component analysis, soft independent modeling of class analogy,

partial least squares discriminant analysis, partial least squares regression and neural networks [75, 87, 88].

Recently LIBS has been applied in forensic related research in an attempt to find applications that can be used in forensic laboratories. Due to the precision issues associated with LIBS the majority of research has been focused on increasing the reliability of LIBS for forensic applications with limited applications to casework. Applications of LIBS analysis have been applied in forensic research to paint [18, 89-92], fibers [93], glass [15-17, 94-99], bodily fluids [100, 101], inks [102], explosives [103-105], and additional applications [106-109]. A recent case in Florida demonstrated one of the first applications of LIBS analysis in casework[110]. The majority of the research presented in the above references applied sampling methods and chemometric techniques to the LIBS data to minimize instrumental precision issues. It is hoped the previous research and the research presented here will improve LIBS to allow for its application to forensic casework.

1.3.2 Fourier Transform Infrared Spectroscopy

FTIR is one of the most powerful techniques for chemical analysis due to its simplicity, sensitivity, speed of analysis, and versatility to many applications [111, 112]. With its ability to provide characteristic molecular information about organic compounds it is a versatile tool which has been adapted to many forensic disciplines. FTIR provides a

nondestructive qualitative and quantitative technique for the analysis of solids, liquids and gases.

Multiple chemometric methods have been applied to FTIR data to analyze and identify specific signature peaks within samples. These methods included: PCA [27, 113-116], multivariate calibration models [113], PLSDA [113], hierarchical clusters analysis (HCA) [27], and soft independent modeling of class analogy (SIMCA) [115, 116].

FTIR instrumentation has been applied to the research of many forensically related samples and application within forensic laboratories. These applications include the analysis of: paint [21, 25, 27, 29, 32, 42, 117-120], inks [119, 121-128], fibers [129, 130], illicit drugs [113, 115, 116, 131-134], explosives [135-137], and other applications [41, 114, 138-142]

1.3.3 Raman spectroscopy

One of the most widely used laser spectroscopy techniques in forensic science is Raman spectroscopy. A Raman spectrum acts as a molecular fingerprint for a sample based on the highly specific chemical information obtained from the vibrational modes of the molecule [143-147]. Raman is a nondestructive technique which can be used on organic, inorganic, biological, and aqueous samples in the forms of solid, liquid, or gas. It can be applied using any laser excitation wavelength at day or night; however the

fluorescence from excitation at short wavelengths favors the use of longer wavelength lasers. Additionally, Raman has the ability to be implemented as a long range detection and field portable method.

Chemometric techniques have been applied to Raman data to improve the weak spectral signal associated with Raman analysis. Techniques such as PCA [143], self-modeling curve resolution [144], and HCA [145] have been applied to Raman data to assist in separating spectral signal from interferences.

Raman instrumentation has been used in research applications in many of the forensic disciplines which include: fibers [34, 131, 148-154], explosives [145, 155-164], gunshot residue [165], polymers [166], illicit drugs [167], paint [21, 26, 31, 35, 41, 42, 117, 118, 154, 168-173], bodily fluids [174-181], inks [119, 182-186], and additional applications [143, 187]. From these and many other applications, Raman has been very useful in forensic examinations through traditional Raman and new emerging Raman techniques.

1.3.4 Gas Chromatography-Mass Spectrometry

The detection and identification of chemical compounds using the combination of gas chromatography and mass spectrometry is setting precedents in analytical research and industrial fields. GC-MS analysis performs separation of complex mixtures to provide mass spectra of individual compounds. The instrumentation achieves separation by the

gas chromatography portion and detection and identification by the mass spectrometry portion [188-190]. Both quantitative and qualitative information can be obtained for the compound being analyzed. There are many varieties of GC-MS systems with the ideal combination of components being based on the desired results from a designed experiment. GC-MS does require volatile sample components, sample preparation, and careful calibration, but its greatest drawback is the high cost of the systems [188-190]. Despite the high costs, these systems are prevalent in research and crime laboratories.

Many chemometric techniques have been used for GC-MS data analysis which include: PCA [58, 59, 191-194], statistical pairwise comparison methods [58, 195], TFA [191, 192], SIMCA [193], artificial neural networks (ANN) [59], and discriminant analysis [194].

GC-MS analysis of many forensic related topics have recently been investigated in addition to its well established application in forensic laboratories for evidence analysis. These applications include the analysis of: bodily fluids and illicit drugs [116, 196-204], fire debris [58, 59, 62, 65, 67, 191-194, 205-212], explosives [195], inks [213-220], paints [22, 24, 28, 33, 221] and other applications [222].

CHAPTER 2: MULTIVARIATE STATISTICS

2.1 Soft Classification Scheme

A soft classification scheme provides the ability to classify a test sample into one, multiple or none of the classes included within a library data set, while a hard classifier requires the classification of the test data into one of the library classes. The soft classification scheme applied in the research used a combination of multiple statistical methods which will be discussed in further detail in the following sections.

The first step of the classification scheme was the application of PCA and TFA to obtain correlation values between library classes and mixtures. The highest correlations identified the compounds in the mixture most related to compounds present in the library. The second step, the Bayesian decision theory, provided the means to perform the combined steps as a soft classification method. The Bayesian decision theory calculations used the correlations obtained for the TFA to calculate posterior probabilities from the kernel distribution functions. Based on the posterior probabilities the classification of a compound present in the mixture was identified.

Each step of the classification scheme was performed by codes prewritten in the software or codes written in-house. Both MatLab (MathWorks, Natick, MA, USA) and R (The R Project for Statistical Computing, http://www.r-project.org) were used to create the codes used.

2.1.1 Principal Components Analysis

Principal Components Analysis, PCA, is a data reduction method that derives new latent variables which are linear combinations of the original data. It is often used in data analysis to reduce a data set with a large number of variables to a smaller group of descriptive variables for the data [223, 224]. Another way to look at PCA is to consider it as a rotation of the axes within an original coordinate system to produce a new set of axes that are orthogonal. These axes, or variables, are ordered based on the decreasing amount of variation within the original data each new variable represents. [223]. It is an unsupervised learning, or exploratory data analysis, technique; this means it makes no assumptions of the presence or absence of groupings within the original data. PCA also allows for multivariate data to be visualized by plotting the data in score and loading plots [223]. Separation is not maximized by PCA but visualization of the data may provide relevant information in determining the number of principal components to retain for further data analysis. It also allows for separation of the noise and the relevant data information [223]. While PCA is useful for data reduction it can be greatly influenced by outliers and scaling within the data [223], therefore prior to PCA data should be checked for outliers and normalized.

When performing PCA, the main goal is to determine the line of best fit which is defined as the first variable, or first principal component [223]. It represents the direction in the variable space that best preserves the distances between the samples, therefore

defining the maximum variance of the principal components [224]. The second principal component is defined as the line orthogonal in direction to principal component one [223, 224]. Again, it represents the maximum possible variance of the principal component in that direction. If additional principal components are necessary then they are defined as being orthogonal to all previous principal components that are in the direction that represents the maximum possible variance of the data projected in that direction [223].

Equation (2.1) is the underlying data model for PCA and data should conform to this equation for meaningful results.

$$d_{i,k} = \left[\sum_{j=1}^{n} r_{i,j} c_{j,k}\right] + error \tag{2.1}$$

where the r and c matrices are physically significant parameters and n is the number of terms required to reproduce the data [225]. The dataset, *d*, is an *i* by *k* matrix where *i* is the row designator, which corresponds to the sample, and k is the variable designation, which refers to the wavelength. The variable *j* represents the eigenvectors and corresponding scores.

Each data set can be shown in matrix notation:

$$[D] = [R][C] + [E] \tag{2.2}$$

Where principal components are given in each column of the scores matrix [R], each row of the loadings matrix [C], and the dataset is represented in [D] [225]. The scores and loadings matrices are a set of abstract values that do not provide a physical solution. The loading matrix has an ortho-normal relationship between the members of a set of vectors which are normalized to one; this is shown in equation (2.3).

$$\sum_{k} c_{jk} \cdot c_{jk} = 1 \tag{2.3}$$

To produce the [R] and [C] matrices, singular value decomposition is performed on the data matrix by equation (2.4):

$$[D] = [U][S][V]^T \tag{2.4}$$

The three singular value decomposition matrices [U], [S], and [V] correspond to the matrices in equation (1.2) by the following two equations (2.5) and (2.6):

$$[R] = [U] \times [S] \tag{2.5}$$

$$[C] = [V]^T \tag{2.6}$$

where the scores matrix [R] corresponds to the product of the [U] and [S] singular value decomposition matrices and the loadings matrix [C] corresponds to the transpose of the [V] singular value decomposition matrix.

Within the matrix [C] the values in the rows are ranked in descending order of significance based on the amount of variance in the data. The first principal component is represented in the first row of [C] and accounts for the largest variance in the data set [D]; each subsequent row corresponds to an additional principal component. The retention of multiple principal components results in the addition of the variance in the data that is accounted for by each eigenvector. The number of principal components, n, retained depends on the amount of variance to be reproduced for the data set, without including error. By retaining only the principal components determined to be significant it will reduce the data set to principal components required to reproduce a specified fraction of the variance in the data. If all principal components are considered significant then the total amount of variance retained would be 100%. The principal components that are not retained are associated with noise within the data. From this point the ortho-normal abstract solutions [R] and [C] can be used as input for

discriminant analysis or transformed into physically-significant values by target factor analysis.

There are multiple methods for determining the number of principal components required for retention. Some methods include scree plots, determination of rank by median absolute deviation (DRMAD), and retention of a specified amount of variance. Scree plots are a graphical representation of the amount of variance represented cumulatively for the principal components. Determination of the number of principal components by this method is done by observing the point where the curve of the scree plot begins to level off. It is likely that any principal components after the curve has begun to level off will contain noise in the sample rather than significant variance. The DRMAD test, a statistical method used for identifying outliers [226], is another method used to determine the number of principal components to be retained. The MAD, centered on the median value and defined by the median of the absolute value differences between the data and median, as shown in equation (2.7).

$$MAD = median\left|\left|x_i - median(x_i)\right|\right| \tag{2.7}$$

where an outlier (x_{out}) is defined as:

$$\frac{\left|\left|x_{out} - median(x_i)\right|\right|}{MAD} > 5 \tag{2.8}$$

Each successive eigenvalue is tested to determine if it is an outlier relative to the set of eigenvalues, inclusive of the value being tested (i.e., eigenvalue 1 is tested as an outlier against all n eigenvalues, then eigenvalue 2 is tested as an outlier against eigenvalues 2-n, etc.). When all of the outliers have been determined, the remaining eigenvalues correspond to eigenvectors which contribute to noise in the data. The number of principal components retained will correspond to the number of outliers observed due to the outliers representing variance of that data. The final method that will be discussed is the retention of a specified amount of variance. The cumulative variance for each principal component can be determined by summing the variance of the previous factors with the current principal component variance. If a specified variance for retention is desired, for example to keep multiple tests at consistent parameters, then the number of principal components corresponding to the cumulative variance can be selected.

Once the desired number of retained principal components has been determined, PCA data reduction is complete. Equation (2.9) redefines Equation (2.2)

$$[D^{\ddagger}] = [R^{\ddagger}][C^{\ddagger}] \tag{2.9}$$

where $[C^{\ddagger}]$ would be the loading matrix composed of the reduced number of rows of eigenvectors and $[R^{\ddagger}]$ would be the scores matrix of the reduced number of columns of scores. $[D^{\ddagger}]$ represents the data matrix reproduced without the fraction of the error

removed by PCA. The scores and loadings still do not represent physically meaningful data but can be used in additional data analysis techniques, such as Target Factor Analysis, to reproduce real data.

2.1.2 Target Factor Analysis

Target Factor Analysis (TFA) is a method which uses the abstract data from PCA to obtain physically meaningful data by a mathematical transformation. The main goal of TFA is to identify one or more spectra that fall within the same subspace as the principal components from PCA [225]. The technique uses an *n x n* transformation matrix, [T], and the [$R^{\ddagger}$] matrix, which is the row matrix produced by PCA for the sample [225]. The [$R^{\ddagger}$] matrix is transformed into physically meaningful data by Equation (2.10).

$$[\bar{R}] = [R^{\ddagger}][T] \tag{2.10}$$

where $[\bar{R}]$ is the transformed scores in the form of a row matrix. The [$C^{\ddagger}$] matrix is transformed in a similar manner by Equation (2.11).

$$[\bar{C}] = [T]^{-1}[C^{\ddagger}] \tag{2.11}$$

where the transformed column matrix $[\bar{C}]$ is the product of the inverse transformation $[T]^{-1}$ post-multiplied by $[C^{\ddagger}]$. A combination of Equation (2.9) and (2.11) shows the relationship between $[R^{\ddagger}]$, $[C^{\ddagger}]$, and $[D^{\ddagger}]$.

$$[D^{\ddagger}] = [R^{\ddagger}][T][T]^{-1}[C^{\ddagger}] \tag{2.12}$$

The entire matrix [T] or $[T]^{-1}$, does not need to be found for equation (2.12) to be useful. We can find one column in [T], or one row in $[T]^{-1}$, at a time.

In TFA, predicted vectors can be individually compared against test vectors, $\bar{\bar{C}}_n$, which means a set of real factors can be determined based on a set of test vectors taken from a library of spectra [225]. Equation (2.13) is used to find a transformation vector, T'_n, which is post-multiplied by the reduced-dimensionality matrix $[C^{\ddagger}]$ in Equation (2.14) to obtain the predicted vector, $\bar{C}_n$.

$$T'_n = \bar{\bar{C}}_n[C^{\ddagger}]^T \tag{2.13}$$

$$\bar{C}_n = T'_n[C^{\ddagger}] \tag{2.14}$$

Pearson correlation coefficients are then used to calculate the degree of correspondence between the test and predicted vector. The correlation coefficient is

calculated by equation (2.15) which is the division of the covariance by the product of the individual standard deviations [18, 30, 227, 228]. The variables x and y from equation (2.15) represent two analytical samples. The correlation coefficient can range from -1 to +1, with the greater the absolute value of the coefficient indicating a stronger correspondence between the two variables. The Pearson's correlation coefficient is commonly used for the analysis of data that is not normally distributed [18, 30, 227].

$$r = \frac{\sum(x_i - \bar{x})\,(y_i - \bar{y})}{\sqrt{\sum(x_i - \bar{x})^2 \sum(y_i - \bar{y})^2}} \tag{2.15}$$

The greater the similarity between the test and predicted vector, the closer to one the Pearson correlation will fall.

2.1.3 Bayesian Soft Classification

Many of the techniques discussed so far have been hard classification methods, which will assign a sample to the library class it is most similar to. While these methods are useful for pure samples, issues can arise when mixture samples or samples with a significant background signal are investigated. For samples that do not clearly classify as one library class, soft classification methods are preferred as they allow for multiple or no classification. The Bayesian method performed for the analysis in this research will be modified to perform as a soft classification method.

The Bayesian decision theory is applied to a classification problem that has multiple classes by equation (2. 16):

$$P(\omega_i|r) = \frac{p(r|\omega_i)P(\omega_i)}{\sum_i p(r|\omega_i)P(\omega_i)} \quad (2.\ 16)$$

where $P(\omega_i|r)$is the posterior probability, $p(r|\omega_i)$ is the class-conditional probability and $P(\omega_i)$ is the prior probability of classification to the ω_i class [229] The vector r contains the parameters that characterize each class; one parameter, the correlation obtained from the TFA analysis will be the focus of this research. For each class the prior probabilities will be equal to the inverse of the number of classes, which allows the prior probabilities in the numerator and the prior probabilities, once factored out of the summation, in the denominator of equation (2. 16) to be canceled.

The class-conditional probabilities, $p(r|\omega_i)$, in equation (2. 16) will be approximated by the kernel function shown in equation (2.17) [229]. The kernel function determines the shape of the distributions while the bandwidth determines the width [230]. The kernel function is not the only way to express the class-conditional probabilities, $p(r|\omega_i)$, but it is used to calculate the class-conditional probabilities as a superposition of Gaussian functions centered at the n_i correlation values for each class,ω_i.

$$p(r|\omega_r) = \frac{1}{n_i}\sum_{j=1}^{n_i}\frac{1}{h_i\sqrt{2\pi}}e^{\left[\frac{1}{2h_i^2}(r-r_j)^2\right]}$$

(2.17)

In equation (2.17) the variable h_i represents the adjustable bandwidth. This is calculated by equation (2.18).

$$h_i = 0.9A_i n_i^{1/5}$$

(2.18)

The variable A_i is the adaptive estimate of the distribution in the correlations for class ω_i; calculated by equation (2.19):

$$A_i = min\left(s_i\, {R_i}/{1.34}\right)$$

(2.19)

where s_i is the standard deviation of the Pearson correlations for class ω_i and R_i is the inter-quartile range of the correlations for class ω_i. A_i is set as the minimum of the two values s_i and ${R_i}/{1.34}$.

The $p(r|\omega_i)$ functions were calculated with the bandwidth determined by equation (2.18) These functions provide a mean integrated squared error within 10% of the ideal for t-

distributions, multimodal distributions and log-normal distributions which have skewness up to 1.8 [229, 230]. For each class, the class-conditional probabilities, $p(r|\omega_i)$, are based on the distributions of Pearson correlations between the predicted and test spectra. For every set of TFA results the correlations for each class will change, which will result in a change in the calculated class-conditional probabilities and distribution of each class. Therefore, a set of class-conditional probabilities, $p(r|\omega_i)$, should be calculated after each TFA analysis. Due to the change in the class-conditional probabilities for each TFA analysis, the calculation of the posterior probabilities must also be modified.

A few options are available for the modification of the posterior probability calculation. The first option is to calculate the posterior probabilities, $P(\omega_i|r)$, at a specified correlation, *r*, by equation (2. 16) [229]. Issues are encountered which results in the posterior probabilities, $P(\omega_i|r)$, varying considerably over a small range of *r* due to low class conditional probabilities. The second option is the calculation of the posterior probabilities, $P(\omega_i|r)$, at *r=1*, to obtain perfect correlation between the test and predicted spectra. This option results in a very strict requirement for the identification of data factors and would result in posterior probabilities not being calculated for many samples. The final option, and a less stringent approach, would be to define a lower limit, r_{LL}, and identify the class with the highest probability for a correlation between the test and predicted spectra that falls above r_{LL}. A posterior probability is then calculated for the integrated area under $p(r|\omega_i)$ for the correlations that fall above r_{LL}. While the

interval for *r* is technically [-1, 1] it is possible that the integrated area under the class conditional-probability may be less than one, based on equation (2.17). If *r* is less than one a finite bandwidth will occur, which would result in the possibility that $p(r|\omega_i)$ would not reach zero at *r*=1. An approximation of the area for *r*>r_{LL} by $1 - I_i[-1, r_{LL}]$ can be used to address the issue, where $1 - I_i[-1, r_{LL}]$ is the integrated area under $p(r|\omega_i)$ for the limits -1 and r_{LL}.

Once the integrated area under $p(r|\omega_i)$ has been calculated based on the lower correlation cutoff a final criteria of a defined significance level, α, is set to determine whether a posterior probability should be calculated. The value of $1 - I_i[-1, r_{LL}]$ will need to exceed a significance level of α to calculate a $P(\omega_i|[r_{LL}, 1])$ for a class ω_i [229]. The α value corresponds to a statistical level of significance for the assignment of a posterior probability to a given class for a minimal probability of observing r>r_{LL}. Once the two criteria have been satisfied the modified calculation of the posterior probability is performed using equation (2.20) [229].

$$P(\omega_i|[r_{LL}, 1]) = \frac{(1 - I_i[-1, r_{LL}])P(\omega_i)}{\sum_i (1 - I_i[-1, r_{LL}])\, P(\omega_i)} \tag{2.20}$$

which allows for the calculation of posterior probabilities for a single, multiple or no classes. If a test sample has one or more classes with class conditional probabilities meeting the lower correlation cutoff and significance level a posterior probability will be

calculated for all of the classes. If none of the classes have class conditional probabilities meeting the criteria then no posterior probability will be calculated. By applying the method this way the sample will not be required to be classified to the class with the highest posterior probability. Instead, the samples are allowed to be classified into multiple classes or remain unassigned. This is done by using the posterior probabilities to approximate the degree of class membership; for example if there are three potential classes a sample could be assigned to, two of the classes may have a posterior probability of 0.5 and the third a posterior probability of 0, resulting in an even distribution of the degree of class membership between the two classes.

2.2 Discriminant Analysis

Discriminant analysis (DA) is a supervised multivariate statistical technique used to achieve maximum separation of a specified data set by maximizing the between-class variance while minimizing the within-class variance [223, 231]. Two forms of discriminant analysis will be focused on in the research presented here, linear (LDA) and quadratic (QDA). Both DA methods find one or more functions, linear or quadratic latent variables, of the x-variable of the data for classification [223].

The differences between the two forms of discriminant analysis are the assumptions necessary for the application of each method and the number of parameters needed. LDA requires the assumption of equal covariance matrices and normal distribution

within the groups. While QDA does not require the covariance matrices to be equal it does require a larger number of minimum samples due to the increased number of parameters necessary. Equations (2.21) and (2.22) demonstrate the number of parameters necessary for the application of LDA (5 parameters) and QDA (18 parameters), respectively, for a data set with four variables [232]:

$$x = a + bx_1 + cx_2 + dx_3 + ex_4 \tag{2.21}$$

$$x = a + bx_1 + cx_2 + dx_3 + ex_4 + fx_1x_2 + \cdots + jx_3x_4 + kx_1^2 + \cdots + kx_4^2 \tag{2.22}$$

Due to the required number of variables for LDA and QDA, discriminant analysis is restricted to data sets with classes that contain the same number of samples as required variables or less. To meet this restriction, PCA can be performed prior to DA to reduce the dimensionality of the data set and reduce the number of variables [233]. Whether the full or reduce data sets are analyzed, data will be set up in matrix form for each class of the data set [231]:

$$class1 = \begin{bmatrix} d_{11} & d_{12} \\ d_{21} & d_{22} \\ \cdots & \cdots \\ d_{n1} & d_{n2} \end{bmatrix} \qquad class2 = \begin{bmatrix} t_{11} & t_{12} \\ t_{21} & t_{22} \\ \cdots & \cdots \\ t_{n1} & t_{n2} \end{bmatrix} \tag{2.23}$$

The mean of each class and the entire data set should be calculated:

$$\mu_x = \sum_n p_n \mu_n$$

(2.24)

where μ_n are the individual class means, p_n are the prior probabilities for each class, and μ_x is the mean of the entire data [223, 231]. The prior probabilities are defined as the natural probability of a sample belonging to one class prior to classification [223] and are used to provide more accurate predictions of classification. These prior probabilities can be assumed to be equal in Fisher DA [223].

Using the individual means the covariance matrix of each class can be calculated by equation (2.25):

$$cov_n = (x_n - \mu_n)(x_n - \mu_n)^T$$

(2.25)

From the covariance matrix the within-class and between-class scatter can be determined by equations (2.26) and (2.27) to calculate the criteria for the class separation:

$$S_w = \sum_n p_n (cov_n)$$

(2.26)

$$S_b = \sum_n (\mu_n - \mu_3)(\mu_n - \mu_3)^T$$

(2.27)

where S_w is the within-class scatter, or the expected covariance for each class, and S_b is the between-class scatter, or the covariance of a data set with members that are the mean vectors of each class [231]. The optimizing criterion in LDA for the class dependent cases is determined by the equations (2.25) and (2.27) to give equation (2.28).

$$criterion_n = inv(cov_n)S_b$$

(2.28)

For the class dependent cases, the number of classes defines the number of optimizing criteria that are required for each class [231]. A set of eigenvectors, which represent a one-dimensional subspace of the vector space of the transformation, are linearly independent if their corresponding eigenvalues are non-zero. The linear combinations of the eigenvectors represent the vector space of the transformation the criterion equation [231]. Once the transformation space has been determined, the data set is transformed:

$$transformed_{set_n} = transform\_n^T x\ dataset\_n$$

(2.29)

Once the data is transformed it is classified using a distance measurement. The distance measurement used in this research was the Mahalanobis distance. The Mahalanobis distance is calculated by equation (2.30):

$$d_M = \sqrt{\left[\left(x_j - x_k\right)^T cov^{-1}(x_l - \bar{x})\right]} \tag{2.30}$$

where x_j and x_k are points in the transform space and x_l is the class vector. It reflects the distribution in the transformation space and the covariance matrix of the data points [223, 234]. The Mahalanobis distance also considers the probability of the sample being grouped into a class based on the size, direction and positioning of the covariance matrix to the two points being compared [234]. The data point will be classified to the class to which it has the smallest Mahalanobis distance.

Once the sample has been classified, a confusion matrix is produced to determine the number of correct/incorrect classifications based on class and the percentage of correct classifications for individual class and overall data.

The discriminant analysis was performed using SYStat (Cranes Software International, Chicago, IL, USA).

2.3 Hypothesis Testing

One of the major goals for forensic analysis is to determine whether two samples are consistent with originating from the same or different sources, without the need to specifically identify the source. To achieve this goal, an appropriate statistical approach would be hypothesis testing. Hypothesis testing is a statistical decision making process to conclude whether two samples are discriminated based on a level of statistical significance. The level of significance is defined by an operator, for example alpha. There are two hypotheses that can be reached, the null or alternative hypotheses. The null hypothesis concludes that two samples are consistent with the same source based on the parameters known as test statistics, while the alternative hypothesis states the contrasting conclusion [30, 227]. Test statistics are defined for the specific test being performed and will be discussed in detail for the nonparametric permutation test [30, 227]. It is common to base results solely on the null hypothesis by stating it is either accepted or rejected based on acquired results. The determination of whether the null hypothesis is accepted or rejected is based on calculated p-values from the defined test statistics [30, 227]. The p-values are defined as the probability of observing a particular test statistic if the null hypothesis is presumed true [30, 227, 235]. Therefore, if the p-value exceeds the defined significance level then the null hypothesis is rejected.

In hypothesis testing there are two forms of statistical errors that can occur. The first is a Type I error, which is a rejection of the null hypothesis when it is true [30, 227, 235].

The second is the Type II error, which is the failure to reject a false null hypothesis [30, 227, 235]. In analysis it is sometimes difficult to maintain the two errors at the specified significance level, therefore it is common to minimize one error with the allowance of the other error to exceed the significance level. This approach could be overly optimistic for the data results. Therefore, it is necessary to maintain a balance between the two errors, with both ideally falling below the significance level. Further discussion of data analysis and the handling of the errors will be discussed in following sections.

In hypothesis testing the data can be assumed to be normally distributed which would lead to the use of parametric methods for analysis or no assumption of distribution could be made and nonparametric methods would be pursued. Deviations from the normal distribution can occur and often do in nature, with many distributions being asymmetric. Deviation from normal distribution can occur from the use of an inappropriate scaling of the data, sampling technique, sample heterogeneity and many other causes [236]. When deviations from normal distributions are observed steps should be taken to ensure the data is correctly analyzed. Transformations, such as the Fisher Transformation which will be discussed below, can be used to adjust the distribution or nonparametric methods can be explored. The focus of this work will be on nonparametric methods due to the non-normal distribution exhibited by LIBS data [18].

Each step of the classification scheme was performed by codes prewritten in the software or codes written in-house. Both MatLab (MathWorks, Natick, MA, USA) and R

(The R Project for Statistical Computing, http://www.r-project.org) were used to create the codes used.

2.3.1 Nonparametric Permutation Test

The nonparametric permutation test is an example of a hypothesis test which can be used in the statistical analysis of analytical samples. The nonparametric permutation test is a valuable test due to the guarantee of a specified significance level without requiring the assumption of a normal distribution of the data [18, 30, 227].

To perform the nonparametric calculations the Pearson's product-moment correlation coefficient was calculated, which was described previously in section 2.1.2. The Fisher transformation can then be applied as a variance stabilizing transformation to the Pearson's correlation coefficients [18, 30, 227]. The application of the transformation maintains an approximately constant variance for all the coefficient values and is calculated using Equation (2.31) [18, 30, 227, 228].

$$z = \frac{1}{2}\ln\frac{(1+r)}{(1-r)} \tag{2.31}$$

The test statistic for the nonparametric test is W_k, which is defined by Equation (2.32) [18, 30, 227].

$$W_k = \frac{W_1 + W_2}{c\big(c-1) + d(d-1)\big)} - \frac{W_3}{cd}$$

$$W_1 = \sum_{(a,b)\in S_1} f_{a,b} \qquad W_2 = \sum_{(a,b)\in S_2} f_{a,b} \qquad W_3 = \sum_{a\in S_1 b\in S_2} f_{a,b}$$

(2.32)

In equation (2.32), W_1 and W_2 are summations of the Fisher transformation of the Pearson correlation coefficients for the specified number of spectra from samples 1 and 2, defined as c and d respectively. W_3 is the summation of the Fisher transformation of the Pearson correlation coefficients for the between sample spectra from samples 1 and 2 [18, 30, 227].

The total number of spectral comparisons that can be made for samples 1 and 2 is defined by k in Equation (2.33), where m and n represent spectra from samples 1 and 2 respectively. Therefore, if six spectra from each sample were compared, a comparison of twelve spectra, there would be a total of 942 possible spectral comparisons [18, 30, 227].

$$k = (c + d)!/(c!\, d!)$$

(2.33)

The p-value for the nonparametric test is the proportion of k values that are greater or equal to the observed W_0 [18, 30, 227]. When two spectral sets are comprised of spectra from the same sample, the original partition of the spectra will not differ significantly from the permuted sets. Therefore, the test statistic, W_k, will fall within the distribution of W values and yield a high p-value. At a defined confidence interval of 95%, also referred to as a significance level of 5% (or α=0.05), any sample comparison with a p-value greater than α=0.05 would not be discriminated and the null hypothesis would be accepted [18, 30, 227]. On the other hand, when the two spectral sets are comprised of spectra from different samples, the original partition will differ significantly from the permuted sets and yield a test statistic that exceeds the majority of the other W values [18, 30, 227]. Therefore, most, if not all, the W values will fall below the W_0 and yield a low p-value. The sample comparisons with p-values less than α=0.05 would not discriminated and the null hypothesis would be rejected.

2.3.2 Hoteling's T-Test

The Hoteling's T-test is a multivariate t-test for two independent samples. It is a special case of the multivariate analysis of variance (MANOVA) which can be used to analyze data with one independent variable with two levels and multiple dependent variables

[237, 238]. A combined mean of the dependent variables is found for each group and the independent samples are compared based on their vector means.

Hoteling's test statistic, T^2, is found by:

$$T^2 = \frac{n_1 n_2}{(n_1 + n_2)} * (\bar{x} - \bar{y})' * W^{-1} * (\bar{x} - \bar{y}) \tag{2.34}$$

where n_1 and n_2 are the number of samples per class; ẋ and ẏ are the average sample scores for each principal component per class [238]. W^{-1} is found by taking the inverse of the W matrix found by the following equation:

$$W = \frac{1}{(n_1 + n_2 - 2)} * (cov_1 + cov_2) \tag{2.35}$$

where cov_1 and cov_2 are the covariance matrices for the two classes [238]. The scores corresponding to the desired number of retained principal components are mean centered for each class. From the mean centered data the covariance matrix for each class is found from the multiplication of the transposed mean centered data matrix by the mean centered data matrix.

Once the T^2 value has been calculated and is determined to follow an F distribution on p and degrees of freedom, then a critical value can be obtained from tables for the set α level [238]. The F distribution is calculated by (2.36) and the degrees of freedom are calculated by (2.37). The table value and the calculated values are compared to determine whether the samples are discriminated or not; if the calculated value falls above the table value then the samples are found to be discriminated from each other.

$$F = \frac{(n_1 + n_2 - p)}{(n_1 + n_2 - 2)} * T^2 \tag{2.36}$$

$$degrees\ of\ freedom = n_1 + n_2 - p - 1 \tag{2.37}$$

2.3.3 Wilcoxon Rank Sum Test

The Wilcoxon Rank Sum test, also known as the Mann-Whitney test, is the nonparametric version of the parametric t-test for comparison of two independent samples of continuous distribution [236, 239]. The only assumption made is that the samples have the same form of distribution; otherwise it is a distribution free method [236]. The Wilcoxon Rank Sum test is one of the most powerful nonparametric tests for samples which have the same form of distribution [236]. Compared to the two sample t-test, the Wilcoxon Rank Sum test is not as sensitive to outliers, skewness and

differences in variance, but it is sensitive to change in location and shape of distributions [236, 239].

The test is performed based on the order, or rank, the data from two samples fall [236, 239, 240]. For our case, the order would be based on the nonparametric permutation test p-values for two samples. The null hypothesis tested by Wilcoxon Rank Sum test assumes the distribution of data (or p-values) from sample one is the same as the distribution of data (or p-values) from sample two [236, 239]. The test statistic is U, which is calculated by equations (2.38) and (2.39):

$$U_1 = mn + \frac{m(m+1)}{2} - R_1 \tag{2.38}$$

$$U_2 = mn + \frac{n(n+1)}{2} - R_2 \tag{2.39}$$

where R_1 and R_2 are the sum of ranks for sample one and sample two respectively and m and n are the sample size respectively [236].

The smaller of the two Us is considered the test statistic which is used to calculate the p-value for the distribution. The p-value, w_2, is calculated by equation (2.40) and (2.41) depending on whether U_1 or U_2 is determined as the test statistic [236]:

$$w_2 = \frac{U_2}{mn} \tag{2.40}$$

$$w_1 = \frac{U_1}{mn} \tag{2.41}$$

The p-value is used to determine whether the null hypothesis should be accepted or rejected [236]. If the p-value is greater than the critical value (for our calculations an alpha=0.05) the null hypothesis is not rejected and the two samples are considered not to be statistically different. On the other hand, if the p-value is less than or equal to the critical value the null hypothesis is rejected and the distribution of the two samples are considered to be statistically different.

CHAPTER 3: INSTRUMENTAL METHODS

3.1 Laser Induced Breakdown Spectroscopy (LIBS)

3.1.1 Ocean Optics LIBS Instrumental Setup

Part of the LIBS research was performed on a commercial LIBS instrument (model LIBS2000+) from Ocean Optics (Dunedin, FL, USA). A wavelength of 1064nm is emitted by a Nd:YAG Q-switched, pulsed laser (Big Sky Lasers, model CFR200, Bozeman, Montana, USA), with a pulse width of 9 ns. A single lens with a focal length of 7.5 cm is used to focus the laser energy onto the sample. The sample is positioned on a moveable stage within an enclosed chamber. The X and Y directions can be adjusted using the moveable stage to optimize the position of the sample to the laser. The lens can be adjusted for larger samples to ensure the focal length is maintained by a knob on the right side of the sample chamber [14, 16-18, 30, 241].

Positioned 45° to the incident laser beam is a set of bifurcated optical fibers which collect the emitted light from the plasma. The optical fibers are connected to seven individual linear CCD array spectrometers with a detection range of 198.14 to 965.43 nm. A spectral resolution in the range of 0.04-0.07 nm/channel is obtained by the spectrometers, giving a resolution of approximately 10,000 for the instrument. The data detected by the spectrometers is sent to a computer operating Ocean Optics OOILIBS

software. The software controls the laser sampling by controlling the Q-switch within the laser, the timing for the delay, the integration time, and records the spectrum. The software refers to the initial delay as the Q-switch. The Q-switch is a shutter located within the cavity of the laser which is used to generate high pulse energies. When the shutter is closed the photons at the laser wavelength do not stimulate emission, therefore the population inversion between the upper and lower transitions become large. Once the Q-switch is opened, the stored energy is released in a pulse of high energy. The high energy pulse is capable of ablating the sample and creating the plasma [237, 238, 242]. The setup of the instrument is illustrated in Figure 1 [30, 241]. This instrumentation was used for the analysis of automobile paint and glass samples, bones, and metal transfer data collection.

Figure 1: Ocean Optics LIBS 2000+ Setup. Laser control, spectrometer, and laser attached to sample chamber illustrated.

3.1.2 Table Top LIBS Instrumental Setup

The second LIBS instrument used for the research was an in-house system in Professor Martin Richardson's research laboratory at The Center for Research and Education in Optics and Lasers (CREOL) [243]. A schematic of the instrumental setup is shown in Figure 2. This instrumentation setup used a Q-switched Nd:YAG laser (Brilliant, Quantell – Bozeman, MT, USA) with a pulse repetition rate of 10 Hz. The laser fundamental output was 1064 nm with pulse duration of approximately 6 ns. To allow the laser to perform at optimal parameters and reduce the energy to approximately 15 mJ a light-valve composed of a ½ wave plate and a polarizing cube was used. A plano-

convex lens with a focal length of 7.5 cm was used to focus the laser pulse on the sample, with a resultant irradiance of 2.73 x 10^9 W/cm^2.

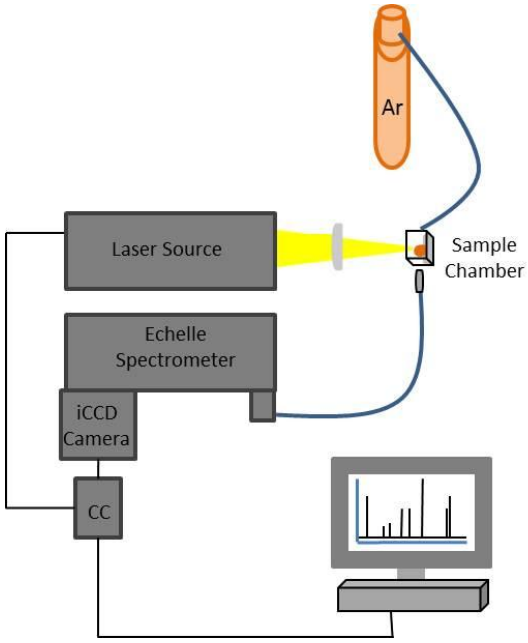

Figure 2: CREOL LIBS setup

Samples were placed in a quartz cuvette which was positioned perpendicular to the laser beam. Air or argon could be flowed through the cuvette depending on the atmosphere desired for sampling. No alterations were necessary for air sampling; a small tube was inserted into the cuvette cap with a flow of argon.

Collection of the plasma emission was performed by an f/2 UV-transmissive collimating ball-lens (74-UV – Ocean Optics, Dunedin, FL) coupled to a 1-meter UV transmissive 50µm core fiber (HRE-FBR-1M – Princeton Instruments, Trenton, NJ). The fiber was

attached to a 250 mm Echelle spectrometer (Acton HRE, Princeton Instruments) combined to a 512 x 512 pixel GenII iCCD camera that had a MgF_2 input window and a P46 phosphor (PI-MAX2, Princeton Instruments). The instrumental setup gave a resolution of approximately 6000 over the spectral range of 200 to 900 nm. Collection of spectra was performed with a delay of 158 ns after the laser pulse and integrated over a 10 μs interval. This collection allowed for the continuum to be minor related to the line emission. The electronic gain was set at 100. Spectral data was collected by a Princeton Instruments WinSpec 32-bit Windows® software package which had an Echelle module from Roper Scientific. NIST (National Institute of Standards and Technology) traceable calibrated irradiance lamps (Deuterium lamp 63945 and Quartz Tungsten Halogen lamp 63355 – Oriel Instruments, Stratford, CT) were used to measure the spectral response of the system and correct the spectra. This instrumentation was used for the organic compounds and polymer mixtures.

3.2 Fourier Transform Infrared Spectroscopy – Attenuated Total Reflectance (FTIR-ATR)

3.2.1 Instrumental Setup

For the research involving FTIR analysis, an ATI Mattson Infinity Series FTIR attached to a Spectratech IR Plan Advantage IR Microscope with an ATR attachment was used,

illustrated in Figure 3. The instrument contained a Helium-Neon (HeNe) laser with a maximum of one milliwatt of continuous output power at 632.8 nm. The analysis was done using an ATR module attached to the IR-Plan Advantage microscope in transmittance mode. The coupled instrumentation allowed for trace amounts of samples to be analyzed. The parameters for data collection were set using the Thermo Electron Corporation OMNIC software. The background spectrum could be set to be acquired pre or post sampling and was subtracted by the software. The desired number of scans and resolution can be set within the software, with a collection range of 600-1799cm^{-1} [30, 241]. This instrumentation was used for the analysis of organic compounds and automobile paint samples.

Figure 3: FTIR instrumentation setup.

3.3 Raman Spectroscopy

3.3.1 Instrumental Setup

For the portion of the research involving Raman analysis, an R-3000 series Raman system from Ocean Optics (Dunedin, FL, USA) was used. A computer with RSIscan software was used for the parameter selection and collection of the spectrum. The background spectrum was collected prior to each sample collection while no laser signal was emitting and was automatically subtracted by the software.

The instrument was setup two ways for sample collection, illustrated in Figure 4. The first setup utilized a sampling compartment which accompanied the instrument. The sample was placed into a vial and the fiber optic was positioned within an opening at an optimum distance. For the second setup the laser output was focused onto the sample through a polarized light microscope. An interface was attached between the eyepiece and the objectives of the microscope which allowed the laser light to be focused onto the sample. The scattered light was then sent back through the optical pathway and collected through the same interface into the detector. This instrumentation was used for the analysis of organic compounds.

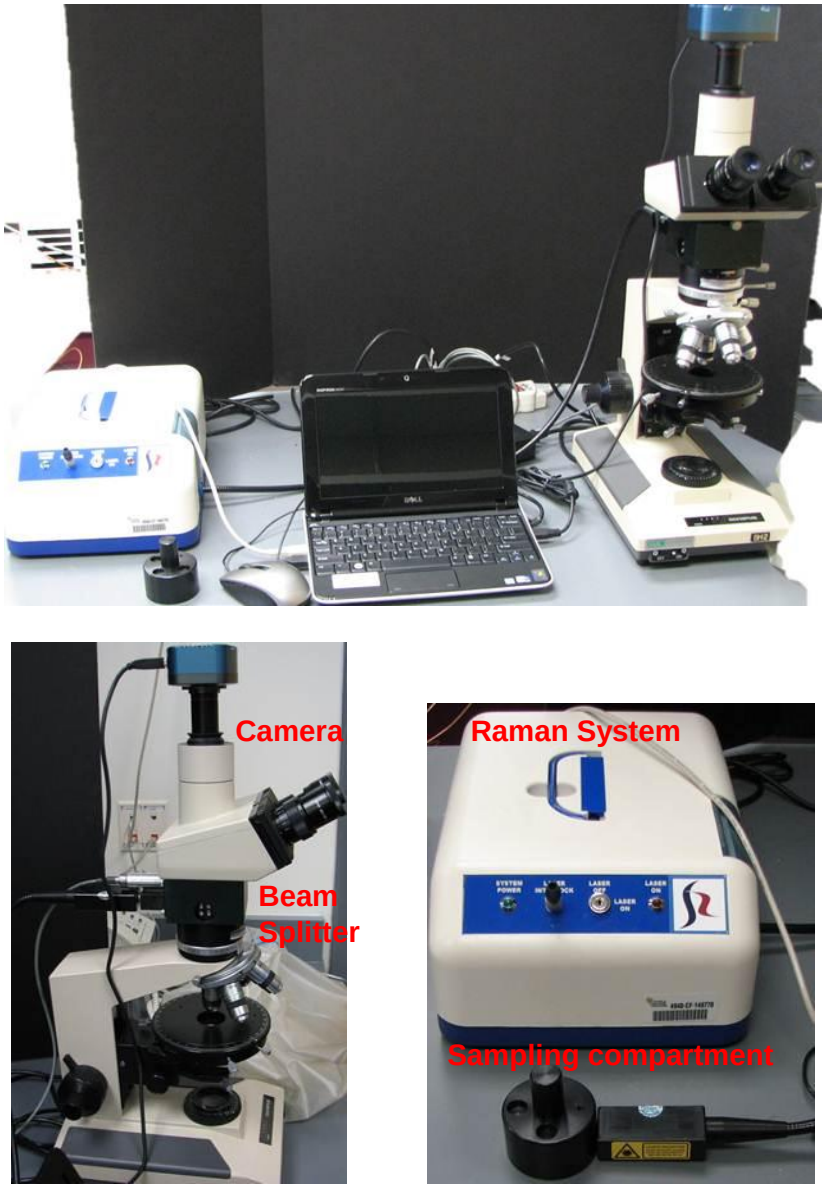

Figure 4: Raman Setup a) full setup including Raman system, computer, microscope, and sampling chamber; b) microscope setup with camera and beam splitter attachments; c) sampling compartment and Raman system

3.4 Gas Chromatography Mass Spectrometry (GC-MS)

3.4.1 Instrumental Setup

The GC-MS analysis for this research was performed on an Agilent 6890 gas chromatograph interfaced to an Agilent 5973 mass spectrometer, shown in Figure 5. An auto sampler was connected to the chromatograph for analysis of multiple samples. Instrumental parameters will be further expanded upon in the following chapter. This instrument was used for the analysis of fire debris samples.

Figure 5: GC-MS instrumentation used for research.

CHAPTER 4: EXPERIMENTAL

4.1 Laser Induced Breakdown Spectroscopy Experimental

Multiple data sets were analyzed by LIBS for this research, and therefore optimization of each method's parameters was required for each data set. In the following section, a description of the instrumental parameters for each data set will be given. In addition to the instrumental parameters, collection order and spectral averaging methods will be focused on. The optimization of the instrumental and collection parameters is a crucial part in LIBS analysis due to the shot-to-shot variance and reproducibility issue seen as discussed in the introduction of the instrument.

One of the first experimental method parameters to be addressed for optimizing the application of LIBS instrumentation was the order of sample collection. Two collection orders were used in the analyses, random order and consecutive order, depending on the samples. As previously discussed, LIBS is prone to shot-to-shot variance and reproducibility issues, in addition some of the samples collected in the research were highly similar in nature. With highly similar samples any variance whether due to instrumental precision, contamination, or trace effects in the sample can greatly affect the outcome of the results. Randomization of the collection order encompasses the variance caused by shot-to-shot variance or instrumental error into the data results. Randomization requires the data set to be completely random in sample and spectra

order, therefore the collection of spectra for all samples is spread over the full collection time frame. For analysis of samples that are not highly similar in nature, consecutive collection order may be used. Consecutive order is performed when all spectra of a single sample are collected in order and all samples within one data set are collected together. This approach prevents issues with instrumental drift within samples and data sets but does not address shot-to-shot variance. In samples that are not highly similar in nature, the small shot-to-shot variance does not affect the outcome of the results in the same manner as in highly similar samples.

The second experimental parameter decided upon when sampling with LIBS was the type of spectral averaging performed. It has been determined that averaging multiple shots to comprise a single spectrum improves signal to noise and reduces shot-to-shot variance. There are three averaging methods: drill down, multiple points, and a combination of drill down and multiple points, illustrated in Figure 6. Drill down averaging is performed when all shots to be averaged are collected on the same spot of the sample. This approach is useful when acquiring data on heterogeneous samples as it encompasses multiple layers of the sample into a single spectrum. Ablation through thin samples may occur when multiple shots are taken or confinement issues may be encountered with thick samples as each shot goes further into the sample. Confinement of the laser pulse can result in distortion of the plasma which affects the outcome of the results. The second averaging method is multiple points averaging, which is the collection of the average shots over multiple areas of the sample. During

collection of spectrum using multiple points averaging the sample is moved to prevent the same area from being sampled. This method is useful when the sample is known to be homogenous throughout and when confinement affects may be an issue. It does not allow for cleaning shots to be performed prior to sampling. The third method is a combination of drill down and multiple points; for example 10 shots are averaged, with 5 shots collected in 2 spots. This allows for some sampling of multiple layers of the sample without encountering a large amount of confinement effects but also prevents results from being influenced solely by the surface layer of the sample. All three averaging methods and collection order methods have advantages and disadvantages, therefore the results desired from the experiment should be considered prior to collection.

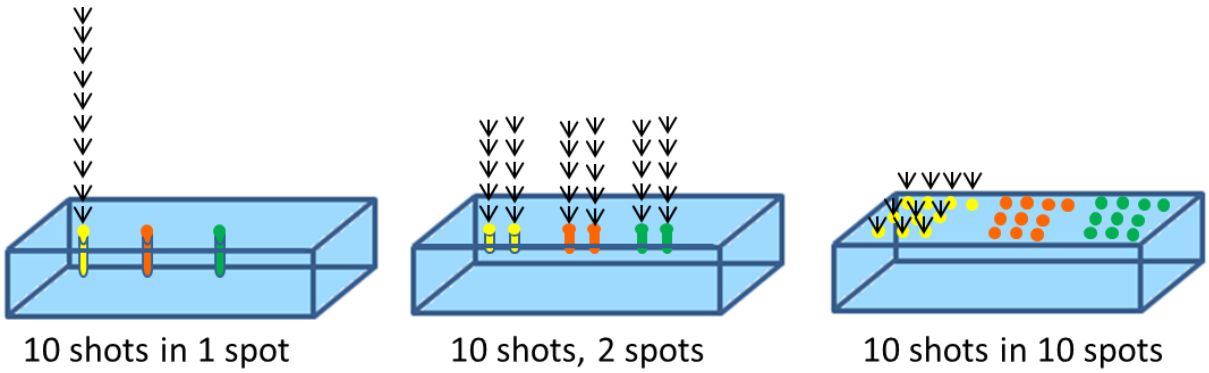

Figure 6: Demonstration of three spectral averaging methods.

4.1.1 Automobile Paint

Automobile paint chips were collected from South Carolina Law Enforcement and a local junkyard in Bithlo, FL. The 90 paint samples that were collected came from different make, manufacturer, year (1987-2006), and color automobiles. The make, manufacturer and year of the car were determined by the vehicle identification number (VIN). Microscopic examination with a stereomicroscope (34 x magnifications) allowed for the determination of the number of layers present in each sample. The number of layers ranged from 3-7, with the higher number of layers attributed to after manufacture paint jobs. Table 1 summarizes the number of samples for each group of color, number of layers, and presence of effect pigments with a more detailed table of manufacturer, make, year, color, effect pigment, substrate and number of layers which is given in APPENDIX A.

If the samples were still attached to their substrate upon collection they were removed using a razor blade and mounted on a glass microscope slide. The paints were secured by a smooth coat of softened (200 °C) polyisobutylene to ensure the samples would lay flat for the analysis. Polyisobutylene was selected because it gave little to no LIBS signal, therefore providing no contribution to the paint spectrum.

Data sets were separated based on the color, presence/absence of effect pigment, and the number of layers for each paint samples for the analysis. These parameters were

determined by visual and microscopic examination. These parameters would be easy to identify and would provide initial discrimination between samples prior to the need for a more intensive analysis method. As the paints could be separated by these parameters prior to LIBS analysis, only samples within each data set were compared by the statistical analyses.

The LIBS parameters were optimized for the sampling of the automobile paint samples. The laser energy was 31 mJ/pulse with a 5 μs detector delay. The spectra were collected in an air atmosphere with ambient temperature and pressure. The focusing lens and optic were adjusted to the optimal position for the laser focus on the samples and collection of the plasma. Each spectrum was comprised of an average of five drill down shots. The average of five shots was determined to be ideal for the collection of all the layers present in each sample without completely passing through the samples; a few of the samples with the smallest number of layers were sampled completely through. Drill down was preferred over multiple points averaging as it allowed spectral data on all layers present in paint to be collected. For each sample twelve spectra were collected. Due to potential instrumental drift, the twelve spectra for one sample were collected consecutively and all samples of one data set were collected consecutively. The full set of automobile paint samples (all colors/layer/effect pigment data sets) was collected over a four day period but each individual data set was collected within a period of a few hours.

Table 1: Summary of automobile paint samples where 'y' indicates presence of effect pigment and 'n' indicates absence of effect pigment.

Color	Effect Pigment/Layers	Number of Samples	Color	Effect Pigment/Layers	Number of Samples
Red	3y	3	**Green**	3y	2
	4n	4		4y	3
	4y	2		5y	3
	5y	2	**White**	3n	17
Black	3y	2		4n	6
	3n	2		5n	5
	4n	3		6n	4
	5n	2		7n	4
Blue	3y	5	**Silver**	3y	2
	4y	3		4y	4
Tan	3y	4		5y	3
	4y	2			
	5y	4			

4.1.2 Float Glass

The float glass analysis performed for this research was an expansion on initial research performed by Bridge and McIntee [14, 16, 17, 241], which was touched upon in the introduction. Initial studies investigated single pieces of glass originating from a window using nonparametric analysis. In the research presented here, analysis was performed on multiple areas of a single window pane to determine the homogeneity of the window. In addition, multiple window panes were compared to determine the discrimination ability between automobile window panes using the nonparametric permutation test.

Full window pane samples were acquired from a local Orlando junkyard. The full window pane samples that were used are listed in Table 2. Based on the source of the samples, it is not guaranteed the glasses were from the original manufacturer; they may be aftermarket windows.

Full window pane samples were used to acquire spatial information in addition to discrimination ability. To provide this information, five areas were identified for analysis. The five areas, shown in Figure 7, were the (1) upper left, (2) center, (3) lower right, (4) upper right, and (5) lower left. Duct tape was used to mark these areas and ensure they remained intact when the window was broken into smaller pieces. Once the window was broken, the duct taped pieces were separated for analysis. The remaining shattered pieces of glass from each window were saved separately.

Table 2: List of full automobile window panes collected for analysis.

Sample Label	**Year**	**Make**	**Model**
A	1979	VW	Rabbit
B	1978	GMC	Van
C	2000	Volvo	540
D	1992	Honda	Accord
E	1998	Mitsubishi	Galant
F	1998	Mitsubishi	Galant (2)
G	1989	Dodge	Dynasty
H	1993	Mazda	626
I	1997	Chrysler	Sebring
J	2000	Acura	Integra

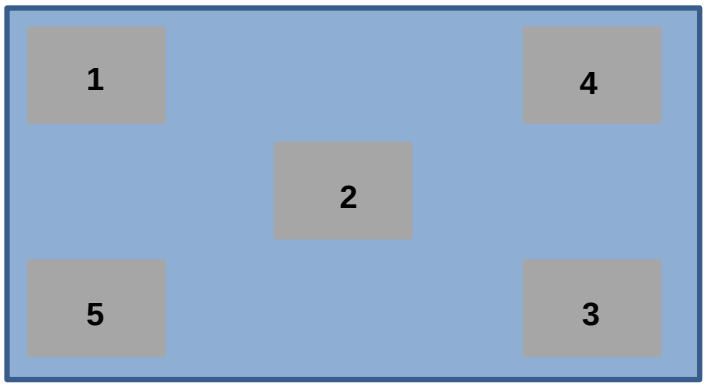

Figure 7: Areas for spatial analysis of automobile glass samples.

Analysis was performed on the non-float side of the glass. This was done to avoid the large presence of tin used during the manufacturing process from overpowering the trace elements in the spectra. The non-float side was determined by the side of the glass that did not fluoresce under short wavelength ultraviolet light (254 nm). Once the non-float side was determined the samples were mounted on microscope slides using double sided tape.

Samples were cleaned prior to analysis. All glass samples were cleaned of dirt initially with deionized water but further cleaning was need on some of the samples. Some of the samples had tinting on the non-float side, therefore a razor blade was used to remove the tinting and cyclohexane was used to remove the remaining adhesive. All samples were cleaned with the cyclohexane whether there was adhesive or not. Before analysis, samples were cleaned one final time with deionized water and allowed to dry.

LIBS analysis was performed using the Ocean Optics LIBS system discussed in the instrumental section. The laser energy was 45 mJ/pulse with a 5 μs detector delay. The spectra were collected in an air atmosphere with ambient temperature and pressure. The focal lens and optic were adjusted to the optimal position for the laser focus on the samples and collection of the plasma.

Three different methods of spectral averaging were performed in the course of the automobile glass research. The three methods were: drill down, partial drill down/multiple point, and multiple points as discussed in the beginning of the LIBS experimental section. For the analysis of glass 10 shots were averaged per spectrum for each of the spectral averaging method. Therefore, the drill down method was 10 shots in one spot; the multiple point method was one shot in 10 spots; and the partial drill down/multiple point method was five shots in two spots. These three spectral averaging methods were tested to ensure the optimal parameters for analysis of the automobile float glass samples. Each provided informational results on the glass samples.

In addition to the spectral averaging method, order of collection was optimized. Due to the highly similar nature of the glass samples produced from the manufacturing process variation from the instrument could have a large effect on the results. Therefore, collecting the samples in a way which incorporated the instrumental variation over time into the spectra helped prevent discriminations based on variation from anything but the

samples. Two methods were tested, consecutive order and random order. From experiments it was determined that the random order would be ideal for collection of these highly similar samples. Therefore, random collection order was used for the remaining analyzes.

Once sampling parameters were optimized, data was collected. The number of spectra collected depended on the analysis performed; with between six and 15 spectra collected per sample, with each spectrum an averaging of 10 shots.

The experimental steps given in this section were written into a standard operating procedure (SOP) to be used when sampling automobile float glass samples with the LIBS. The SOP is shown in APPENDIX B.

4.1.2.1 Multiple Point Spectral Averaging, 10 Windows 3 Areas

Initial experiments were performed to determine the ability of the nonparametric test to discriminate between different automobile windows. The first experiment was performed with all ten window panes and three areas of each of the window panes (areas 1, 2, and 3). The three areas were grouped together as “same window”. Six average spectra were collected in random order on each of the areas, giving a total of 18 spectra grouped as same window for each sample. Each spectrum was an average

of ten spectra taken at different spots on the glass. Discrimination by nonparametric permutation hypothesis testing was calculated for “same window” and “different window” comparisons using an in-house software.

4.1.2.2 Multiple Point Spectral Averaging, 3 Windows 3 Areas

The second LIBS experiment was performed using the three car windows with the most discrimination between areas (C,D, and J) and three areas of each window (1, 2, and 3). The samples were collected in triplicate where three sets of spectra were collected for each sample. For each set, six average spectra were collected in random order. Each spectrum was an average of ten spectra taken at different spots on the glass. Triplicate sampling, was selected because it provided multiple p-values for same sample comparisons. Discriminations by the nonparametric permutation hypothesis test were calculated for same window-same area (SWSA), same window-different area (SWDA), and different window (DW) data using the in-house software.

4.1.2.3 Multiple Point Spectral Averaging, 2 Windows 5 Areas

The third experiment looked at the two windows from the first experiment (D and G) and all five areas of these windows. Twelve spectra, each an average of ten spectra taken at different spots on the glass, were collected on each area in random order.

Discriminations by the nonparametric permutation hypothesis test were calculated for SWSA, SWDA, and DW.

4.1.2.4 Test of Spectral Averaging Method, 10 Windows 5 Areas

The fourth set of experiments used the three spectral averaging methods to analyze the five areas from all ten windows to determine whether variance being observed in the SWDA samples was due to sampling only on the surface. Between twelve and fifteen average spectra were collected per sample for each of the three spectral averaging methods (drill down, partial drill down\multiple points, and multiple points). For each spectral averaging method ten shots were averaged for one spectrum. Once data was collected, the nonparametric permutation hypothesis test was performed to obtain results using in-house software.

4.1.2.5 Discrimination versus Inter-Sample Distance Test

The fifth experiment investigated the discrimination based on distances using a single piece of glass of 3 cm x 1 cm from sample I. The sample was sectioned off into 1 cm x 1 cm blocks as shown in Figure 8, with the first block (A) further subdivided into a ½ cm x 1 cm block. Twelve spectra, each an average of ten spectra taken at different spots

on the glass, were collected in random order on the sample and nonparametric permutation test was performed.

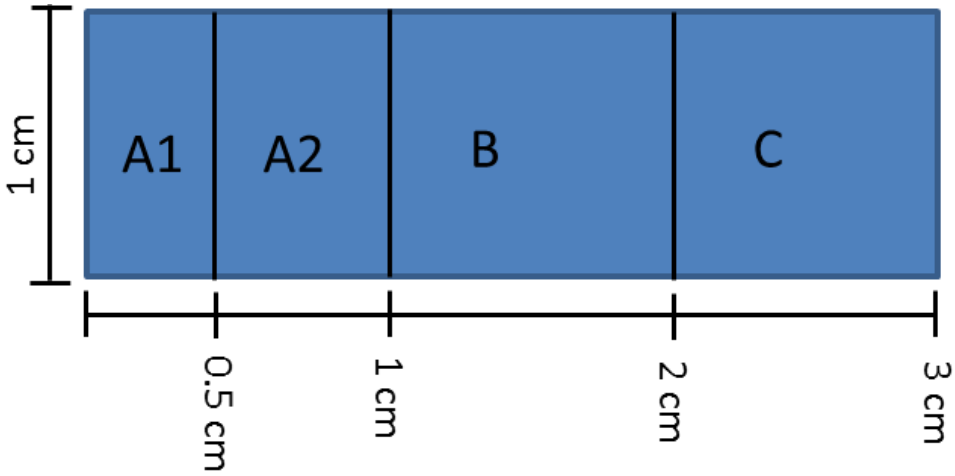

Figure 8: Diagram of grid float glass sample for discrimination based on distance.

4.1.2.6 Nonparametric versus Parametric

To ensure the within window pane spatial variation being observed was not based on the statistical analysis of the samples the spectral data from all five areas of window A was compiled and the Wilcoxon Rank Sum test and a parametric t-test were applied. The twelve to fifteen spectra collected in the 5.1.2.4 experiment were tested for all three spectral averaging methods. The spectra were each an average of 10 shots. The spectral data was used in the Hoteling's t-test (parametric method) and the Wilcoxon Rank Sum test (nonparametric method) to compare the results and ensure the chosen

nonparametric method was performing equivalently to the more accepted parametric method.

4.1.2.7 LIBS Imagining

The final analysis to investigate the within window pane spatial variation was imaging of the LIBS spectral data. This analysis looked at two pieces of glass: a 1 cm x 1 cm piece of glass from window F area two, and a 2 cm x 2 cm piece of glass from window J area five. These pieces of glass were sectioned off into 16 spots for the 1 cm x 1 cm piece of glass and 100 spots for the 2 cm x 2 cm piece of glass as illustrated in Figure 9.

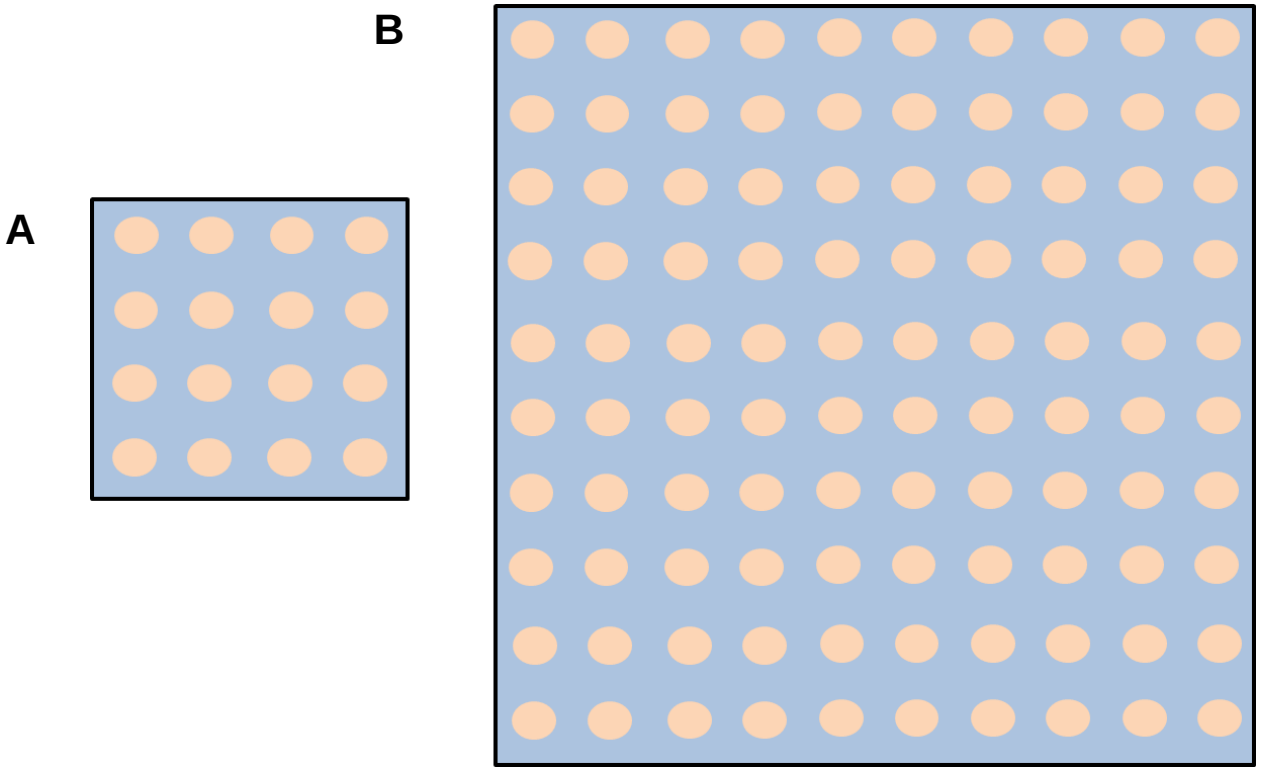

Figure 9: Grids of A) 1 cm x 1 cm and B) 2 cm x 2cm glass data collected for LIBS imaging.

For each spot on the two pieces of glass five spectra were collected. Each spectrum was a single shot and all five spectra were collected in the same spot. This provided spectral data for five layers of the window in each spot. The locations, where five successive spectra were collected, were chosen in random order. Spectra were compiled and PCA was performed to obtain the scores for the data and the scores corresponding to the first three principal components were plotted on an RGB color scale to demonstrate variance within the areas.

4.1.2.8 Blind Tests

The final experiment set consisted of blind tests performed with each spectral averaging method. Five pieces of a window were collected without knowledge of where on the window they came from. Four of the areas were classified as known and the fifth was classified as a questioned. An additional piece of glass was collected from a separate window as another questioned sample. Four areas were classified as the known to try and create a method which would encompass the variance being observed within a single window pane to ensure unknown pieces consistent with the same source would not be discriminated. Fifteen spectra were collected in random order on each piece for each spectral averaging method. For each method ten shots were averaged per spectrum. Data was analyzed by the nonparametric permutation hypothesis test with 100 p-values calculated for each pairwise comparison. The distributions of the p-values were plotted in boxplots by type of comparison (known versus known, known versus questioned one, and known versus questioned two) to determine if questioned samples could be identified as coming from the same window as the known or a different window. Same window comparisons were expected to show uniformly distributed p-values, while different window comparison p-value distributions were expected to cluster at or below the significance level. The Wilcoxon Rank Sum test was then applied to the p-values to provide additional statistical backing of the discriminations or non-discriminations. This step was performed to provide information on the ability of this method for the analysis of glass samples in case work.

4.1.3 Bone

The analysis of bone samples was comprised of samples acquired from Professor John Schultz, Department of Anthropology, University of Central Florida. Bones of different species were acquired including: bird, fish, human, dog, deer, alligator and turtle. Other than species of the bone, little was known about the bones. LIBS sampling was performed on the intact bone with minimal damage to the sample. Issues were encountered with the size of some of the bones and attempts were made to collect slivers of the bone or bone ash for analysis; these presented additional issues of being too thin for the laser shot and increased damage to the sample. Therefore, analysis was limited to small bones that would fit into the LIBS sampling chamber.

Multiple experiments were tested using a range of different bones. More details will be discussed in the following sections on which bones were used for specific tests, but an overview of all bones gathered for the experiments are seen in Table **3**. Bones from different species were acquired along with bones of the same species same animal and different animal (ex. two dog bones from one dog and a third dog bone from a different dog). The variety of bones was used to test the ability of discrimination between bones from different species, bones from different animals in the same species and different bones from the same animal.

Table 3: Bone samples used in LIBS analysis; The first number after a bone indicate which animal they come from, therefore 1.1 and 1.2 come from the same animal, and 1.1 and 2.1 come from different animal. The second number after the sample distinguishes between bones from the same sample, therefore 1.1 and 1.2 are bones 1 and 2 from the same animal.

Bone Samples		
Human 1	Human 2	Fish 1
Fish 2	Human Toe	Human Tarsel
Archeological Human 1.1	Archeological Human 1.2	Archeological Human Cu 1.1
Archeological Human Cu 1.2	Bird Bone 1.1	Bird Bone 1.2
Bird Bone 2.1	Bird Bone 2.2	Deer 1.1
Deer 1.2	Deer 2.1	Deer 2.2
Dog 1.1	Dog 1.2	Dog 2.1
Dog 2.2	Alligator 1.1	Alligator 1.2
Alligator 2	Human Cleaned 1.1	Human Cleaned 1.2
Human Natural	Human Burnt	Human Bleached
Human Tooth Denton 1	Human Tooth Enamel 1	Human Tooth Denton 2
Human Tooth Enamel 2	Pig 1.1	Pig 1.2
Pig 2.1	Pig 2.2	Pig Tooth Denton 1
Pig Tooth Enamel 1	Pig Tooth Denton 2	Pig Tooth Enamel 2
Deer	Turtle 1.1	Turtle 1.2
Turtle Bone 2	Turtle Shell	Soil

Multiple LIBS tests were performed in an effort to determine the appropriate method for analysis of the bones. LIBS parameters were varied depending on the experiment being performed. The laser output ranged between 65- 45 mJ/pulse for the analysis, the delay after the laser pulse was between 2.5 -5 µs.

4.1.3.1 Single shot, Consecutive Sampling

The initial approach to the bone analysis was the analysis of twelve bone samples from different species. Twelve single shot spectra were collected in consecutive order for each bone over the full spectral range. The bones for this experiment are shown in Table 4.

Table 4: Bone samples used for single shot, consecutive sampling.

Bone Samples			
Alligator Bone	Turtle Shell 2 (top side)	Turtle Shell 1 (under side)	Bird Bone 1
Bird Bone 2	Deer Bone	Fish Bone 1	Fish Bone 2
Human Bleached	Human Burnt	Human Tarsal	Turtle Bone

4.1.3.2 Single Shot, Random Sampling

The second set of bone data collected was performed on 37 bones, listed in Table 5, from different species, same species different animal, and same species same animal to determine ability of discrimination. Two sets of five single shot spectra were collected per bone. The data was grouped per sample set (set one and two) and the order of collection for each group was randomized.

Table 5: List of 37 bone samples used in second set of bone data. Bones labeled by species, #.#. First # corresponds to animal; therefore 1.1 and 1.2 come from the same animal while 1.1 and 2.1 come from different animals. The second # corresponds to how many bones from a specific animal, therefore 1.1 and 1.2 are bones 1 and 2 from the same animal.

Bone Samples			
Archeological Human 1.1	Archeological Human 1.2	Bird 1.1	Bird 1.2
Bird 2.1	Bird 2.2	Dog 1.1	Dog 1.2
Dog 2.1	Dog 2.2	Gator 1.1	Gator 1.2
Human Cleaned 1.1	Human Cleaned 1.2	Human Tooth Dent. 1	Human Tooth Dent.2
Deer 1.1	Deer 1.2	Deer 2.1	Gator 2
Human Bleached 4	Human Burnt 3	Human Tooth Enamel 2	Pig 1.1
Pig 1.2	Pig 2.1	Pig 2.2	Human Tooth Enamel 1
Pig Tooth Dent 1.	Pig Tooth Dent. 2	Pig Tooth Enamel 1	Pig Tooth Enamel 2
Turtle 1.1	Turtle 1.2	Turtle 2 Bone	Turtle 2 Shell
Test (Deer)			

4.1.3.3 Average Spectra, Random Order

The final set of data was collected on the four bones listed in Table 6. Twelve average spectra were collected on each bone in random order. Each spectrum was an average of 10 shots collected in different spots on the bone.

Table 6: Samples used for average spectra, random order data set. Bones labeled by species, #.#. First # corresponds to animal; therefore 1.1 and 1.2 come from the same animal while 1.1 and 2.1 come from different animals. The second # corresponds to how many bones from a specific animal, therefore 1.1 and 1.2 are bones 1 and 2 from the same animal.

Bone Samples	
Bird 2.2	Human Finger
Pig 2.1	Pig 2.2

4.1.4 Metal Transfer

Metal transfers were performed using 9 mm bullets acquired from a local gun store (East Orange Shooting Sports, Orlando, Fl). Six brands of bullets (five bullets of each brand), shown in Figure 10, were acquired for the analysis. The bullets, including the brand and jacketing type, are listed in Table 7.

Figure 10: Six standard bullets; from left to right: CCI Blazer (B1), Independence (B2), Remington UMC (B3), Hornady Tap (B4), Winchester Silver-Tip (B5), Winchester hand packed (B6)

Table 7: Description of bullet samples used in metal transfer experiments

Manufacturer	Bullet Type	Jacket	Composition	Bullet Number
CCI	Blazer	Yes	Copper	1
Independence		Yes	Copper	2
Remington	UMC	Yes	Copper	3
Hornady	Tap (hollow-point)	Yes	Copper	4
Winchester	Silver-Tip (hollow-point)	Yes	Unknown metal	5
Winchester	Hand packed	No	Lead	6

The bullets were transferred using two methods on to two different substrates. The first transfer was performed by shooting the bullets through a 1 mm steel plate (the first

substrate) purchased from Home Depot, Orlando, FL. This was performed at the Seminole County Shooting Range by Lt. Jerry Emert from the University of Central Florida Police Department. Four bullets of each brand were shot through the steel plate at a range of approximately seven feet to create the bullet hole metal transfer. The fifth bullet of each brand was saved as a standard to build a data library. Three steel plates were used, with each containing a cluster of four bullet holes for two bullets (except for the CCI bullet where only three bullet holes were made in the substrate). Plates were packaged separately for transportation to prevent any sample contamination and pictures were acquired of each sample prior to transfer with a few examples seen in Figure 11.

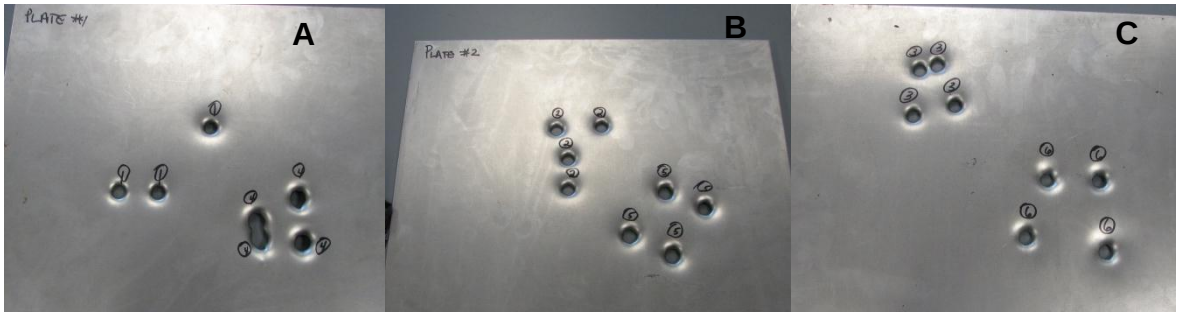

Figure 11: Bullet holes on steel plate backgrounds. A) Plate 1 with 3 bullet holes clustered for bullet 1 and 4 bullet holes clustered for bullet 4; B) Plate 2 with 4 bullet holes clustered for bullet 2 and bullet 5; C) Plate 3 with 4 bullet holes clustered for bullet 3 and bullet 6.

The second method of metal transfer was the transfer of trace amounts of the metal from the bullet jacket to a steel plate and a porcelain tile (the second substrate). This method allowed for the testing of an additional substrate, multiple bullet transfers in one

area, and a less complex sampling surface (flat instead of trying to collect spectra within the bullet holes).

The transfer was performed in two ways: single bullet transfer and multiple bullet transfer. Single bullet transfer was done by taking each bullet individually and creating three separate lines onto the substrates for the single bullet transfer. All six bullets were transferred individually to the two substrates. For the multiple bullet transfer the bullets were transferred individually onto each substrate creating three lines and a second bullet was then transferred over the same places of each substrate to create a more complex transfer. Only three of the bullets were used for the multiple bullet analysis: B3, B5, and B6. These three bullets encompassed a copper jacket (B3, CJ), a metal jacket (B5, MJ) and a non-jacketed bullet (B6, NJ). Listed in Table 8 are the individual and mixture samples that were analyzed. Transfer lines are illustrated in Figure 12 for bullets 3 and 6 onto each substrate. Silver and copper colored flakes can be observed within the red boxes where the transfers occurred.

Table 8: Transfer line individual and mixtures samples and substrates. Mixtures are listed with the first bullet listed being the first bullet transferred to the substrate.

Sample	**Substrate**	**Sample**	**Substrate**
Bullet 1	Steel Plate	Bullet 1	Porcelain tile
Bullet 2	Steel Plate	Bullet 2	Porcelain tile
Bullet 3	Steel Plate	Bullet 3	Porcelain tile
Bullet 4	Steel Plate	Bullet 4	Porcelain tile
Bullet 5	Steel Plate	Bullet 5	Porcelain tile
Bullet 6	Steel Plate	Bullet 6	Porcelain tile
Bullet 5 and 6	Steel Plate	Bullet 5 and 6	Porcelain tile
Bullet 6 and 3	Steel Plate	Bullet 6 and 3	Porcelain tile
Bullet 5 and 3	Steel Plate	Bullet 5 and 3	Porcelain tile

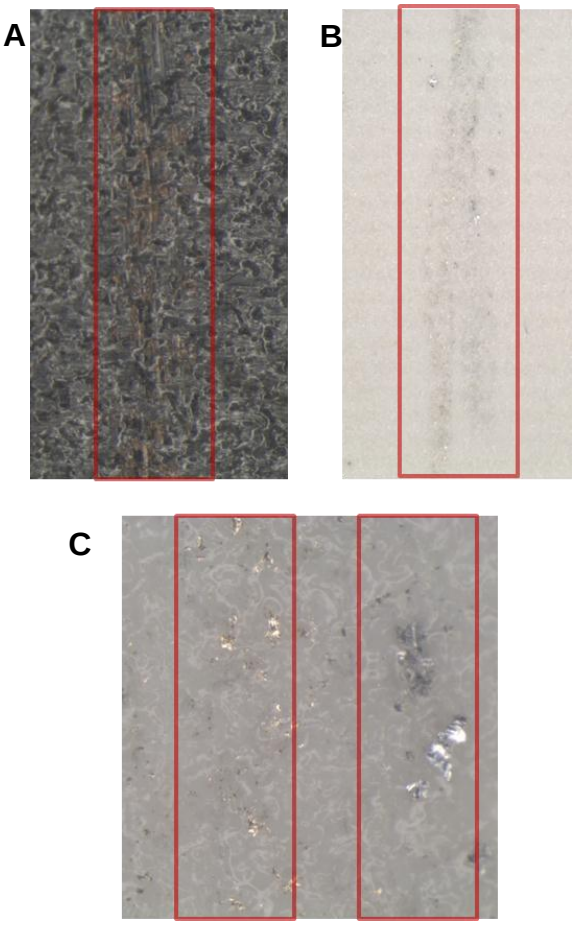

Figure 12: Transfer lines onto steel and porcelain substrates; highlighted in the red box is where the transfer line occurred and visible silver and copper flakes. A) Bullets 3 and 6 onto the steel substrate, B) Bullets 3 and 6 onto the porcelain substrate, C) Close up of Bullet 3 and 6 on the porcelain substrate.

LIBS analysis was performed using the Ocean Optics LIBS 200+ at an average laser output of 45 mJ/pulse and pulse width of 9 ns. The delay was set between 3-6 µs after the laser was fired for each analysis and the spectra were collected from 200 to 900 nm. A library of spectra was collected from the unused bullets. Prior to LIBS analysis the projectile, casing and smokeless powder were separated to ensure safety during LIBS sampling. FDLE Orlando fire arms analyst Christine Murphy assisted with this

separation. A Bullet Puller, a tool which separates the three pieces of the bullet was used. The library was composed of six spectra collected on the projectile portion for each brand of bullet, with each spectrum being a multiple point average of ten shots.

Prior to collection of the bullet hole data the steel plates containing the bullet holes were cut to allow for the bullet holes to be placed in the sampling chamber; each was labeled in a corner to ensure samples were not mixed up and markings did not interfere with sampling. The bullet hole was positioned so that the laser would hit the edge of the bullet hole to ensure collection of spectra where the transfer occurred. For each bullet hole twelve single shot spectra were acquired; holes were labeled as shown in Figure 13. All four bullet holes were sampled over multiple samplings. The spectral data for the bullet holes was acquired over a five month period. Despite the time of collection for the bullet hole data, comparison was made to a single library collected prior to the collection of the first set of bullet hole data. The same library was used for the transfer line data.

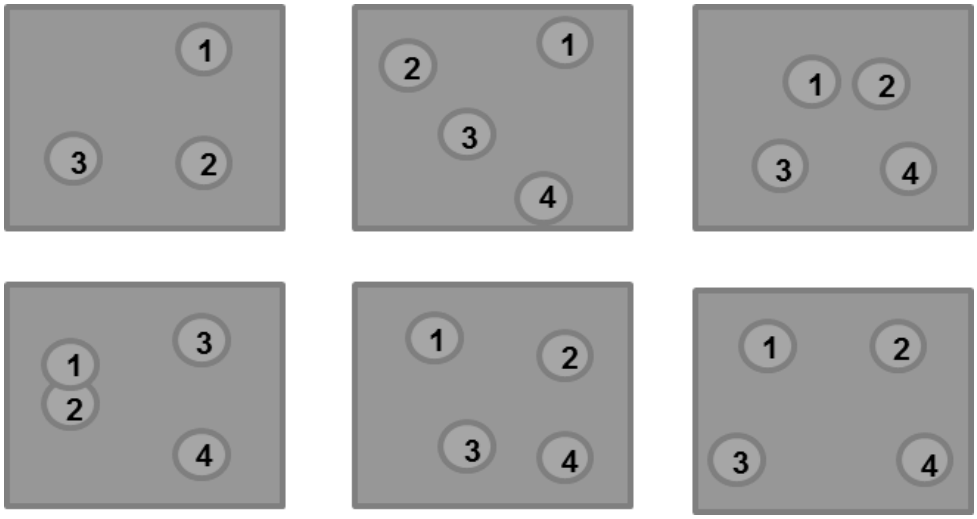

Figure 13: Bullet hole labeling for each bullet cluster. With order from top left corner bullet 1 to bottom right corner bullet 6.

LIBS spectra of the transfer lines on the two substrates were collected with the same instrumentation and energy level as the bullet holes. The delay was 4.5 – 6 μs after the laser was fired and the same spectral range was used. Twelve single shot spectra on each of the lines were collected. The spectra of the transfer lines were collected in random order. For the single bullet transfer the randomization of order was performed so that samples were randomized by substrate; therefore all porcelain samples were collected in random order and then all steel samples. Also each mixture was sampled separately so the randomization was purely for the order of the lines and not the samples (example, all 3,5 porcelain samples collected in random order then all 5,6 porcelain samples).

4.1.5 Organic Compounds and Polymer Mixtures

The LIBS experiment for organic compounds was performed using samples of polymer thin films. Three polymers were prepared to comprise the library and mixtures were made of these three polymers to comprise the test samples. The polymers used included the following solutions: poly styrene in toluene (100 mg/mL), poly acrylonitrile in dimethyl formamide (65 mg/2mL), and nitrocellulose in methyl-ethyl-ketone (200mg/3mL). The mixtures included: nitrocellulose on poly styrene and poly acrylonitrile on poly styrene. A small amount of each polymer solution was pipetted onto a glass slide which had been cut to 8 mm x 8 mm. The polymer solution was then spread using the edge of a clean glass to create a thin film of consistent thickness across the glass; this procedure is known as “doctor-blading”. The solution was allowed to dry and then sampled. The mixtures were prepared in a similar way with the base polymer applied and allowed to dry prior to the second polymer being pipetted in thin lines on top.

Spectra were collected in both air and argon atmospheres. The collection of spectra under argon was performed to minimize the molecular emissions from the air that may interfere with the elements of interest, specifically the N_2 and O_2 contributions and the reaction of N_2 with C and C_2 which results in CN lines. For argon sampling, the sample was placed in a sealed cuvette perpendicular to the laser path. A small tube was

inserted into the cuvette in order to allow argon to flow into the cuvette for two minutes prior to collection.

For each library and mixture sample 50 single shot spectra were obtain in both air and argon using a nanosecond LIBS system in Professor Richardson's laboratory which was assembled by Christopher Brown [243]. The 50 spectra were collected by raster scanning across the samples to ensure collection of the mixture samples with contributions from all components. The spectra were collected from 200-785 nm at wavelength increments of 0.022nm using an Echelle detector. The laser used was a Brilliant 1064 with energy of 15.4 mJ. The gate width and delay were 10 µs and 0.018 µs respectively.

4.2 Fourier Transform Infrared Spectroscopy – Attenuated Total Reflectance (FTIR-ATR) Experimental

4.2.1 Automobile Paint

The automobile paint samples were analyzed on the FTIR instrument previously discussed in the instrumental section with the ATR attachment. The paint samples were the same ones used in the LIBS analysis of automobile paint and are listed in APPENDIX A**.**

The FTIR detector was cooled for 30 minutes with liquid nitrogen prior to collection of the spectra. This was done to reduce the background noise in the spectra. Once the detector was cooled, spectra were collected. The samples were mounted on a glass microscope slide for analysis. Prior to collection, the samples were cleaned with isopropyl alcohol.

OMNI software was used to collect the FTIR spectra. The instrumental parameters were set with a resolution of 4 cm^{-1} and 32 scans were collected. The sample spectra were collected in the range of 400-4000 cm^{-1} with the ATR attachment in contact with the sample. The ATR pressure on the sample was approximately 5 on the sensor. Before the collection of the sample spectrum, the background spectrum was collected with the ATR attachment removed from the sample. It was then subtracted by the software from the sample spectrum.

Twelve spectra were collected per sample in consecutive order to be used for analysis by the nonparametric permutation hypothesis test. Once collected the samples were grouped into two sets of six for analysis by in-house software. The nonparametric permutation hypothesis test was performed on the data for both the original and log of the spectra. Two wavelength ranges were tested also, 400 - 4000cm^{-1} and 650 - 2000cm^{-1}.

4.2.2 Organic Compounds and Polymer Mixtures

The FTIR previously mentioned in the instrumental section was also used in the analysis of organic compounds. Spectra of pure samples were collected to create a library. Table 9 lists the compounds used to comprise the library, with four spectra of each compound collected. Library samples were prepared by placing a small amount of the sample on to a glass microscope slide. The FTIR used in the analysis was attached to a microscope, therefore the microscope was used to ensure crystals of the library samples were in the sampling field and spectra were collected.

Table 9: Organic compounds used to for FTIR spectral library.

Library Compounds	
1,5-Dimethylnaphthalene (1,5-DMN)	2,3-Dinitrotoluene (2,3-DNT)
2,4-Dinitroluene (2,4-DNT)	3,4-Dinitrotoulene (3,4-DNT)
Benzophenone (BP)	Caffeine (Caf)
Theobromine (TB)	Theophylline (TP)
Glass	Paint

The FTIR analysis was performed using the ATR attachment which required contact between the instrument and the samples, with approximate pressure of 5 on the sample. Spectra were collected using the OMNI software from the range of 650-2000 cm^{-1}. The instrument resolution was set at $4cm^{-1}$ and 32 scans were collected. The background spectrum was collected prior to each sample spectra by removing the ATR attachment from contact with the sample. The background spectrum was subtracted

from the sample spectrum by the software. Prior to any analysis the detector was cooled for 30 minutes.

Mixture samples were prepared to test against the library and are shown in Table 10. The mixture samples were prepared by placing a small amount of the compound onto a glass slide. A fingerprint was simulated for the mixture by a gloved finger being pressed to the researcher's forehead to acquire oils. The finger was then touched into the compound on the glass slide to mix the oil and the organic compound. The mixture was then touched to a glass slide or paint chip for transfer onto the substrate. Once transfer was made to the substrate the mixtures were analyzed using the same FTIR procedure as described for the library. Additional spectra were collected for the mixture samples to ensure all compounds were collected at varying amounts throughout the sample.

Table 10: FTIR organic mixture samples

Organic Mixtures	
Benzophenone and paint	Caffeine, fingerprint oil, and glass
2,4-Dinitrotoluene and paint	Theobromine, fingerprint and paint

4.3 Raman Spectroscopy

4.3.1 Organic Compounds and Polymer Mixtures

Raman spectroscopy was the last method for analysis of the organic compounds. The Ocean Optics Raman instrumentation with the 532nm laser interfaced to a polarized light microscope was used to collect a library of compounds and mixture samples.

Clear glass vials containing a small amount of the compounds listed in Table 11 were used to collect the library spectra. For the collection of the library samples the Raman laser was not interfaced to the microscope; it was instead positioned in the separate sampling compartment. The sampling compartment provided for the sample vial and the laser probe to be perpendicular to each other in an enclosed dark space. The probe was in contact with the sample vial during the collection of the spectra. For each library compound, four spectra were collected. A background spectrum was collected prior to each sample spectrum; the background spectrum was collected with the laser off and was subtracted from the spectrum by the software. An integration time of 10 seconds was used for collection.

Table 11: Raman organic compound library samples

Raman Organic Compound Library		
1,5-Dimethylnapthalene	2,3-Dinitrotoluene	2,4-Dinitrotoluene
3,4-Dinitrotoluene	Ammonium perchlorate	Benzophenone
Caffeine	Potassium chlorate	Potassium nitrate
Potassium perchlorate	Sodium chlorate	Sodium nitrate
Sodium perchlorate	TATP	Theobromine
Ammonium nitrate		

Mixture samples were prepared in a similar way to the FTIR mixtures. A small amount of the sample was placed on a glass slide and if necessary crushed to small particles using a metal spatula. A gloved finger was touched to the forehead to ensure oil was present and then touched into the compound. The mixture was then transferred to a clean glass microscope slide. Five mixtures were prepared and are listed in Table 12. The Raman was interfaced to the microscope for the collection of spectra using 10x and 40x objectives. The integration time was increased to 30 seconds per instructions in the instrument manual. Between five and seven spectra were collected per mixture to ensure combinations of the compounds present were collected.

Table 12: Raman mixture samples

Raman Mixture Samples	
Ammonium nitrate and fingerprint (spectra 1-5 at x10, spectra 6-7 x40)	TATP and fingerprint (spectra 1-3 x10, spectra 4-6 x40)
TATP, ammonium nitrate and fingerprint (spectra 1-3 x10, spectra 4-6 x40)	2,4-dnt and fingerprint (all 5 spectra x40)
Theobromine and fingerprint (all 5 spectra x40)	

4.4 Gas Chromatography Mass Spectrometry (GC-MS)

4.4.1 Fire Debris

The fire debris samples were analyzed on an Agilent GC-MS mentioned previously. The instrument used a split/splitless injector where 1 µL of sample was split 50:1 at a temperature of 250°C. A HP-1 (methyl siloxane) chromatographic column with an internal diameter of 0.2 mm, length of 25 m, and film thickness of 0.5 µm was used [191, 205]. A helium carrier gas was kept at a constant flow rate of 34 cm/minute on the column. The oven temperature began at 50°C for 3 minutes. The temperature was ramped at a rate of 10°C/min until the final temperature reached 280°C, where it was held for 4 minutes. The total run time of the analysis was 30 minutes. A scan of 30-350 m/z was performed by the mass analyzer at a scan rate of 2-3 scans/second; which is approximately 6-10 scans per peak. The mass scanning began after a 2 minute solvent delay. The source temperature was set at 230°C and the mass spectrometer line was held at 280°C [191, 205].

On completion of sample analysis, the total ion spectrum (TIS) was compiled. Previous methods used the TIC or EIC to determine the presence and classification of ignitable liquid residues. As illustrated in Figure 14 the TIC sums the ion intensities over all mass-to-charge ratios (m/z) at each mass scan, while the EIC sums the m/z ratios of specific ions at each mass scan. The TIS is produced by summing the intensities for

each m/z value across the entire chromatographic range and normalizing the sum of the intensities to one, which is similar to an average mass spectrum across the chromatographic profile. The TIS provides a 2-dimensional representation of the 3-dimensional data set acquired by GC-MS analysis which is also illustrated in Figure 14. To allow for comparisons of multiple total ion spectra each were normalized to a total intensity of one. The TIS is independent of time unlike the TIC, therefore the issue of retention time shifts from comparison of multiple labs instrumental data was removed. The independence of time and the significant chromatographic information provide enough for a library or database to be created from the TIS. Care should be taken to collect the full chromatographic range as the TIS does require all components including the lightest and heaviest to be complete, otherwise the results are distorted causing issues in data analysis.

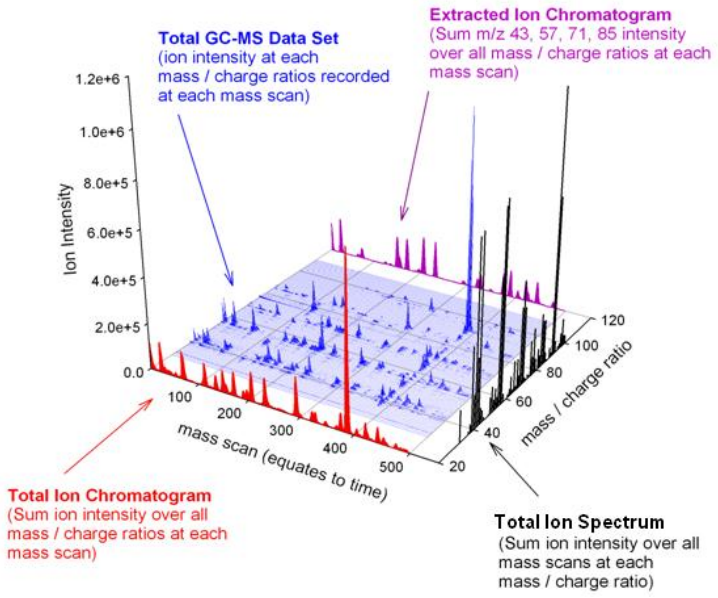

Figure 14: A 3-dimensional representation of GC-MS data.

With a goal of determining a chemometric method of classifying ignitable liquids into their characteristic ASTM classes, a data set was compiled from the online ignitable liquid reference collection developed by the Ignitable Liquids Reference Collection (ILRC) Committee of the Technical Working Group for Fire and Explosions (TWGFEX). The data set consisted of 452 ignitable liquid samples from all ASTM classes, with petroleum distillates broken into heavy (HPD), medium (MPD) and light (LPD). Each summed ion spectrum contained the m/z range of 30-200 and was normalized to sum to one. Two classes, miscellaneous (MISC) and oxygenates (OXY), have caused the biggest problems in previous methods of analysis, therefore the 452 samples were broken into two data sets. Data set one included the miscellaneous and oxygenate classes, therefore keeping all 452 samples; while data set two had the miscellaneous and oxygenate classes removed, therefore retaining 287 samples. The models were composed of the samples listed in the table in APPENDIX C, with the MISC and OXY samples removed for the data set two models and substrates removed when not included in the model. This table was included in the appendices due to the large amount of data included in it.

CHAPTER 5: DATA ANALYSIS

5.1 Fire Debris

The analysis of the fire debris samples was performed by normalization and reduction of the data dimensionality prior to PCA, further reduction by PCA, and classification by discriminant analysis. Initial methods looked at reducing the data prior to PCA analysis by selecting high F-values. For each data set, F-values were calculated by an R code and then weighted by multiplying by the m/z average intensity from the data. F-values represent the ratio of between group variance to within group variance, therefore allowing for the optimum separation between classes to be obtained. To determine the appropriate number of F-values to retain, five sets were tested: 10, 20, 30, 40, and 50. The 50 F-values for each data set are shown in Figure 15. After the initial f-value ions were identified and tested an additional 55 ions were found to be important in distinguishing between the classes, shown in Table 13. These additional ions were identified as being abundant within the ASTM classes and were therefore included in the analysis.

Some of the abundant ions were encompassed in the F-values, the remaining were added at this point. Two ions were also specifically removed if found as one of the top F-values, 32 and 76, due to their presence in the baseline and their ability to dominate

pyrolysis products. The removal of ions 32 and 76 prevented issues with trying to separate between substrates and ignitable liquids in analysis that contain both samples.

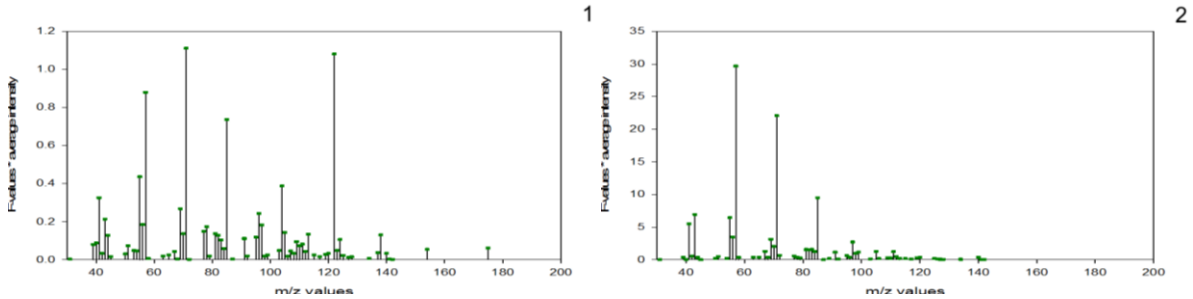

Figure 15: Illustration of selected F-values for 1) data set 1 (all ASTM classes) and 2) data 2 (excluding MISC and OXY classes).

Table 13: Abundant ions found to be characteristic for classification of ASTM classes.

Abundant Ions			
31	65	85	111
39	67	87	112
40	68	91	113
41	69	92	115
42	70	95	117
43	71	96	119
44	72	97	120
45	77	98	125
51	78	99	127
55	79	103	128
56	81	105	134
57	82	106	141
58	83	109	142
63	84	110	

Based on the tests, the optimum selection of ions to retain prior to PCA was determined to be the top 50 F-values plus the additional abundant ions for each data set (excluding ions 32 and 76), listed in Table 14. The total number of ions was different for the two tests. The m/z ratios identified for the ions corresponding to the 50 high F-values differed due to one of the data sets containing the MISC and OXY classes and the other data set not containing them. When the abundant ions were added to the data sets some of the ions had already been included based on the high F-values. The number of abundant ions and ions corresponding to the 50 high F-values differed between the two data sets, therefore resulting in a difference in the total number of ions for the two data sets.

Once the optimum ion selection was determined, the second step of data selection focused on determining the correct normalization technique for the data. The data was normalized by summing the intensities of the m/z to one prior to PCA. Three additional methods of normalizing the data were tested which included: normalizing the m/z ratio summed to one and the sample spectrum summed to one, mean centered, and autoscaled. Mean centering the data involves calculating the average intensity of each m/z and subtracting it from each data point; autoscaling divides the mean centered data by the standard deviation of the intensity of each m/z. Autoscaling is done to prevent domination by a single spectral data line, but results in the loss of the information contained in the relative peak intensity. The normalization methods were used on the

data containing the ions in Table 14. Each normalization method was performed prior to PCA analysis.

Table 14: Ions corresponding to the 50 highest F-values and abundant ions for the two ignitable liquid data sets.

Model One Ions (with MISC and OXY) (50 F-values + abundant ions)		Model Two Ions (without MISC and OXY) (50 F-values + abundant ions)	
31	87	31	87
39	91	39	89
40	92	40	91
41	95	41	92
42	96	42	95
43	97	43	96
44	98	44	97
45	99	45	98
51	103	50	99
53	105	51	103
54	106	53	105
55	109	54	106
56	110	55	110
57	111	56	111
58	112	57	112
63	113	58	113
65	115	63	115
67	117	67	117
68	119	68	119
69	120	69	120
70	123	70	123
71	125	71	126
77	127	77	127
78	128	78	128
79	134	79	134
81	140	81	138
82	141	82	140
83	142	83	141
84		84	142
85		85	

Once the method of determining the retention of significant ions and the normalization method were optimized, substrates were added to the analysis. Each data set was

broken into three models: 1) ignitable liquids and substrates, 2) ASTM classes and substrates, and 3) ASTM classes only. Model 1, consisted of the classification of only ignitable liquid or substrate, while models 2 and 3 consisted of ignitable liquids broken into their ASTM classes.

Once the data was normalized and reduced, classification was performed by LDA and QDA. The LDA and QDA analysis was performed on the scores for the PCA data with the ions listed in Table 14 for each normalization method to create a model for each data set. For each LDA and QDA analysis the number of scores retained corresponded to a specified amount of desired variance.

Once optimal classification of each model was achieved, the models were applied to test samples. The test data consisted of pure ignitable liquids and substrate samples as LDA is a hard classifier and showed poor performance in initial tests of mixtures (ignitable liquid and substrate, or multiple ignitable liquids) samples. LDA and QDA models from both data sets were used in cross validation to classify test samples of pure ignitable liquids and substrates not included in the model.

Model testing was done by steps outlined below and assessed by percentage of correct classifications. Model data was obtained from the ILRC database, while the test data was obtained from large scale and laboratory burns. Data for both the model and test were reduced to the ions defined by the top 50 F-values and abundant ions for the

model. Both were then autoscaled using the averages and standard deviations for the model data. PCA was performed on the model and the desired variance or number of principal components was retained for LDA and QDA analysis. From the PCA data the eigenvectors were used to post-multiply the normalized test data. This provided scores for the test data based on the model PCA. The discriminant functions were evaluated at the projected scores and the sample was assigned to the class having the largest classification function.

5.2 Bone

The bone data was analyzed by data reduction using PCA, LDA and QDA, and nonparametric hypothesis testing. Descriptions of the steps are given in the following sections.

Prior to normalization and PCA data dimension reduction the data was baseline corrected using an in-house software [30, 68]. To perform the baseline correction the peaks and their base are first identified and removed. The baseline is then taken as a local minimum for a defined width and is subtracted from the original spectrum. The process is repeated to give the baseline corrected spectrum. The desired spectral range for analysis was then determined and the bone data was normalized.

The full spectral range was analyzed initially, shown in Figure 16, but the large data sets were either too large for the software or had very long calculation times. To reduce the

size of the data set two approaches were taken: identification of ions corresponding to high F-values and reduction of the spectral ranges. The wavelengths corresponding to high F-values were selected as described in the fire debris section and spectral ranges were tested: 300-500nm and 500-700nm. Of these tested ranges, the results showed the 300-500nm spectral range performed best for the calculations; it was further expanded to 200-500nm which provided results equal to the full spectral range but in a more efficient time frame. Therefore, the ideal spectral range for the analysis of bone sample was determined to be 200-500nm, shown in Figure 17, and was used for the remainder of the data analysis. Two normalization methods were tested: autoscaling the data and setting the maximum equal to one. To set the maximum equal to one, the maximum spectral intensity was found for each sample spectrum and the full spectral data was divided by that value; the method for autoscaling was previously described in the fire debris data analysis section.

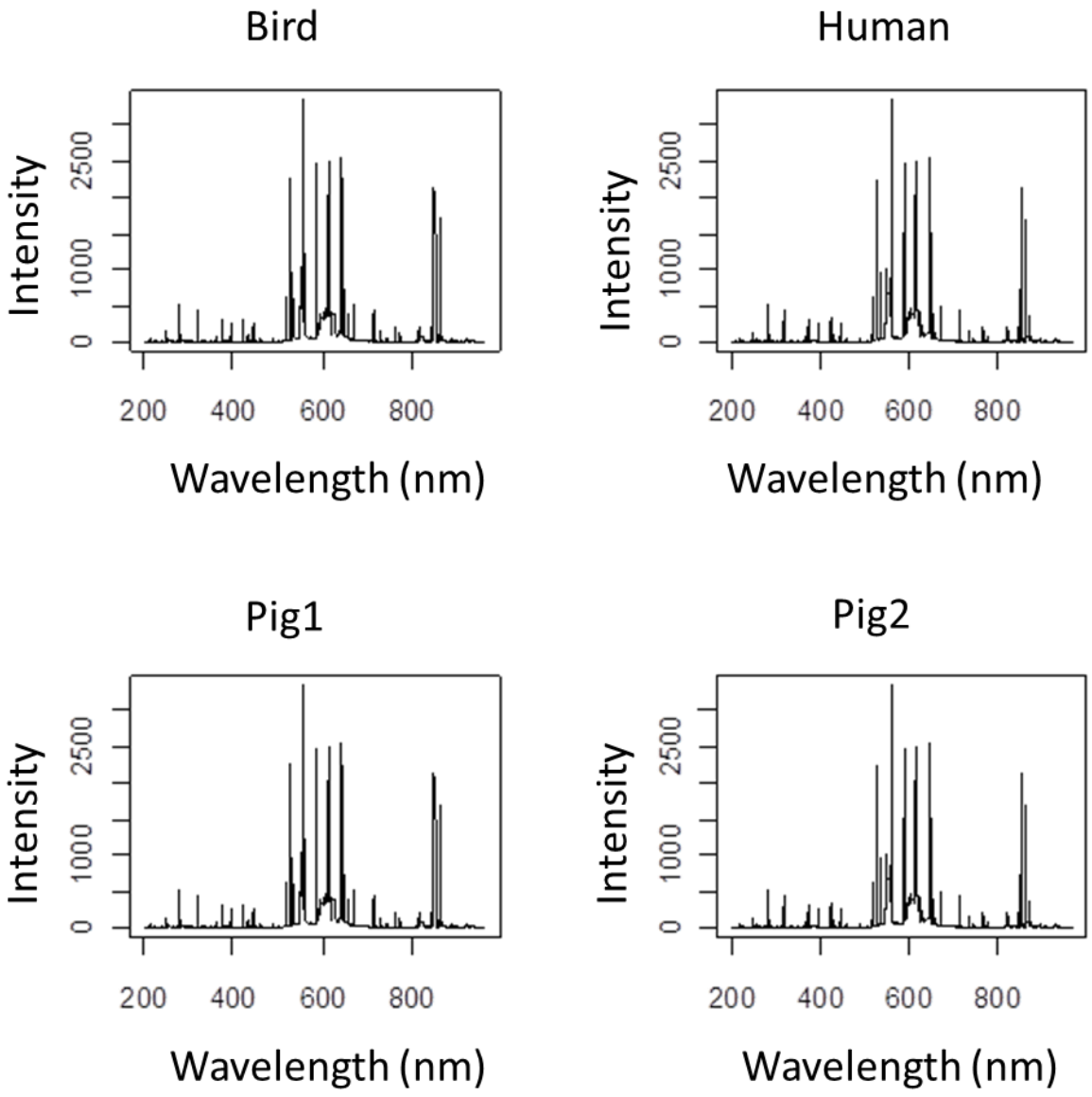

Figure 16: Bone spectra covering the full spectral range (200-900nm) for a bird, human, and two pigs. Spectra are very similar and would be visually very difficult to distinguish between.

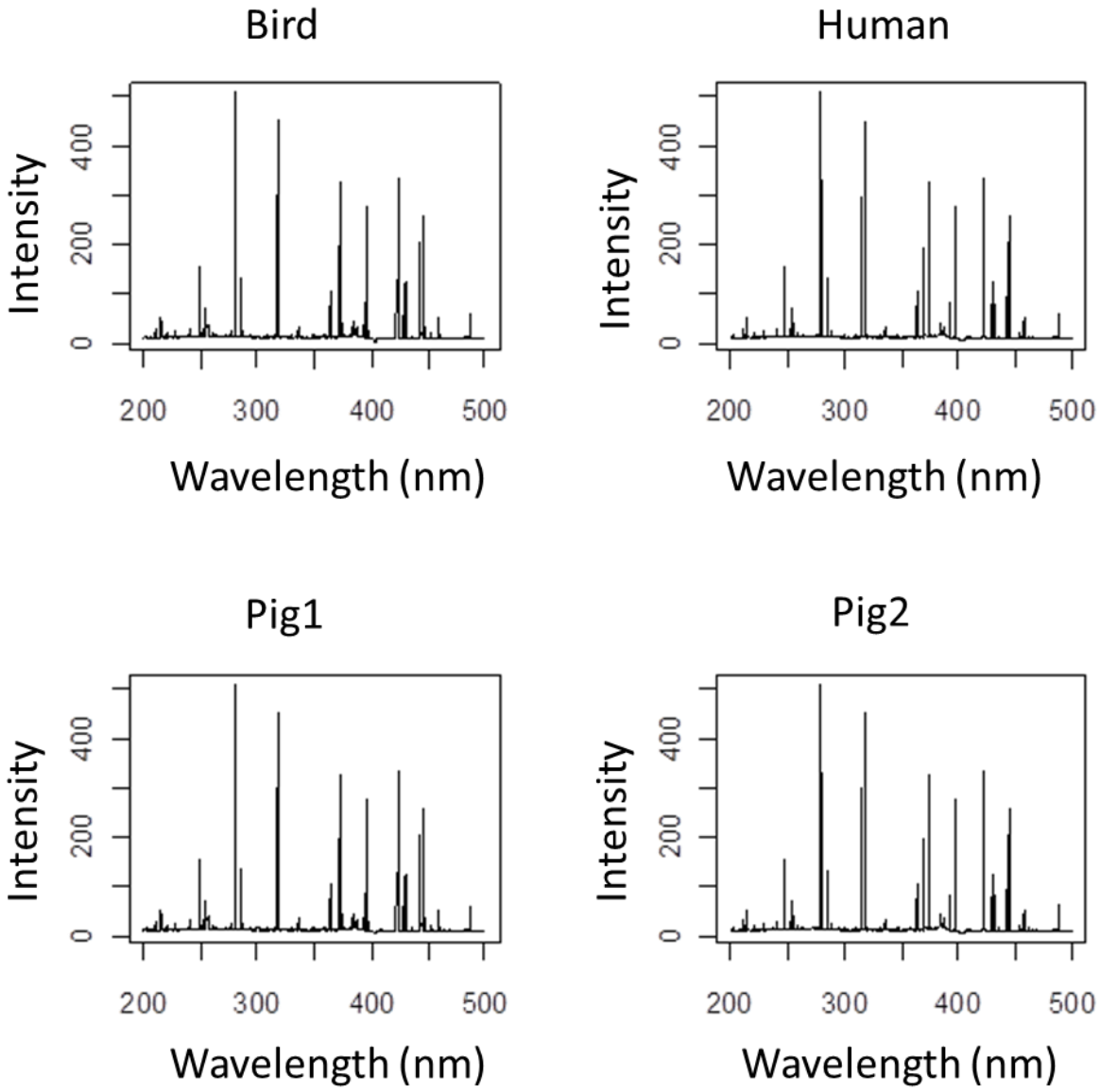

Figure 17: Bone spectra covering the spectral range of 200-500 nm for a bird, human, and two pigs. Again spectra are very similar with slight visual variations.

Once preprocessing was completed on the bone data, PCA was performed to determine the number of principal components to retain for further data analysis. Initial analysis retained between 80-95% of the variance with the number of principal components retained varying depending on the data pretreatment method. In looking at the variance retained in each principal component it was determined that the first principal component contained 95% of the variance. This indicated that the bones were similar in composition for the major components; therefore separation of the bones would be difficult. To provide for more separation between the classes, tests were performed with the removal of the first principal component. The principal components two thru four were retained as they had variance attributed to contributions from the trace components of the bones.

Both LDA and QDA were performed in an attempt to classify the bone spectra into classes by bone and by species. LDA and QDA were performed on data processed by the multiple different processing methods to determine the appropriate combination for analysis. Analysis included baseline corrected and uncorrected data, the two normalization techniques, the multiple spectral ranges, and the variance in number of principal components retained.

In addition to discriminant analysis, the bone data was also analyzed by the nonparametric permutation test. The data was not normalized prior to analysis, but the spectral range was analyzed from 200-900nm and 200-500nm. The spectra were also

baseline corrected using the in-house software discussed previously [30, 68], therefore analysis was performed on the uncorrected and baseline corrected data. For the nonparametric permutation test the original and log intensities were analyzed in addition to the two spectral ranges.

For the nonparametric permutation test analysis software written in house was used to perform the calculations. LIBS experiments were used which had twelve spectra collected per sample; this allowed for 6 spectra to be chosen per comparison out of 12. The significance level was set at $\alpha=0.05$ for all calculations and the Type I and Type II errors were calculated based on the significance level. The percent discrimination was determined based on species and individual bone.

5.3 Organic Compounds and Polymer Mixtures

Organic compounds and polymer mixtures were analyzed with multiple instrumental techniques as discussed previously. This data was also analyzed by multiple multivariate techniques to determine the ideal method for analysis which will be discussed below. These methods included: PCA/TFA, and Bayesian decision theory.

Prior to the spectral collection and data analysis, a few organic compounds in fingerprint oil were examined using a polarized light microscope to ensure transfer of the compound and the oil would occur. Figure 18 a and b show the caffeine, fingerprint, and glass mixture in bright field and crossed polars respectively, while Figure 19 shows the theobromine, fingerprint, and car paint mixture in bright field; all images were collected at 200x magnification. In each of the images the oil from the finger and the organic compound were seen which indicate the method of transfer was successful. Based on these results, spectral data was collected and statistical analysis was performed for the organic compounds in fingerprint oil for the FTIR and Raman experiments.

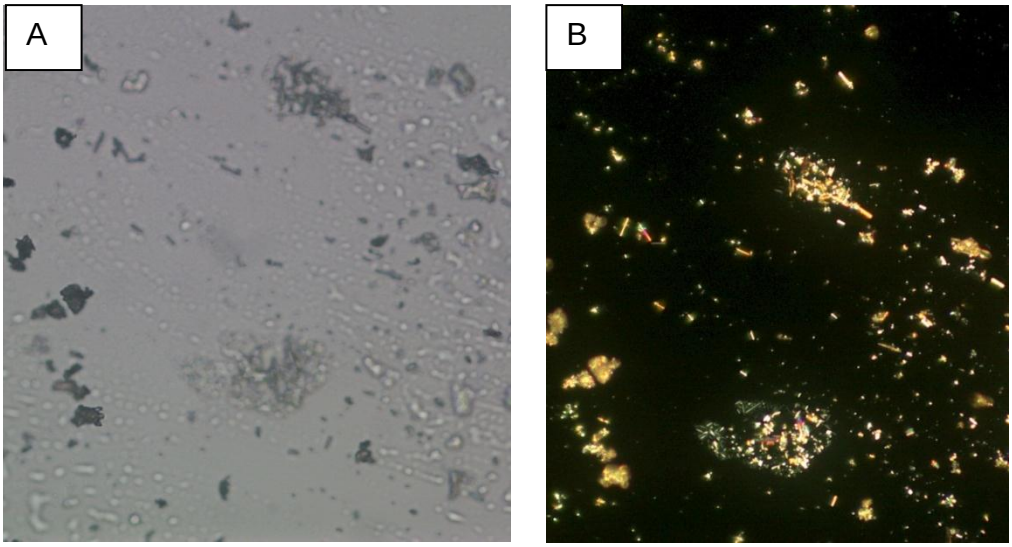

Figure 18: Caffeine, fingerprint, and glass mixture in A) bright field at 200 times magnification and B) crossed polars at 200 times magnification.

Figure 19: Theobromine, fingerprint, and car paint mixture in bright field at 200 times magnification.

5.3.1 LIBS

The PCA/TFA analysis was performed on specific peaks which were selected for the six major emissions for the organic compounds tested: C (247 nm), CN (388 nm), C_2 (516 nm), H (656 nm), N (746 nm) and O (777 nm). The spectra were normalized to one by dividing the intensity of the wavelengths by the sum of the intensity of the spectra. The normalization was performed to offset large variations in spectral intensity which could be caused by variations in laser intensity. The data was again normalized from 0-1 for each emission by finding the minimum and maximum intensity of each emission. Then the intensity minus the minimum value was divided by the maximum minus the minimum. In the spectra collected in argon and air the hydrogen emission line was large and had the potential to dominate the spectra. The CN (388), N (746), and O

(777) became significant contributors in the air data and the C_2 (516 nm) line was a small contributor, which was expected of LIBS in air as the nitrogen in the air could react with the C_2 to from CN emissions. For analysis, data within two standard deviations of the average in the normalized data set was selected.

Three principal components were retained from the PCA of the library for the TFA on the mixture samples. This retained 93% of the variance for the air data set and 95% of the variance for the data set collected under an argon atmosphere. The scores from the first three principal components of the library data sets collected in the argon and the air atmospheres were used in LDA. The LDA was performed on the library samples to determine if separation of library compounds occurred.

DRMAD was used to determine the number of principal components to retain for the PCA\TFA and Bayesian decision theory. The two criteria for calculation of the posterior probabilities were set; with the significance level set at 0.05 and lower correlation cutoffs of 0.8 and 0.9 tested.

5.3.2 FTIR

The FTIR library and mixture spectra for the organic compounds were compiled and the spectral range of 650-2000 cm^{-1} was set equal to zero intensity at the minimum

absorbance value. Once the spectra were zeroed, the spectra were normalized by dividing by the sum of the spectra, which gave spectra summed to one.

Library spectra for the 650-2000 cm^{-1} spectral region are shown in Figure 20. The 1,5-dimethylnaphthalene (1,5-DMN) and benzophenone (BP) compounds both showed characteristics peaks for C-H aromatic ring bends around 800 cm^{-1}. Benzphenone also showed peaks at 1500 cm^{-1} and 1700 cm^{-1} for C=C aromatic stretches and C=O ketone stretches respectively. The dinitrotoluene compounds all had peaks around 800 cm^{-1} for the C-H aromatic ring bends and peaks around 1300 cm^{-1} and 1500 cm^{-1} for the nitro group stretches. The final group of compounds, the fused ring compounds, caffeine (Caf), theobromine (TB) and theophylline (TP) all contained peaks around 1200 cm^{-1} for the C-N amide stretches, 1400 cm^{-1} for the C-H alkane bends, and 1700 cm^{-1} for the C=O stretches. The final two spectra shown are for the backgrounds of glass and paint, which differ significantly from the organic compound spectra. While the major peaks for each of the groups of the library compounds are similar, there are differences between the overall spectra.

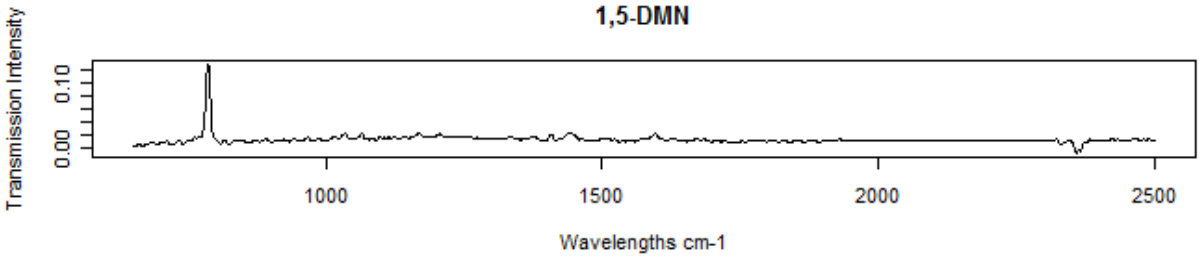
1,5-DMN
Transmission Intensity
0.00
0.10
1000
1500
2000
2500
Wavelengths cm-1

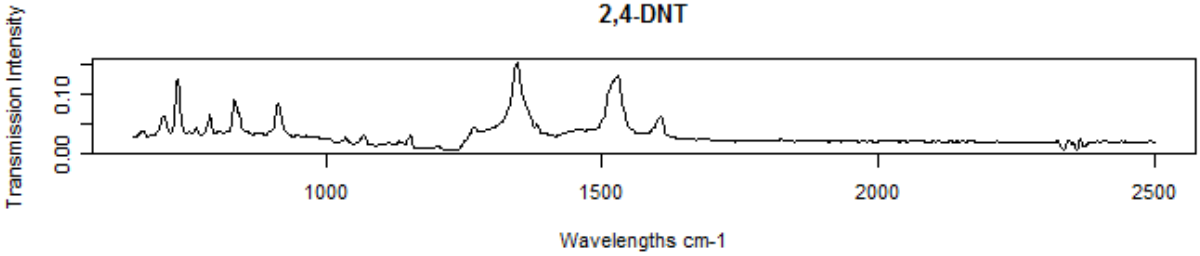
2,4-DNT
Transmission Intensity
0.00
0.10
1000
1500
2000
2500
Wavelengths cm-1

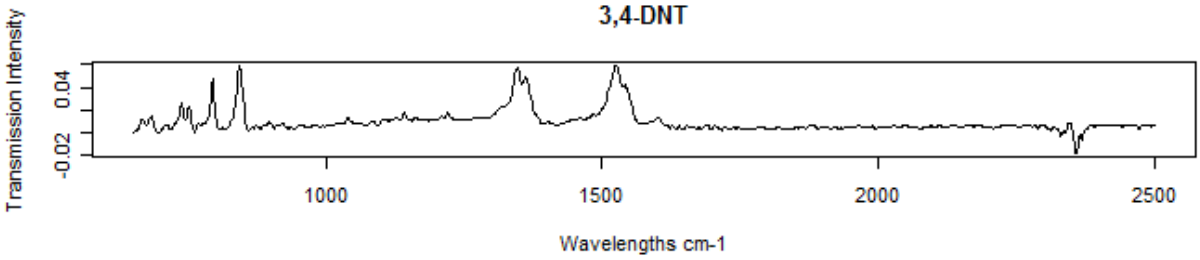
3,4-DNT
Transmission Intensity
-0.02
0.04
1000
1500
2000
2500
Wavelengths cm-1

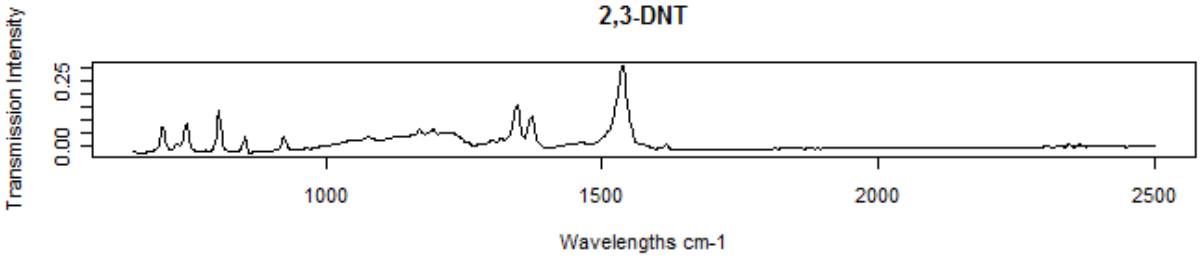
2,3-DNT
Transmission Intensity
0.00
0.25
1000
1500
2000
2500
Wavelengths cm-1

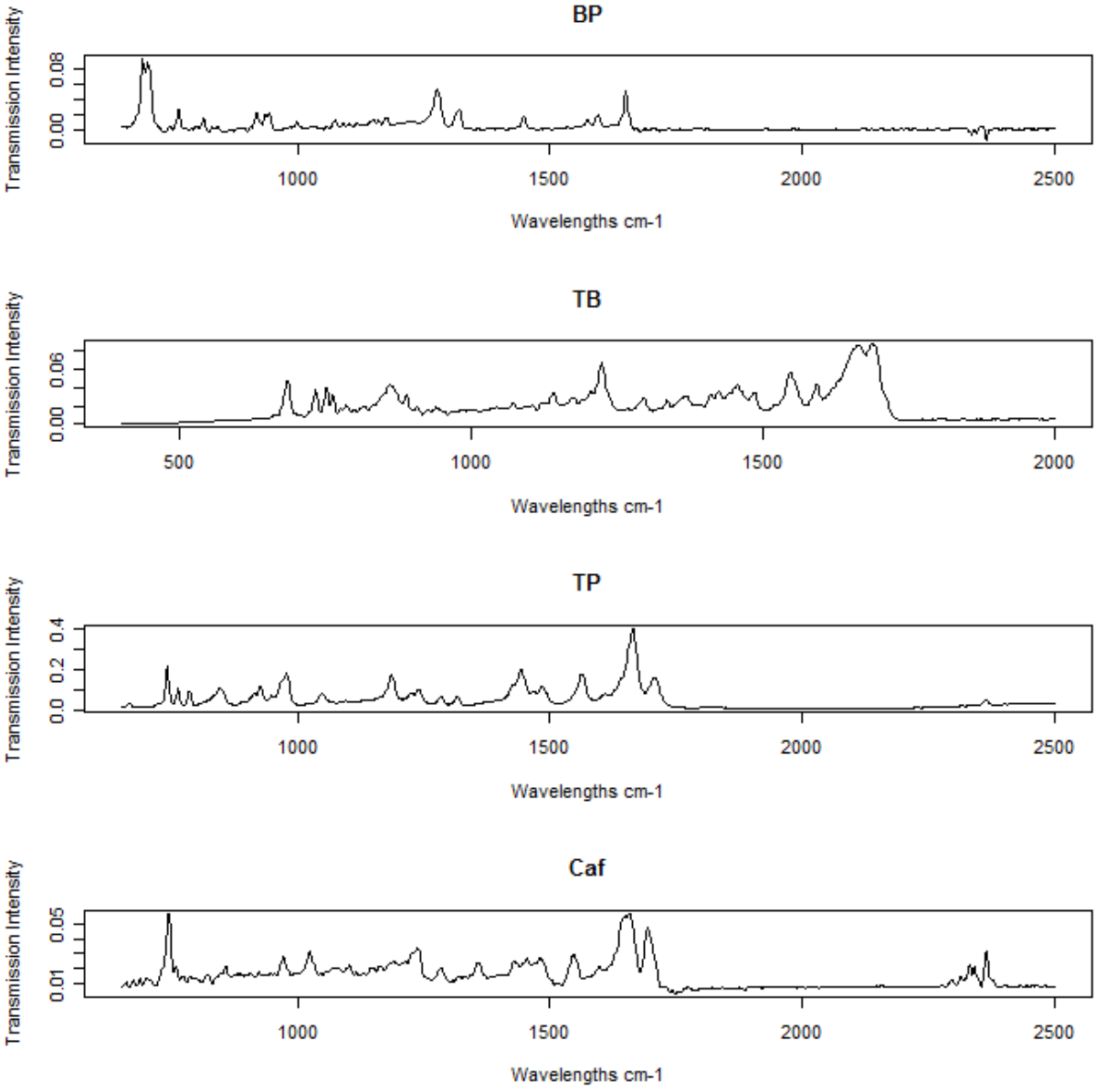
BP
Transmission Intensity
0.00
0.08
1000
1500
2000
2500
Wavelengths cm-1
TB
Transmission Intensity
0.00
0.06
500
1000
1500
2000
Wavelengths cm-1
TP
Transmission Intensity
0.0
0.2
0.4
1000
1500
2000
2500
Wavelengths cm-1
Caf
Transmission Intensity
0.01
0.05
1000
1500
2000
2500
Wavelengths cm-1

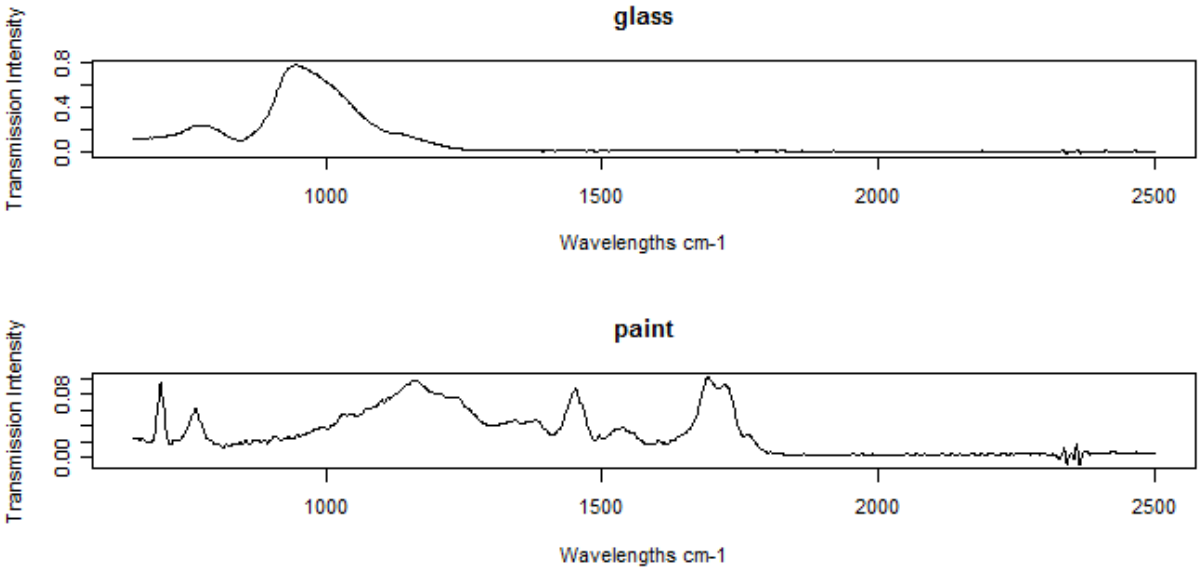

Figure 20: FTIR library spectra.

Examples of the mixture spectra collected are shown in Figure 21. In each spectrum there is varying amounts of spectral contribution from the components within the mixtures.

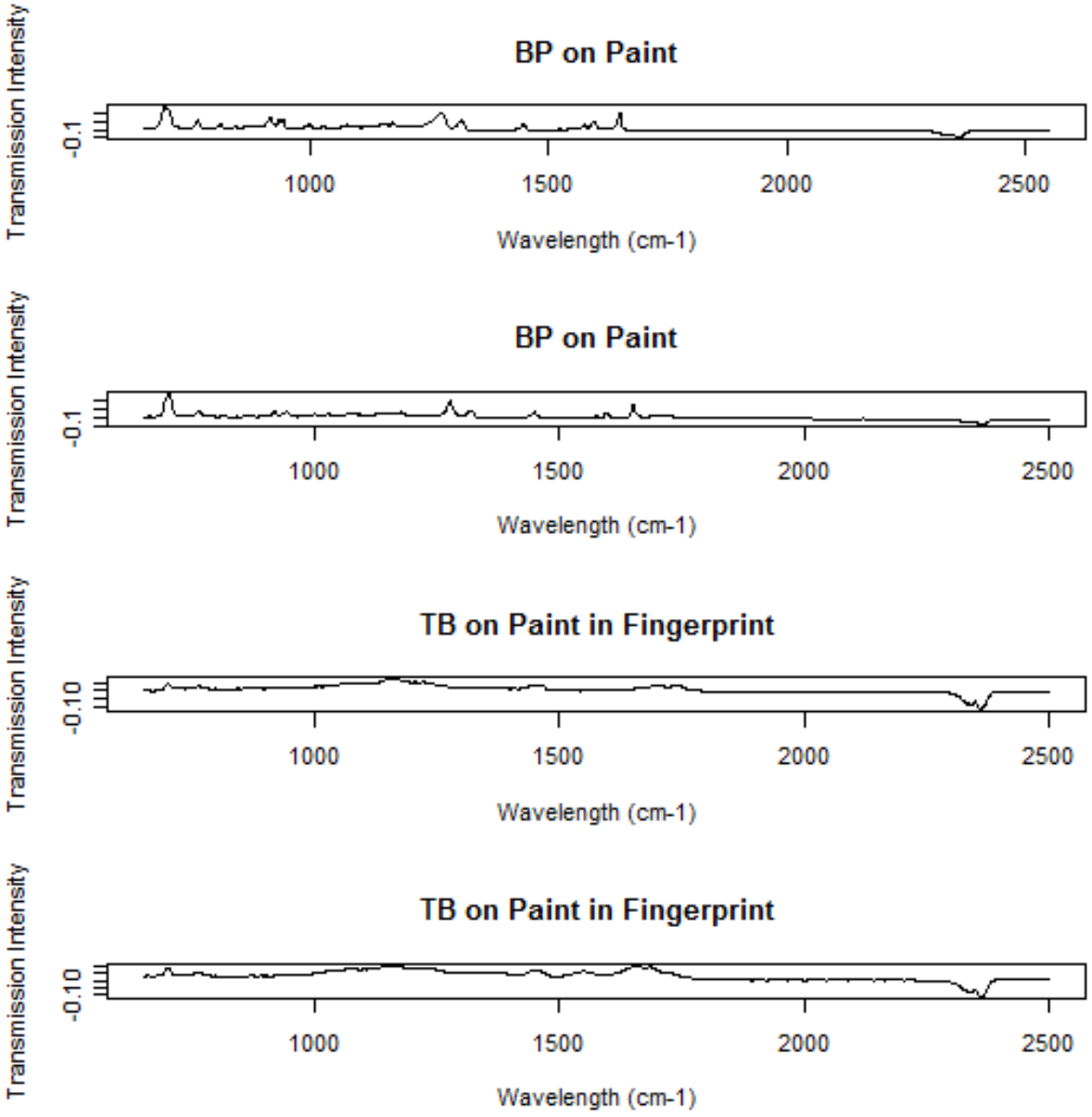
BP on Paint
Transmission Intensity
-0.1
1000
1500
2000
2500
Wavelength (cm-1)
BP on Paint
Transmission Intensity
-0.1
1000
1500
2000
2500
Wavelength (cm-1)
TB on Paint in Fingerprint
Transmission Intensity
-0.10
1000
1500
2000
2500
Wavelength (cm-1)
TB on Paint in Fingerprint
Transmission Intensity
-0.10
1000
1500
2000
2500
Wavelength (cm-1)

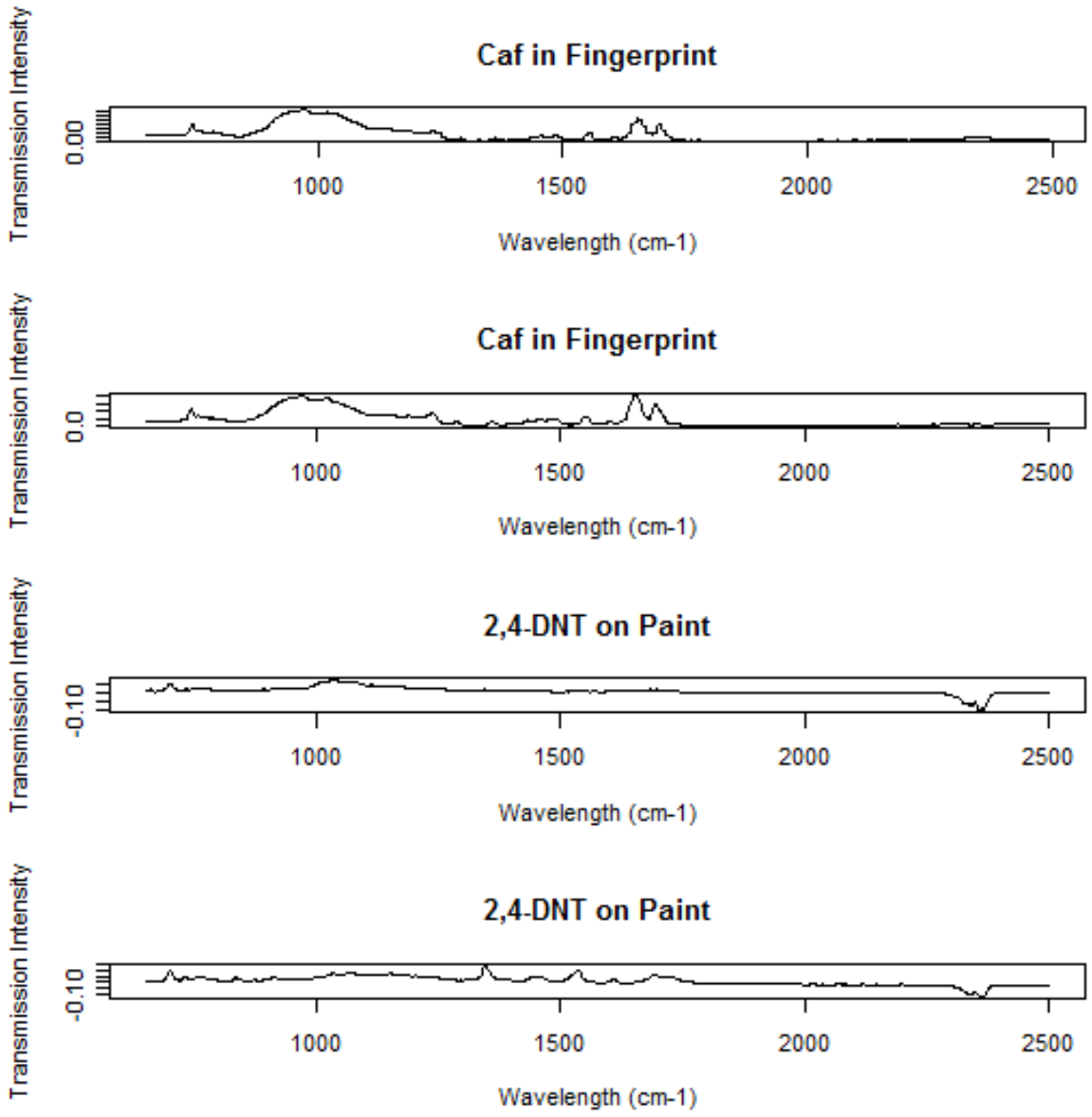

Figure 21: Spectra of FTIR mixture samples.

PCA was used to reduce the data dimensionality to the principal components which contained 95% of the variance. The scores corresponding to the principal components retained were used to perform LDA.

The Bayesian decision theory was performed on the normalized data from 650-2000 cm^{-1}. The significance level was set at 0.05 and the lower correlation cutoff was set at 0.8.

5.3.3 Raman

The spectra for the library and the mixtures were baseline corrected after collection using the software written in-house discussed in section 5.2 [30, 68]. The baseline correction was done to subtract fluorescence out of the spectra, which was seen in a few of the compound spectra. Prior to normalization the spectral lines before 200 cm^{-1} were removed because they contained only the laser line. The data was normalized by summing to 1, where the individual data points were divided by the sum of the spectra, for the spectral region 200-4500 cm^{-1}. The baseline corrected library spectra are shown in Figure 22. Fluorescence was prevalent in the three dinitrotoluene compounds, caffeine, β-hydroxyethyl theophylline, theobromine, 1,5-dimethylnaphthalene and 1,7-dimethylxanthine spectra prior to the baseline correction. Ammonium nitrate and ammonium perchlorate also showed a small contribution from fluorescence.

For each of the chlorate and perchlorate samples (sodium chlorate, potassium perchlorate, potassium chlorate, sodium perchlorate, ammonium perchlorate) the spectra were simple with all the compounds having a peak present around 990 cm^{-1} for

the Cl-O stretch [244]. Ammonium perchlorate shows an additional peak for the amine group around 3300 cm^{-1} [111]. The nitrate compounds (sodium nitrate, potassium nitrate, and ammonium nitrate) also had simple spectra with a single peak between 1000 and 1300 for the N-O stretch [245].

Two of the dinitrotoluene compounds, 2,4-dinitrotoluene (2,4-DNT)and 2,3-dinitrotoluene (2,3-DNT), had very similar spectra while the third, 3,4-dinitrotoluene (3,4-DNT), had no apparent peaks. The two compounds with characteristics peaks had weak spectra due to the strong fluorescence contributions, but showed peaks for the nitro groups around 1300 cm^{-1} and 1500 cm^{-1}. In addition they had very weak peaks for the aromatic C-H stretches at 3010 cm^{-1}. The 3,4-DNT spectra was dominated with fluorescence prior to baseline correction and resulted in a very weak peak in the 1300 cm^{-1} region which could be associated with the nitro group. TATP had a spectrum with a low intensity peak around 2970 cm^{-1}, the C-H stretch for the methyl groups.

The 1,5-DMN and benzophenone spectra both contained aromatic peaks for: aromatic C-H out-of-plane bends between 600-900 cm^{-1}, aromatic C-H stretches around 3010 cm^{-1}, and alkene C=C stretches between 1500-1600 cm^{-1}. The 1,5-DMN had an additional peak near 1350 cm^{-1} for the C-H alkane stretch for the methyl groups, while benzophenone had a peak around 1700 cm^{-1} for the C=O ketone stretch.

The most complex spectra seen were for the fused ring compounds (theobromine, caffeine, 1,7-dimethylxanthine, and β-hydroxyethyl theophylline). These four compounds all had peaks in the 1300 cm^{-1} region for the C-N amide stretches and 3300 cm^{-1} region for the N-H amide stretches. Peaks for the C-H alkane stretches were also seen around 2970 cm^{-1} and 1700 cm^{-1} for the C=O stretches. B-hydroxyethyl theophylline also had a peak around 1200 cm^{-1} for the C-O stretch.

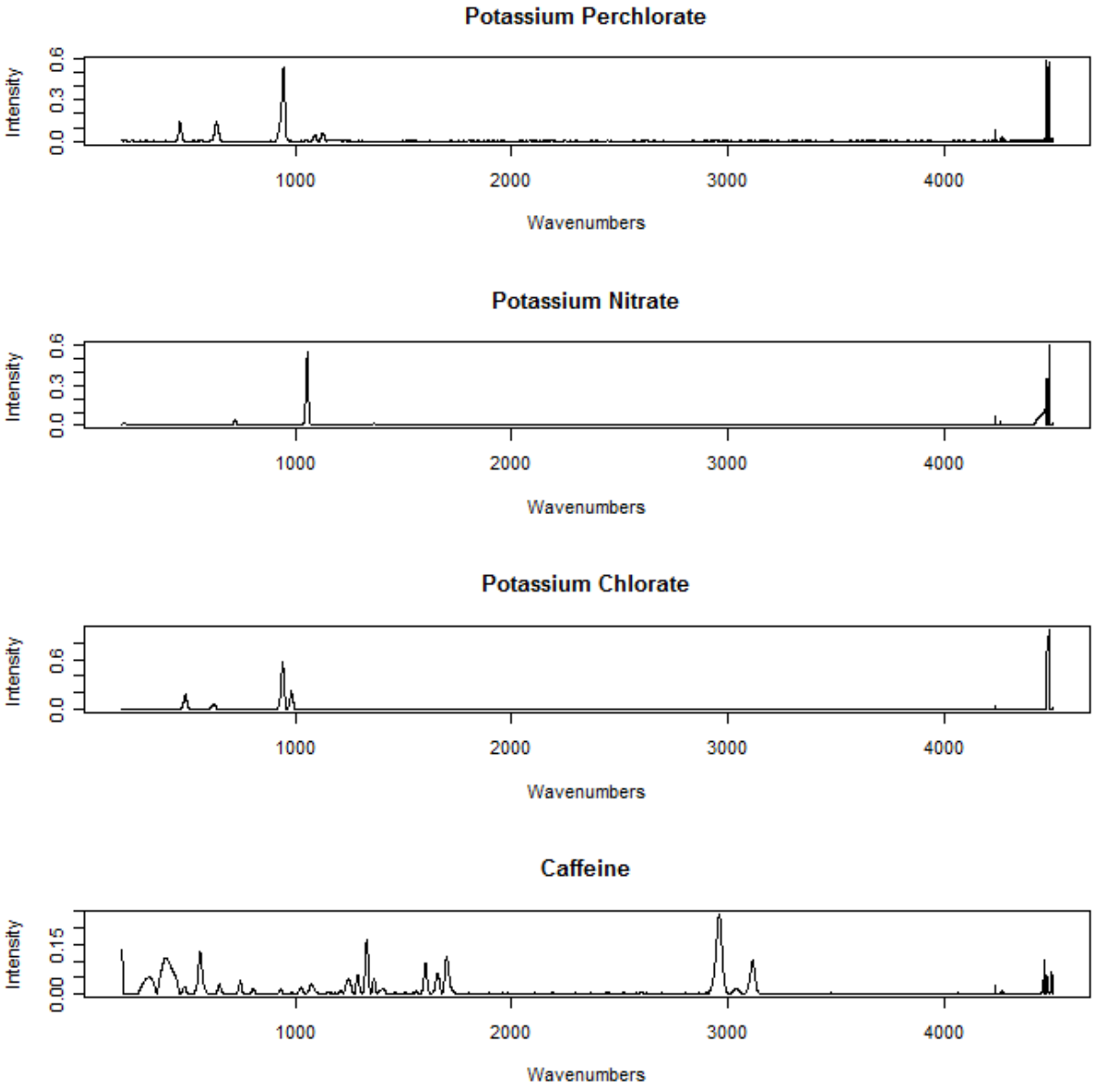
Potassium Perchlorate
Intensity
0.0
0.3
0.6
1000
2000
3000
4000
Wavenumbers
Potassium Nitrate
Intensity
0.0
0.3
0.6
1000
2000
3000
4000
Wavenumbers
Potassium Chlorate
Intensity
0.0
0.6
1000
2000
3000
4000
Wavenumbers
Caffeine
Intensity
0.00
0.15
1000
2000
3000
4000
Wavenumbers

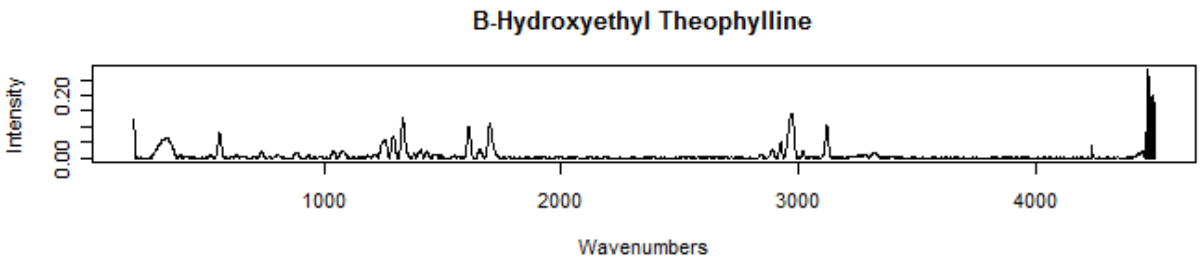
B-Hydroxyethyl Theophylline
Intensity
0.00
0.20
1000
2000
3000
4000
Wavenumbers

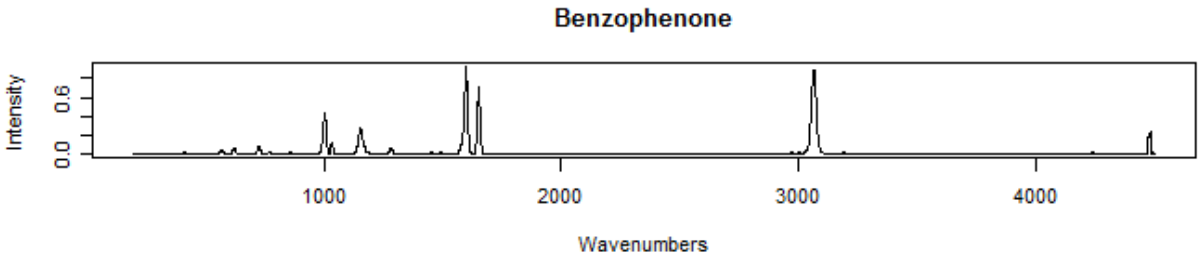
Benzophenone
Intensity
0.0
0.6
1000
2000
3000
4000
Wavenumbers

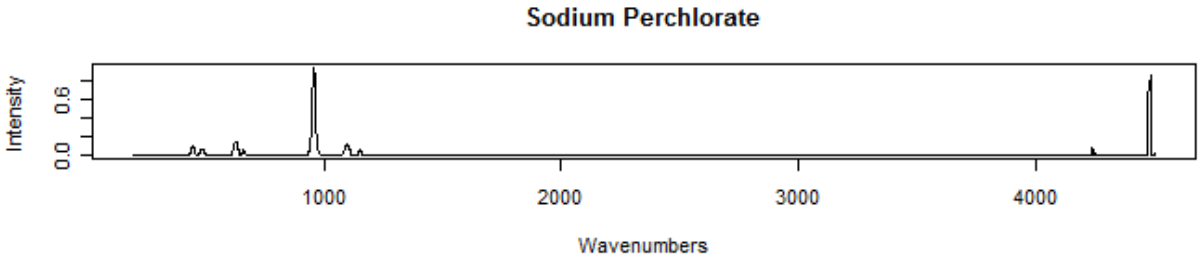
Sodium Perchlorate
Intensity
0.0
0.6
1000
2000
3000
4000
Wavenumbers

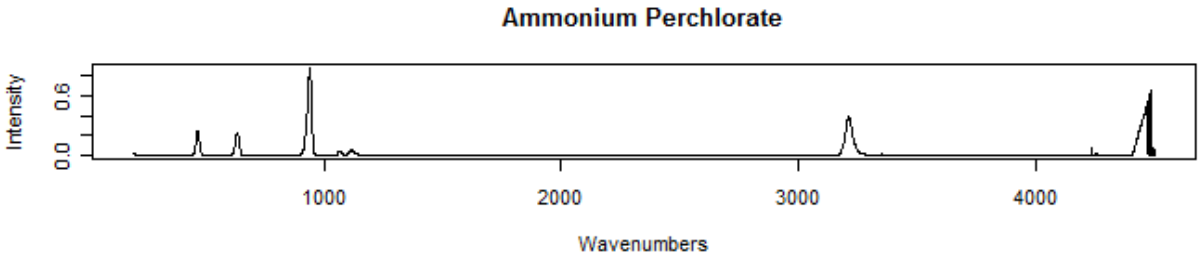
Ammonium Perchlorate
Intensity
0.0
0.6
1000
2000
3000
4000
Wavenumbers

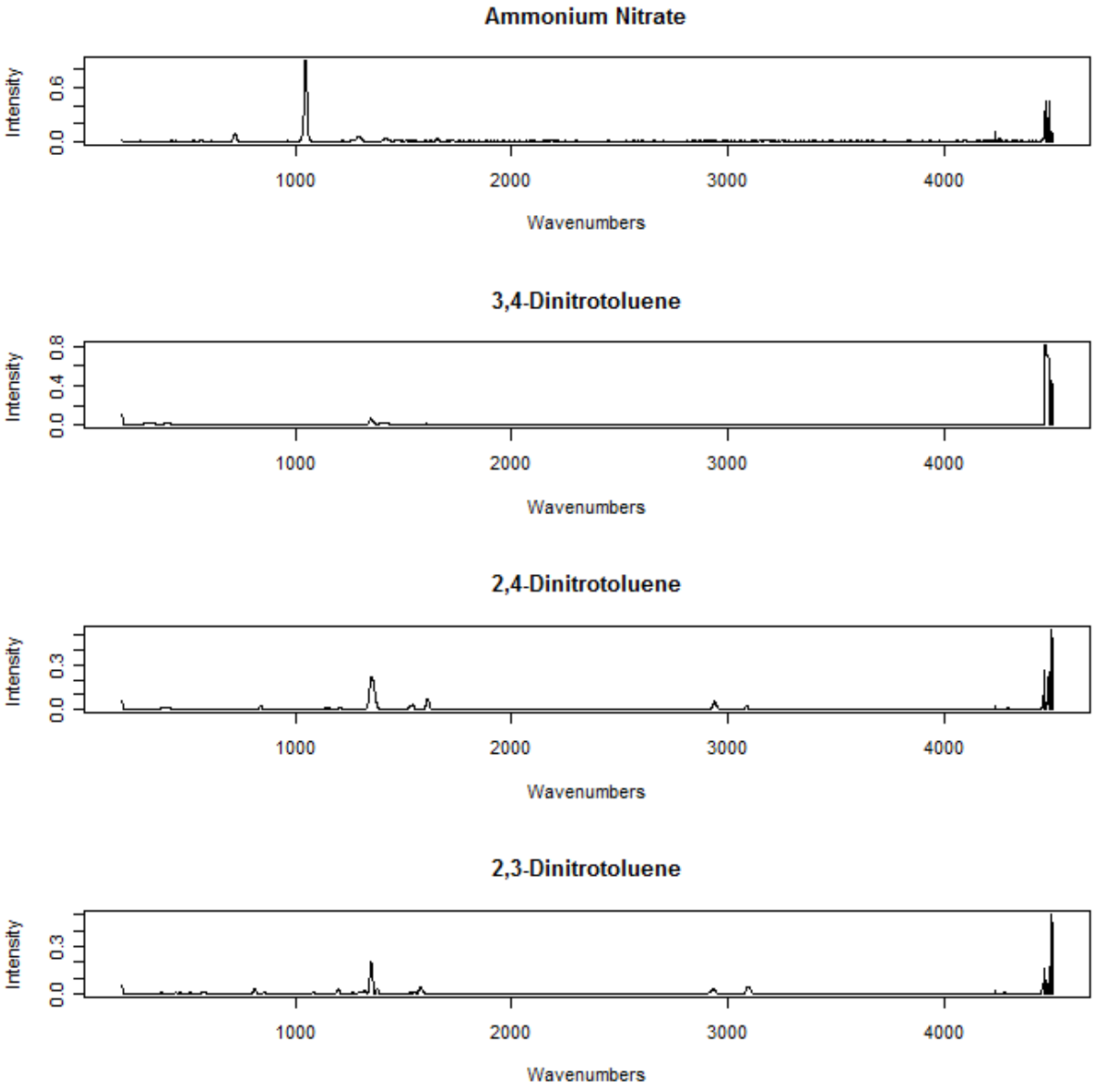
Ammonium Nitrate
Intensity
0.0
0.6
1000
2000
3000
4000
Wavenumbers
3,4-Dinitrotoluene
Intensity
0.0
0.4
0.8
1000
2000
3000
4000
Wavenumbers
2,4-Dinitrotoluene
Intensity
0.0
0.3
1000
2000
3000
4000
Wavenumbers
2,3-Dinitrotoluene
Intensity
0.0
0.3
1000
2000
3000
4000
Wavenumbers

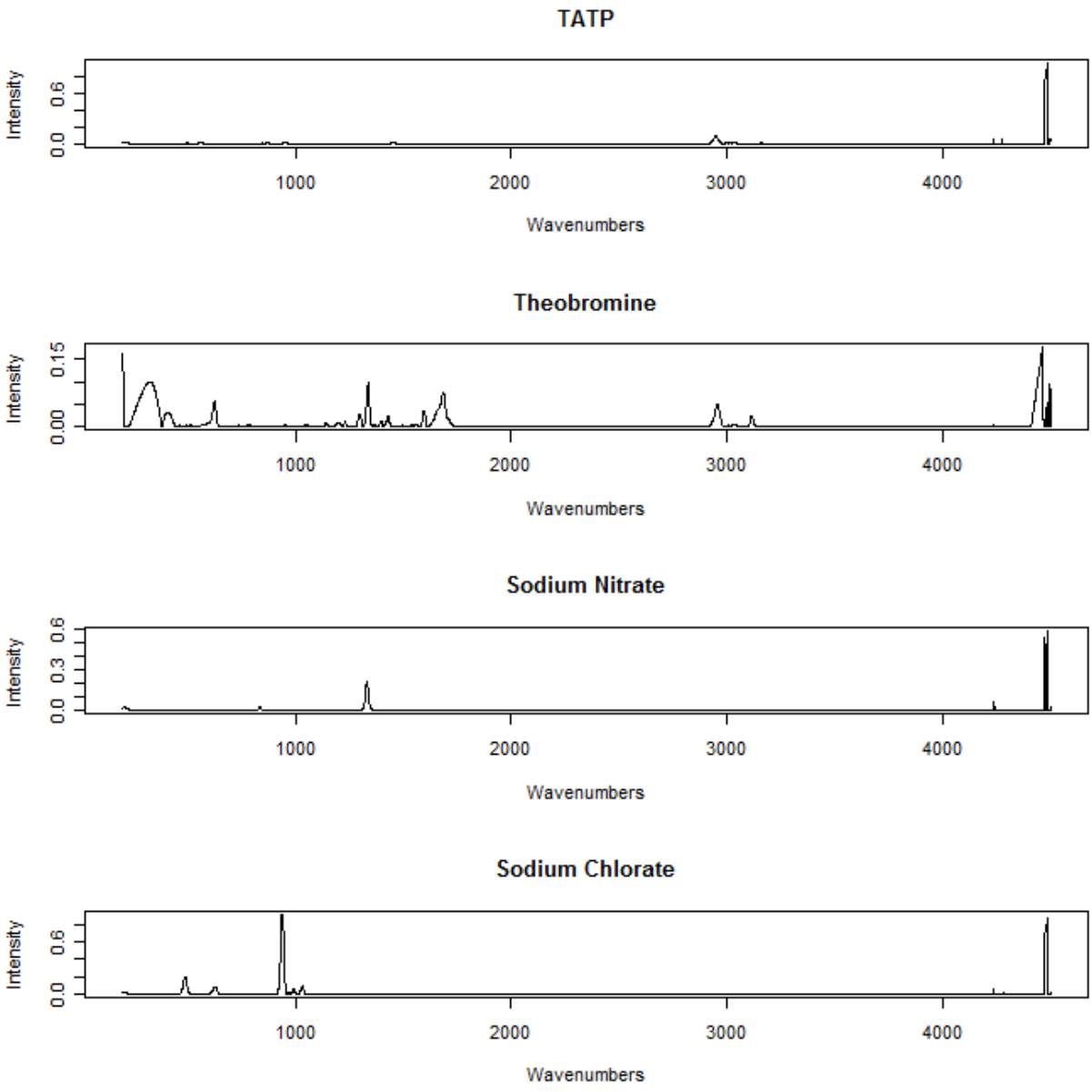
TATP
Intensity
0.0
0.6
1000
2000
3000
4000
Wavenumbers
Theobromine
Intensity
0.00
0.15
1000
2000
3000
4000
Wavenumbers
Sodium Nitrate
Intensity
0.0
0.3
0.6
1000
2000
3000
4000
Wavenumbers
Sodium Chlorate
Intensity
0.0
0.6
1000
2000
3000
4000
Wavenumbers

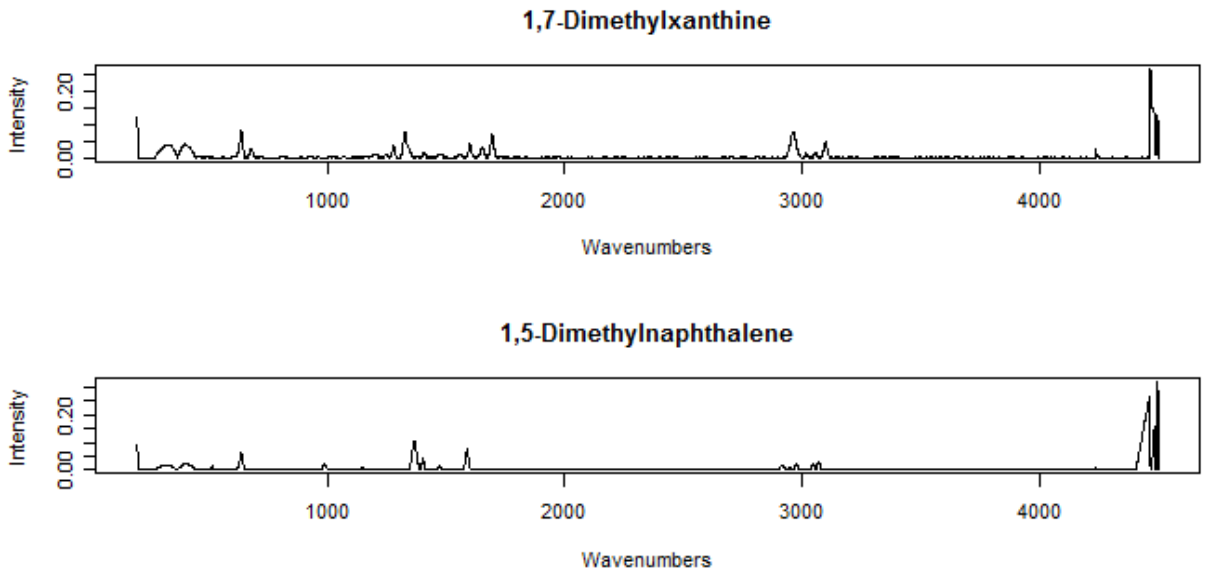

Figure 22: Background corrected Raman spectra for the library compounds in the spectra range 200-4500cm^{-1}.

The mixture spectra were also baseline corrected for the 200-4500 cm^{-1} spectral region. The spectra are shown in Figure 23. As can be seen, the spectra are of much lower intensity but still contain spectral characteristics of the compounds present in the mixture.

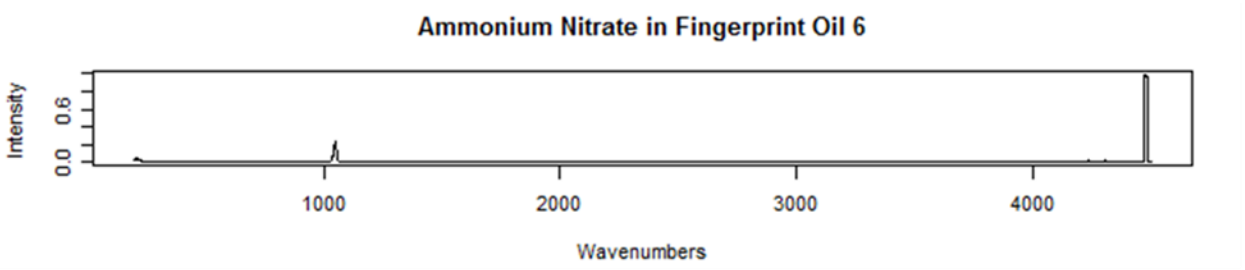
Ammonium Nitrate in Fingerprint Oil 6
Intensity
0.0
0.6
1000
2000
3000
4000
Wavenumbers

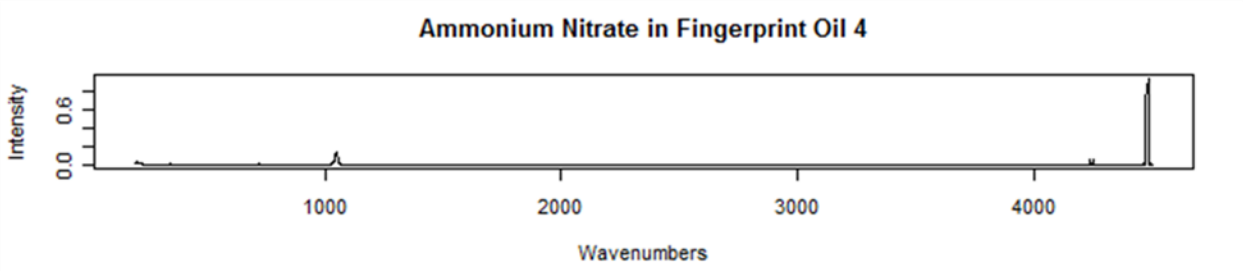
Ammonium Nitrate in Fingerprint Oil 4
Intensity
0.0
0.6
1000
2000
3000
4000
Wavenumbers

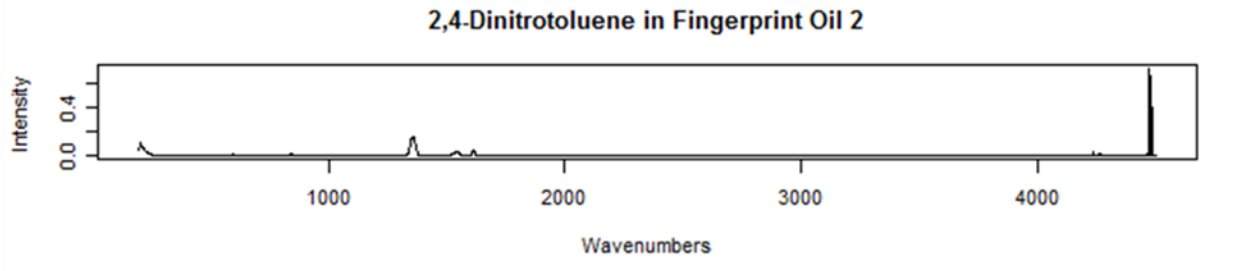
2,4-Dinitrotoluene in Fingerprint Oil 2
Intensity
0.0
0.4
1000
2000
3000
4000
Wavenumbers

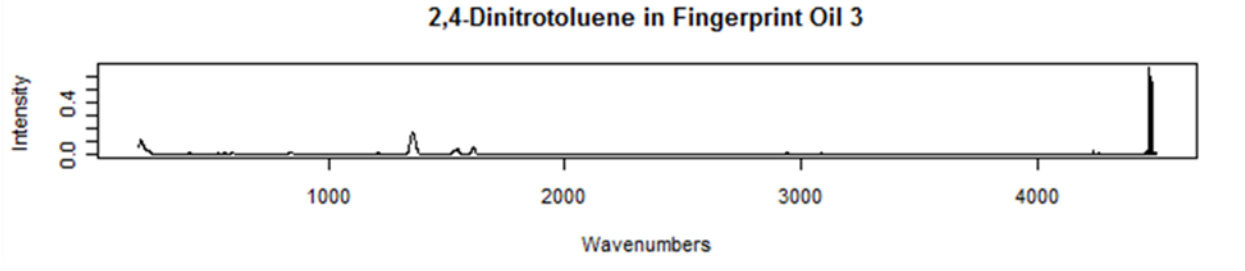
2,4-Dinitrotoluene in Fingerprint Oil 3
Intensity
0.0
0.4
1000
2000
3000
4000
Wavenumbers

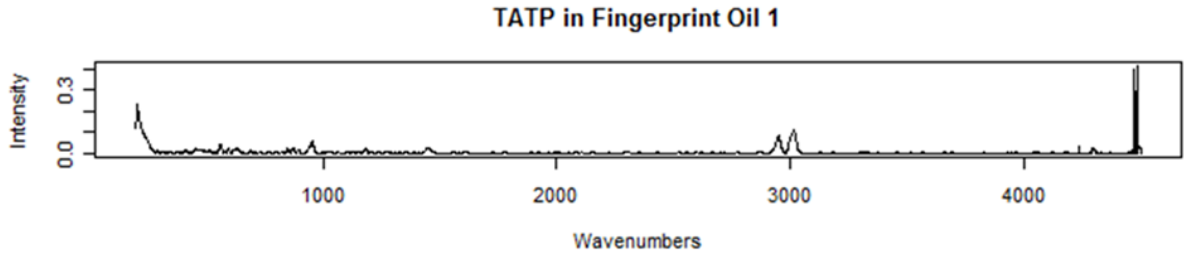
TATP in Fingerprint Oil 1
Intensity
0.0
0.3
1000
2000
3000
4000
Wavenumbers

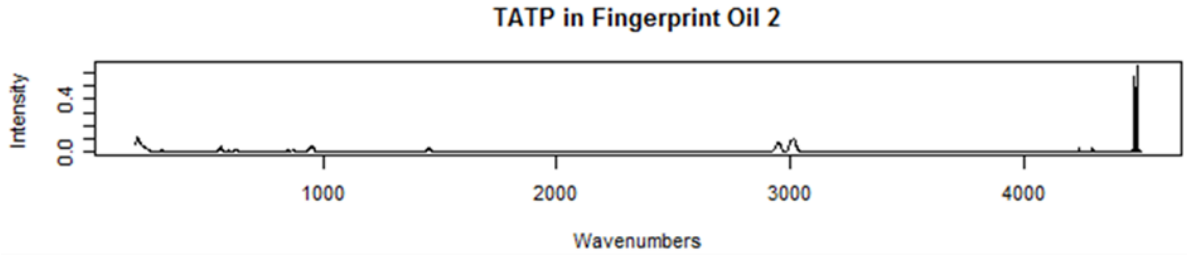
TATP in Fingerprint Oil 2
Intensity
0.0
0.4
1000
2000
3000
4000
Wavenumbers

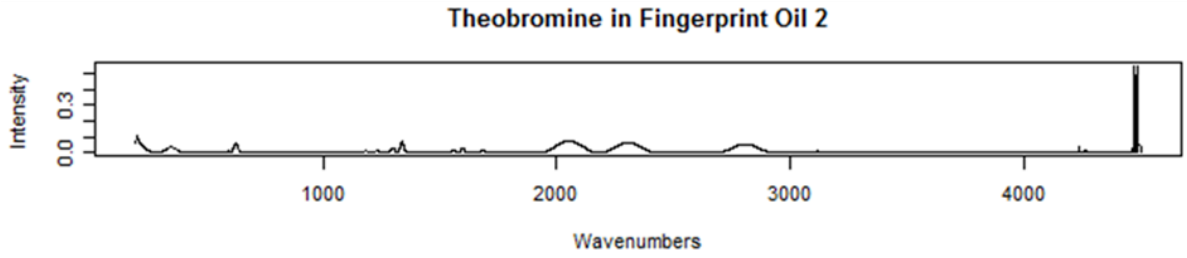
Theobromine in Fingerprint Oil 2
Intensity
0.0
0.3
1000
2000
3000
4000
Wavenumbers

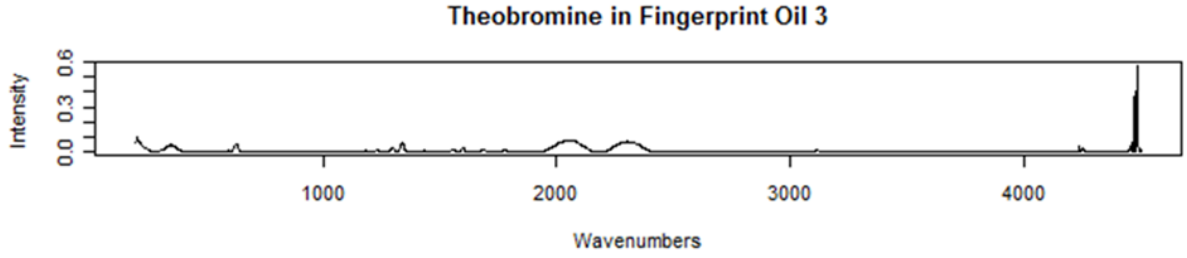
Theobromine in Fingerprint Oil 3
Intensity
0.0
0.3
0.6
1000
2000
3000
4000
Wavenumbers

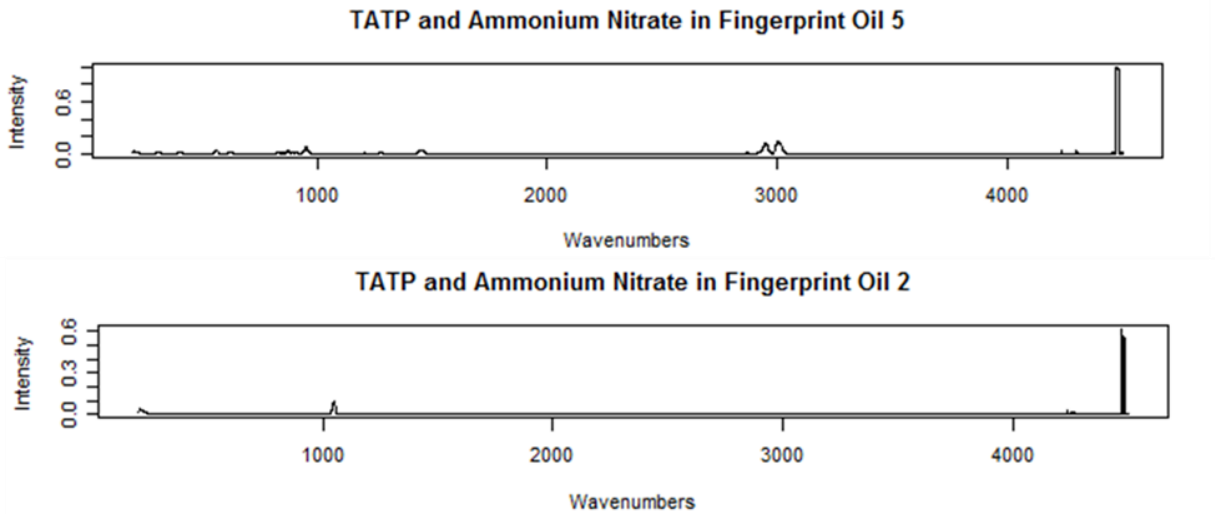

Figure 23: Raman mixture spectra, background corrected in the spectral range of 200-45000 cm^{-1}

PCA\TFA, LDA, and Bayesian decision theory were performed with retention of principal components required for 95% of the variance to be retained. The Bayesian decision theory was performed with a lower correlation cutoff of no less than 0.8 and a significance level of 0.05.

5.4 Metal Transfers

The LIBS spectra of the metal transfer data was condensed to a spectral range of 200 to 500 nm for PCA/TFA. This reduction still maintained characteristic spectral information but reduced the number of points from 13696 to 5626, therefore reducing

the data analysis time. Each transfer experiment (library, bullet holes, individual and mixture transfer on steel plate, and individual and mixture transfer on porcelain tile) data was normalized by summing the intensity of the emissions of each spectrum to one. Figure 24 illustrate examples of each spectra contained in the library for each bullet.

PCA/TFA and Bayesian decision theory analysis were performed by retaining the number of principal components defined by the DRMAD. The data was analyzed with a lower correlation cutoff of 0.8 and 0.9. The significance level was set at 0 and 0.05, with 0 classifying only the samples falling at the lower correlation cutoff.

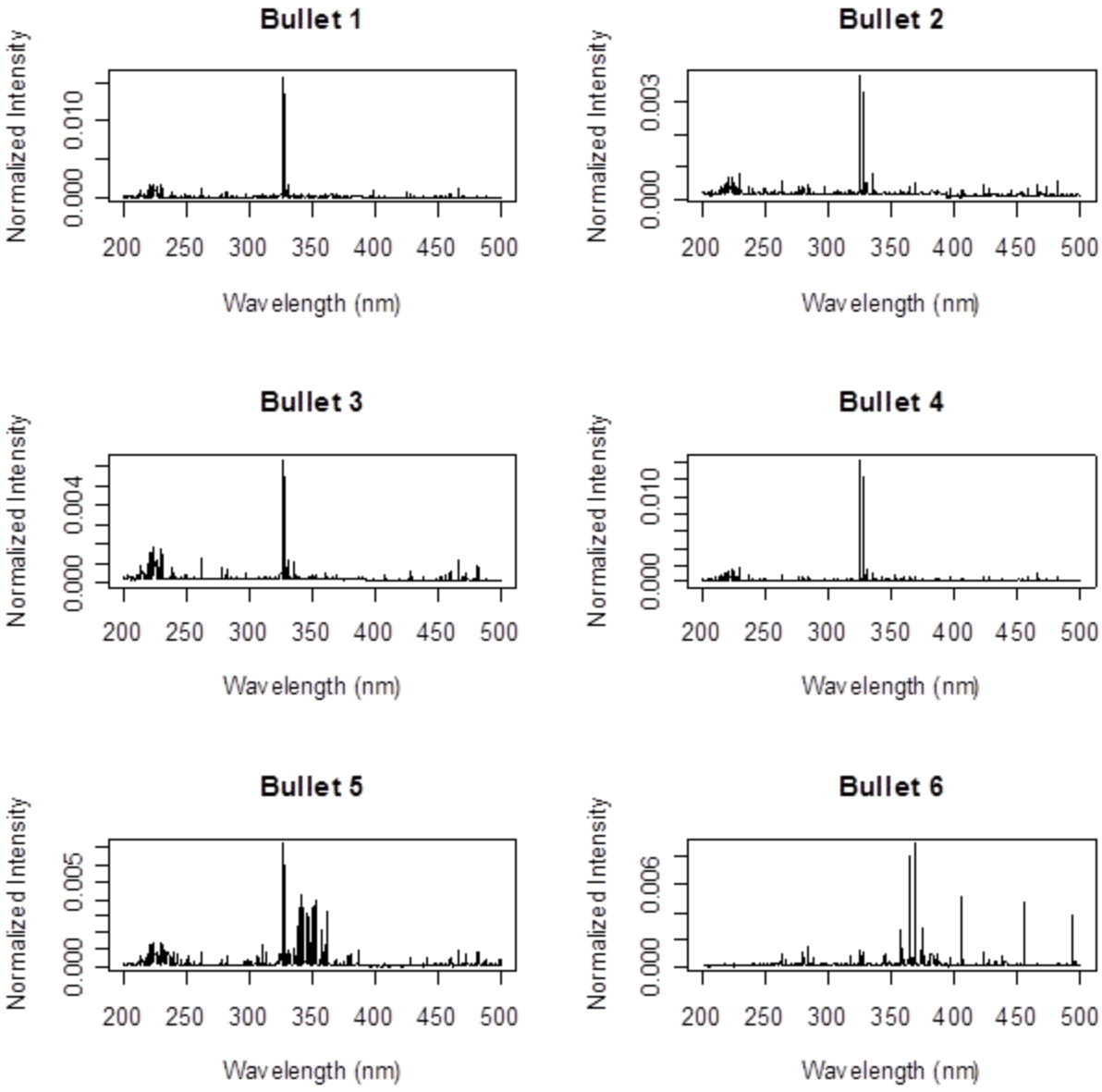

Figure 24: Examples of normalized spectra for each bullet in the metal transfer library.

5.5 Automobile Paint

Based on the parameters described in the experimental chapter, LIBS spectra of paint samples were collected. Spectrum from each dataset illustrated noticeable differences in spectral patterns observed for the different colors, effect pigments, and layers. Examples of spectra collected for each class can be seen in Figure 25. The white paint spectrum contained a significant underlying broad emission. These emissions were present in each white paint spectrum and were present even after the sharp atomic and molecular emissions disappeared. The underlying emissions are attributed to metal components within the white paint.

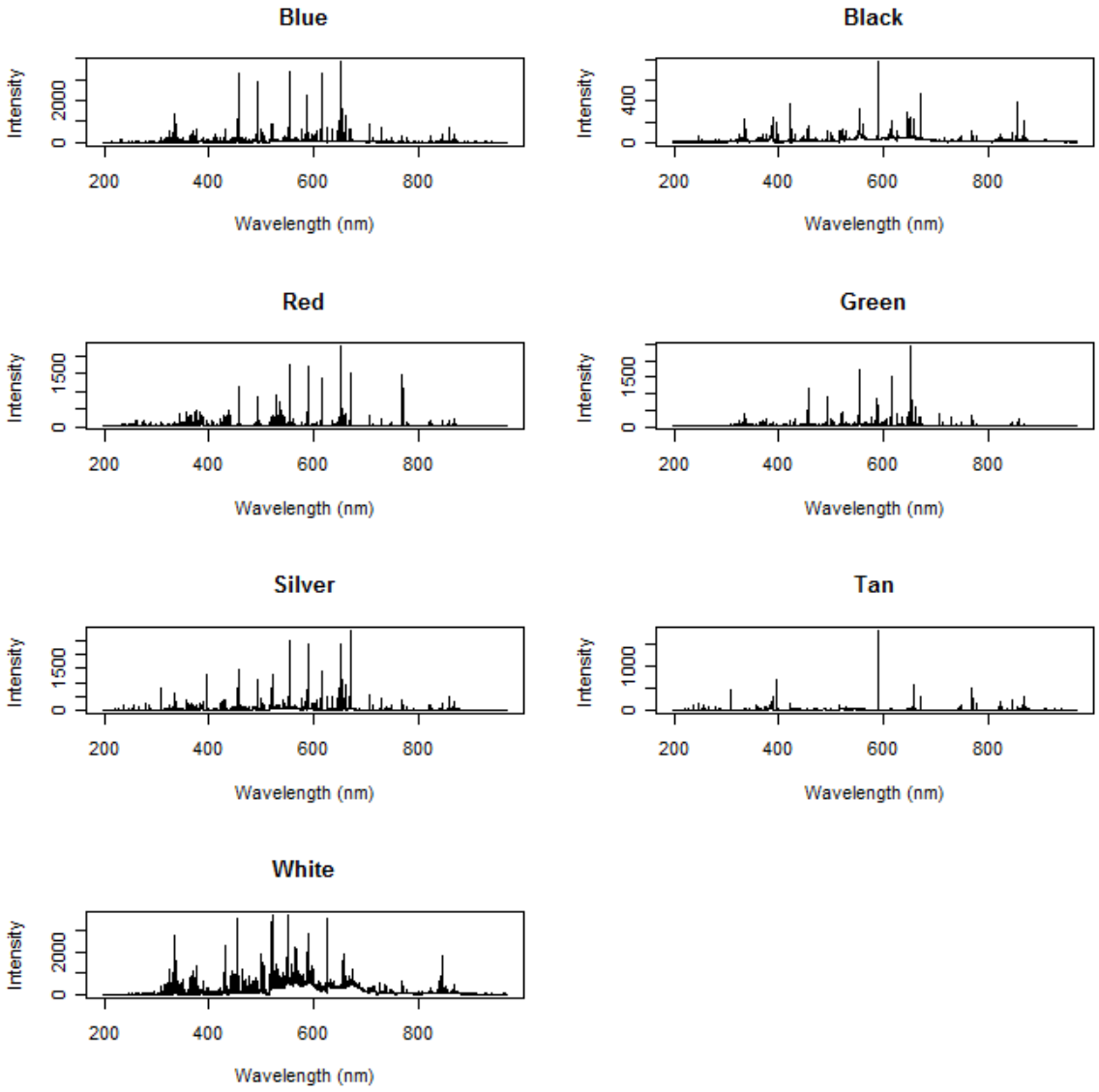

Figure 25: Spectra for datasets of each color containing three layers and effect pigments (except for black and white paint spectra which do not contain effect pigments). Spectra correspond to the following make, model and year: blue- 2002 Honda Accord, black – 1998 Nissan Altima, red- 1995 Chevrolet S-10, green- 2001 Honda Accord, silver- 2004 Chevrolet Cavalier, tan- 2000 Saturn SC2, white- 2000 Chrysler Voyager.

The LIBS spectra of the paint samples were collected for the full spectral range, with no preprocessing of the data. Data files were compiled with odd numbered spectra grouped into one file and even numbered spectra grouped into the second file for each sample. This grouping was performed to prevent results from being effected by potential spectrometer drift by spacing the comparisons over the full collection period. Each group contained six spectra.

The nonparametric permutation hypothesis test was performed using software written in-house [16, 18, 30, 227] with a significance level of $\alpha=0.05$. A single comparison was made between each set of spectra, producing one p-value per spectral comparison. A summary of discriminations, non-discriminations, Type I errors, and Type II errors from comparisons of same samples and different samples was compiled.

5.6 Automobile Float Glass

LIBS float glass samples had spectra that were similar between windows and within windows as seen in Figure 26 and Figure 27 respectively. This similarity makes the ability to discriminate between the samples visually difficult; therefore, the nonparametric permutation hypothesis test was used for the analysis of the spectral data.

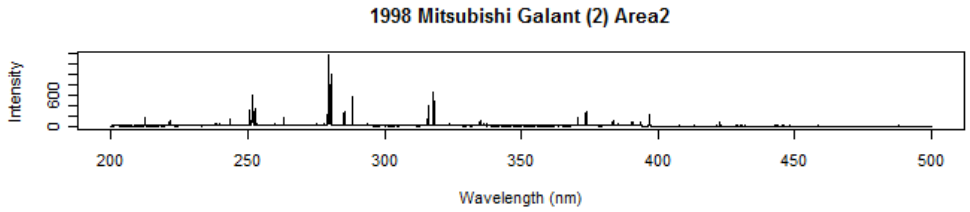
1998 Mitsubishi Galant (2) Area2
Intensity
0
600
200
250
300
350
400
450
500
Wavelength (nm)

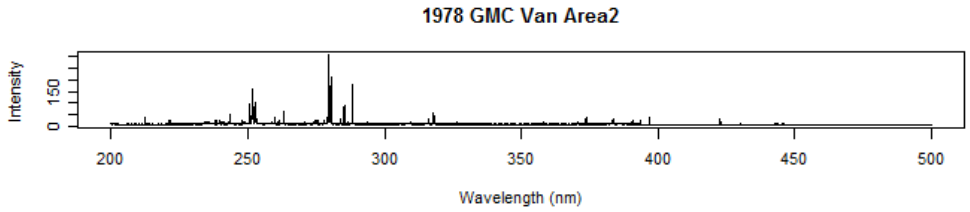
1978 GMC Van Area2
Intensity
0
150
200
250
300
350
400
450
500
Wavelength (nm)

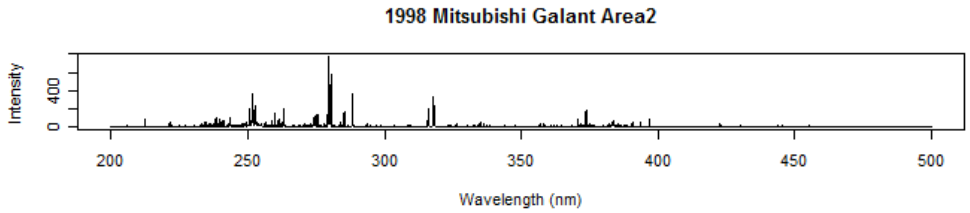
1998 Mitsubishi Galant Area2
Intensity
0
400
200
250
300
350
400
450
500
Wavelength (nm)

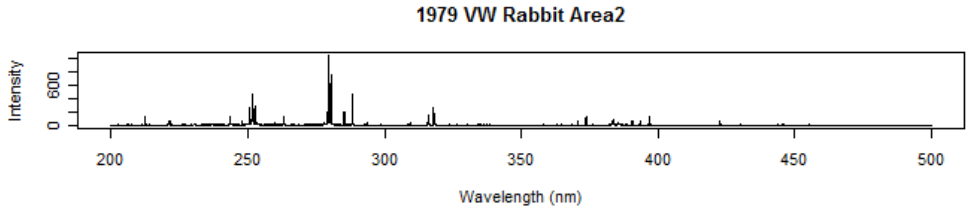
1979 VW Rabbit Area2
Intensity
0
600
200
250
300
350
400
450
500
Wavelength (nm)

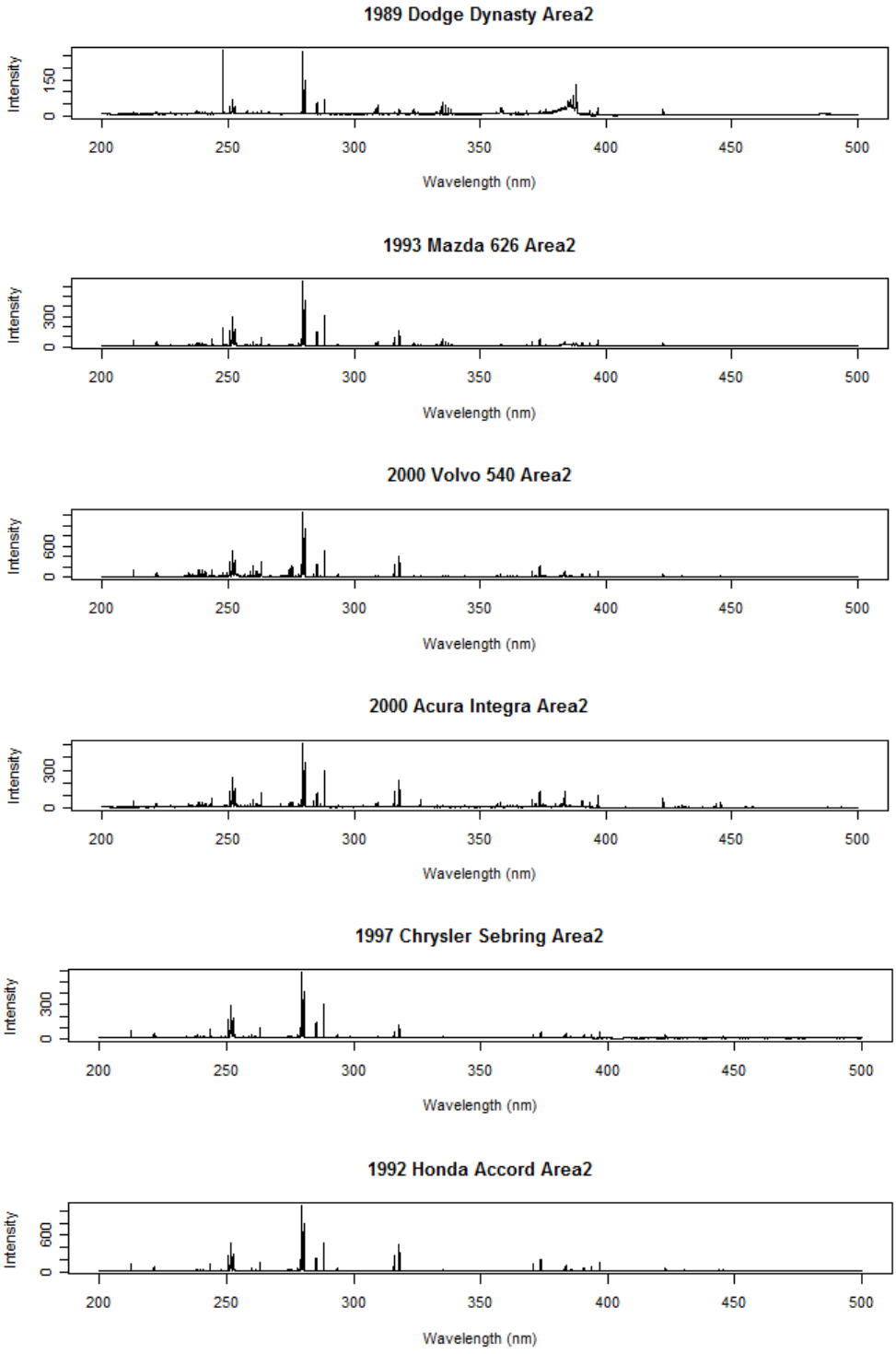

Figure 26: Spectra of each of the full window panes from the center area of the window. Spectral range plotted 200-500nm.

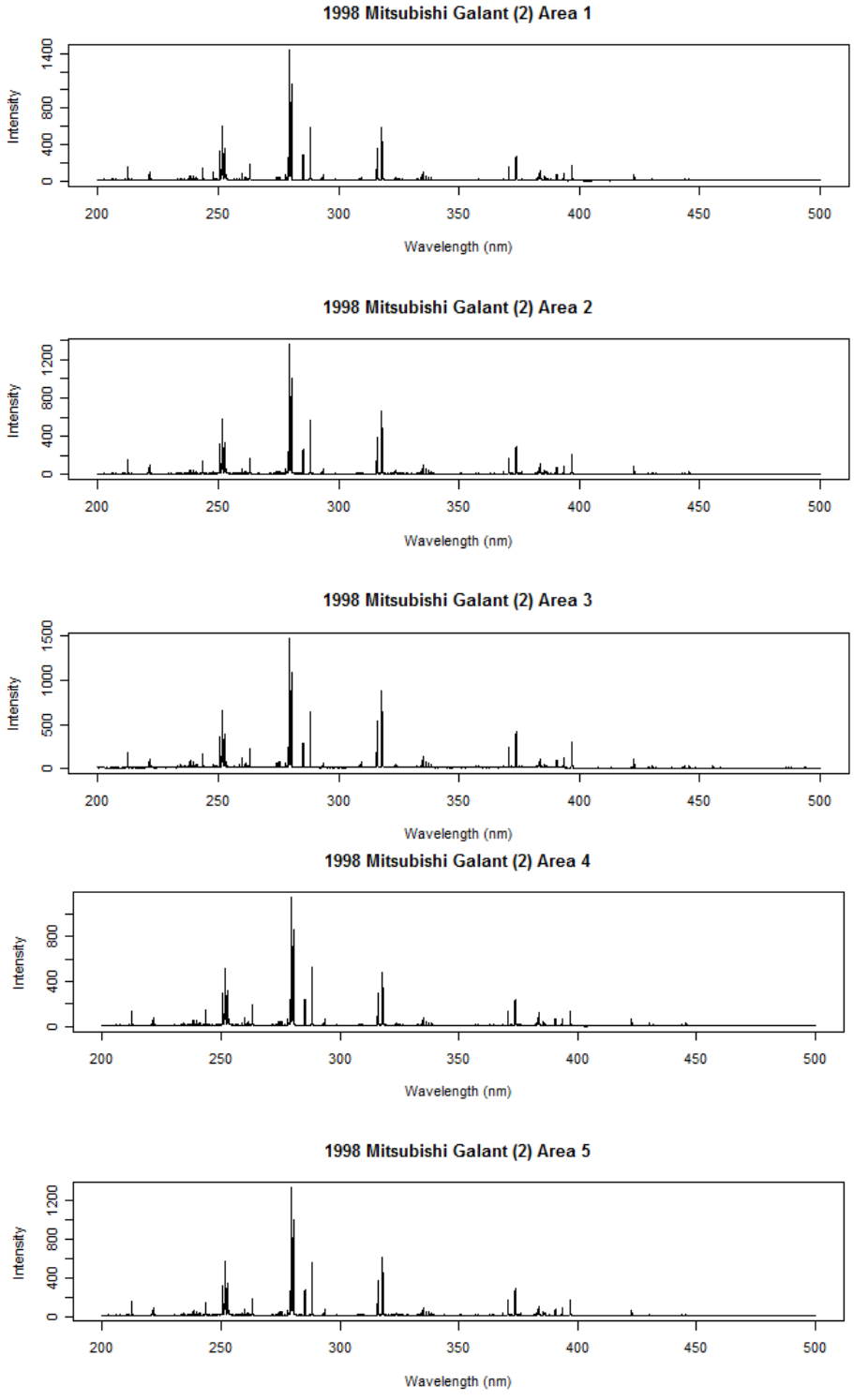

Figure 27: Spectra of window A from areas 1-5. These spectra demonstrate the similarities with slight differences in the spectra.

Based on the parameters described in the experimental chapter, LIBS spectra of automobile float glass samples were collected. LIBS spectral data in the range of 200-500 nm was used for the nonparametric analysis. This spectral range was selected because it incorporated characteristic spectral lines for the glass samples without eliminating important lines. In addition, the reduction of spectral range decreased the analysis time. Besides the reduction of the spectral range, no preprocessing of the data was performed.

Nonparametric permutation test was performed using two in-house software programs. The nonparametric permutation test was performed with a significance level of $\alpha=0.05$. Each method performed the nonparametric permutation test using the 12 choose 6 method, selection of six spectra for each sample for a total of twelve spectra per comparison. The original software provided one unique pairwise comparison per each set of data spectra; therefore one p-value was obtained per each spectral comparison. The second software program provided the option to input the number of unique pairwise comparisons desired for each set of data spectra. For each data set comparison, 100 unique pairwise comparisons were calculated which provided 100 p-values for each data set comparison. A summary of discriminations and non-discriminations from comparisons of same samples and different samples were compiled along with Type I and Type II error.

The Wilcoxon Rank Sum test was applied to the automobile float glass samples to determine whether samples from the same window-different areas and different windows were statistically different. The nonparametric p-values were used for the calculation. The data was set up with three groups: known versus known, known versus questioned one and known versus questioned two. The known group contained the p-values for the comparisons of four areas from a single window pane; known versus questioned one contained the p-values for the comparisons of the known to a fifth area of the same window pane; and known versus questioned two contained the p-values for the comparisons of the known to a different window.

The Wilcoxon Rank Sum test was then compared to the Hoteling's t-test to determine whether the nonparametric methods applied in the current research performed similarly to a more common parametric method.

The Wilcoxon Rank Sum test was performed using the p-values obtained for the comparisons of the different areas of window A by the nonparametric permutation test with a significance level of 0.05. The Hoteling's t-test was applied to scores obtained from PCA of the spectral data for the five areas of window A which had been normalized to sum to one. The scores corresponding to the first three principal components were retained and the Hoteling's T-test was applied to the data at a significance level of 0.05.

The final step in the data analysis of automobile float glass was the imaging of the LIBS spectral data. The data was normalized to sum to one and PCA was performed on each layer of the glass for the two data sets. The scores for the first three principal components were found for each layer and normalized from 0-1. The normalized scores were then plotted on an RGB color scale where the red component corresponded to the scores for the first principal component, the green component corresponded to the scores for the second principal component and the blue component corresponded to the scores for the third principal component. The scores were plotted to illustrate based on color the contributions from each principal component at each spot and layer within the glass. From the colors demonstrated it was possible to determine whether spatial variation was being observed within the window panes and if domains were present in the small area.

CHAPTER 6: RESULTS AND DISCUSSIONS

6.1 Fire Debris

As discussed previously, the fire data was viewed multiple ways to determine the ideal parameters to produce the best classification of the fire debris model and test data. With tests for multiple data normalization methods for both data sets, it was determined LDA and QDA classification performed best when the number of ions retained corresponded to the top 50 F-values and the additional abundant ions with the data normalized by autoscaling. For each model the optimal method for classifying the data was determined based on the number of ions, principal components, and variance retained, and correct classification percentages for the total and individual classes.

In addition to the two data sets (data set 1 – all ASTM classes and data set 2- ASTM classes excluding MISC and OXY), subsets were investigated. For each data set two subsets were created with the addition of substrate data. One subset consisted of classifying the data only as ignitable liquid (IL) or substrate (SUB), while the other subset consisted of classify the data as one of the ASTM classes or substrate. The addition of these subsets allowed for further investigation of the classification ability of the LDA and QDA models. The data, when grouped as IL versus SUB, was successfully distinguished into the two major types of fire debris samples; while the

ASTM classes versus SUB subsets investigated the more difficult issue of discriminating between IL and SUB in addition to correctly classifying IL into their ASTM classes, shown in Table 15. Results from the data sets containing only IL and the subsets for each of the three tested normalization methods are shown in Table 16. As can be seen, the autoscaled LDA and QDA data without ions 32 and 76 gave the best results when comparing number of principal components/variance and classification percentages.

The LDA results for data set two when retaining 95% of the variance with and without substrates had an overall correct classification rate of 90%; while data set one with and without substrates, had an overall correct classification rate of approximately 72%. The data performed very well for the IL versus SUB subsets with LDA results at 98% for both data sets with the retention of 95% of the variance. These results indicate that the optimal parameters were achieved with the retention of the top 50 F-values and additional abundant ions and the normalization method of autoscaling the data. Further, these results show that ignitable liquids and substrates can be identified correctly with this method. ASTM classes were more difficult to correctly classify, but correct classifications were achieved with LDA over 70% of the time for the autoscaled data.

In comparison, QDA performed better than LDA when the data set fit the criteria for its use. In IL versus SUB, QDA had high correct classification percentages into the two groups, while it performed at least 10% better than LDA for ASTM classifications.

Unfortunately, the large number of parameters required for QDA prevented its use with the retention of larger numbers of principal components, therefore limiting the extent of improvement possible with this method.

Table 15: Summary of fire debris tests to determine ideal ion retention and normalization technique. Each test has listed the number of ions and principal components along with individual and total class correct classification percentages.

Columns not normalized with 32 76	**Ions**	**PC**	**Ar**	**Gas**	**HPD**	**ISO**	**LPD**	**MISC**	**MPD**	**NP**	**NormA**	**Oxy**	**Sub**	**Total**
ASTM (-MISC and OXY)	64	6	93	73	88	69	96		84	94	94			85
ASTM + SUB (-MISC and OXY)	69	8	89	85	96	86	92		77	94	94		80	85
ASTM	60	10	78	81	92	89	83	22	86	94	100	54		69
ASTM + SUB	67	12	78	81	88	80	83	15	85	94	100	53	80	67
Columns not normalized wo 32 76														
ASTM (-MISC and OXY)	62	6	93	73	88	71	96		84	94	88			85
ASTM + SUB (-MISC and OXY)	67	8	85	85	94	86	96		78	94	100		87	86
ASTM	58	9	81	73	92	86	83	16	84	94	100	57		67
ASTM + SUB	65	11	59	77	88	86	88	12	85	94	100	43	85	65
Columns normalized with 32 76														
ASTM (-MISC and OXY)	64	10	85	85	85	83	92		88	94	94			88
ASTM + SUB (-MISC and OXY)	69	18	89	85	96	86	92		77	94	94		80	85
ASTM	60	15	81	77	85	54	96	30	83	94	82	59		67
ASTM + SUB	67	14	63	81	88	77	58	24	81	94	76	57	83	66
Columns normalized wo 32 76														
ASTM (-MISC and OXY)	62	10	89	88	85	89	92		84	94	94			88
ASTM + SUB (-MISC and OXY)	67	17	63	81	77	86	88		89	94	100		80	84
ASTM	58	14	70	85	88	51	96	28	82	94	82	60		66
ASTM + SUB	65	18	78	81	90	54	96	30	81	94	76	61	80	69
Mean centered wo 32 76														
ASTM (-MISC and OXY)	62	8	93	77	90	86	96		78	94	100			86
ASTM + SUB (-MISC and OXY)	67	10	78	81	94	86	96		82	94	94		85	86
ASTM	58	12	81	73	92	89	96	23	80	94	100	53		68
ASTM + SUB	65	14	81	81	92	89	92	20	80	94	100	51	83	69
Standardized wo 32 76														
ASTM (-MISC and OXY)	62	14	93	88	94	91	96		83	94	100			90
ASTM + SUB (-MISC and OXY)	67	24	81	92	81	94	96		91	94	100		92	90
ASTM	58	20	81	81	96	94	96	30	80	94	100	66		72
ASTM + SUB	65	27	81	88	96	94	92	26	89	94	100	66	83	73
ASTM 3 PC LDA	58	3	78	69	89	37	92	13	65	88	76	46		55
ASTM 3 PC QDA	58	3	85	85	92	83	96	31	88	94	94	59		72
ASTM 3 PC LDA (-MISC and OXY)	62	3	89	73	90	40	96		67	88	88			75
ASTM 3 PC QDA (-MISC and OXY)	62	3	85	88	92	94	96		91	94	100			92
ASTM + SUB 3 PC LDA (-MISC and OXY) 49.7%	67	3	74	81	85	89	96		73	94	100		52	77
ASTM + SUB 3 PC QDA (-MISC and OXY) 49.7%	67	3	85	88	85	97	96		87	94	100		70	86
ASTM + SUB 3 PC LDA	65	3	78	69	85	54	83	16	68	94	76	59	50	58
ASTM + SUB 3 PC QDA	65	3	70	73	92	86	83	17	77	94	94	56	55	63

Table 16: Summary of fire debris tests to determine ideal ion retention and normalization technique for grouping of IL and SUB.

Using ILRC & SUB (ILRC NOT divided into classes, columns not normalized, wo 32 76)					
LDA	**Ions**	**PC**	**IRLC**	**SUB**	**Total**
(-)MISC + OXY samples	67	8	98	87	96
Including MISC + OXY samples	65	11	90	87	90
QDA					
(-) MISC + OXY samples	67	8	99	93	98
Including MISC + OXY samples	65	11	96	98	97
LDA - Mean centered data					
(-) MISC + OXY samples	67	10	95	82	93
Including MISC + OXY samples	65	14	94	82	93
(-) MISC + OXY samples 80% variance	67	5	95	83	93
Including MISC + OXY samples 80% variance	65	6	88	78	87
(-) MISC + OXY samples 3 PCs (73%)	67	3	86	87	86
Including MISC + OXY samples 3 PCs (64%)	65	3	81	95	83
QDA - Mean centered data					
(-) MISC + OXY samples	67	10	99	92	98
Including MISC + OXY samples	65	14	97	98	97
(-) MISC + OXY samples 80% variance	67	5	97	93	96
Including MISC + OXY samples 80% variance	65	6	90	92	91
(-) MISC + OXY samples 3 PCs (73%)	67	3	90	90	90
Including MISC + OXY samples 3 PCs (64%)	65	3	87	90	88
LDA - Standardized data					
(-) MISC + OXY samples	67	24	99	90	98
Including MISC + OXY samples	65	27	100	85	98
(-) MISC + OXY samples 80% variance	67	11	100	82	97
Including MISC + OXY samples 80% variance	65	13	99	87	98
(-) MISC + OXY samples 3 PCs (49.7%)	67	3	96	70	91
Including MISC + OXY samples 3 PCs (47%)	65	3	92	63	88
QDA - Standardized data					
(-) MISC + OXY samples	67	24	100	98	99
Including MISC + OXY samples	65	27	100	100	100
(-) MISC + OXY samples 80% variance	67	11	98	93	97
Including MISC + OXY samples 80% variance	65	13	99	98	99
(-) MISC + OXY samples 3 PCs (49.7%)	67	3	92	72	89
Including MISC + OXY samples 3 PCs (47%)	65	3	86	70	84

Once optimization of the data processing and data analysis parameters was achieved the next step was to apply the model to test data to determine the classification of samples not included in the model. As described in the experimental method, the PCA/LDA and PCA/QDA models were applied to test fire debris data, shown in Table 17, to obtain new scores and classify the test data.

Table 17: Sample, identification number, and classification for test fire debris data.

Sample	ID Number	Class	Sample	ID Number	Class	Sample	ID Number	Class
IKEA Pillow	B2sub1	SUB	Aroma Glow-Mixed Berries	455	NormA	Mastercraft Odorless Paint Thinner & All Purpose Cleaner	495	MPD
Curtains	B2sub2	SUB	Interlux 2333N Reducing Solvent	456	OXY	Mastercraft Low Odour Varsol	496	MPD
IKEA Coffee Table	B2sub3	SUB	Interlux 355 Vinyl-Lux Solvent	457	OXY	Mastercraft Liquid Sander	497	AR
IKEA Bedsheet	B2sub4	SUB	Interlux 2316N Reducing Solvent	458	OXY	Recochem Methylene Chloride Free Paint Remover	498	AR
IKEA Comforter	B2sub5	SUB	Interlux Solvent 202 Fiberglass Wash	459	OXY	Home Paint Thinner	499	MPD
IKEA Duvet Cover	B2sub6	SUB	Interlux Interstrip 299E Paint Remover	460	OXY	Recochem Clear Kerosene	500	MPD
IKEA Chair Frame	B2sub7	SUB	Interlux Solvent 333 Brushing Liquid	461	HPD	Mastercraft Brush & Roller Cleaner	501	AR
IKEA Bed Headboard	B2sub8	SUB	Pettit Ablative Thinner 185	462	OXY	Recochem Lacquer Thinner	502	OXY
IKEA Paper Lamp Shade	B2sub9	SUB	Interlux Solvent 216 Special Thinner	461	HPD	Mastercraft Lacquer Thinner	503	OXY
IKEA Couch	B2sub10	SUB	Ace Lacquer Thinner High Strength	464	OXY	Mastercraft Portable Burner Fuel	504	OXY
IKEA Chair Padding	B2sub11	SUB	Ace Paint Thinner, 100% Mineral Spirits	465	MPD	STP Fuel Injector & Carb Cleaner	505	HPD
IKEA Slated Bed Base	B2sub12	SUB	Pettit Brushing Thinner 120/T-10	466	MISC	Kama Sutra Lamp Oil	506	ISO
IKEA Mattress	B2sub13	SUB	E85	467	OXY	Goo Gone Cleaner	507	ISO
IKEA Dresser	B2sub14	SUB	Bio-Diesel	468	OXY	Orange Glo Wood Polish & Conidtioner	508	ISO
Women's fashion shirt	B2sub15	SUB	B99 Biodiesel Fuel	469	OXY	Prestone Cold Start	509	MPD
Children's Embroidered Jeans	B2sub16	SUB	B5 Biodiesel	470	OXY	Lamplight Ultrapure Lamp Oil	510	Norm A

Sample	ID Number	Class	Sample	ID Number	Class	Sample	ID Number	Class
Women's Swim Suit	B2sub17	SUB	Kero-Klean Kerosene Fuel Treatment	471	OXY	Ecoflame Lighting Gel	511	OXY
Women's Tank Top	B2sub18	SUB	Pro-Mix 2-cycle Engine Oil	472	MPD	Watco Satin Wax	512	MPD
Women's Dress Shorts	B2sub19	SUB	Strypeeze	473	OXY	LePage Contact Cement Thinner/Cleaner	513	LPD
Men's T-shirt	B2sub20	SUB	3M Citrus Base Cleaner	474	MISC	LePage PolyClens Paint Brush/Roller Cleaner	514	AR
Women's Silk Skirt	B2sub21	SUB	Summer Comfort Citronella		NP	Jet Pep E85, unweathered	525	OXY
Children's Leggings	B2sub22	SUB	Strypeeze	476	MISC	Jet Pep E85, 25% weathered	526	OXY
Women's Spaghetti Strap Shirt	B2sub23	SUB	Minwax Wood Finish	477	MPD	Jet Pep E85, 50% weathered	527	OXY
Women's Spaghetti Strap Shirt	B2sub24	SUB	Speedy Spar Varnish	478	MPD	Jet Pep E85, 75% weathered	528	OXY
Women's Dress Pants	B2sub25	SUB	Majic Polyurethane Enamel	479	MPD	Howard Restor-A-Finish	529	OXY
Women's Jeans	B2sub26	SUB	Barb-o-lite Charcoal Lighter	480	HPD	Old Harbor Candles Citronella Outdoor Lamp Oil	530	HPD
Children's L/S Shirt	B2sub27	SUB	Homestar Citronella Torch Fuel	481	MPD	Savogran Dirtex Liquid Cleaner	531	OXY
T-shirt	B2sub28	SUB	Fred's Fuel Injector Cleaner	481	MPD	Carr's Diesel	532	HPD
T-shirt	B2sub29	SUB	Big Lots Odorless Charcoal Lighter Fluid	483	ISO	Ace Flight Service Jet A	533	MISC
Women's Pajama Pants	B2sub30	SUB	Crown Low Odor Mineral Spirits	484	NP	Ace Flight Service LL 100	534	MISC
Carpet used in Burn 2 (5/10)	B2sub31	SUB	Citgo Off Road Diesel	485	HPD	Holiday Gasoline 88.5 Octane	535	Gas
Stoddard Solvent	446	MPD	Gulflite Charcoal Starter	486	ISO	Holiday Gasoline 87 Octane	536	Gas

Sample	ID Number	Class	Sample	ID Number	Class	Sample	ID Number	Class
Paraffin Oil	447	MISC	Kwal Howells Lacquer Thinner	487	OXY	Aero Tech LL 100	537	MISC
3 in One Professional High Performance penetrant Spray	448	MISC	Safeway Charcoal Lighter	488	MPD	Kingsford Charcoal Lighter	538	MPD
Omega Castor Synthetic Engine Fuel	449	OXY	Nasco Spirits of Turpentine	489	MISC	Klean Strip Odorless Mineral Spirits Substitute	539	NP
TRX 2.5 Racing Engine Top Fuel	450	OXY	Startex VMP&P Naphtha	490	LPD	Flood Penetrol	540	MISC
HPI Racing Power Fuel	451	OXY	Nasco Lacquer Thinner	491	OXY	Klean Strip VM&P Naphtha	541	MPD
Kingsford Odorless Charcoal Lighter	452	MPD	Loew Cornell Odorless Brush Cleaner & Thinner	492	ISO	Biodiesel 100%	542	OXY
Startex MEK	453	OXY	Loew Cornell One-Step Oil Brush Cleaner & Conditioner	493	ISO	E85 gasoline	543	Gas
Klean Strip Acetone	454	OXY	Better Way Brush Cleaning Fluid and Oil Paint Solvent	494	ISO	Biodiesel 100%	544	OXY

Models based on data set one and two were applied to the test data. A total of 89 ignitable liquids and 31 substrates were included in the test data; except when data set two was applied to the test, for this test the MISC and OXY samples were removed leaving 47 ignitable liquids and 31 substrates. The models were applied to the data sets classified as ASTM classes with the inclusion and exclusion of substrates and for data sets classified as IL and SUB. For data set one there were three models tested: Model 1 included only the pure ignitable liquids for classification into the ASTM classes; Model 2 included the ignitable liquids and substrates for classification into IL or SUB; and Model 3 included the pure ignitable liquids and substrates for classification into the ASTM classes or SUB. For data set two there were also three models: Model 4 included only the pure ignitable liquids for classification into the ASTM classes; Model 5 included the ignitable liquids and substrates for classification into IL or SUB; and model 6 included the pure ignitable liquids for classification into the ASTM classes and SUB. For each model, PCA and LDA were performed on the model data to give test data corresponding to both methods. The number of principal components retained for the LDA analysis corresponded to 80% of the variance, which provided good results without the retention of an excess number of principal components. QDA was not used for the model application because the number of parameters needed to perform the analysis exceeded the number of samples in some of the classes.

Prior to the application of the model to the test data, plots were created to demonstrate the distribution of the classes within the model. The plots were created using the

canonical scores which were acquired by multiplying the PCA scores by the canonical functions obtained from LDA. The number of canonical scores is equal to the number of classes in the model minus one [232, 246]. The canonical scores were plotted for models 2, 3, 5 and 6.

Models 2 and 5 each had one canonical variate due to the models only containing two groups; therefore the Gaussian distributions of these two models were plotted as shown in Figure 28 and Figure 29 respectively. As can be seen in both plots the ignitable liquids and substrates distributions overlap slightly but the majority of the two groups were separated. More separation was observed in model 5, which is likely due to the removal of the broad MISC and OXY classes.

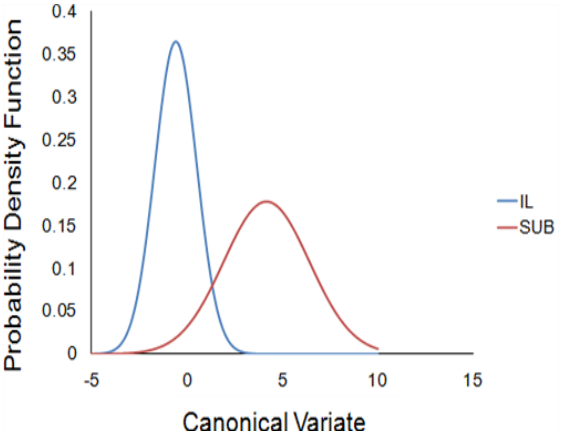

Figure 28: Canonical variate plot for model 2

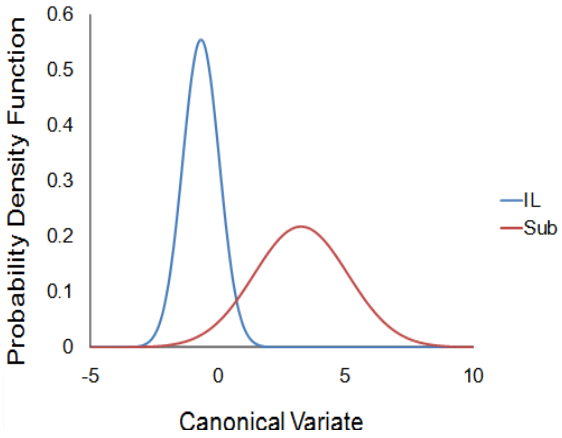

Figure 29: Canonical variate plot for model 5

Models 3 and 6 had the potential to have 10 and 8 canonical variates respectively, but only the first three were plotted due to the inability to visualize the higher dimensions. Figure 30 and Figure 31 illustrate the distributions of the ASTM classes. For model 3 there is a great deal of overlap of the MISC and OXY classes with the other nine classes, which results from the broad criteria for classification of the MISC and OXY.

Model 6 classes were more separated with only slight overlap between the ASTM classes and substrates being mostly separated from the ignitable liquid classes. Only two classes were not separated at all; these two classes were the isoparaffins (ISO) and the normal alkanes (NA). This lack of separation can be explained by the similarity of the two groups as ISOs are branched alkanes.

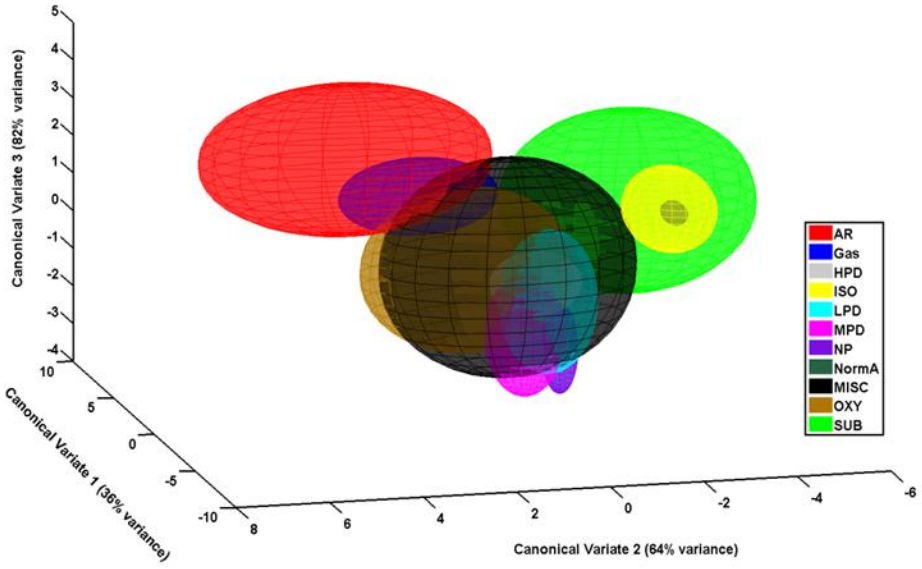

Figure 30: Canonical variate plot for model 3.

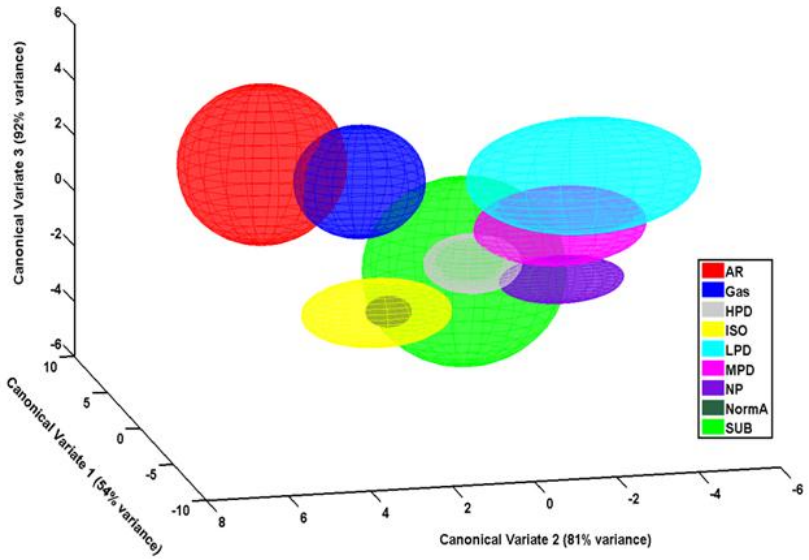

Figure 31: Canonical variate plot for model 6.

The first model, ignitable liquids only classified by ASTM classes, required the retention of 10 principal components to reach 80% of the variance. Shown in Table 18 are the correct classification percentages for the model, with the majority of the ASTM classes correctly classifying at 70% or above. The overall correct classification percentage was 66% with the MISC and OXY classes having the lowest classification rates as expected. When this model was applied to the test data, the overall correct classification rate was 60% with individual classifications shown in Table 19. The majority of misclassifications resulted from samples going to groups that were similar in spectral pattern for both the model and the test data.

Table 18: Model 1 – Classification percentages from LDA analysis of model.

	AR	Gas	HPD	ISO	LPD	MISC	MPD	NP	NormA	OXY	%correct
AR	20	4	0	0	0	1	0	0	0	2	74
Gas	3	20	1	0	0	0	0	0	0	1	80
HPD	0	0	44	0	0	0	1	3	0	0	92
ISO	0	0	1	28	2	0	0	0	4	0	80
LPD	0	0	0	0	23	0	0	1	0	0	96
MISC	3	13	16	9	8	23	10	9	0	3	24
MPD	0	0	4	0	0	10	72	9	0	0	76
NP	0	0	1	0	0	0	0	15	0	0	94
NormA	0	0	0	1	0	0	0	0	16	0	94
OXY	1	4	1	0	10	10	3	3	1	38	54
Total	27	41	68	38	43	44	86	40	21	44	66

Table 19: Model1 – Classification percentages of test data based on model LDA.

	AR	Gas	HPD	ISO	LPD	MISC	MPD	NP	NormA	OXY	%correct
AR	0	0	0	0	0	0	0	0	0	0	N/A
Gas	3	6	0	0	1	1	0	0	0	0	55
HPD	0	0	1	0	0	0	0	0	0	0	100
ISO	0	0	0	1	0	0	0	0	0	0	100
LPD	0	0	0	0	1	0	0	0	0	0	100
MISC	0	0	0	0	1	2	0	1	0	0	50
MPD	0	0	1	0	0	1	4	1	0	0	57
NP	0	0	0	0	0	0	0	0	0	0	N/A
NormA	0	0	0	0	0	0	0	0	1	1	50
OXY	0	1	0	0	0	1	0	1	0	5	62
Total	3	7	2	1	3	5	4	3	1	6	60

Model 2, ignitable liquid and substrates classified as IL and SUB, required the retention of 13 principal components to reach 80% of the variance. Table 20 shows LDA correctly classified the model into IL or SUB with an overall classification rate of 98%. The application of the model to the test data resulted in the overall classification rate dropping to 61%. As seen in Table 21, IL had a 94% correct classification rate while substrates had a low correct classification rate of 32%. The low substrate classification

was attributed to the substrates incorrectly classifying into the IL class due to the inclusion of the MISC and OXY classes.

Table 20: Model 2 - Classification percentages from LDA analysis of model.

	IL	**SUB**	**%correct**
IL	448	4	99
SUB	8	52	87
Total	456	56	98

Table 21: Model 2 – Classification percentages of test data based on model LDA.

	IL	**SUB**	**%correct**
IL	33	2	94
SUB	28	13	32
Total	61	15	61

Model 3, ignitable liquid and substrate classified as ASTM classes and SUB, was the final model including the MISC and OXY classes and the most difficult for classification. To obtain 80% of the variance 13 principal components were retained. The model performed well for the majority of the classes, with correct classification rates of about 70% for all but the MISC and OXY classes. The overall correct classification rate for this model was 70%, the highest for the models so far. When applied to the test data, the overall correct classification rate was slightly less than half at 45%. Correct classification rates of about 60% were seen for the majority of the classes except MISC, OXY and SUB. The majority of misclassifications were observed for the substrate class, with the ASTM classes having minimal misclassifications. Many of the

misclassifications of the substrates were attributed to the inclusion of the broad groups of MISC and OXY. Table 22 shows the individual classifications for the LDA of the model, while Table 23 shows them for the test data.

Table 22: Model 3 - Classification percentages from LDA analysis of model.

	AR	Gas	HPD	ISO	LPD	MISC	MPD	NP	NormA	OXY	SUB	%correct
AR	19	5	0	0	0	0	0	0	0	2	1	70
Gas	2	22	1	0	0	0	0	0	0	0	0	88
HPD	0	0	45	0	0	0	1	2	0	0	0	94
ISO	0	0	1	26	2	0	0	0	6	0	0	74
LPD	0	0	0	0	23	0	0	1	0	0	0	96
MISC	3	10	15	7	7	27	11	9	1	4	0	29
MPD	0	0	4	0	0	9	73	9	0	0	0	77
NP	0	0	1	0	0	0	0	15	0	0	0	94
NormA	0	0	0	2	0	0	0	0	15	0	0	88
OXY	1	4	1	0	9	7	4	3	1	41	0	58
SUB	0	0	1	1	1	2	0	4	0	1	50	83
Total	25	41	69	36	42	45	89	43	23	48	51	70

Table 23: Model 3 – Classification percentages of test data based on model LDA.

	AR	Gas	HPD	ISO	LPD	MISC	MPD	NP	NormA	OXY	SUB	%correct
AR	0	0	0	0	0	0	0	0	0	0	0	N/A
Gas	2	7	0	0	1	1	0	0	0	0	0	64
HPD	0	0	2	0	0	0	0	0	0	0	0	100
ISO	0	0	0	1	0	0	0	0	0	0	0	100
LPD	0	0	0	0	1	0	0	0	0	0	0	100
MISC	0	0	0	1	1	1	0	1	0	0	0	25
MPD	0	0	0	0	0	1	4	1	0	0	0	67
NP	0	0	0	0	0	0	0	0	0	0	0	N/A
NormA	0	0	0	0	0	0	0	0	1	1	0	50
OXY	0	0	0	0	0	2	0	1	0	5	0	63
SUB	0	2	4	0	4	2	2	2	0	13	12	29
Total	2	9	6	2	7	7	6	5	1	19	12	45

The fourth model, ignitable liquids only by ASTM classes with the exclusion of the MISC and OXY groups, required the retention of 7 principal components to reach 80% of the

variance. The LDA of the model had a total correct classification of 89% with no classes having a classification percentage below 74%. Individual classification percentages can be seen in Table 24. When the model was applied to the test data the total correct classification was again fairly high at 77%. The majority of the classes had correct classification rates above 65%, with the ISO class being the only one to fall below with a classification percentage of only 38%. The majority of the misclassified ISO samples were classified as normal alkane which was a result of the ISO group engulfing the normal alkane group within the model. Individual classifications for the test data are seen in Table 25.

Table 24: Model 4 - Classification percentages from LDA analysis of model.

	AR	Gas	HPD	ISO	LPD	MPD	NP	NormA	%correct
AR	24	3	0	0	0	0	0	0	89
Gas	1	23	1	0	0	0	0	0	92
HPD	0	0	41	0	0	3	4	0	85
ISO	0	0	0	26	2	0	0	7	74
LPD	0	0	1	0	23	0	0	0	96
MPD	0	0	1	0	0	87	7	0	92
NP	0	0	1	0	0	0	15	0	94
NormA	0	0	0	2	0	0	0	15	88
Total	25	26	45	28	25	90	26	22	89

Table 25: Model 4 – Classification percentages of test data based on model LDA.

	AR	Gas	HPD	ISO	LPD	MPD	NP	NormA	%correct
AR	4	1	0	0	0	0	0	0	80
Gas	1	2	0	0	0	0	0	0	67
HPD	0	0	7	0	0	0	0	0	100
ISO	0	0	0	3	0	0	0	5	38
LPD	0	0	0	0	2	0	0	0	100
MPD	0	0	1	0	0	14	2	0	82
NP	0	0	0	0	1	0	2	0	67
NormA	0	0	0	0	0	0	0	2	100
Total	5	3	8	3	3	14	4	7	77

Model 5, ignitable liquids and substrates classified as IL or SUB without MISC and OXY classes required 8 principal components to reach 80% of the variance. LDA of the model data provided a total correct classification of 96%, and both classes had correct classifications above 80% as seen in

Table 26. When the model was applied to the test data, the total correct classification was 96% with both classes correctly classifying above 95% as seen in Table 27 . This model demonstrates the ability to distinguish between ignitable liquids and substrates; it also further indicates that the issue with model 2 was the classification of substrates as IL due to the MISC and OXY classes.

Table 26: Model 5 - Classification percentages from LDA analysis of model.

	IL	**SUB**	**%correct**
IL	283	4	99
SUB	11	49	82
Total	294	53	96

Table 27: Model 5 – Classification percentages of test data based on model LDA.

	IL	**SUB**	**%correct**
IL	45	2	96
SUB	1	30	97
Total	46	32	96

Model 6, ignitable liquids and substrates using ASTM classes excluding MISC and OXY was the final model tested. To retain 80% of the variance, 8 principal components were

kept for the LDA analysis. The total correct classification for the model was 82% with all classes correctly classifying at or above 60%, as shown in Table 28. ISO had the lowest correct classification rate, 60% with the majority of its misclassifications going to normal alkanes, which as seen in model 4 was attributed to the ISO group engulfing the normal alkane group for the model. When applied to the test data, the correct classification percentage was 86%. Test data had lower correct classification percentages, but all classes correctly classified at or above 60% as seen in Table 29.

Table 28: Model 6 – Classification percentages from LDA analysis of model.

	AR	**Gas**	**HPD**	**ISO**	**LPD**	**MPD**	**NP**	**NormA**	**SUB**	**%correct**
AR	24	3	0	0	0	0	0	0	0	89
Gas	1	22	1	0	0	0	0	0	1	88
HPD	0	0	45	0	0	1	2	0	0	94
ISO	0	0	1	21	2	0	0	11	0	60
LPD	0	0	0	0	23	1	0	0	0	96
MPD	0	0	9	0	0	77	9	0	0	81
NP	0	0	1	0	0	0	15	0	0	94
NormA	0	0	0	4	0	0	0	13	0	76
SUB	0	7	4	0	0	2	2	0	45	75
Total	25	32	61	25	25	81	28	24	46	82

Table 29: Model 6 – Classification percentages of test data based on model LDA.

	AR	**Gas**	**HPD**	**ISO**	**LPD**	**MPD**	**NP**	**NormA**	**SUB**	**%correct**
AR	3	2	0	0	0	0	0	0	0	60
Gas	0	2	0	0	0	0	0	0	1	67
HPD	0	0	7	0	0	0	0	0	0	100
ISO	0	0	0	5	0	0	0	3	0	63
LPD	0	0	0	0	2	0	0	0	0	100
MPD	0	0	1	0	0	14	2	0	0	82
NP	0	0	0	0	1	0	2	0	0	67
NormA	0	0	0	0	0	0	0	2	0	100
SUB	0	1	0	0	0	0	0	0	30	97
Total	3	5	8	5	3	14	4	5	31	86

The LDA results for the first three models demonstrate the issues with the MISC and OXY classes. These classes are broad in criteria and encompass a large variety of samples and spectral patterns, as discussed in the introduction. These criteria result in misclassification of ignitable liquids and substrates into these classes because MISC and OXY encompassed multiple spectral patterns causing overlap with the more well-defined ASTM classes. The models were improved with the removal of these classes as shown in the second set of three models. The classification of ignitable liquid and substrates without MISC and OXY samples included improved a great deal, demonstrating correct classification as IL or SUB. Improvements were also seen in the ASTM classifications, with the majority of misclassifications for all models resulting from classification into classes of similar spectral pattern. The removal of the broad MISC and OXY classes forced the samples in the remaining ASTM classes that were most similar. The models were created and classifications were based on samples present in the model, therefore it was expected when the models were applied to the test data, which were not present in the model, that classifications would drop some. In addition, the test data set was smaller in size demonstrating a large effect on the classification percentage with one or two misclassifications.

6.2 Bone

6.2.1 Discriminant Analysis

6.2.1.1 Single Shot, Consecutive Sampling

The initial test of the bone experiment was to investigate methods for analysis of bones by LIBS. It was seen in the spectra that the bones were going to appear very similar in chemical structure and a statistical technique would be needed for discriminating between species or different animals of the same species. First, twelve bone samples, shown in Table 4, were analyzed by LIBS using twelve single shot spectra collected in consecutive order. The full spectral range was analyzed (200-900 nm) and the data was normalized to the maximum intensity equal to one. Thirty-two high F-values were determined by the methods described in the fire debris section and are shown in Table 30.

Table 30: Spectral wavelengths corresponding to high F-values for initial experiment.

High F-Value Wavelengths (nm)			
588.91396	588.8596	589.51145	588.96832
589.457.17	854.33028	589.02267	589.56572
589.61997	866.38027	854.24145	589.07701
588.80522	866.29317	646.09807	589.67422
643.75362	589.40289	854.4191	558.76555
766.50248	589.1315	558.82428	819.5816
559.35253	766.54635	649.20004	558.88301
616.0905	643.80961	589.72847	589.18567

The data corresponding to the selected wavelengths was normalized by autoscaling the data and PCA was performed. LDA was performed using scores for four principal components, which contained 95% of the variance, on the data grouped as species, results shown in Table 31. The human bones were not grouped together because they were known to have been processed differently from each other. As can been seen in Table 31 correct classification percentages were fairly low for the majority of the classes with only two classes having above an 80% correct classification: human burnt (100%) and turtle (92%). It can be seen that all of the misclassifications of human bones were into classes of other human bone classes, therefore indicating the processing did not alter the overall composition of the bone drastically. The total correct classification percentage was only 63%.

QDA was performed using scores for five principal components, which contained 96% of the variance, and the data was again grouped. From the LDA results it was decided to group the humans as one class. Turtle bone and shell were classified together in this test also. The correct classification percentages can be seen in Table 32 the results greatly improved with QDA and the grouping of the human bones; this was attributed to QDA not requiring the assumption of equal covariance matrices. The lowest classification percentage was 86% for the turtle shell. This may be due to variation between the top and bottom of the shell which were grouped together. The total correct classification rate was 91%.

Table 31: LDA results for twelve initial bone samples.

	Alligator	Bird	Deer	Fish	Human Bleached	Human Burnt	Human Tarsal	Turtle	Turtle Shell	%correct
Alligator	5	1	1	4	2	0	0	0	0	38
Bird	0	12	0	0	1	0	10	0	0	52
Deer	0	0	9	3	0	0	0	0	0	75
Fish	8	0	3	11	2	0	0	0	0	46
Human Bleached	0	0	0	0	9	0	4	0	0	69
Human Burnt	0	0	0	0	0	11	0	0	0	100
Human Tarsal	0	0	0	0	4	0	8	0	0	67
Turtle	0	0	0	0	1	0	0	11	0	92
Turtle Shell	8	0	0	0	2	0	0	0	14	58
Total	21	13	13	18	21	11	22	11	14	63

Table 32: QDA results for twelve initial bone samples.

	Alligator	**Bird**	**Deer**	**Fish**	**Human**	**Turtle**	**% correct**
Alligator	12	0	0	0	0	0	100
Bird	0	21	0	0	3	0	88
Deer	0	0	12	0	0	0	100
Fish	2	0	1	21	0	0	88
Human	0	2	0	0	34	0	94
Turtle	4	0	0	1	0	31	86
Total	18	23	13	22	37	31	91

6.2.1.1 Single Shot, Random Sampling

PCA analysis was performed on the baseline corrected spectral range from 200-500nm. This was done to reduce the size of the data set and because characteristic data was determined to be contained in that range. Two normalization methods were also analyzed: sum to maximum equal to one and autoscaling. LDA was performed on 95% and 80% of the variance, unfortunately QDA could not be performed due to the number of samples in each bone group being too small and the number of principal components required to retain for these variances was too large. When the bones were analyzed individually to determine the ability to distinguish between bones from the same animal or same species, the LDA results had approximately 100% correct classification for each class but a small data set was used with a large number of groups to sort between. Therefore, bones were grouped by species to obtain large group population. Classes of bird, human, dog, gator, deer, pig and turtle were tested.

The data normalized to the maximum equal to one required the retention of scores for nine principal components to reach 95% of the variance within the data. The overall correct classification percentage was just over half at 55%. The individual class results can be seen in Table 33, with the highest correct classification being for bird at 89% and lowest being for deer at 33%.

Table 33: LDA results for normalization to maximum equal to 1 while retaining 95% of the variance.

	Bird	**Deer**	**Dog**	**Gator**	**Human**	**Pig**	**Turtle**	**%correct**
Bird	8	1	0	0	0	0	0	89
Deer	1	4	3	0	0	3	1	33
Dog	0	0	7	0	0	2	0	78
Gator	2	0	1	6	0	0	0	67
Human	2	2	5	1	15	1	4	50
Pig	3	4	2	1	2	8	1	38
Turtle	1	0	1	0	2	0	8	67
Total	17	11	19	8	19	14	14	55

Autoscaling the data required a very large number of principal components, 84, to be retained to reach 95% of the variance. The total correct classification rate was 98%, with the majority of the classes having 100% correct classification rates, and the lowest being for dog at 89%. Individual class results can be seen in Table 34.

.

Table 34: LDA results for normalization by autoscaling while retaining 95% of the variance.

	Bird	**Deer**	**Dog**	**Gator**	**Human**	**Pig**	**Turtle**	**%correct**
Bird	9	0	0	0	0	0	0	100
Deer	0	11	0	0	1	0	0	92
Dog	0	0	8	0	0	1	0	89
Gator	0	0	0	9	0	0	0	100
Human	0	0	0	0	30	0	0	100
Pig	0	0	0	0	0	21	0	100
Turtle	0	0	0	0	0	0	12	100
Total	9	11	8	9	31	22	12	98

The same set of data was analyzed with the removal of the tooth data for both human and pig. It was decided to remove these bones from the analysis because they have different elemental composition than the other bones being examined, therefore potentially causing misclassifications. The removal of the teeth improved the results for the two normalization techniques by a small amount, 59% for maximum equal to zero and 100% for autoscaling. Similar results were observed when the teeth were separated into new classes: human teeth and pig teeth.

The results showed that normalization of the data by autoscaling required the retention of a large number of scores due to the small difference in variance between successive principal components. Therefore, normalization by setting the maximum equal to one was determined to be the ideal method despite the lower results shown in this experiment. This method was also chosen for further analysis because jackknife classification results were distorted from the classification matrix when the data was normalized by autoscaling, but the two classification matrices were not distorted when

the data was normalized by maximum equal to one. The jackknife method analyzes the data by removing one sample and testing it against the remainder of samples to determine its classification, whereas the classification method previously discussed includes the sample being tested within the model. Jackknife results for normalizing by setting the maximum emission intensity equal to one were within 5 to 10% of the classification matrix, with the maximum difference being 35% (for the deer class); jackknife results for normalization by autoscaling were up to 95% different from the classification matrix with the minimum difference being 60% (for the bird and turtle classes).

6.2.1.3 Average Spectra, Random Order

The final approach using discriminant analysis for bone samples was to reduce the number of scores retained to allow for both LDA and QDA to be performed. When the scores retained to reach a specified variance were analyzed it was determined that the score for the first principal component contained the majority of the variance with the remainder containing only small percentages. It was decided to eliminate the scores for the first principal component from the analysis, which consisted of 95% of the variance, and retain the scores for the next three principal components. This was performed on a smaller data set, Table 6. The spectral range (200-500nm) was normalized by maximum equal to one and PCA was performed.

Scores for principal components two thru four consisted of 3.5%, 0.7%, and 0.3% of the variance respectively. The data was grouped two ways, with classes for each pig bone (where the bones were different bones from the same pig) and with a class containing all of the pig bones. The LDA results using the two methods of grouping the pig bones were improved from previous discriminant analysis tests. Results are shown in Table 35 and Table 36, where total correct classification was 85% for pigs separated and 92% with pigs grouped. The Jackknife classifications were also high, with the total correct classifications 77% for pigs separated and 83% for pigs combined. The largest difference between the two classification methods was 17%.

Table 35: LDA results for scores for principal components 2-4 and pig bones separated.

	Bird	**Human**	**Pig 2.1**	**Pig2.2**	**%correct**
Bird	9	3	0	0	75
Human	1	11	0	0	92
Pig 2.1	0	0	11	1	92
Pig 2.2	1	0	1	10	83
Total	11	14	12	11	85

Table 36: LDA results for scores for principal components 2-4 and pig bones combined into one group.

	Bird	**Human**	**Pig**	**%correct**
Bird	9	3	0	75
Human	0	12	0	100
Pig	1	0	23	96
Total	10	15	23	92

The smaller number of principal components used allowed for QDA to be performed on the data. QDA performed very well on the data, with results seen in Table 37 and

Table 38. The total correct classifications were 90% and 94% for pigs separated and combined respectively. Jackknife results for the QDA were also fairly high, with total correct classification at 83% for pigs separated and 88% for pigs combined. The largest difference between the jackknife classifications and the original classifications was 16%.

Table 37: QDA results for scores for principal components 2-4 and pig bones separated.

	Bird	**Human**	**Pig 2.1**	**Pig2.2**	**%correct**
Bird	9	2	0	1	75
Human	0	12	0	0	100
Pig 2.1	0	0	12	0	100
Pig 2.2	1	0	1	10	83
Total	10	14	13	11	90

Table 38: QDA results for scores for principal components 2-4 and pig bones combined into one group.

	Bird	**Human**	**Pig**	**%correct**
Bird	10	2	0	83
Human	0	12	0	100
Pig	1	0	23	96
Total	11	14	23	94

While these results were on a very small scale, they show potential for the use of LIBS and discriminant analysis for the classification of bones based on species with appropriate parameters applied.

6.2.2 Hypothesis Testing

In the previous section the application of discriminant analysis was discussed for bone samples for classification of the bones by species. In this section, the results of the nonparametric permutation test will be discussed for discrimination between bone samples.

The data set analyzed consisted of four bones, shown in Table 6. Twelve average spectra (10 shots from multiple spots on the bone averaged per spectra) were collected in random order for each sample. Analysis of bones from the same individual may be highly similar in nature which could result in high error rates if the instrumental fluctuations were not accounted for by randomizing the order of collection. The nonparametric permutation test was performed on the full spectral range (200-900nm) and the 200-500 nm spectral range.

The nonparametric permutation test was performed using the 12 choose 6 method with significance level of 0.05. Both the p-value and log p-value data was tested for discrimination capability of the individual bone samples. Results are shown in Table 39, with the best results being seen for the data collected using the reduced spectral range. For both spectral ranges the Type II error was high for the log p-value data, while the Type I error was kept approximately at or below the significance level. The p-value data had low Type I errors for both spectral ranges. The Type II error was kept below the

significance level for the 200-500 nm range, while the full spectral range had a very high Type II error.

Table 39: Nonparametric permutation test results for second set of LIBS bone spectra.

Parameters	Discrimination percent	Type II error	Type I error
200-500 nm Range P-values	95.83	4.17	0.00
Full Spectral Range P-Values	79.17	20.83	0.00
200-500 nm Range Log P-Values	83.33	16.67	8.33
Full Spectral Range Log P-Values	83.33	16.67	0.00

Based on this small test it was shown that the p-values and reduced spectral range provided better discrimination capability than the full spectral range. This is attributed to the full spectral range having peaks within the 200-500nm range which gave discrimination between the bones but also contained peaks that were found in all the bones and environment which caused problems in discriminating between them.

The data set was analyzed further by increasing the number of comparisons made in the nonparametric permutation test calculation to 100 pairwise comparisons per two samples. For example, 100 p-values were returned for comparisons of bird versus human. The increase in number of comparisons allowed for a better estimate of Type I and Type II errors. Due to the significance level being set at $\alpha=0.05$, it was necessary to perform at least 20 comparisons to truly observe the Type I error, (1 out of 5 should

result in a Type I error). The results of this data set were similar to what were seen in the smaller calculation for the 200-500 nm range p-values. The discrimination percentage between different samples was 92% with a Type I error of 6% and Type II error of 8%. The boxplot below, Figure 32, shows the distribution of the data for the 100 comparisons based on grouping them as same bone comparison or different bone comparison. Separation can be seen between the two groupings, which demonstrate the ability to discriminate bones coming from different animals by the nonparametric permutation test.

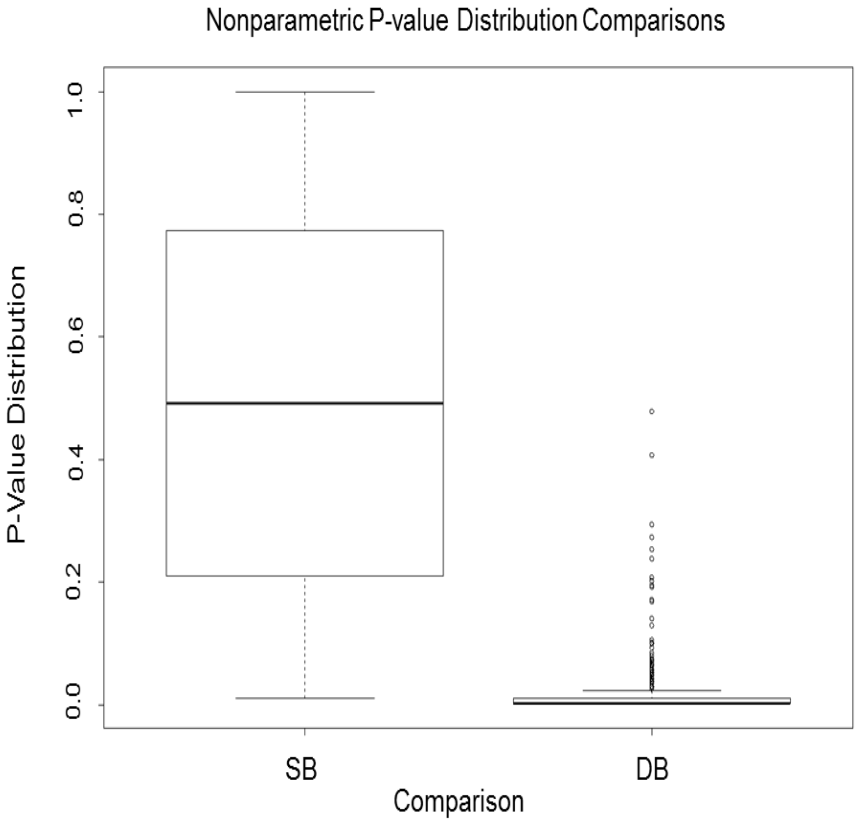

Figure 32: Boxplot illustrating the p-value distribution over same bone comparisons (SB) and different bone comparisons (DB) for 100 comparison nonparametric calculation.

6.3 Organic Compounds and Polymer Mixtures

6.3.1 LIBS

6.3.1.1 PCA/TFA

PCA was performed on the library data for both the air and argon data. For each data set three principal components were retained which kept 93% of the data for the air data set and 95% of the data for the argon data set. Figure 33 shows the loadings of the different emissions for the first three principal components for the air data. All the emissions contributed significantly and nearly equally in the first principal component, accounting for approximately 80% of the variance. The second principal component had significant contributions from the CN, C_2, and O emissions, which accounted for approximately 10% of the overall variance. The argon data, Figure 34, showed significant and nearly equal contributions of all the emissions in the first principal component. The hydrogen emission was the most significant contribution in the principal component.

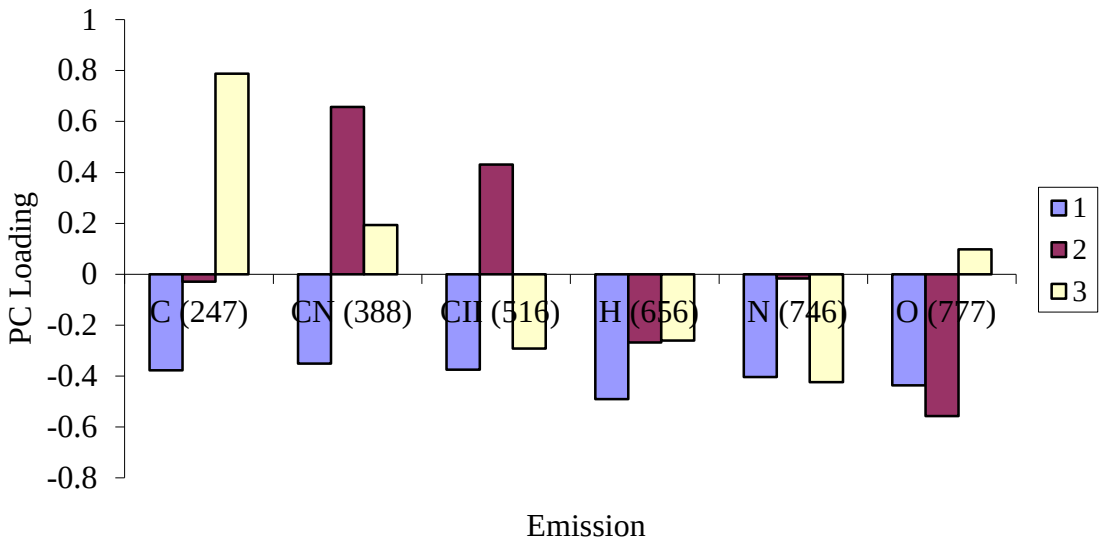

Figure 33: Loadings for air data of the specified spectral emissions for the LIBS organic polymer library.

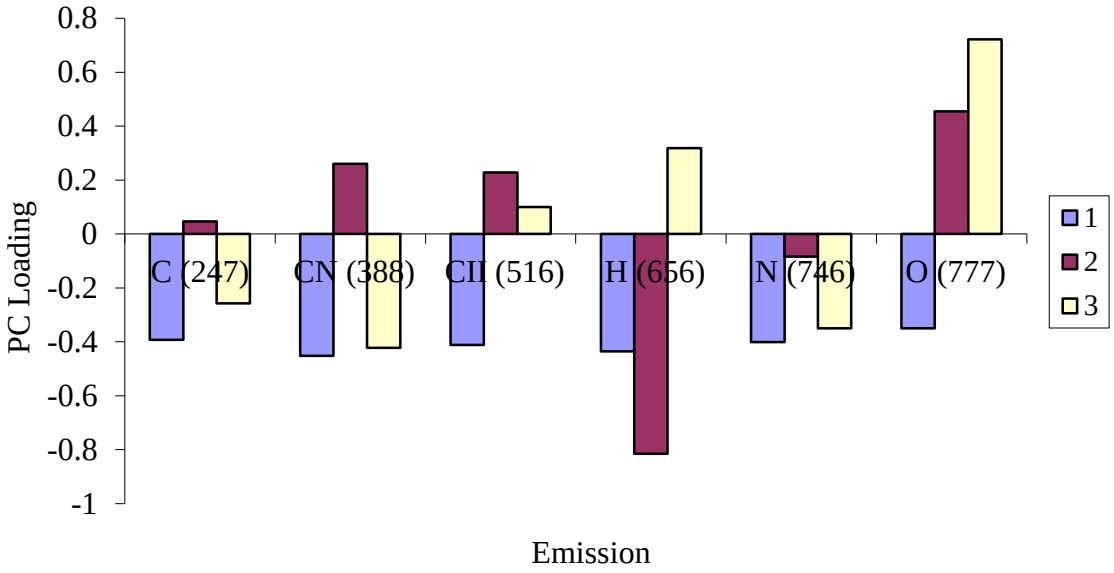

Figure 34: Loadings for argon data of the specified spectral emissions for the LIBS organic polymer library.

The first three principal component scores were plotted for each data set. Figure 35 shows the air data which exhibits no significant separation of the poly acrylonitrile (AN) and poly styrene (PS) library scores. The nitrocellulose (NC) library scores were slightly separated to the right of the plot. The nitrocellulose likely differed from the other two compounds as it contains a large number of nitrogen and oxygen groups, while poly styrene contains only carbon and hydrogen and poly acrylonitrile contains carbon, hydrogen and nitrogen. The structures are shown in Figure 36. The CN contribution in the poly styrene was attributed to the interaction with the nitrogen in the air, therefore giving it the same elements as poly acrylonitrile.

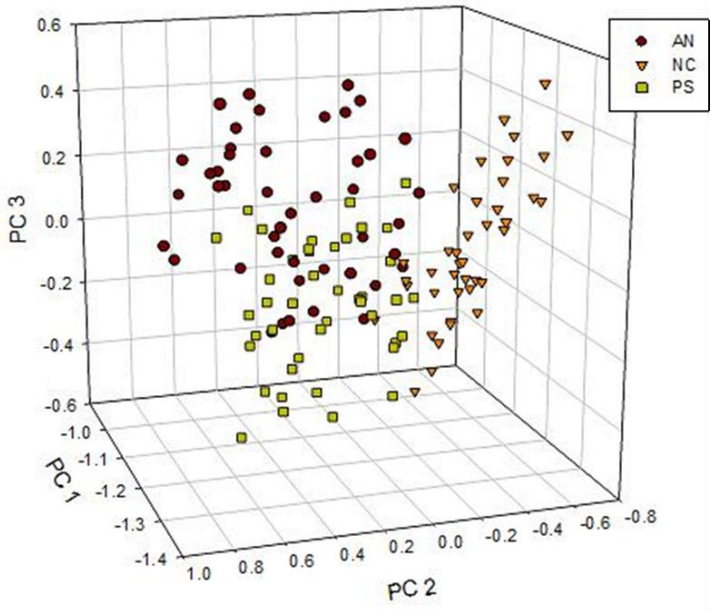

Figure 35: Scores plot for air library data.

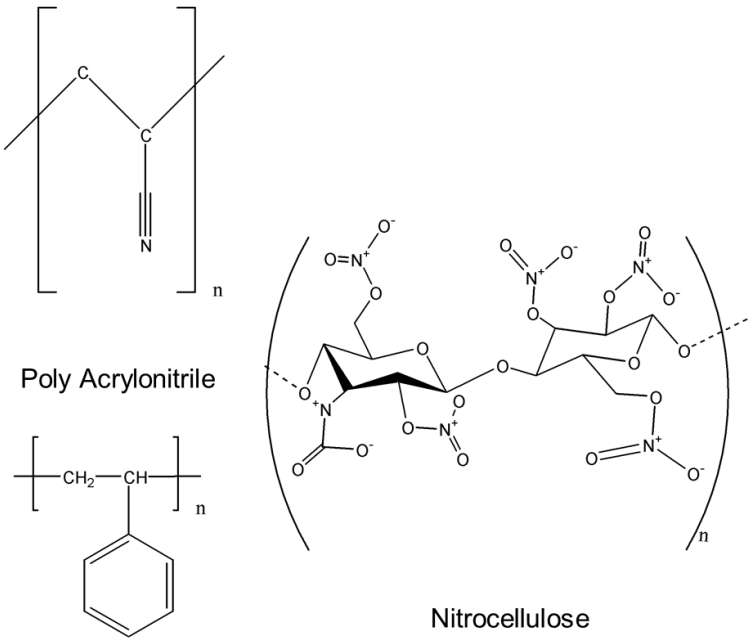

Figure 36: Organic compound structures for LIBS analysis.

The argon data, shown in Figure 37, had separation between the poly acrylonitrile, nitrocellulose, and poly styrene library scores. The interactions of the compounds with the air were not present in this data analysis, therefore each compound differed in elemental composition with poly styrene only having carbon and hydrogen, poly acrylonitrile having carbon, hydrogen and nitrogen, and nitrocellulose having carbon, hydrogen, nitrogen and oxygen. The differences in the elemental composition of the compounds resulted in the separation seen.

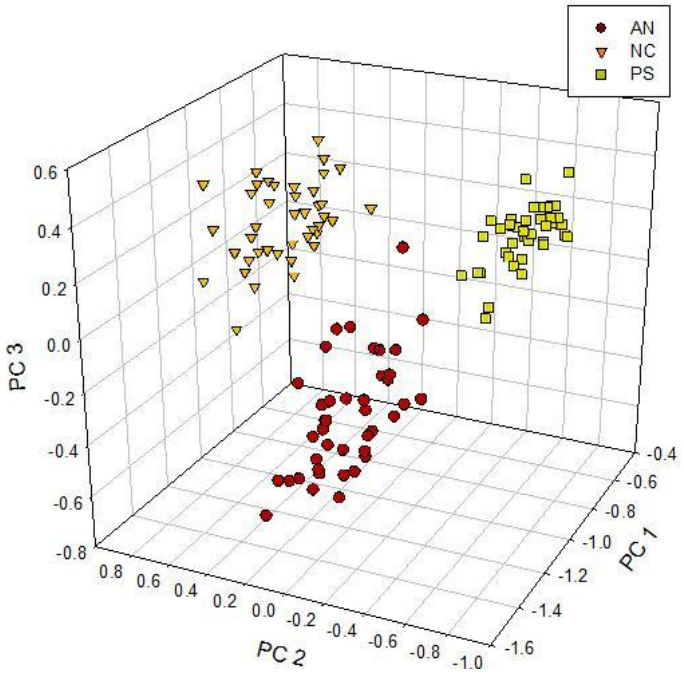

Figure 37: Scores plot for argon library data.

Using the library scores a model was created to project scores for the mixture data. The mixture data was multiplied by the transpose eigenvectors of the library to provide the projected mixture scores. This allowed for these projected scores to be plotted over the library clusters. Both the air and argon data set mixtures were projected for the poly acrylonitrile/poly styrene mixture and the nitrocellulose/poly styrene mixture.

Figure 38 shows the poly acrylonitrile/poly styrene mixture projected scores for the air data. As can be seen, the projected mixture scores fall outside the library clusters. The nitrocellulose/poly styrene mixture in air scores fell within the model scores, though

most of them fell among the poly styrene and poly acrylonitrile model scores, as seen in Figure 39. Some projected scores fell within the library model nitrocellulose scores.

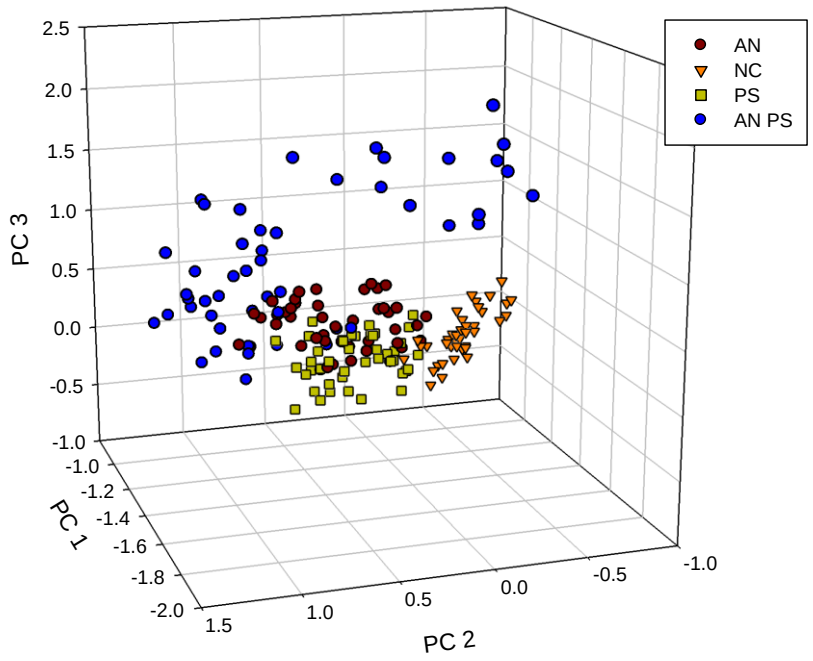

Figure 38: Poly acrylonitrile/poly styrene mixture in air projected scores plotted on the library model.

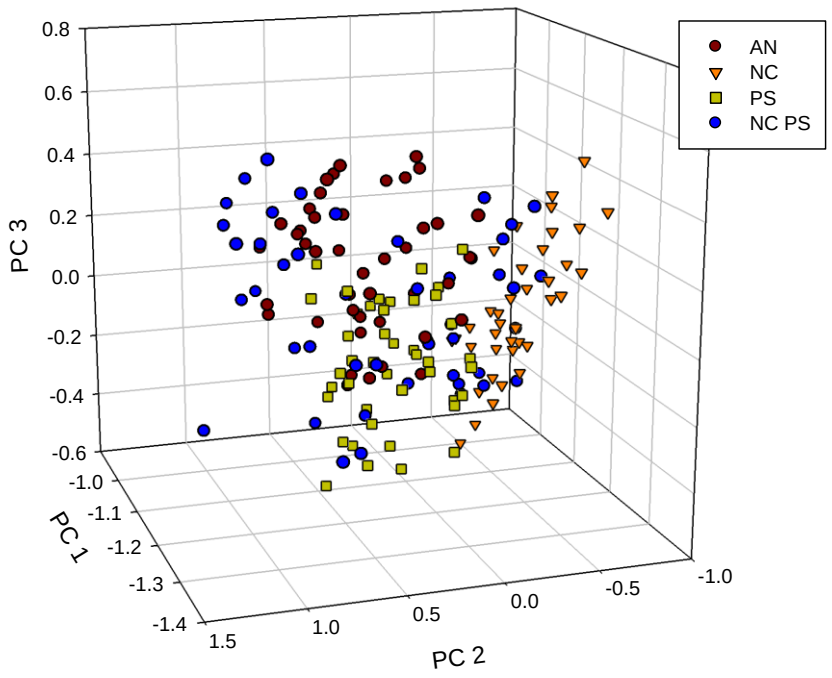

Figure 39: Nitrocellulose/poly styrene mixture in air projected scores plotted on the library model.

The projected scores for the poly acrylonitrile/poly styrene mixture collected in argon are shown in Figure 40. As can be seen, the projected scores fell mostly over the library poly styrene cluster with a few of the scores stretching out over the poly acrylonitrile library cluster. The nitrocellulose/poly styrene mixture projected scores also fell within the library poly styrene and nitrocellulose clusters, as shown in Figure 41.

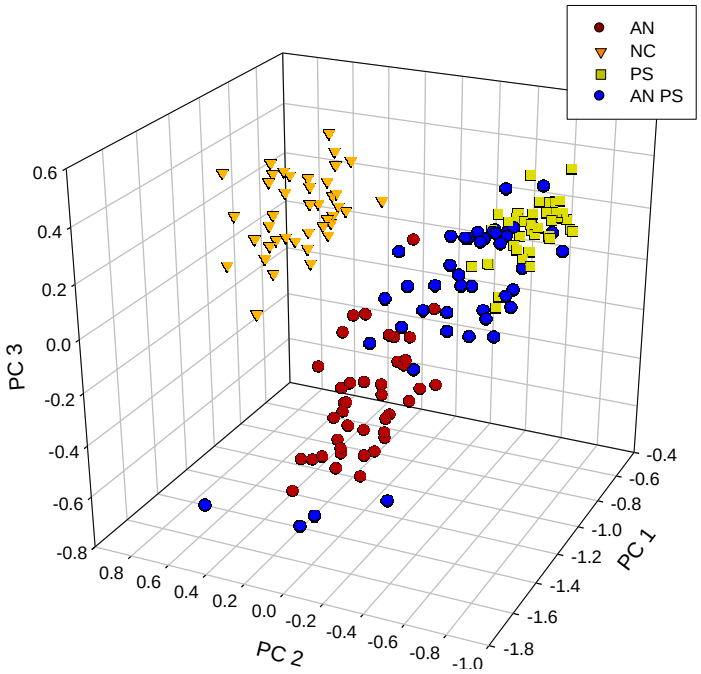

Figure 40: Poly acrylonitrile/poly styrene mixture in argon projected scores plotted on the library model.

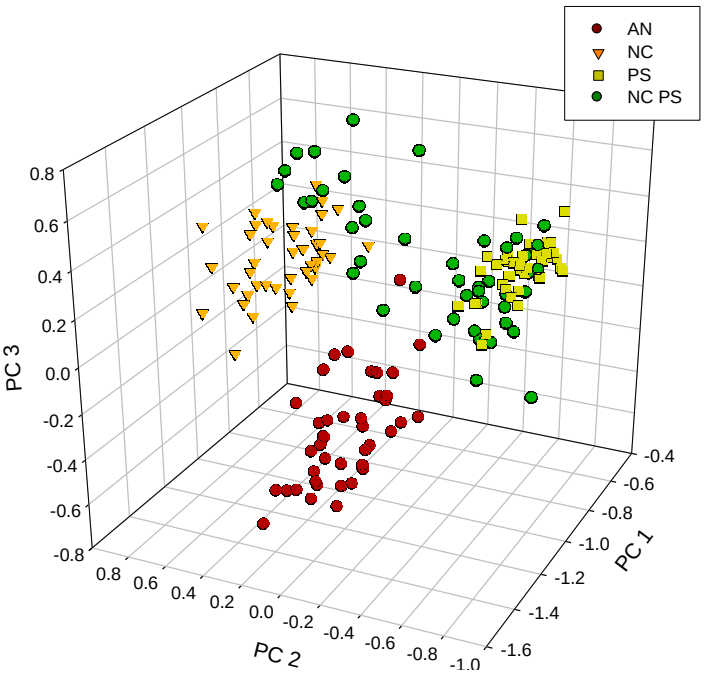

Figure 41: Nitrocellulose/poly styrene mixture in argon projected scores plotted on the library model.

TFA analysis was then performed on the individual mixture reduced data for both the air and argon data sets. The correlations for the two mixtures in air are listed in Table 40. Poly styrene was present in each mixture, but the model did not separate the poly acrylonitrile and poly styrene scores well. Therefore, the correlations between the test and resulting vectors for the poly acrylonitrile/poly styrene mixture do not show a strong prediction for either polymer present in the mixture. The nitrocellulose/poly styrene mixture had better results with an average correlation of 0.87 for nitrocellulose and 0.73 for poly styrene. These correlations give a stronger indication of the presence of nitrocellulose in the mixture. While poly styrene had a higher correlation than poly acrylonitrile, they were still close. This is attributed to the lack of separation of these two polymers in the PCA model.

Table 40: TFA correlation values for two mixtures in air.

Test Vector	**Nitrocellulose/Poly styrene Average Correlation**	**Poly acrylonitrile/Poly styrene Average Correlation**
Poly acrylonitrile	0.518	0.569
Nitrocellulose	0.870	0.333
Poly styrene	0.734	0.354

The TFA analysis for the individual mixture spectral data in argon performed better than the air, as seen in Table 41. For both the poly acrylonitrile/poly styrene and the nitrocellulose/poly styrene mixtures poly styrene had the highest correlation. This is expected as both mixtures had poly styrene as the base polymer and a strong overlap

was seen for the projected scores with the library model for poly styrene. The nitrocellulose/poly styrene mixture had lower correlations observed for the nitrocellulose component, 0.73, but a significantly lower correlation for the poly acrylonitrile, 0.017. The low poly acrylonitrile correlation indicated there was no contribution from that compound while contributions for the nitrocellulose and poly styrene are being observed. The poly acrylonitrile/poly styrene mixture did not perform as well with a correlation of 0.34 for poly acrylonitrile and 0.10 for nitrocellulose. While poly acrylonitrile did have a slightly higher correlation than nitrocellulose it is expected with additional analysis only poly styrene would be identified.

Table 41: TFA correlation values for two mixtures in argon.

Test Vector	**Nitrocellulose/Poly styrene Average Correlation**	**Poly acrylonitrile/Poly styrene Average Correlation**
Poly acrylonitrile	0.017	0.338
Nitrocellulose	0.734	0.100
Poly styrene	0.925	0.967

6.3.1.2 Bayesian Decision Theory

The Bayesian decision theory was applied to the LIBS organic polymer library and mixture data to obtain posterior probabilities. It was determined a lower correlation cutoff of 0.8 with a significance level of 0.05 was the most appropriate for the data analysis, therefore the results discussed below were all acquired using these

parameters. Bayesian decision theory results were obtained for the air and argon data for each of the two polymer mixtures.

The air data for the poly acrylonitrile on poly styrene was obtained using one component and 81% of the variance. The only compound demonstrating a posterior probability at the given parameters was poly acrylonitrile, with a posterior probability of 1. Figure 42 below shows the kernel distributions of the correlations with respect to the posterior probabilities. Broad curves were seen for the kernel distributions due to setting the bandwidth, *h*, equal to 0.05 rather than calculating a value based on the distribution of *r* values. The mixture correctly classified one of the components of the mixture. Interestingly, it did not classify the base polymer which was present in the sample at a much greater quantity.

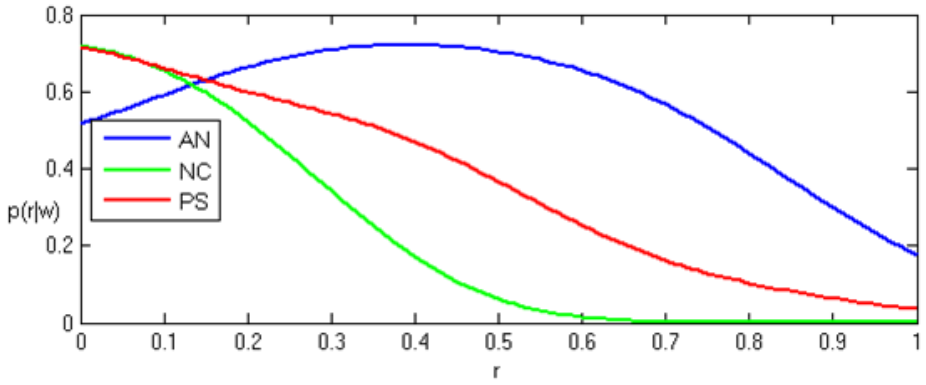

Figure 42: Correlation versus posterior probability distribution plot for poly acrylonitrile on poly styrene thin film mixture in air.

The second mixture in air, nitrocellulose on poly styrene performed well. All three library compounds had contributions when two principal components were used with 99% of the variance. While all three library compounds had posterior probabilities greater than 0, poly acrylonitrile had a posterior probability of 0.13 while the two other compounds present in the mixture had posterior probabilities that were higher and approximately equal. Nitrocellulose had a posterior probability of 0.45 and poly styrene had a posterior probability of 0.42. Figure 43 shows the kernel distribution of the classes where the nitrocellulose and poly styrene distributions are seen to be approximately equal in contribution.

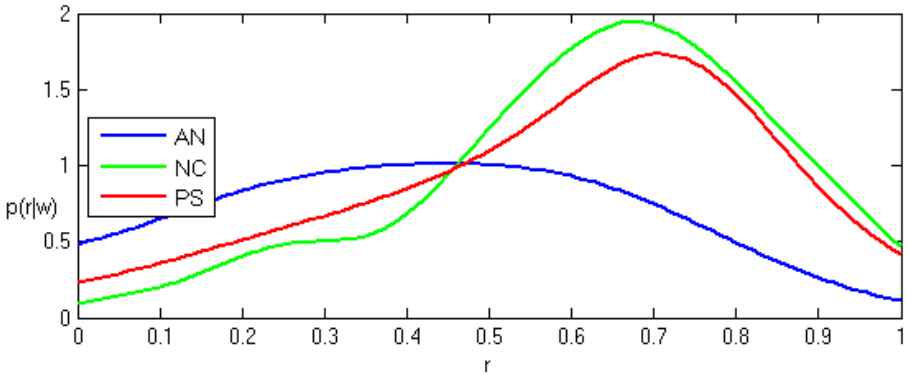

Figure 43: Correlation versus posterior probability distribution plot for nitrocellulose on poly styrene thin film mixture in air.

Next the data collected in the argon atmosphere was analyzed using the Bayesian decision theory. The poly acrylonitrile on poly styrene mixture used two principal components containing 99% of the variance for the analysis. Figure 44 below shows

the kernel distributions for the library compounds corresponding to the contributions observed in the mixture. The poly acrylonitrile did not have a posterior probability calculated at the set parameters; therefore its contribution to the mixture would remain unclassified. The poly styrene had the highest posterior probability of 0.77 and nitrocellulose had a low posterior probability of 0.23. Poly styrene was the base polymer and present in the largest quantity for the mixture which was attributed to it having the high posterior probability observed. Based on these results the test was capable of classifying one of the mixture components with the second component remaining unclassified.

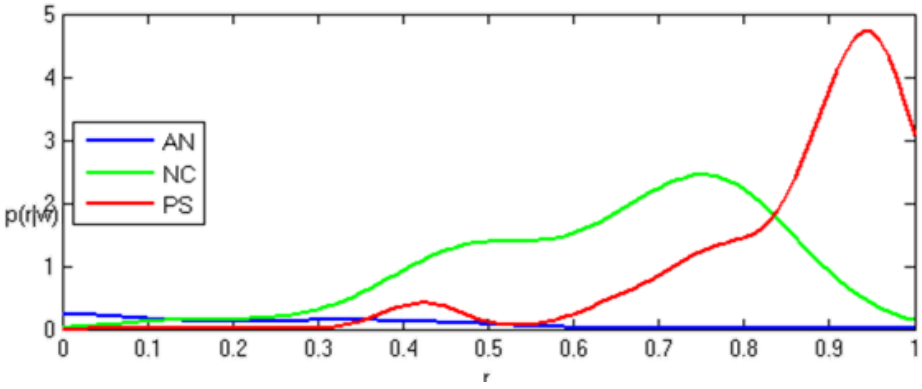

Figure 44: Correlation versus posterior probability distribution plot for poly acrylonitrile on poly styrene thin film mixture in argon.

The final mixture, nitrocellulose on poly styrene, also used two principal components containing 99% of the variance for the analysis. The two compounds present in the mixture had posterior probabilities greater than zero, with the poly acrylonitrile not

contributing at the specified parameters. The nitrocellulose had a low posterior probability of 0.15 while the poly styrene had a high posterior probability of 0.85. The higher posterior probability for poly styrene is attributed to it being the base polymer and being present in a greater amount. Figure 45 shows the kernel distributions for the library compounds corresponding to the mixture and it can be seen that both nitrocellulose and poly styrene have contributions above the 0.8 correlation cutoff. Both components of the mixture would have been classified at the parameters set forth for this test.

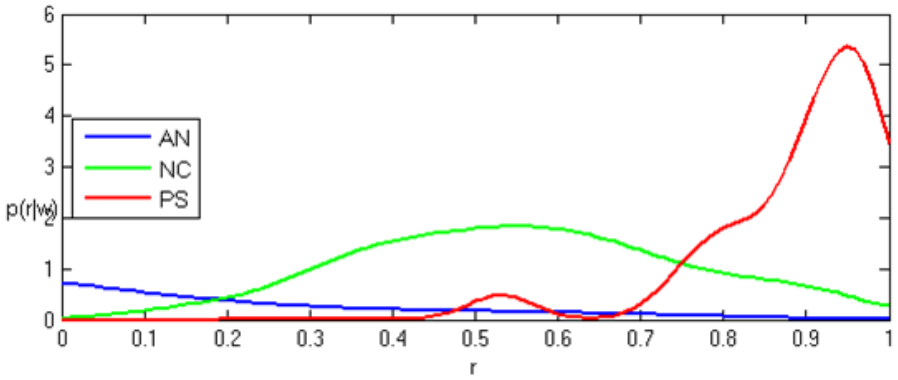

Figure 45: Correlation versus posterior probability distribution plot for nitrocellulose on poly styrene thin film mixture in argon.

The calculations for the Bayesian decision theory demonstrates the difficulty associated with classifying organic LIBS data. As has been observed from the tests to this point, the similarity of the sample spectral contributions cause difficulty in classifying. The argon data performed very well for the classification of the poly styrene data which is

attributed to the large contribution of this compound in the mixture as it was the base polymer. The polymers applied on top of the base polymer were not as successfully detected, which was attributed to poor contribution from these compounds in the spectral data. The air data demonstrated overall lower results which were attributed to the interaction of the plasma with the air atmosphere.

6.3.2 FTIR

6.3.2.1 PCA/TFA

PCA was performed on the library of organic compounds prior to analysis of the mixtures to observe whether grouping occurred between the library compounds. If grouping did not occur for the library compounds it would be unlikely that the TFA would perform well for the mixture samples. The analysis was performed independent of the background as the library did not include the background samples. Eigenvalues were obtained which defined the amount of variance retained by each principal component. The first six principal components contained 95% of the data variance, shown in Table 42.

Table 42: Variance contained in principal components for PCA of FTIR library.

Principal Component	Cumulative variance
1	0.632
2	0.765
3	0.854
4	0.917
5	0.946
6	0.963

To determine the spectral characteristic contributing to this variance, the eigenvectors corresponding to the first seven principal components were plotted in Figure 46. As can be seen a great deal of spectral characteristics were observed for the spectral range of 600-2000cm^{-1}. The plot shows that the eigenvectors corresponding to the principal components of five and six begin to incorporate some noise along with spectral characteristics. Figure 47 shows the eigenvectors corresponding to principal components one through four, which shows characteristic spectral peaks with reduced amount of noise.

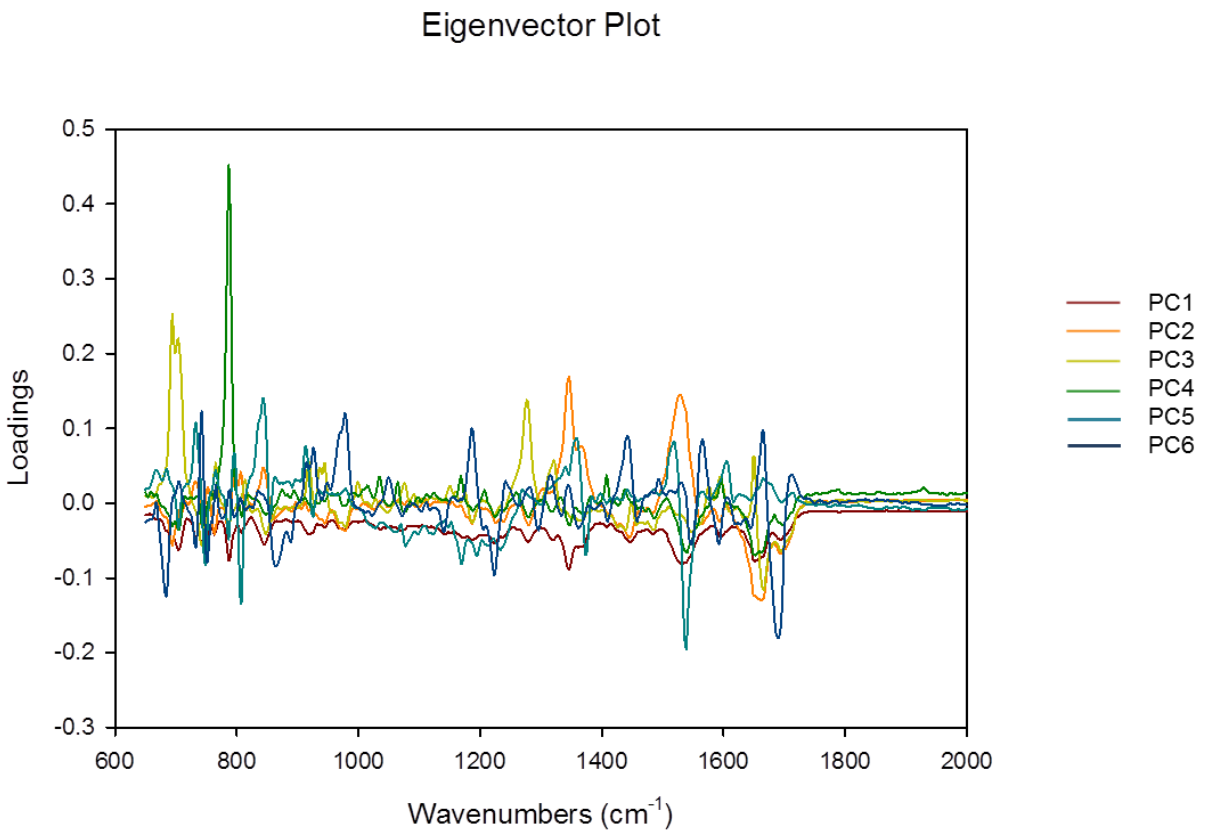

Figure 46: Eigenvectors corresponding to the first seven principal components for the FTIR library.

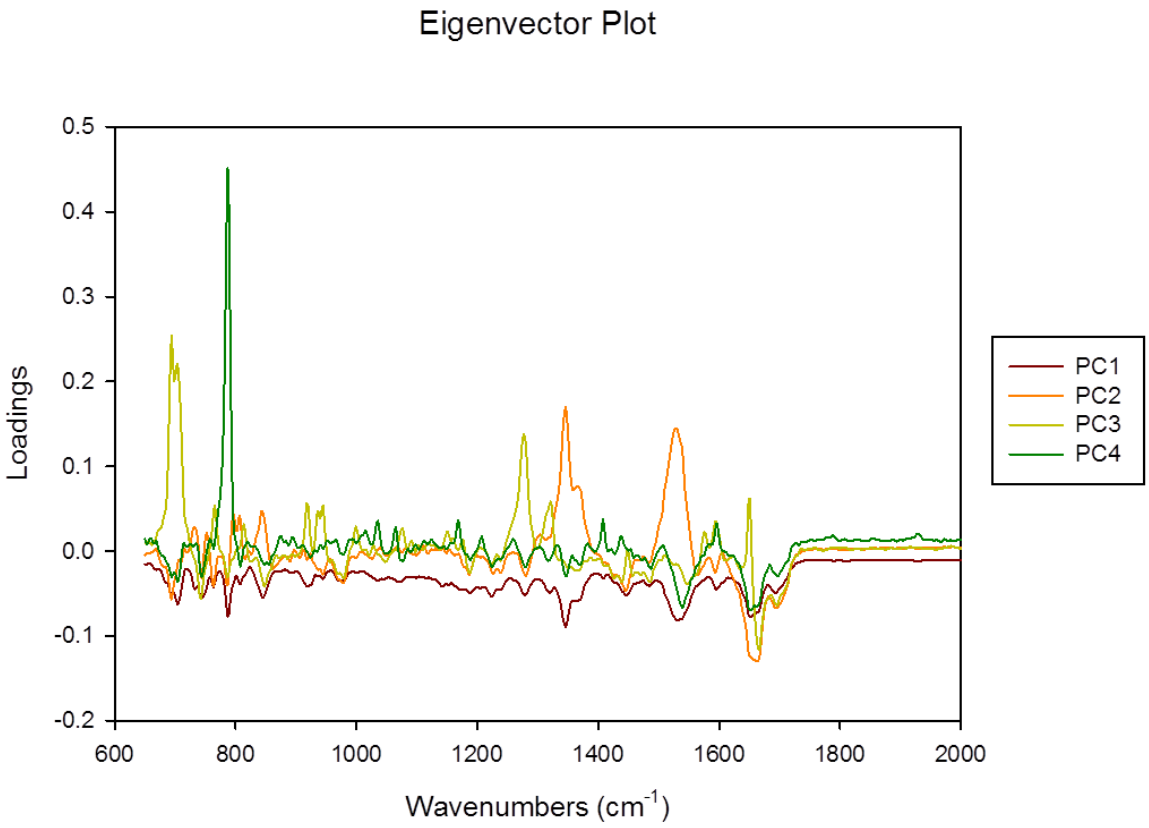

Figure 47: Eigenvectors corresponding to the first four principal components for the FTIR library.

The first principal component contains contributions from peaks in the fingerprint region, attributed to the C-H aromatic ring bends in the dinitrotoluene compounds. It also shows contributions in the spectral range of 1300 to 1700 cm^{-1}, which contained characteristic peaks for all of the library compounds. The second principal component did not show as much contribution within the fingerprint region but show stronger contributions in the 1300 cm^{-1} and 1500 cm^{-1} region which are attributed to the nitro groups of the dinitrotoluene compounds. The third principal component also had contributions within the range of the 1300 cm^{-1} and 1500 cm^{-1}. In addition it showed a

contribution from the alkene C=C and C=O stretches in the region of 1600 to 1700 cm^{-1}. The fourth principal component showed a strong contribution in the 700 cm^{-1} range which was seen in many of the compounds, which was attributed to the C-H aromatic stretches. It also had a contribution around the 1700 cm^{-1} range, again from the C=C and C=O stretching. The first four principal components appear to encompass contribution from all of the library compounds.

The scores were plotted for the first three principal components as it is difficult to visualization larger dimensions. Figure 48 demonstrates the initial separation being observed in the first three principal components which shows clustering into three groupings. The groupings show promise for the application of the library to mixture samples to obtain identification of individual compounds present in the mixture.

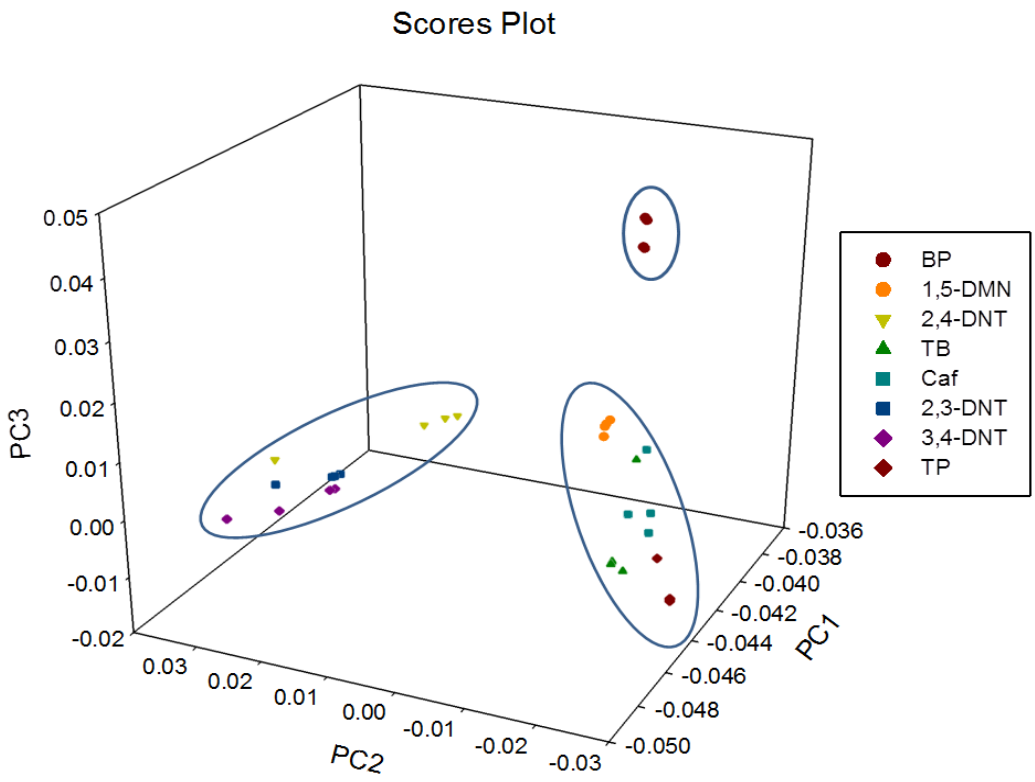

Figure 48: Scores corresponding to the first three principal components for the FTIR library.

The first grouping fell to the bottom left of the plot and contained three compounds: 2,3-DNT, 2,4-DNT, and 3,4-DNT. It was expected these three compounds would cluster together as they differ only by the position of the nitro groups, as shown in Figure 49. While there was clustering of these compounds away from the other library compounds there was also separation of these compounds within the cluster, indicating the probability of differentiation between these compounds.

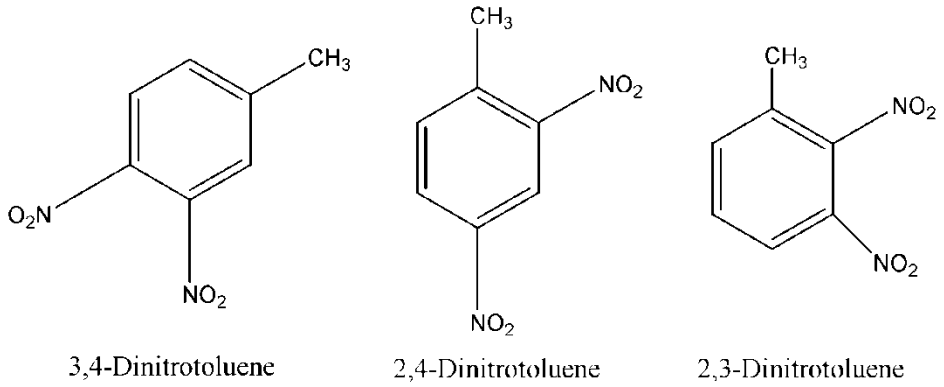

Figure 49: Library compounds in second grouping of FTIR scores plot.

The second grouping in the scores plot fell in the bottom right of the plot and contained the library compounds: 1,5-DMN, theobromine, caffeine and theophylline. Within this cluster there was also separation of the compounds. Theobromine, caffeine, and theophylline, which differ by number of and position of methyl groups, shown in Figure 50, show some separation between each compound. The 1,5-DMN fell at the top of the cluster separated slightly from the other three compounds. The final cluster contained only benzophenone, shown in Figure 52, and fell in the upper right portion of the plot.

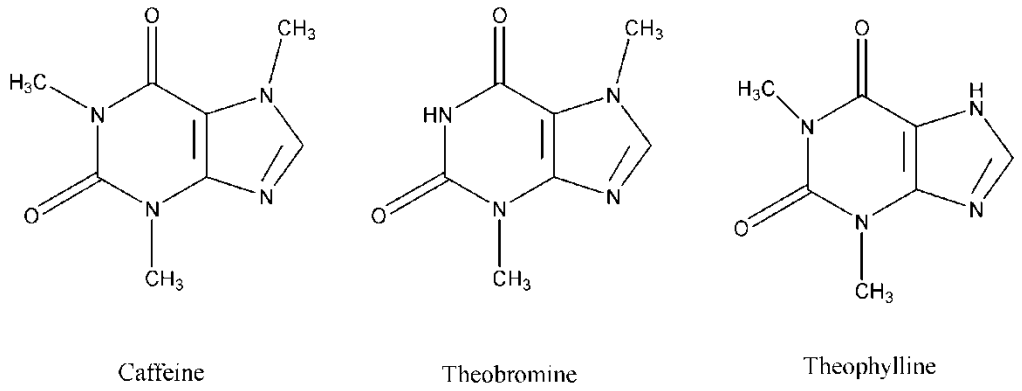

Figure 50: Library compounds in one section of the third grouping of FTIR scores plot.

TFA was performed on the normalized data from the mixture to provide correlation. DRMAD was used to determine the number of principal components that were retained for the analysis of each of the mixtures.

The first mixture was 2,4-DNT on a white car paint sample. Six principal components were retained which accounted for 99% of the variance. Results showed the highest correlations for the 2,4-DNT, with an average correlation of 0.961. The next highest correlation was 0.814 for 3,4-DNT, which showed separation of the compound present in the mixture from the other library compounds despite the similarity in structure of some of the compounds. As can be seen in Figure 51, 2,4-DNTand 3,4-DNT differ only in the placement of one of the nitro groups.

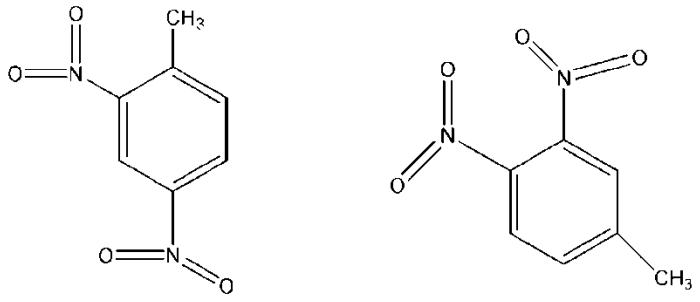

Figure 51: 2,4-dinitrotoluene and 3,4-dinitrotoluene structures.

The second mixture was benzophenone on a white car paint sample. Two principal components were retained for the analysis which accounted for 96% of the variance. The highest correlation was for benzophenone, with an average correlation of 0.923. All other library compound correlations fell much lower; the closest was caffeine with a correlation of 0.308. The library did not contain a compound with a structure similar to benzophenone, seen in Figure 52, which was apparent by the significantly lower correlations seen for the remaining library compounds.

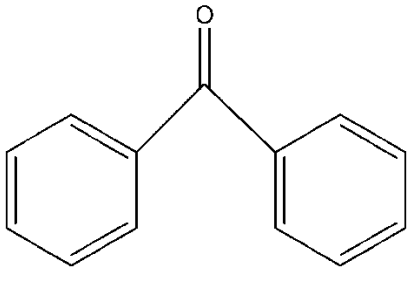

Figure 52: Structure of benzophenone

For the mixture of caffeine and fingerprint oil on glass four principal components were retained to account for 99% of the variance. Caffeine had the highest correlation with an average correlation of 0.892. The two closest library correlations were at 0.715 for theobromine and 0.688 for theophylline which are both one methyl group different in structure from caffeine, shown in Figure 50. Again, this mixture demonstrates separation of the organic compounds despite the similarity in structure.

TB and fingerprint oil on a white car paint was the final mixture. Two principal components were retained which accounted for 98% of the variance. The highest correlation was for TB at 0.525. As was seen with the caffeine mixture, the closest correlations were for the two compounds with similar structures, caffeine (0.473) and theophylline (0.328). Overall, the correlations were lower for this mixture which indicates low spectral contributions from the organic compound in the mixture.

The results of these mixtures demonstrate separation of the different organic compounds by PCA\TFA analysis despite library samples of similar structure and background contributions. As FTIR is a molecular spectroscopy technique the structures with differences in only the position of the functional groups could be distinguished between.

6.3.2.2 Bayesian Decision Theory

The Bayesian decision theory was applied to the library and mixture data to obtain posterior probabilities. This was done as there were multiple spectra collected for each mixture which contained varying contributions of the organic compounds and the backgrounds. It was determined a lower correlation cutoff of 0.8 with a significance level of $\alpha=0.05$ was the most appropriate for the data analysis; therefore the results shown below were acquired using these parameters.

The first mixture analyzed was the benzophenone in a fingerprint on car paint. The plot in Figure 53 shows the distributions for the library compounds corresponding to this mixture. As can be seen, the distribution for benzophenone falls above the lower correlation cutoff of 0.8 and the remaining compounds fall below. The posterior probability for benzophenone was calculated to be 1. This was calculated using one principal component, which contained 89% of the variance. The remaining library compounds did not reach the criteria for calculation of posterior probabilities. Therefore, benzophenone was the only compound that would have a probability of classification for this mixture.

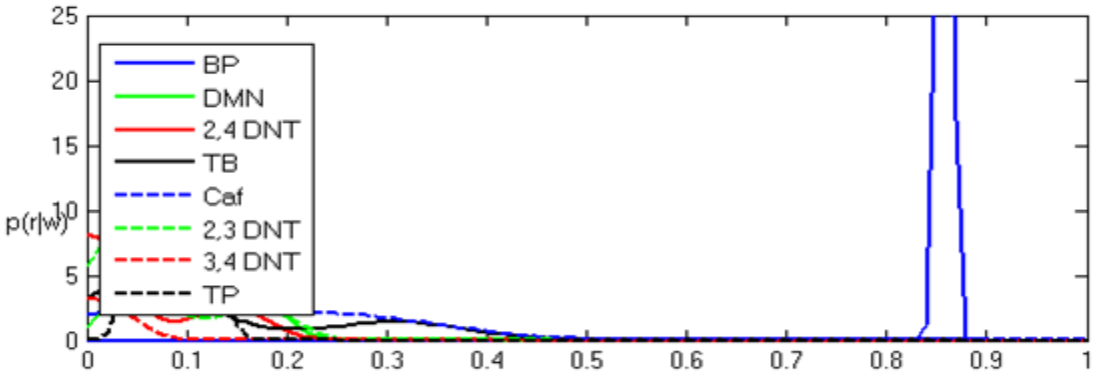

Figure 53: Correlation versus posterior probability distribution plot for benzophenone in a fingerprint on a car paint mixture.

The second mixture analyzed was the caffeine in fingerprint oil on a glass slide. This mixture had the highest posterior probability for caffeine of 0.88 and a small posterior probability of theobromine, 0.12. Figure 54 shows the caffeine distribution falling just below a 0.9 correlation. A small amount of the theobromine curve falls above the lower correlation cutoff of 0.8. Theobromine and caffeine are very similar in structure which has been shown in previous sections which explains the presence of theobromine. Three principal components were used for this analysis and encompassed 99% of the variance. Again, the result showed the correct classification of the compounds present in the mixture.

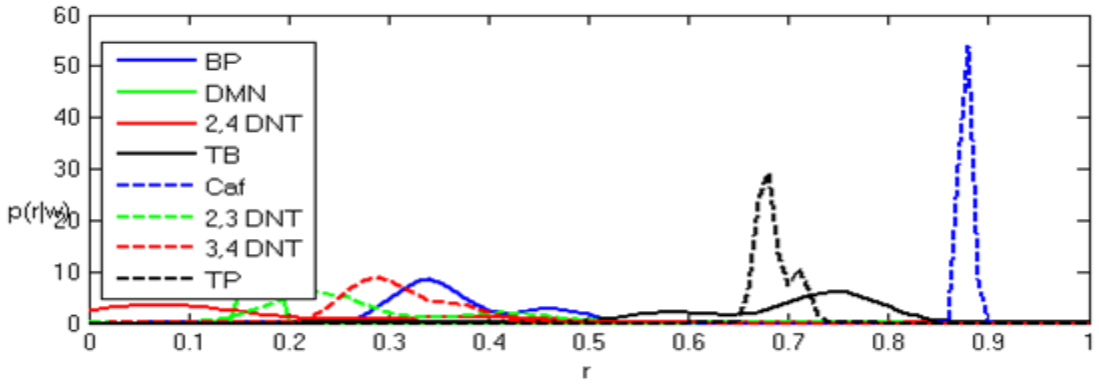

Figure 54: Correlation versus posterior probability distribution plot for caffeine in fingerprint oil on a glass slide mixture.

The 2,4-DNT in fingerprint oil on car paint mixture performed similarly to the caffeine mixture. The 2,4-DNT had distributions falling above the lower correlation cutoff of 0.8 as shown in Figure 55. In addition to 2,4-DNT, part of the distribution for 3,4-DNT fell above the lower correlation cutoff. Both had posterior probabilities calculated, with 2,4-DNT having a posterior probability of 0.57 and 3,4-DNT having a posterior probability of 0.43. Five principal components were used in the analysis with 99 % of the variance being accounted for. The contribution of the 3,4-DNT is attributed to the similarity of it in structure to the 2,4-dinitrotoluene.

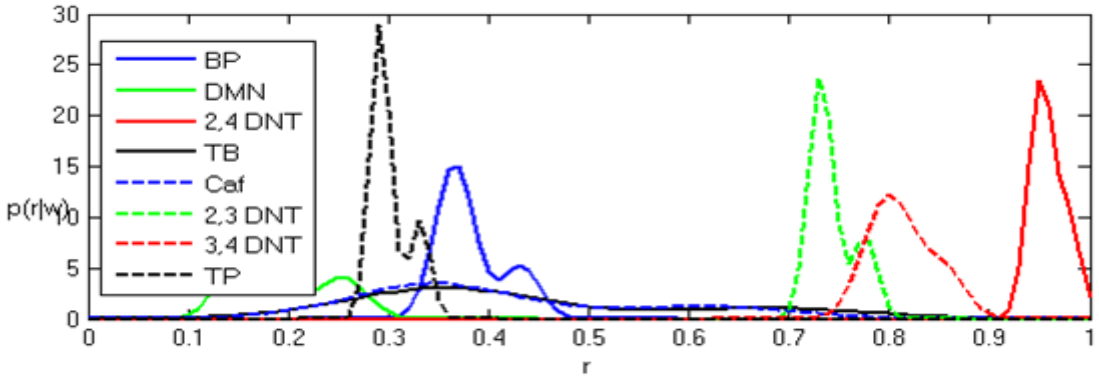

Figure 55: Correlation versus posterior probability distribution plot for 2,4-dinitrotolune in fingerprint oil on car paint mixture.

The final mixture for analysis was the theobromine in fingerprint oil on a car paint. This mixture did not perform as well as the previous mixtures with none of the distributions falling above the criteria for calculation of posterior probabilities, shown in Figure 56. As previous tests have shown, this indicates the theobromine was not present at a large enough quantity for detection. The analysis was performed with one principal component which encompassed 96% of the variance.

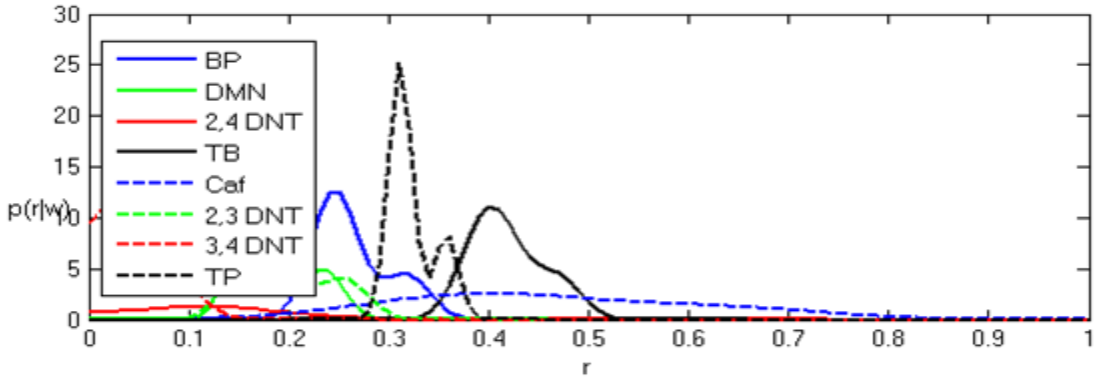

Figure 56: Correlation versus posterior probability distribution plot for theobromine in fingerprint oil on car paint mixture.

The Bayesian decision theory performed well for these mixtures with only one mixture not classifying its organic component and one mixture having a posterior probability calculated for a compound not present in the mixture.

6.3.3 Raman

6.3.3.1 PCA/TFA

The PCA analysis of the library samples provided information on the distribution of the spectral range throughout the eigenvectors and the clustering of the library compound scores. For the PCA, twelve principal components were necessary to retain 95% of the variance, with the cumulative percent of the principal components shown in Table 43.

Table 43: Percent of variance contained in each principal component for Raman library data.

Principal Component	Cumulative %
1	0.259
2	0.507
3	0.613
4	0.691
5	0.762
6	0.826
7	0.867
8	0.897
9	0.915
10	0.932
11	0.948
12	0.959

Eigenvector plots were prepared to observe the spectral contribution per principal component. Figure 57 shows the eigenvector plot for the first 12 principal components. As can be seen a great deal of the spectral peaks are accounted for in the region of 200 to approximately 1500 cm^{-1} and in the 3000cm^{-1} region. Most of the library compounds contained spectral peaks that were observed in those spectral regions. The variance for the first 12 principal components appears to be comprised of characteristic spectral peaks of the library compounds with little to no noise. Contributions from 600-800 cm^{-1} were seen corresponding to aromatic C-H stretching in a few of the principal components. Also around 900 cm^{-1}, strong contributions were observed for the Cl-O stretching. Contributions were seen in a few of the principal components in the 1300 cm^{-1} which were attributed to the amide C-N, nitro, and alkane C-H groups. The other nitro stretch was also observed in quite a few of the principal components in the 1500 cm^{-1} range. Principal component seven had a high contribution from the C=O and aromatic ring C=C in the range of 1500 to 1700 cm^{-1}. The final group of contributions was seen in the range of 3000 cm^{-1} and was attributed to the amide N-H (3300 cm^{-1}), alkane C-H (2850 cm^{-1}) and aromatic C-H (3010 cm^{-1}).

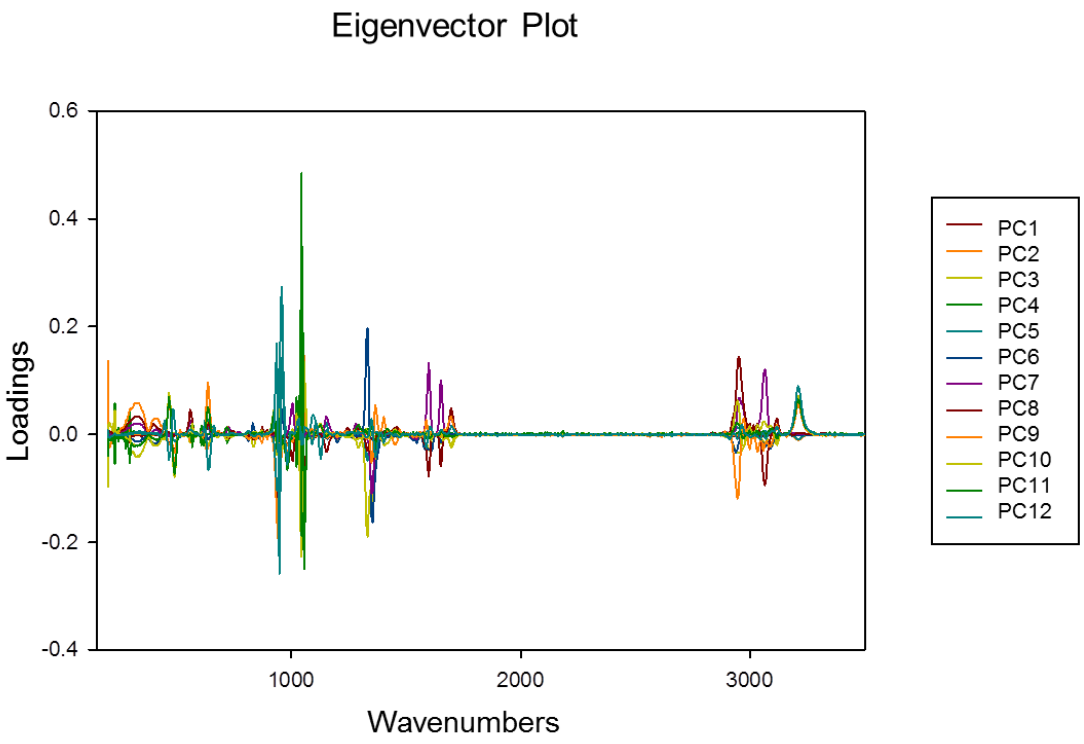

Figure 57: Eigenvector plot for first 12 principal components for the Raman library.

As a plot of twelve dimensions would be difficult to observe, therefore a scores plot of the first three principal components was plotted, Figure 58, to observe if any separation was seen between the library compounds. The plot demonstrates the initial separation into four groups. The upper left of the plot shows grouping of five compounds: potassium chlorate, sodium chlorate, potassium perchlorate, ammonium perchlorate, and sodium perchlorate. These five compounds, shown in Figure 59, are similar in structural components as they contain a chlorate or perchlorate.

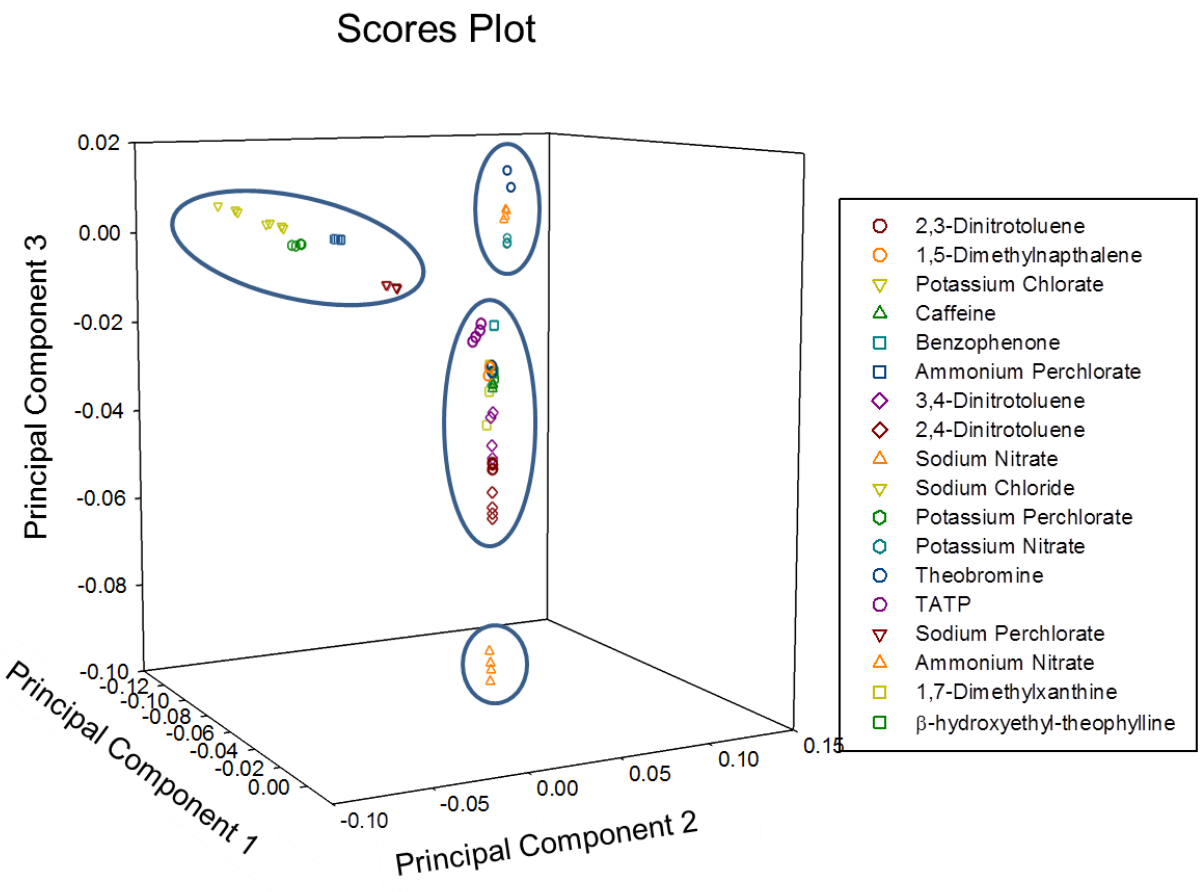

Figure 58: Scores plot of first 3 principal components for the Raman library.

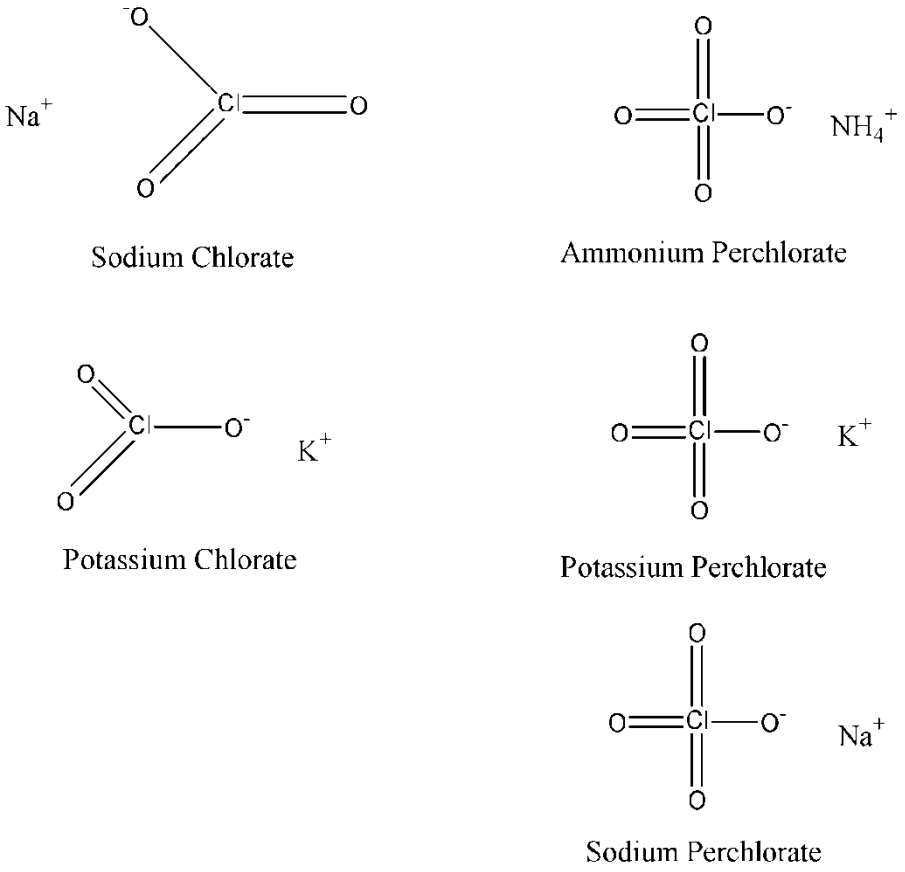

Figure 59: Compounds in group one of library score plot.

The second group clustered in the upper right of the plot showed grouping of three compounds: theobromine, ammonium nitrate, and potassium nitrate. These compounds, shown in Figure 60, consist of nitrates and an alkaloid.

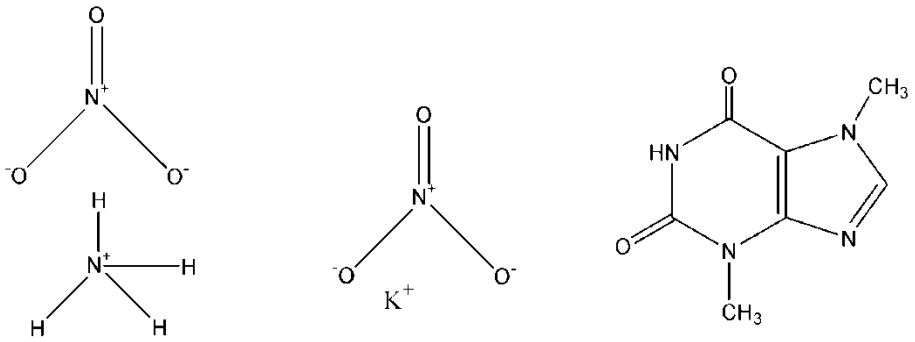

Figure 60: Compounds in group two of library scores plot.

The third grouping contained at the bottom center of the plot showed only sodium nitrate. This compound, shown in Figure 61, was significantly separated from the other nitrate compounds.

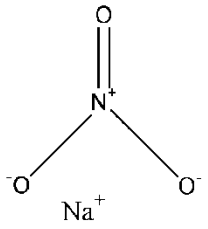

Figure 61: Compound in group three of library scores plot.

The final cluster of compounds fell in the middle of the plot and contained the remaining nine compounds. The compounds, shown in Figure 62, included aromatic and peroxide compounds. This plot only shows the first three principal components, containing only 61% of the data variance, but it showed promise of separation of the library compounds.

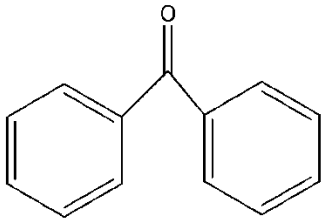

Benzophenone

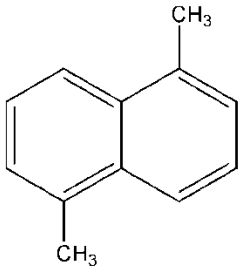

1,5-Dimethylnaphthalene

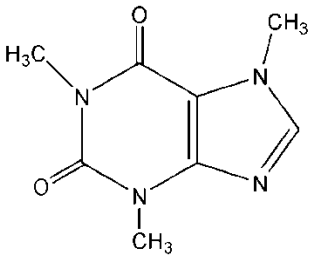

Caffeine

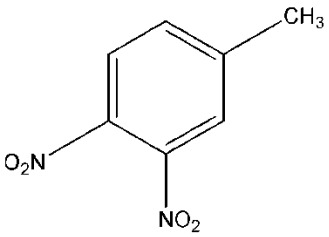

3,4-Dimethylnitrotoluene

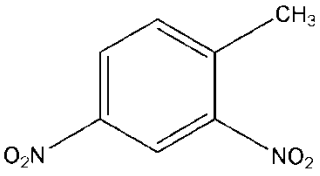

2,4-Dimethylnitrotoluene

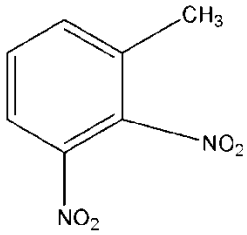

2,3-Dimethylnitrotoluene

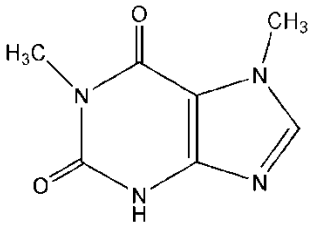

1,7-Dimethylxanthine

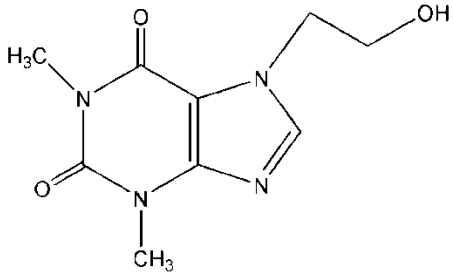

B-Hydroxyethyl-theophylline

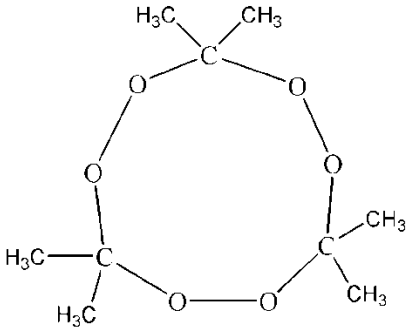

Triacetone Triperoxide

Figure 62: Compounds in group four of library scores plot.

The TFA data of the mixtures provided correlation values for the identification of the components present in the mixture. As mentioned in the experimental section, the number of principal components retained corresponded to keeping 95% of the variance. The substrate and fingerprint oils were not included in the library for the analysis, which allowed for the identification of the organic compounds independent of the background.

The TFA for the first mixture, ammonium nitrate in fingerprint oil on a glass slide required the retention of two principal components to keep 95% of the variance. The highest average correlation was seen for ammonium nitrate, 0.989. All other correlations fell much lower, with the closest being seen for potassium nitrate at 0.743.

The next mixture, 2,4-DNT in fingerprint oil on a glass slide also required two principal components to keep 95% of the variance. The highest correlation was seen for 2,4-DNT, 0.843. Again, the highest correlation corresponded correctly to the component present in the mixture. The two closest correlations were the other two dinitrotoluene compounds in the library: 2,3-DNT at 0.6312 and 3,4-DNT at 0.559. Despite the structures differing only by the position of the nitro groups, TFA successfully identified the correct nitrotoluene compound with a significant separation in correlation values of the other two compounds.

The TATP in fingerprint oil on a glass slide mixture also required two principal components to keep 95% of the variance. TATP also had the highest correlation value

of 0.611. While this was a lower correlation than the previous mixtures, it was still significantly higher than the correlations for the remaining library compounds. The closest correlation was 0.264 for caffeine.

The theobromine in fingerprint oil on a glass slide mixture required two principal components to keep 95% of the variance. This mixture did not perform as well as the previous mixtures, with the correlation for theobromine being the third highest at only 0.117. The two library compounds with higher correlations were sodium nitrate, 0.228, and 3,4-DNT, 0.137. The low correlations for the library compounds was attributed to the theobromine being collected in significant amounts within in the analyzed spectral data. These results demonstrate the need to collect multiple spectra and ensure that all components of a mixture are sampled for analysis.

The final mixture combined two organic compounds in a fingerprint to make a more complex mixture. The ammonium nitrate and TATP mixture in fingerprint oil on a glass slide required three principal components to retain 95% of the variance. Ammonium nitrate had the highest correlation for the mixture at 0.983, while TATP had the third highest correlation of 0.664. The second highest correlation was 0.727 for potassium nitrate. The remainder of the organic compounds had correlations that were significantly lower than these three compounds. The method successfully identified one of the compounds in the mixture and performed well for the second compound. Potassium nitrate likely had a high correlation due to the similarity in the structure of it

and ammonium nitrate. Overall, TFA performed well for this mixture with the two compounds being identified with high correlations.

TFA results were successful at identifying, with the highest correlation, the library compounds present in the mixtures, expect for the theobromine mixture. For the theobromine mixture which did not identify the mixture compound, all library compounds had low correlations which indicated none of the library compounds were very similar to the mixture. This result was attributed to the lack of organic compound in the mixture and demonstrates the need to ensure the mixture is thoroughly sampled to obtain spectral characteristics of all components present.

6.3.3.2 Bayesian Decision Theory

The Bayesian decision theory was applied to the library and mixture data as discussed previously for the FTIR samples. The posterior probabilities were calculated, which corresponded to each library compound, and the mixtures were classified as containing the library compound that had the highest posterior probability or multiple compounds with approximately equal posterior probabilities; if the data did not fit the criteria, the sample was left unclassified. A lower correlation cutoff of 0.8 with a significance level of $\alpha=0.05$ was used to acquire the results.

The first mixture analyzed was the 2,4-DNT in fingerprint oil on a glass slide. This mixture performed ideally, with 2,4-DNT having a posterior probability of 1 and all other compounds having a posterior probability of 0. The principal components were used which encompassed 99% of the data.

The second mixture was ammonium nitrate in fingerprint oil on a glass slide. Ammonium nitrate had the highest posterior probability of 0.8226. Theobromine was the only other compound that showed a posterior probability above 0; it had a posterior probability of 0.1774. The contribution for theobromine was small compared to ammonium nitrate indicating that the compound present in the mixture would be the most prevalent for identification. Only one principal component was used for the analysis which encompassed 95% of the variance.

The TATP in fingerprint oil on a glass slide mixture did not perform as well as the previous two methods. All of the distributions fell significantly below the lower correlation cutoff, resulting in a posterior probability of 0 for all of the classes. Again, only one component was used for the analysis which encompassed 97% of the variance. While the mixture compound was not identified, there were also no compounds incorrectly classified. This result indicates the lack of contribution of the organic compound in the spectral data for classification.

The theobromine in fingerprint oil on a glass slide mixture also did not perform well. One principal component was used which encompassed 88% of the variance. All of the library compounds had a posterior probability of zero due to all of the distributions falling below the lower correlation cutoff. This is again attributed to the poor contribution of organic compound in the collected spectra for this mixture.

The final mixture of TATP and ammonium nitrate in fingerprint oil on a glass was the most complex mixture for the analysis. It contained two compounds from the library that could be identified by the method. The analysis used three principal components to encompass a variance of 99%. Three compounds had posterior probabilities that were not equal to 0. The highest corresponded to ammonium nitrate, 0.7036, which was present in the mixture. The other two compounds had much lower posterior probabilities of 0.1658 and 0.1307 for theobromine and TATP respectively. The ammonium nitrate contribution of the mixture was correctly classified with TATP also being classified but at a much smaller contribution. The theobromine contribution was attributed to the clustering observed for the aromatic and peroxide compounds in the scores plot. Overall, the results showed the ability to classify both mixture compounds, with one of the compounds having a larger contribution.

Overall, the Bayesian decision theory analysis performed well for the Raman data with all but two of the mixtures being classified correctly. Those two mixtures remained unclassified due to lack of data necessary for classification as opposed to incorrectly

classifying. There were a few compounds not present in the mixture that had low posterior probabilities in some of the mixtures, but these posterior probabilities fell much lower than the posterior probability for the mixture compound. In addition, those compounds were the library compounds similar in structure to the mixture compounds and clustered near them in the scores plots.

6.4 Metal Transfers

6.4.1 PCA/TFA

PCA/TFA was first performed on the normalized metal data as the initial step in the background independent classification of metal transfer samples. The results obtained from the initial TFA provided correlations of the transfer data to the metal library. Tests were performed using the number of principal components determined to be needed by DRMAD.

The first sets of TFA results to be discussed are the single bullet transfer data to both porcelain and steel. The number of required principal components ranged from between 2 and 8, with approximately 100% of the variance being retained per analysis. Table 44 shows the specific number of principal components per transfer line, in addition to the highest correlation and correlation class from each analysis. For all of the porcelain substrate transfer, the highest correlation corresponded to the class of

bullet used for the transfer. The steel substrate samples also performed well, with only the three metal jacket bullet lines (MJ) misclassified as the copper jacket bullet (CJ). The correlations for the MJ class were at most 0.08 less than the CJ correlations for those samples. As seen in Figure 24, both the metal and copper jacketed bullets demonstrated strong copper emission lines which was attributed to the similarity in the correlation values. For both substrates the correlations were high, with the lowest correlation seen for the correct class being 0.75 for a MJ sample on porcelain. This data set demonstrated the ability to classify on multiple substrates a single metal transfer.

The second set of data tested by this technique was the multiple transfer data. Again, two substrates were tested: porcelain and steel. DRMAD was used to determine the number of principal components to be retained, which ranged between 2 and 6. Results for approximately 100% of the variance are shown in Table 45.

On the porcelain substrate, all of the CJ/MJ samples on porcelain had the highest correlations correspond to the two metals present within the transfer lines; the NJ class consistently had significantly lower correlations for these samples. The CJ/NJ samples also had the highest correlations corresponding to one of the metals present in the transfer, with CJ having correlations above 0.9 for all of the transfers. One of the CJ/NJ samples had NJ correlations above 0.89, but the remaining of these transfer lines had correlations for NJ falling below the MJ class (NJ<0.3 and MJ~0.7). The final set of

porcelain samples, MJ/NJ, had correlations that were very similar for all of the library classes. For two of the samples the CJ class had higher correlations than either the MJ or NJ class (CJ~.60, MJ & NJ ~ 0.55; CJ~ 0.90, MJ & NJ ~0.80). For the final line, the MJ and NJ classes had the highest correlations (MJ ~ 0.83, NJ ~ 0.88, and CJ~ 0.70).

On steel, similar results were observed for the multiple transfer lines. For the CJ/MJ transfers, the CJ class had the highest correlations (>0.85) with the MJ having the second highest (0.65-0.90). For these transfer lines, the NJ class had correlations far below the other two classes (<0.2). The CJ/NJ lines also performed very well on steel, with both CJ and NJ having high correlation values (CJ>0.08 and NJ>0.85). The MJ class correlations were separated from the other two classes for these lines (~.65). The final set of multiple transfer lines, MJ/NJ, demonstrated similar results to the MJ/NJ transfer lines on porcelain. All three groups again had similar correlation values, with little separation between the samples. For two of the MJ/NJ lines the NJ class had correlations higher than the other two classes (>0.89), with the MJ and CJ having correlations of approximately 0.35. In the final MJ/NJ line the CJ and NJ classes both had correlations around 0.85 with the MJ class falling at correlation values approximately at 0.70.

Both the porcelain and steel multiple transfers lines demonstrated the ability to classify at least one of the bullets used to create the metal transfer. Difficulties were observed in classifying both metals, which was attributed to three causes. The first was the

method of transfer, where one metal was transferred and then a second was transferred directly on top of the first. The transfer of the second bullet potentially masked or removed the first metal therefore reducing the presence and detection of the first metal. The second cause of difficulty was the transfer ability of the metals. The NJ metal was seen to easily transfer on both substrates as it was made of lead which is a soft metal. The CJ metal demonstrated decent transfer to both substrates, but the MJ was difficult to transfer. The MJ was composed of a metal alloy which consisted of hard metals, therefore making transfer difficult. The final cause of difficulty of classifying the samples was attributed to the similarity in the copper line contributions in the CJ and MJ spectra. The higher correlations or similar correlations for the CJ when MJ was present in the mixture were attributed to the similarity in the spectral lines of the two metals.

The final set of metal transfer TFA correlations obtained were for the bullet holes. The results were lower for these transfers as they presented a more complex sampling surface and transfer scenario. Of the CJ bullets, seven of the fifteen bullet holes had average correlations of 0.70 or greater for the CJ class. For one of these seven bullet holes, the NJ class had an even higher average correlation of 0.91 than the 0.87 for the CJ class; though the highest individual correlation did correspond to the CJ class (0.94). The high correlation for the NJ class was attributed to the steel plate as both it and the NJ bullets were composed of lead. The other eight samples had low correlations (0.5 and below) for all of the classes indicating poor transfer for these bullet holes. All four of the MJ bullet holes had overall low correlations. The highest correlation observed was 0.7 for one of the bullet holes which corresponded to the CJ class, but the MJ class

had a correlation within 0.1. The final bullet holes, created by the NJ bullets, all had very high correlations for the NJ class (0.88 and above). The other two classes, MJ and CJ, fell significantly below with correlations less than 0.15 for these samples. Table 46 shows the highest correlation for each bullet hole, classification, and number of principal components retained by DRMAD for the bullet hole data.

Again, the bullet hole data demonstrated similar difficulties to the multiple transfer data with the harder metals (CJ and MJ) not transferring as well as the softer metal (NJ). In addition, LIBS is best when used on a flat surface; therefore the convex surface of the bullet holes added complexity to the metal transfer. The results demonstrated the increased difficulty for the three transfer scenarios.

Table 44: TFA results for single metal transfer data; in red are the samples that did not have the highest correlation for the library class present on the sample.

Sample	Substrate	Principal Components Retained	Highest Correlation	Highest Correlation Class	Sample	Substrate	Principal Components Retained	Highest Correlation	Highest Correlation Class
B1a	Porcelain	5	0.94	CJ	**B1a**	Steel	5	0.91	CJ
B1b	Porcelain	4	0.91	CJ	**B1b**	Steel	3	0.91	CJ
B1c	Porcelain	8	0.94	CJ	**B1c**	Steel	5	0.93	CJ
B2a	Porcelain	5	0.9	CJ	**B2a**	Steel	6	0.98	CJ
B2b	Porcelain	4	0.92	CJ	**B2b**	Steel	4	0.91	CJ
B2c	Porcelain	6	0.87	CJ	**B2c**	Steel	6	0.93	CJ
B3a	Porcelain	5	0.93	CJ	**B3a**	Steel	4	0.94	CJ
B3b	Porcelain	4	0.92	CJ	**B3b**	Steel	5	0.92	CJ
B3c	Porcelain	4	0.94	CJ	**B3c**	Steel	4	0.94	CJ
B4a	Porcelain	5	0.88	CJ	**B4a**	Steel	7	0.93	CJ
B4b	Porcelain	4	0.88	CJ	**B4b**	Steel	7	0.94	CJ
B4c	Porcelain	6	0.92	CJ	**B4c**	Steel	4	0.93	CJ
B5a	Porcelain	5	0.85	MJ	**B5a**	Steel	2	0.86	CJ
B5b	Porcelain	3	0.75	MJ	**B5b**	Steel	6	0.87	CJ
B5c	Porcelain	3	0.89	MJ	**B5c**	Steel	2	0.84	CJ
B6a	Porcelain	6	0.94	NJ	**B6a**	Steel	3	0.91	NJ
B6b	Porcelain	3	0.95	NJ	**B6b**	Steel	4	0.92	NJ
B6c	Porcelain	5	0.94	NJ	**B6c**	Steel	6	0.96	NJ

Table 45: TFA results for single metal transfer data; in red are the samples that did not have the highest correlation for the library class present on the sample.

Sample	Substrate	Principal Components Retained	Highest Correlation	Highest Correlation Class	Sample	Substrate	Principal Components Retained	Highest Correlation	Highest Correlation Class
3,5	Porcelain	2	0.95	CJ	**3,5**	Steel	4	0.94	CJ
3,5	Porcelain	3	0.94	MJ	**3,5**	Steel	4	0.94	CJ
3,5	Porcelain	2	0.63	CJ	**3,5**	Steel	5	0.91	MJ
3,6	Porcelain	3	0.95	CJ	**3,6**	Steel	4	0.93	CJ
3,6	Porcelain	2	0.96	CJ	**3,6**	Steel	3	0.94	CJ
3,6	Porcelain	3	0.95	CJ	**3,6**	Steel	4	0.95	CJ
5,6	Porcelain	6	0.91	NJ	**5,6**	Steel	3	0.93	NJ
5,6	Porcelain	4	0.94	CJ	**5,6**	Steel	6	0.91	NJ
5,6	Porcelain	3	0.62	CJ	**5,6**	Steel	5	0.86	CJ

Table 46: TFA results for bullet hole transfer data; in red are the samples that did not have the highest correlation for the library class present on the sample.

Sample	Principal Components Retained	Highest Correlation	Highest Correlation Class	Sample	Principal Components Retained	Highest Correlation	Highest Correlation Class
BH1	5	0.87	CJ	**BH4**	3	0.85	CJ
BH1	4	0.83	CJ	**BH4**	2	0.24	CJ
BH1	3	0.41	CJ	**BH4**	2	0.47	NJ
BH2	4	0.87	CJ	**BH4**	4	0.94	CJ
BH2	4	0.55	CJ	**BH5**	4	0.70	CJ
BH2	3	0.56	NJ	**BH5**	3	0.61	MJ
BH2	3	0.45	CJ	**BH5**	4	0.44	CJ
BH3	3	0.74	CJ	**BH5**	4	0.54	MJ
BH3	5	0.85	CJ	**BH6**	4	0.93	NJ
BH3	2	0.57	CJ	**BH6**	4	0.89	NJ
BH3	3	0.63	CJ	**BH6**	4	0.93	NJ
				BH6	3	0.95	NJ

6.4.2 Bayesian Decision Theory

The Bayesian decision theory was applied next to the metal transfer data as described previously for classification of the test samples against a library. Lower correlation cutoffs between 0.9 and 0.7 were tested along with classification significance levels between 0 and 0.05.

The first sets of sample results to be discussed are the single bullet transfer lines onto porcelain and steel substrates. Figure 63 and Figure 64 illustrate examples of each bullet transfer line on porcelain and steel respectively. As can be seen, the porcelain background contributes many additional spectral lines to the transfer spectra, while the steel background has a smaller contribution.

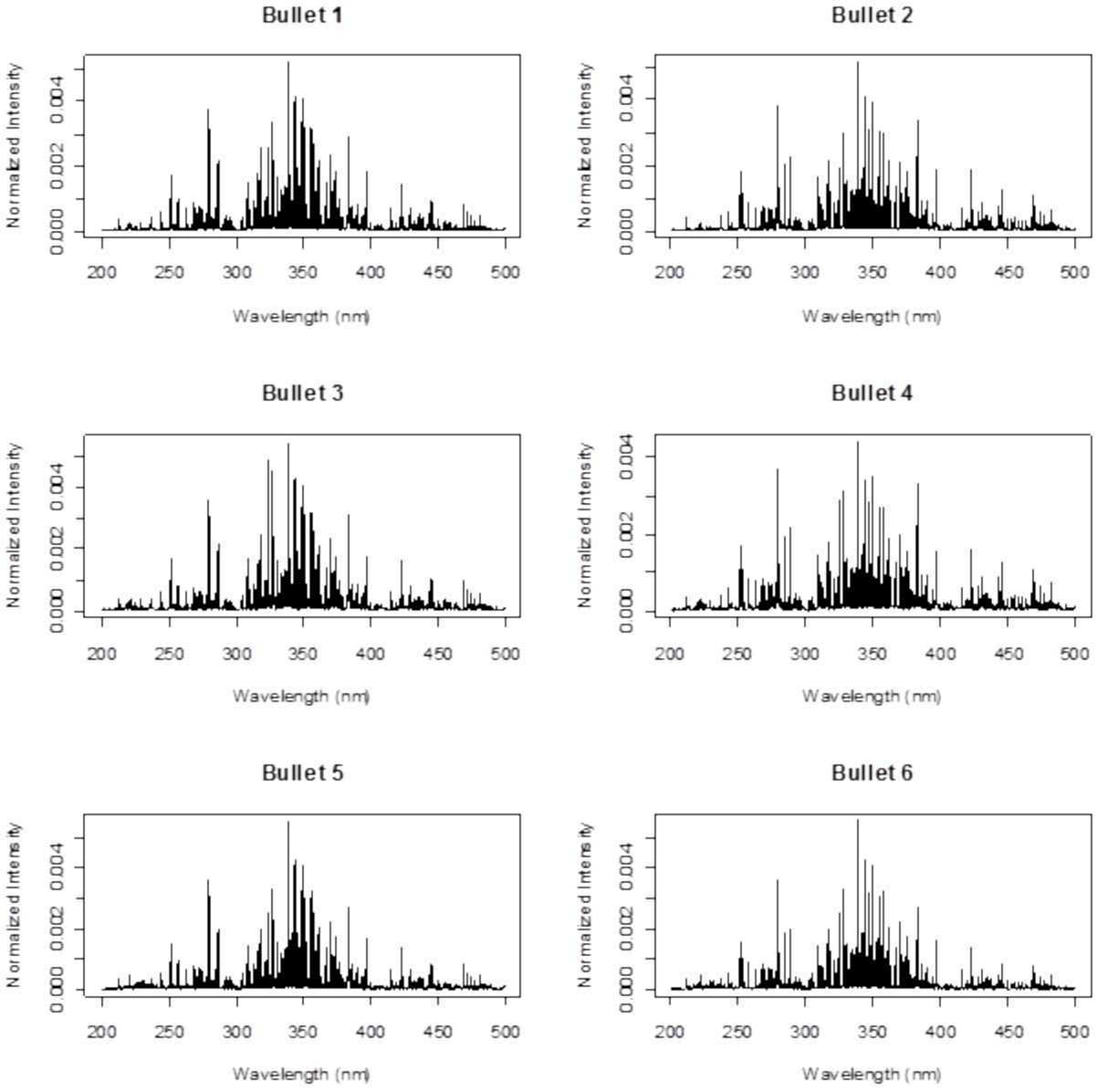

Figure 63: Example normalized spectra of each individual bullet transfer line onto porcelain, labeled by the bullet used to make the transfer.

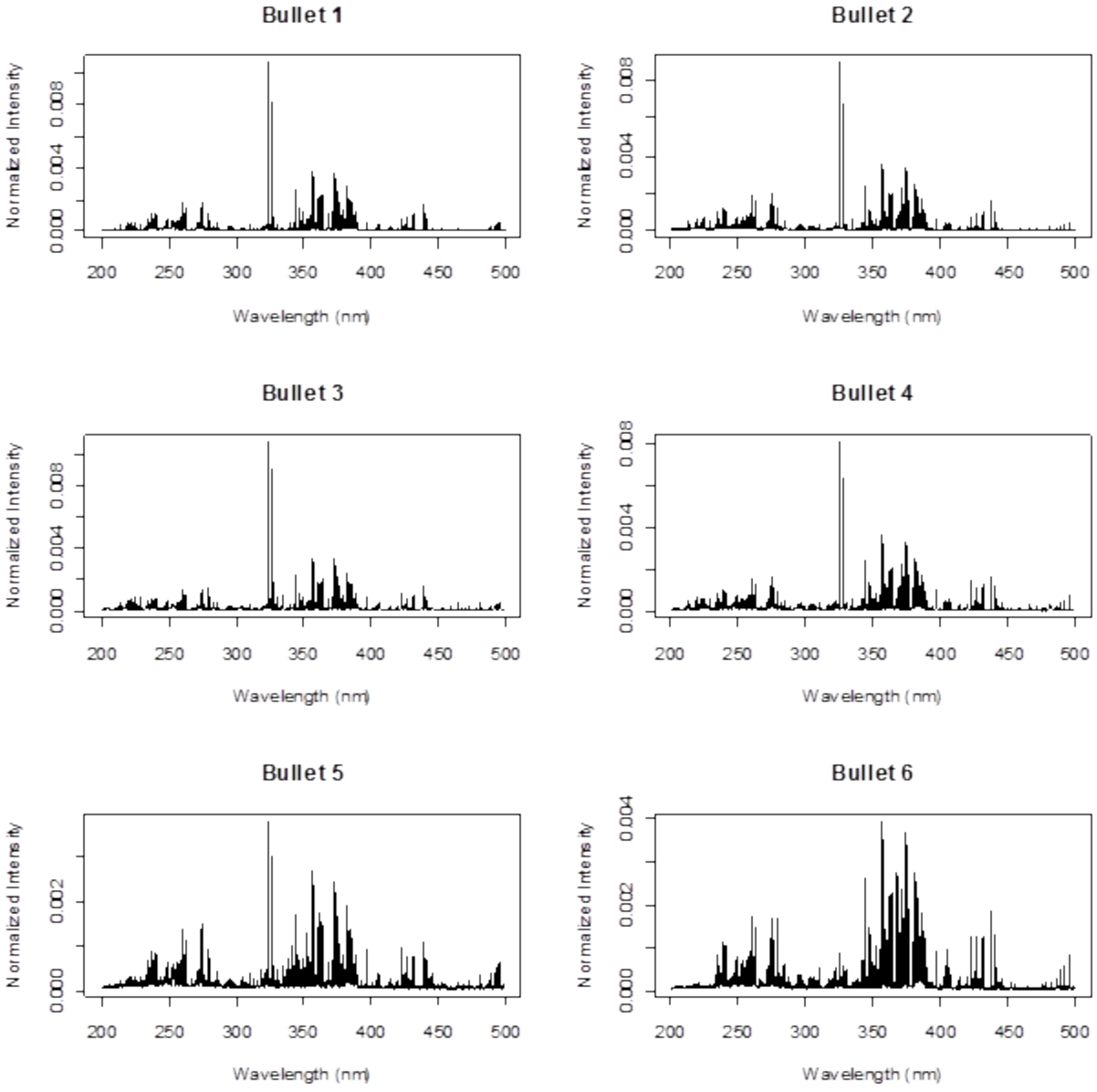

Figure 64: Example normalized spectra of each individual bullet transfer line onto steel, labeled by the bullet used to make the transfer.

The classification significance level was initially set at 0, where the sample would need to fall at or above the lower correlation cutoff to be classified. For lower correlation

cutoffs of 0.9 and 0.8 all but two of the single transfer lines on both substrates, porcelain and steel, correctly classified. The two lines that did not classify were both MJ lines on the steel substrate. These two samples had very low correlation values, as can be seen in Figure 65 a and b, therefore not reaching the lower correlation cutoff to be classified. Figure 66 a and b illustrate plots for the CJ and NJ lines, respectively, on the porcelain substrate; these show much higher correlations for the bullet class present in the sample. As can be seen in all of the single transfer line plots, the CJ and MJ classes which had more spectral similarities fell closer together, whereas the NJ class distribution fell separate.

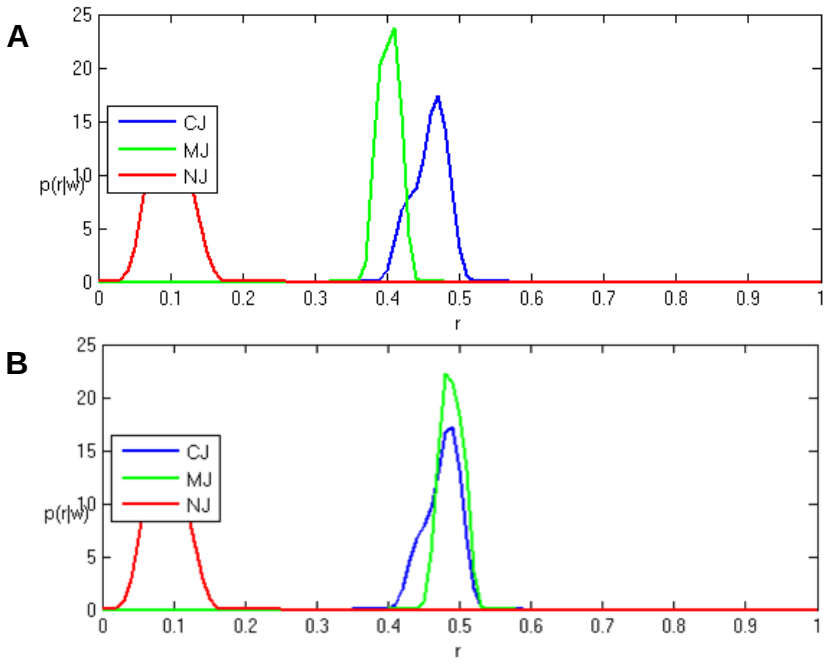

Figure 65: Bullet 5 (MJ) single bullet transfer lines on steel correlation versus posterior probability distribution plot for A) bullet 5 line a and B) bullet 5 line c.

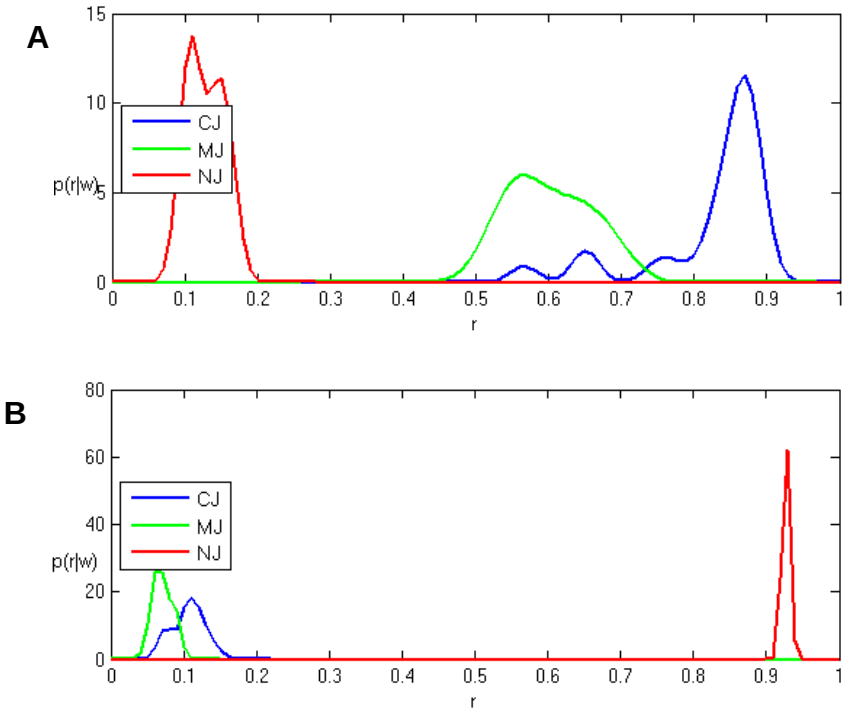

Figure 66: Single bullet transfer lines on porcelain correlation versus posterior probability distribution plots for A) bullet 1 (CJ) line b and B) bullet 6 (NJ) line b.

When the same lower correlation cutoffs were used (0.9 and 0.8) but the classification significance level was set at α=0.01, a confidence interval of 99%, the number of unclassified samples increased and a single misclassification occurred. For a lower correlation cutoff of 0.9, there were three samples not classified and no misclassifications. All of the unclassified samples were MJ on steel. For a lower correlation cutoff of 0.8, there were three samples not classified and one misclassification. The unclassified samples were all MJ, with one on the porcelain substrate and the other two on the steel substrate. The only misclassification was for

MJ on steel. The sample was classified as CJ instead of MJ. Figure 67 illustrates the distribution of the two groups and the overlap observed between them.

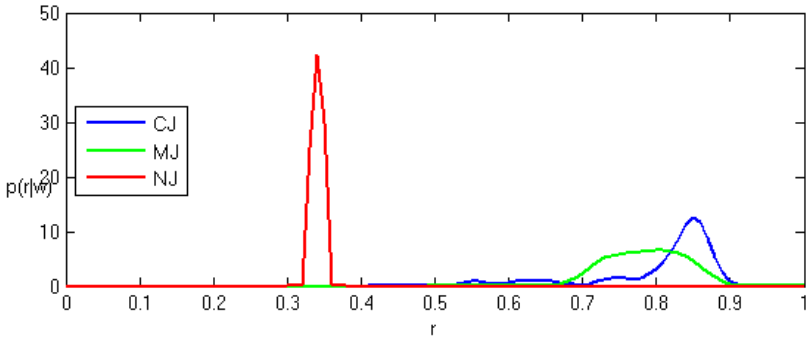

Figure 67: Single bullet transfer line for bullet 5 onto steel correlation versus posterior probability distribution plot. Illustrates overlap between CJ and MJ group causing a misclassification of the sample.

When the classification significance level was set at α=0.05, a confidence interval of 95%, again the number of unclassified samples increased with one misclassification. When the lower correlation cutoff was set at 0.9, there were ten samples not classified and no misclassifications. These samples consisted of four CJ bullets on porcelain, three MJ bullets on porcelain and three MJ bullets on steel. For the lower correlation cutoff of 0.8, the same three samples did not classify as were seen with a classification significance level of α=0.01 and there was one misclassification. The only misclassification came from one MJ bullet on steel, where the sample was classified as CJ instead of MJ, shown in Figure 67.

Based on this data set, the best results were achieved with a lower correlation cutoff of 0.8 with the same results being seen for classification significance levels of α=0.01 and α=0.05. The results for classification significance level of α=0.05 are shown in Table 47, with the posterior probability, number of not classified samples, and the average probability distribution function for the classified samples given. The results demonstrate the ability to classify the metal transfers independent of the background. Figure 68 a and b show the average probability distribution function plots for the samples on porcelain and steel for classification significance level of 0.05. These plots demonstrate the overall ability to correctly classify the metal bullet contributing to the transfer for each of the single line transfers.

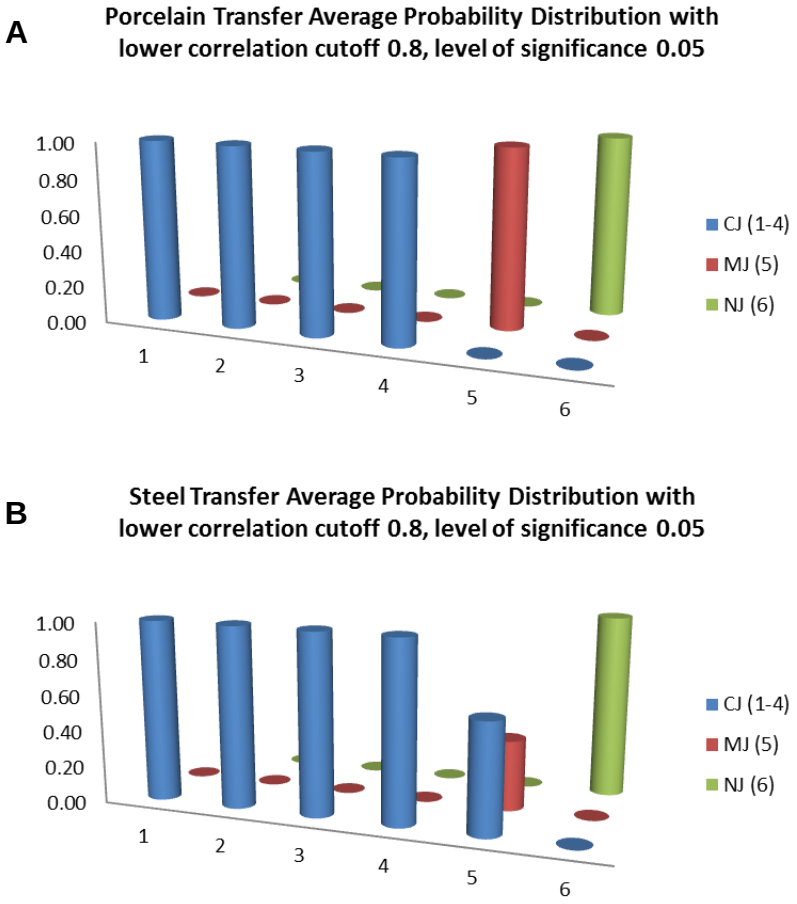

Figure 68: Plots A and B show the average probability distribution for the classified samples for lower correlation cutoff of 0.8 and classification level of significance of 0.05. The numbers on the x-axis indicate the bullet which was transferred to the substrate. A) Porcelain single bullet transfer, B) Steel single bullet transfer

Table 47: Results for single bullet transfers onto porcelain and steel substrates with a lower correlation cutoff of 0.8 and classification level of significance of 0.05.

Single Bullet Transfer Lower Correlation Cutoff 0.8, Classification Level of Significance 0.05													
Substrate	Sample	Posterior Probability			Total Number of Transfers	Not Classified	Probability Distribution Function				Average Probability Distribution Function		
		CJ	MJ	NJ			CJ	MJ	NJ	Not Classified	CJ	MJ	NJ
Porcelain	B1	3	0	0	3	0	1	0	0	0	1	0	0
	B2	3	0	0	3	0	1	0	0	0	1	0	0
	B3	3	0	0	3	0	1	0	0	0	1	0	0
	B4	3	0	0	3	0	1	0	0	0	1	0	0
	B5	0	2	0	3	1	0	0.67	0	0.33	0	1	0
	B6	0	0	3	3	0	0	0	1	0	0	0	1
Steel	B1	3	0	0	3	0	1	0	0	0	1	0	0
	B2	3	0	0	3	0	1	0	0	0	1	0	0
	B3	3	0	0	3	0	1	0	0	0	1	0	0
	B4	3	0	0	3	0	1	0	0	0	1	0	0
	B5	0.61	0.39	0	3	2	0.20	0.13	0	0.67	00.61	0.39	0
	B6	0	0	3	3	0	0	0	1	0	0	0	1

The second method of metal transfer was multiple transfer lines on the porcelain and steel substrates. Three sets of transfers were tested for both substrates with three lines per transfer; the transfers consisted of CJ and MJ, CJ and NJ, and MJ and NJ transfers. Figure 69 thru Figure 74 illustrate four spectra per transfer type. Multiple spectra for each sample are shown to illustrate the variation of contribution of each component of the sample based on different areas of the sample. The analysis was again performed with two lower correlation cutoffs (0.9 and 0.8) and three classification significance levels (0, 0.01, 0.05).

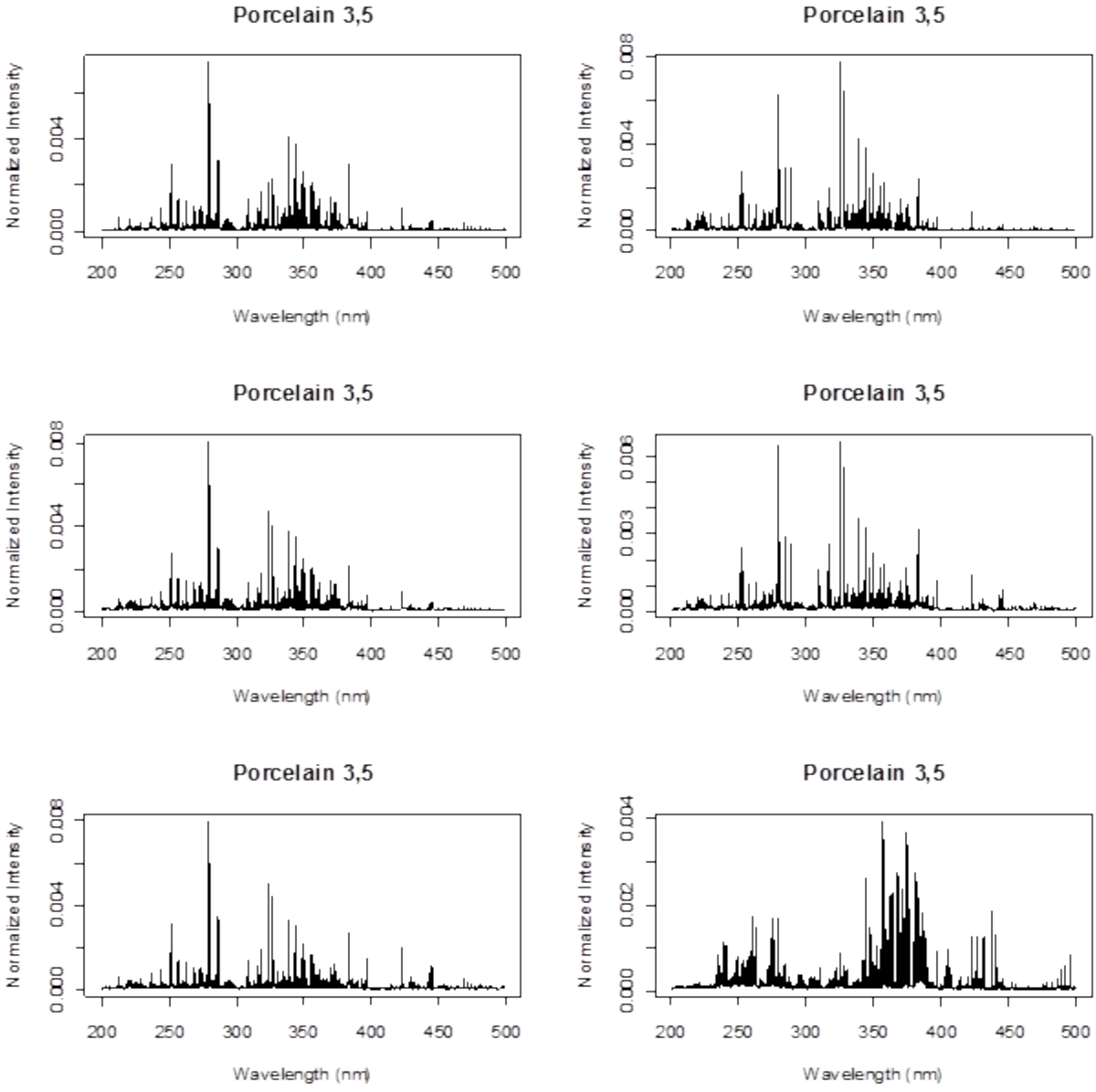

Figure 69: Six of the twelve spectra collected on porcelain 3,5 transfer lines which demonstrate variation in spectral lines observed per spectra.

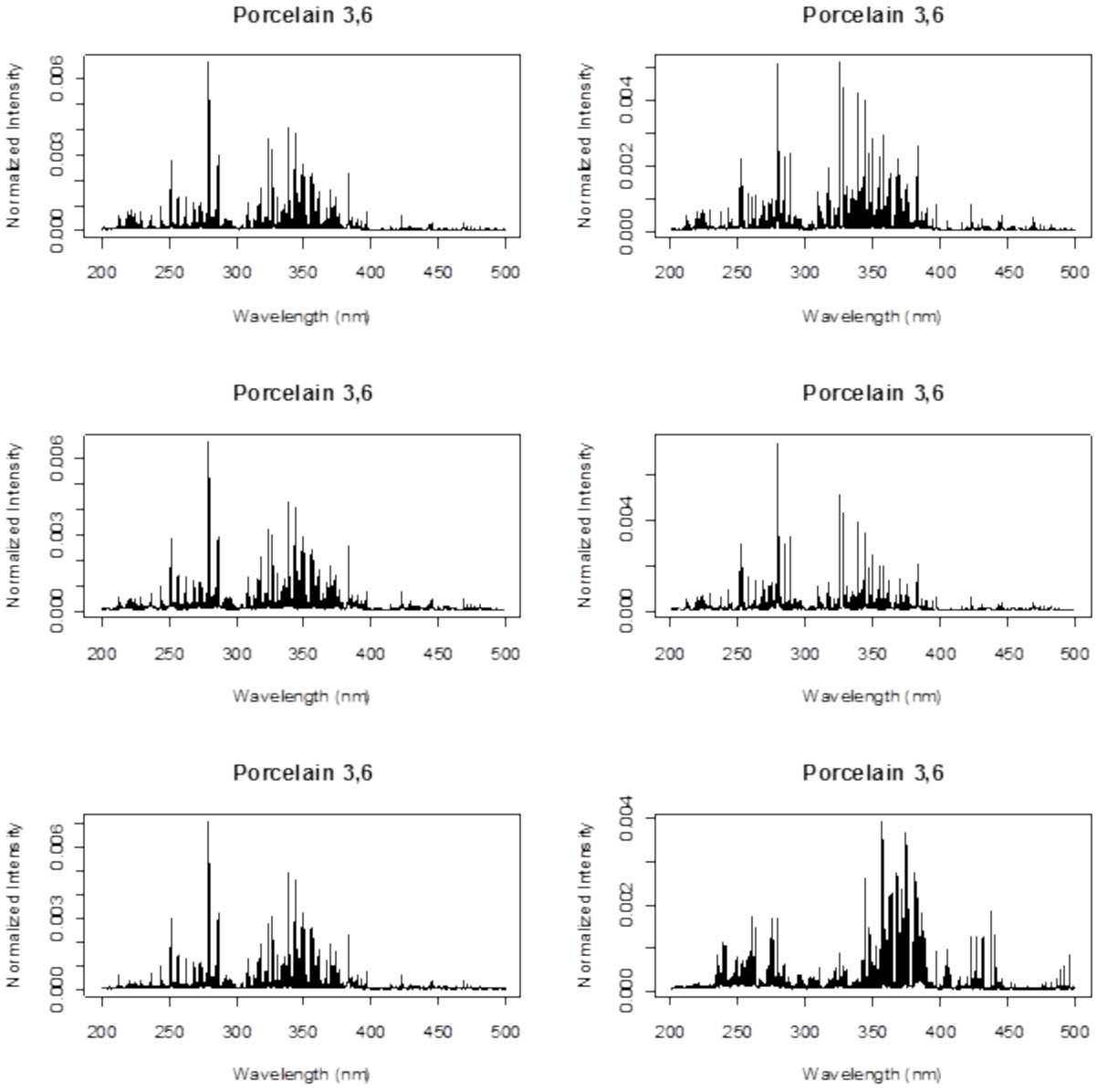

Figure 70: Six of the twelve spectra collected on porcelain 3,6 transfer lines which demonstrate variation in spectral lines observed per spectra.

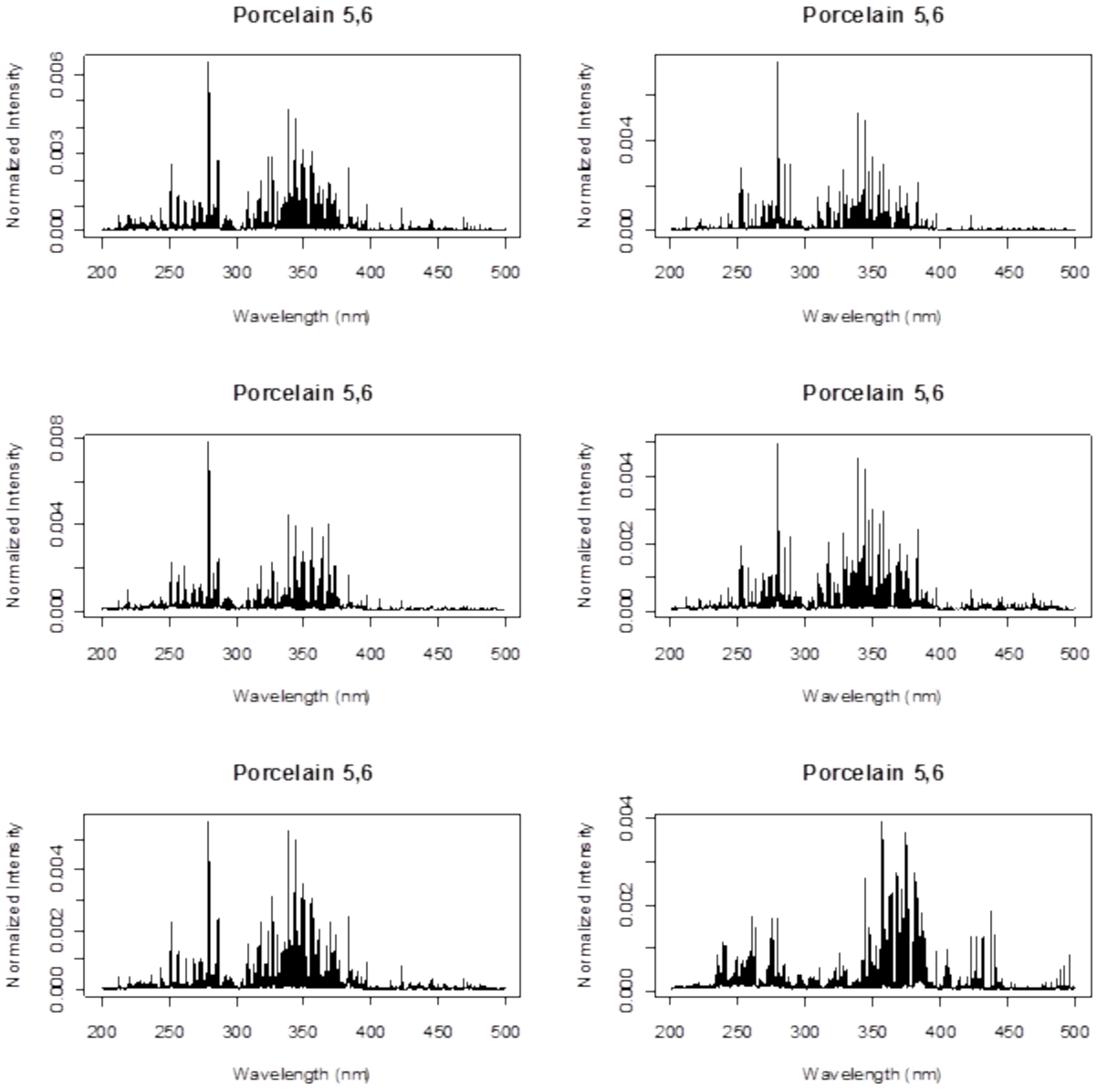

Figure 71: Six of the twelve spectra collected on porcelain 5,6 transfer lines which demonstrate variation in spectral lines observed per spectra.

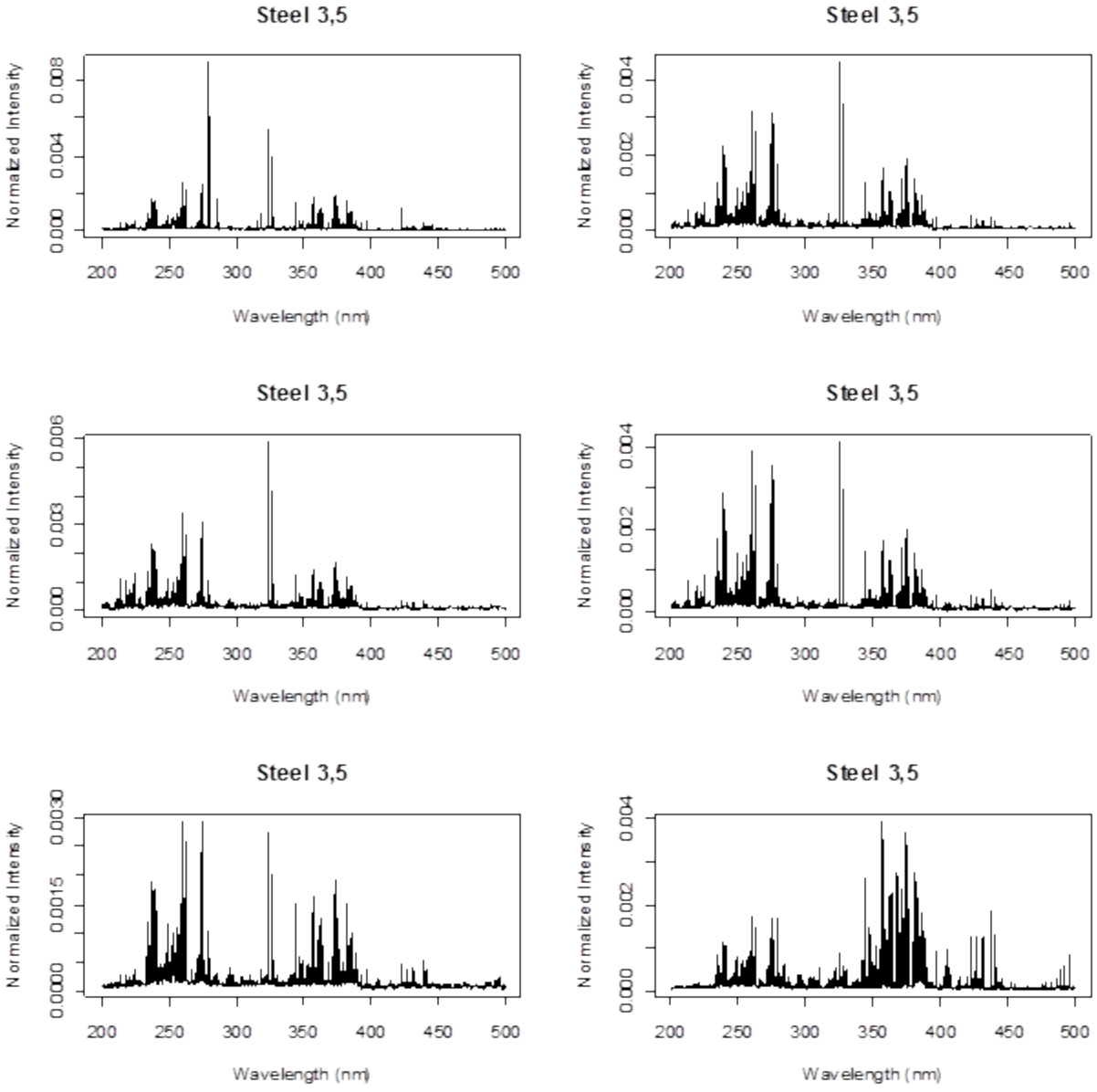

Figure 72: Six of the twelve spectra collected on steel 3,5 transfer lines which demonstrate variation in spectral lines observed per spectra.

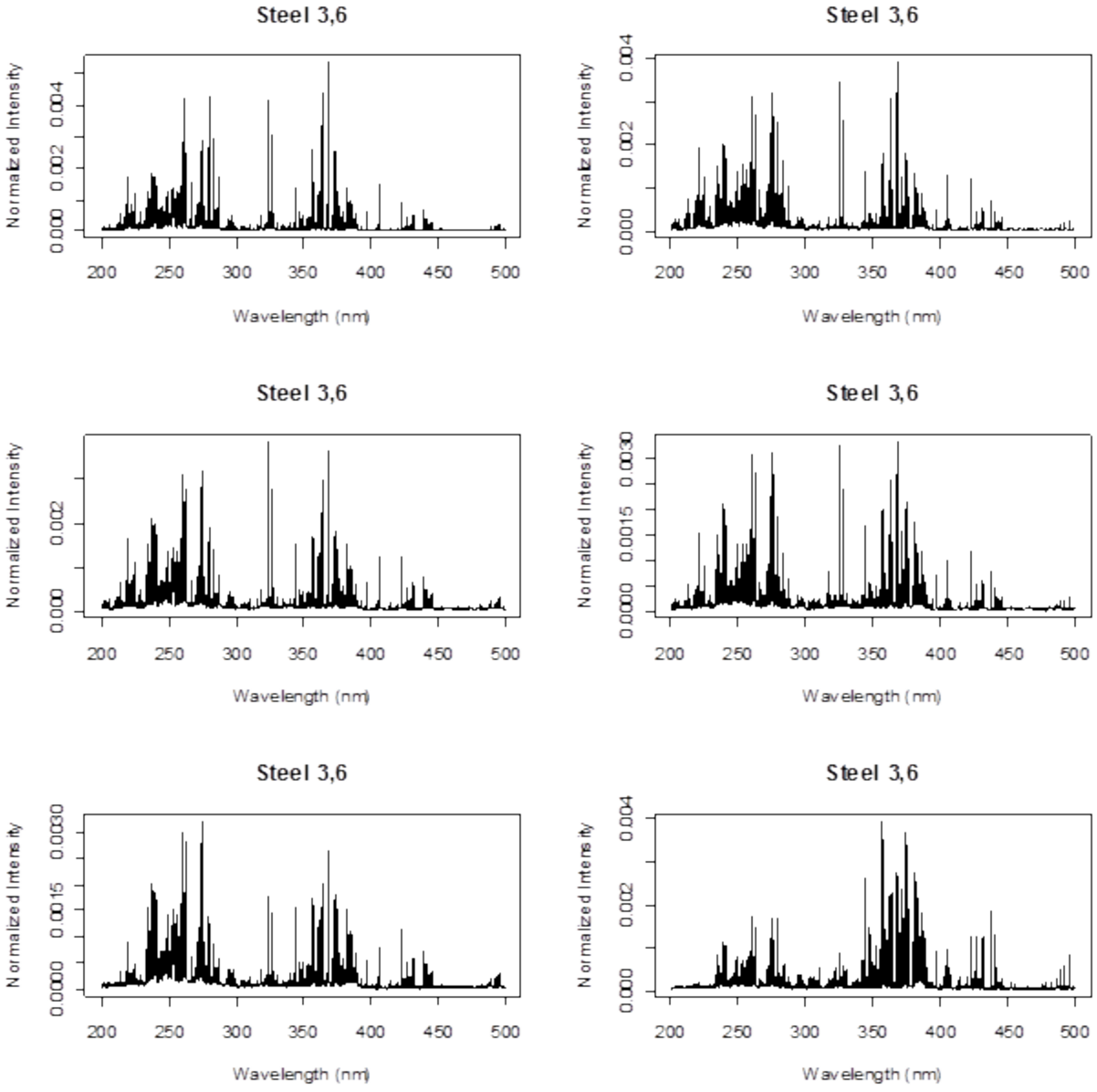

Figure 73: Six of the twelve spectra collected on steel 3,6 transfer lines which demonstrate variation in spectral lines observed per spectra.

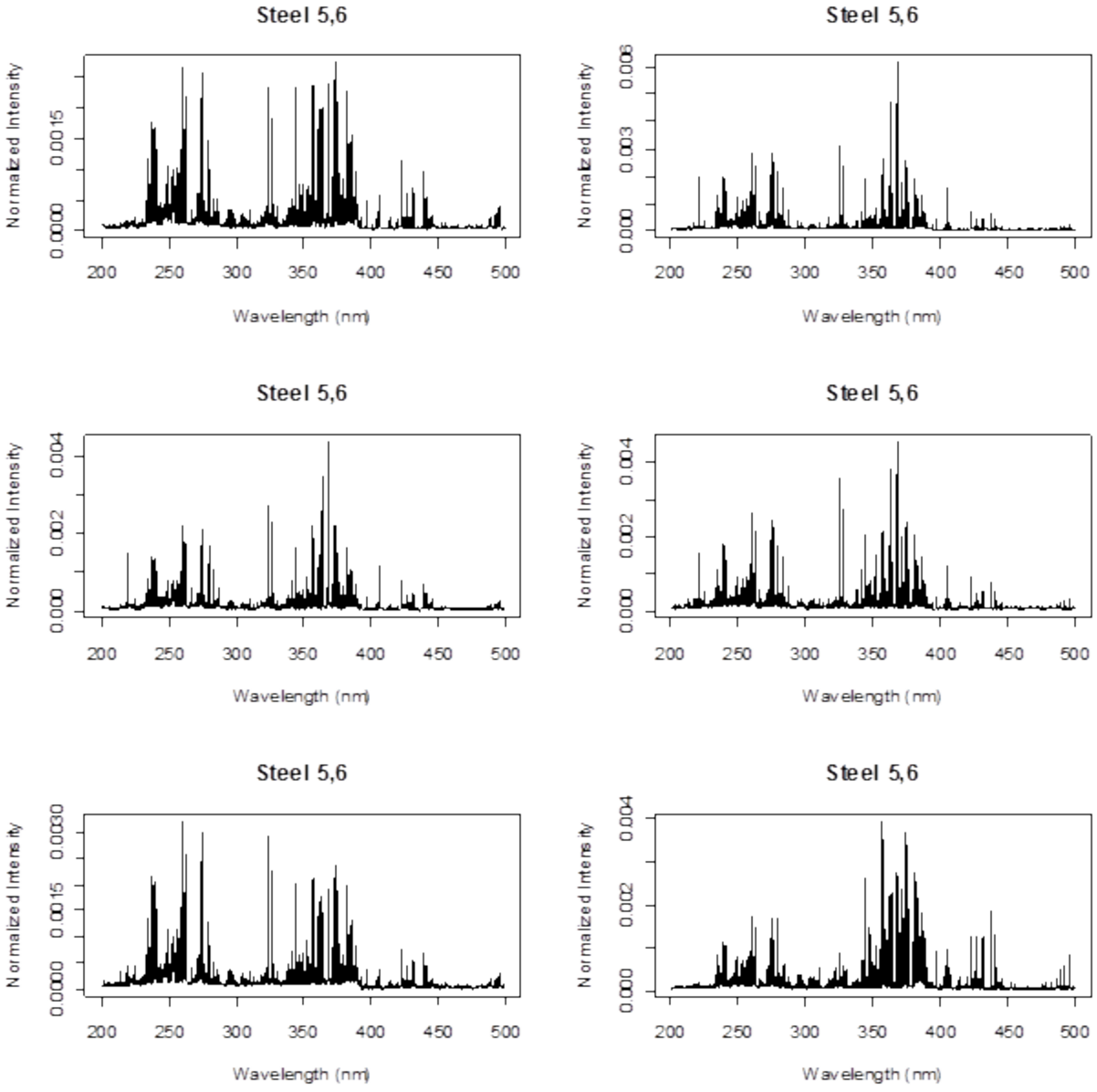

Figure 74: Six of the twelve spectra collected on steel 5,6 transfer lines which demonstrate variation in spectral lines observed per spectra.

The first analysis was performed with the two lower correlation cutoffs, 0.9 and 0.8, with the classification significance level of α=0. For the lower correlation cutoff of 0.9 the porcelain substrate had two samples that were not classified at all, a CJ/MJ and a MJ/NJ sample. The remaining seven samples correctly identified one of the two metal contributions but none of the samples identified multiple contributions. There was one misclassification at these parameters, a MJ/NJ sample classified incorrectly as CJ. On the steel substrate all of the samples classified, with eight of the lines correctly classifying one of the metal contributions and two of the samples correctly classifying both metal contributions. The two samples that classified both metals were both CJ/NJ transfers. One of the MJ/NJ lines classified multiple components, with one of the components correctly classifying as NJ and the second component misclassifying as CJ. For the lower correlation cutoff of 0.8, the results for the multiple transfer lines on both substrates were equal to results for a lower correlation cutoff of 0.9.

When the classification significance level was lowered to α=0.01, the results were similar to the previous classification significance level of α=0 for both substrates. The porcelain substrate again had no samples classify both metal components at lower correlation cutoffs of either 0.9 or 0.8. The same two samples were again not classified and the same misclassification occurred. The steel substrate had one MJ/NJ sample not classify either metal contribution at a lower correlation cutoff of 0.9, but all samples classified at least one component at a cutoff of 0.8. At both the 0.9 and 0.8 cutoffs, the two CJ/NJ samples had both of the metal contributions correctly classified. For a cutoff

of 0.8, one of the MJ/NJ samples classified two components; one of the components was classified correctly as NJ and the other misclassified as CJ.

The final classification significance level tested for this set of data was $\alpha=0.05$. For the porcelain substrate the results were the same as for the significance level of $\alpha=0.01$. At a cutoff of 0.9 on the steel substrate, all but one MJ/NJ sample correctly classified one of the components. Two of the CJ and NJ samples correctly classified both of the metal components, and none of the samples incorrectly classified. For the cutoff of 0.8, all of the samples correctly classified one of the metal components. Two of the CJ/NJ samples correctly classified both metal components, while one of the MJ/NJ samples classified two components NJ and CJ, with the CJ classification being an incorrect classification.

Figure 75 A-F illustrates the correlation versus posterior probability distribution for one of the transfer lines for each multiple bullet transfer for both substrates.

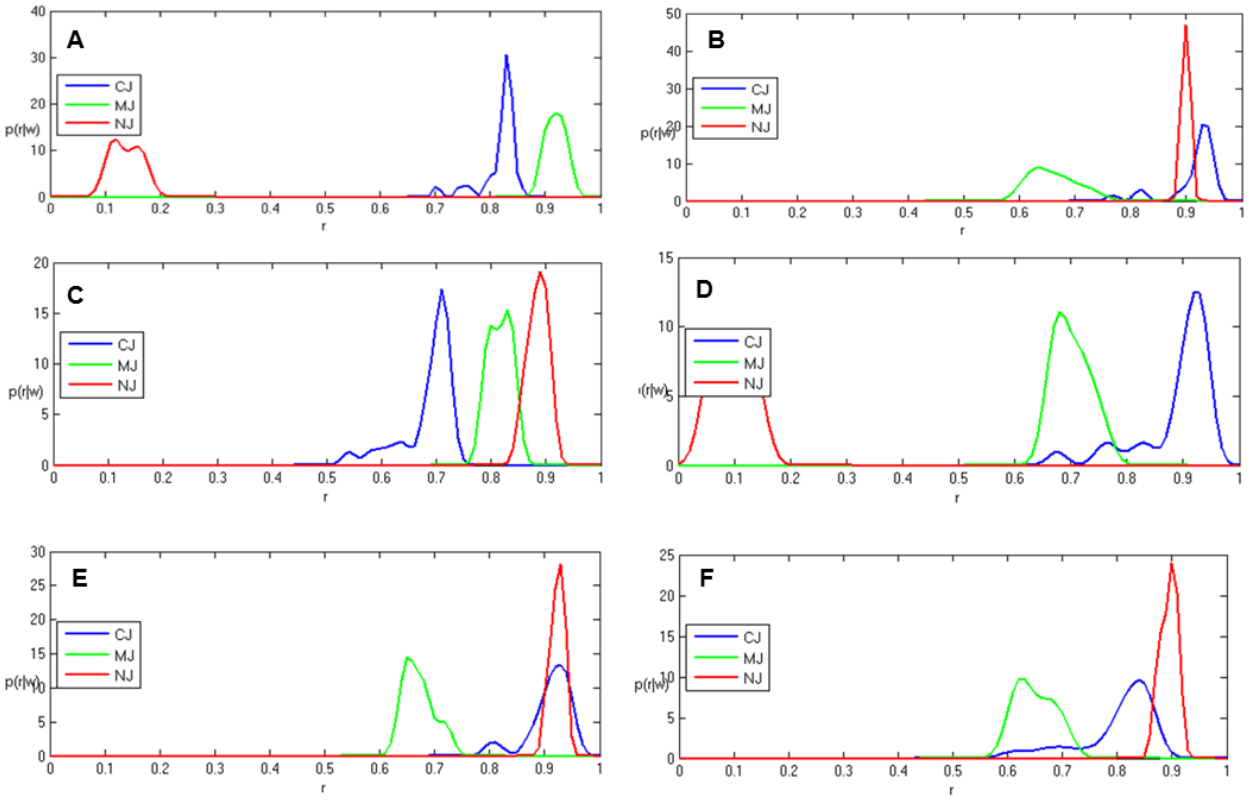

Figure 75: Multiple bullet transfer lines on porcelain (A-C) and steel (D-F) correlation versus posterior probability distribution plots for A) bullet 3 and 5 (CJ/MJ), B) bullet 3 and 6 (CJ/NJ), C) bullet 5 and 6 (MJ/NJ), D) bullet 3 and 5 (CJ/MJ), E) bullet 3 and 6 (CJ/NJ), F) bullet 5 and 6 (MJ/NJ). All represent a correct classification for a minimum of one sample except E where CJ falls higher than the MJ curve.

Overall, the best classification was achieved with a lower correlation cutoff of 0.8 and a significance level of α=0.5. The results for multiple transfer lines are shown in Table 48, with the posterior probability, number of samples not classified and average probability distribution of classified samples included. The results again show the overall ability to classify the samples independent of the background, with a small number of unclassified samples and a minimal number of misclassifications. Figure 76 illustrates the average probability distribution function for the classified samples. All the samples

shown illustrate contributions from the two metals present in the sample, with the exception of sample six which had contribution from CJ instead of MJ.

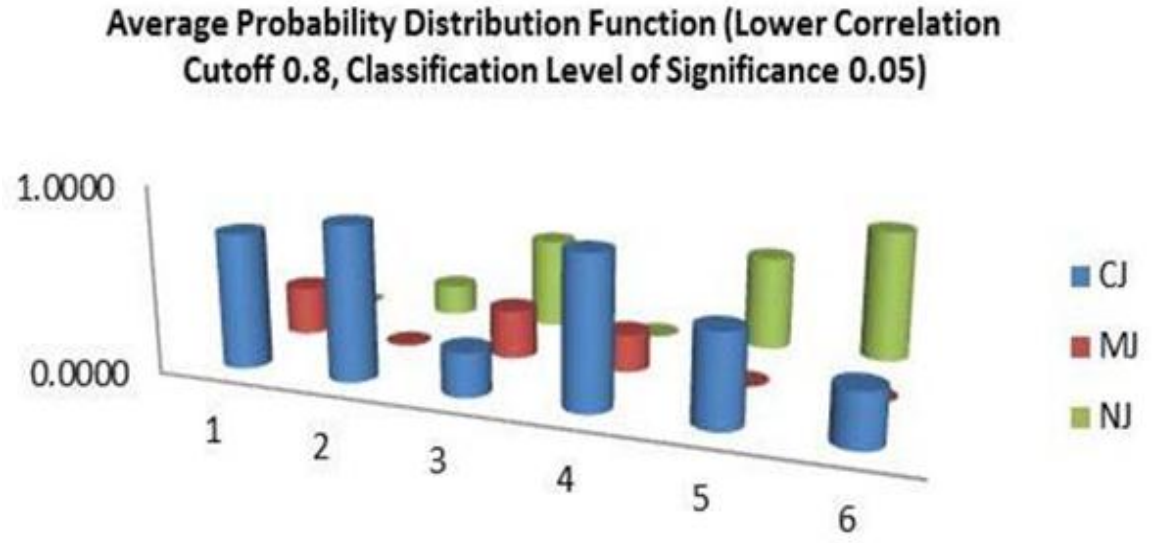

Figure 76: Average probability distribution function chart for multiple transfers onto porcelain (1-3) and steel (4-6). On porcelain: Sample 1 – CJ/MJ, Sample 2 – CJ/NJ, Sample 3 – MJ/NJ; On steel: Sample 4 – CJ/MJ, Sample 5 – CJ/NJ, and Sample 6 – MJ/NJ.

Table 48: Results for multiple bullet transfers onto porcelain and steel substrates with a lower correlation cutoff of 0.8 and classification level of significance of 0.05.

Multiple Bullet Transfer Lower Correlation Cutoff 0.8, Classification Level of Significance 0.05													
Substrate	Sample (Bullet #)	Posterior Probability			Total Number of Transfers	Not Classified	Probability Distribution Function				Average Probability Distribution Function		
		CJ	MJ	NJ			CJ	MJ	NJ	Not Classified	CJ	MJ	NJ
Porcelain	3,5	1.46	0.53	0	3	1	0.49	0.18	0	0.33	0.73	0.27	0
	3,6	2.49	0	0.51	3	0	0.83	0	0.17	0	0.83	0	0.17
	5,6	0.47	0.53	1	3	1	0.16	0.18	0.33	0.33	0.24	0.26	0.50
Steel	3,5	2.40	0.60	0	3	0	0.80	0.20	0	0	0.80	0.20	0
	3,6	1.46	0	1.54	3	0	0.49	0	0.51	0	0.49	0	0.51
	5,6	0.85	0	2.15	3	0	0.28	0	0.72	0	0.28	0	0.72

As can be seen, the number of classified samples decreased from the single bullet transfer to the multiple bullet transfer on the same substrates. This was expected with the increased complexity of the sample matrix, but the results were still promising with the majority of the samples correctly classifying at least one of the components.

The third method of metal transfer was the bullet hole samples. These samples were a single metal transfer onto a substrate, but the sampling had to be performed within the contours of the bullet holes. This irregular surface caused additional complexity of obtaining optimum focal positions as the ideal surface for LIBS is a flat surface. In addition to the irregular surface, the spectral data for the bullet holes were collected over a five month period and compared to a library compiled of data collected prior to the first set of bullet hole data. The time frame between the collection of the spectra within the library and the bullet hole data may cause significant variation to be observed due to instrumental fluctuations which could result in poor correlations between the library and bullet hole spectra. Twenty three bullet holes were analyzed by the method, with four bullet holes per bullet with the exception of bullet one where only three bullet holes were sampled. Spectra for a bullet hole created by each of the six bullets are shown in Figure 77. As done in the two prior methods, two lower correlation cutoffs were tested (0.9 and 0.8) and three classification significance levels (0, 0.01, and 0.05).

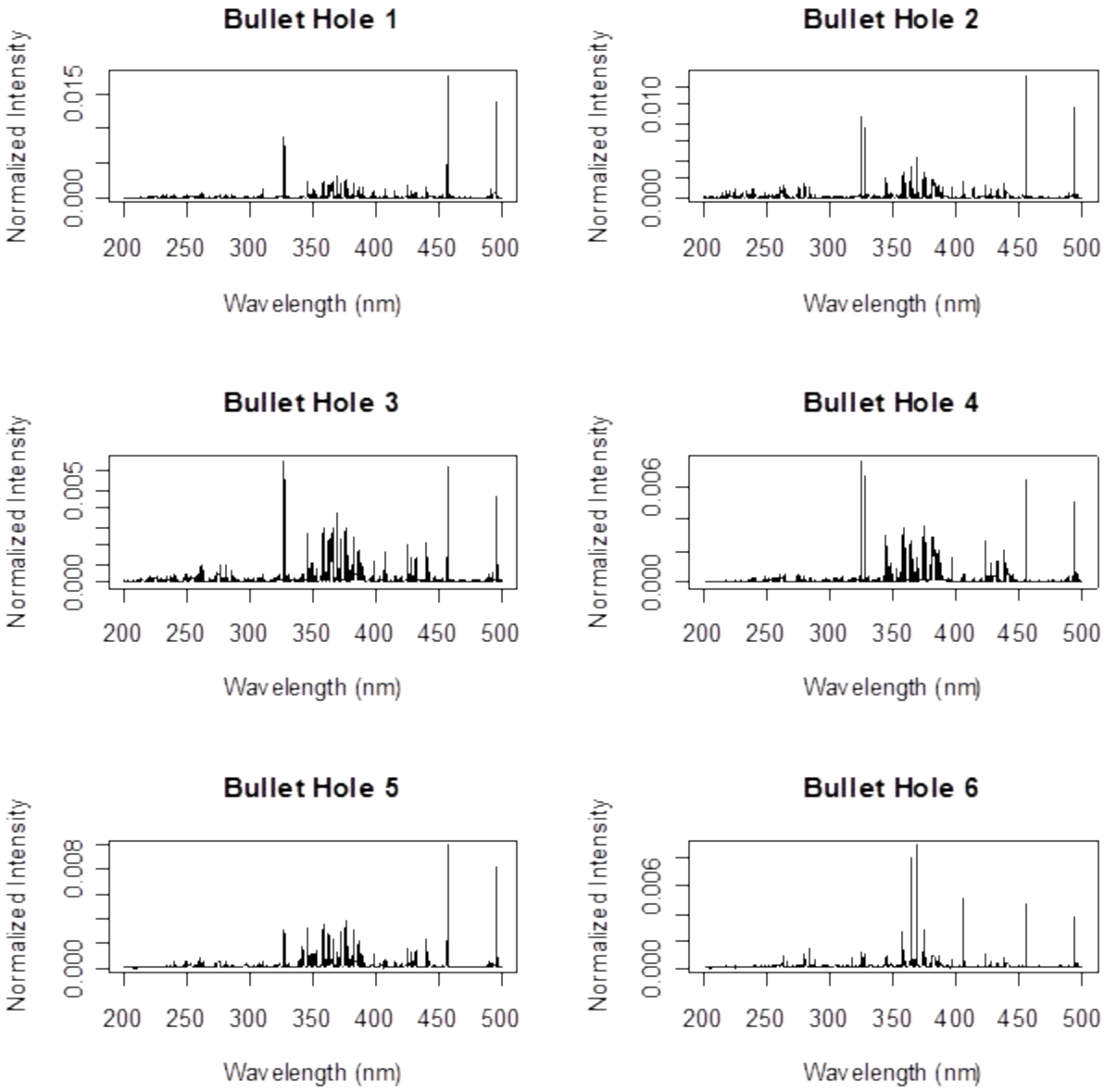

Figure 77: Examples of a normalized spectrum for a bullet hole created by each of the six bullets in the research.

At a significance level of α=0, only nine of the twenty three bullet holes were classified at a cutoff of 0.9. Of these nine samples, one CJ bullet was misclassified as NJ; the

remaining eight samples were correctly classified and corresponded to the four NJ bullet holes and four of the CJ bullet holes. At a cutoff of 0.8, sixteen of the twenty three bullet holes were classified. Five of these bullet holes misclassified; all five of the misclassified bullets were CJ bullets classified as NJ. The remaining eleven correctly classified bullet holes consisted of seven CJ bullets and the four NJ bullets.

At a significance level of α=0.01, six bullet holes of the twenty three were classified at a cutoff of 0.9 and ten at a cutoff of 0.8. For the cutoff of 0.9, one CJ bullet misclassified as an NJ bullet. The remaining five bullets correctly classified as three NJ and two CJ. For the cutoff of 0.8, one CJ bullet misclassified as a NJ bullet. The remaining nine bullets correctly classified as four NJ and five CJ bullets.

At the final significance level of α=0.05, four bullet holes of the twenty three were classified at a cutoff of 0.9 and ten were again classified at a cutoff of 0.8. Of the four bullet holes classified at 0.9, three were correctly classified as NJ and one CJ bullet was incorrectly classified as NJ. For the 0.8 cutoff, the same CJ bullet hole misclassified as NJ. The remaining nine bullet holes were classified as four NJ and five CJ bullets.

Figure 78 A-F illustrates the distributions for the bullet holes created by one of each of the six bullets. Shown are examples of: D) a misclassification for BH4; A,C, and F) correct classifications for BH1, BH3, and BH6; and B,E) non-classifications for BH2

and BH6. The majority of the bullet hole samples resembled the B and E plots for BH2 and BH6 with the distributions falling at low correlations.

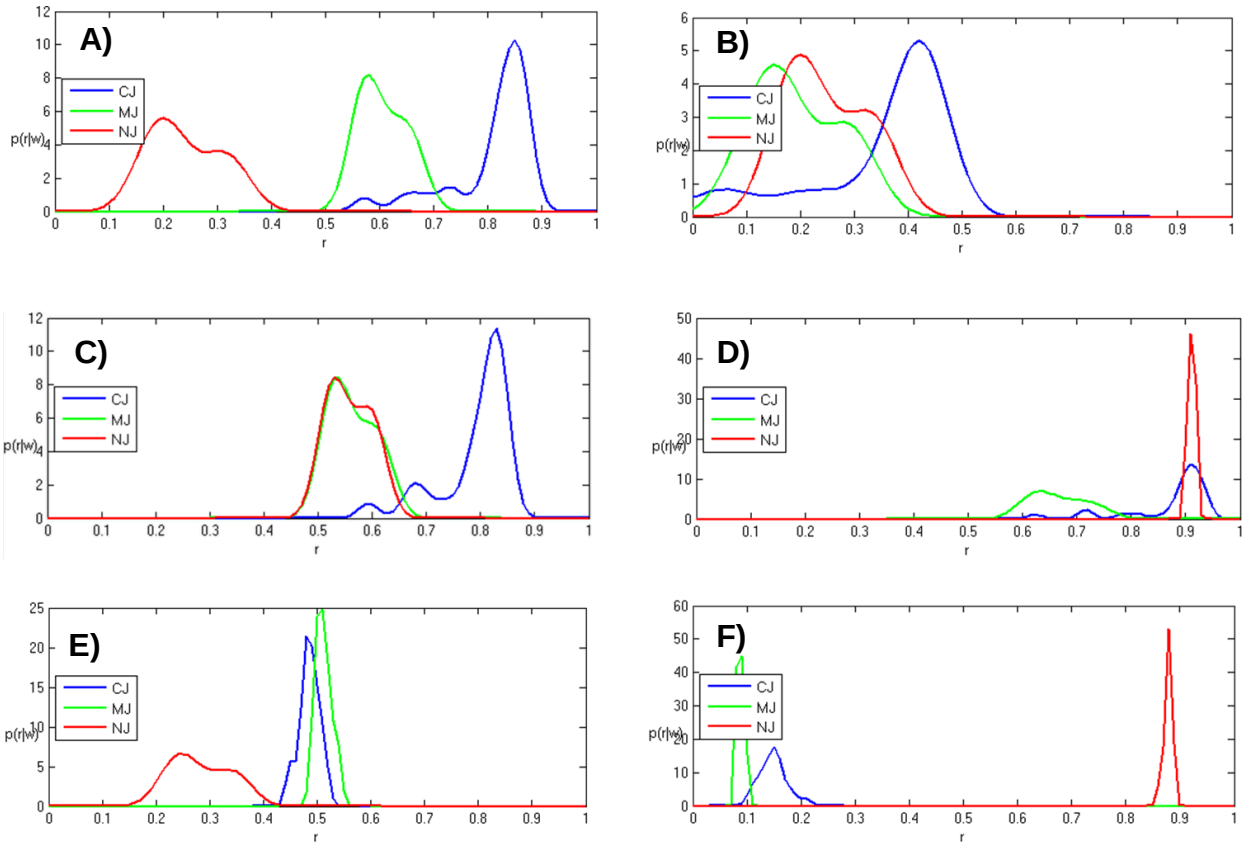

Figure 78: Bullet hole correlation versus posterior probability distribution plots for A) correct classification for BH1 (CJ) B) nonclassification of BH2 (CJ), C) correct classification of BH3 (CJ), D) incorrect classification of BH6 (CJ), E) nonclassification of BH5 (MJ), F) correct classification of BH6 (NJ).

Again the results for a lower correlation cutoff of 0.8 and significance level of α=0.01 and α=0.05 provided similar results. Shown in Table 49 are the results for the cutoff of 0.8 and significance level of α=0.05. The results illustrated the challenges associated

with the complexity of the sample, but show the ability to provide a conservative classification of the samples independent of the background with minimal misclassifications. Figure 79 illustrates the average probability distribution function for the classified samples based on a correlation lower cutoff of 0.8 and a significance level of α=0.05. As can be seen all but bullet 5 (MJ) correctly classified. Bullet 4 (CJ) had a small contribution that classified as NJ, but the posterior probabilities were highest for CJ.

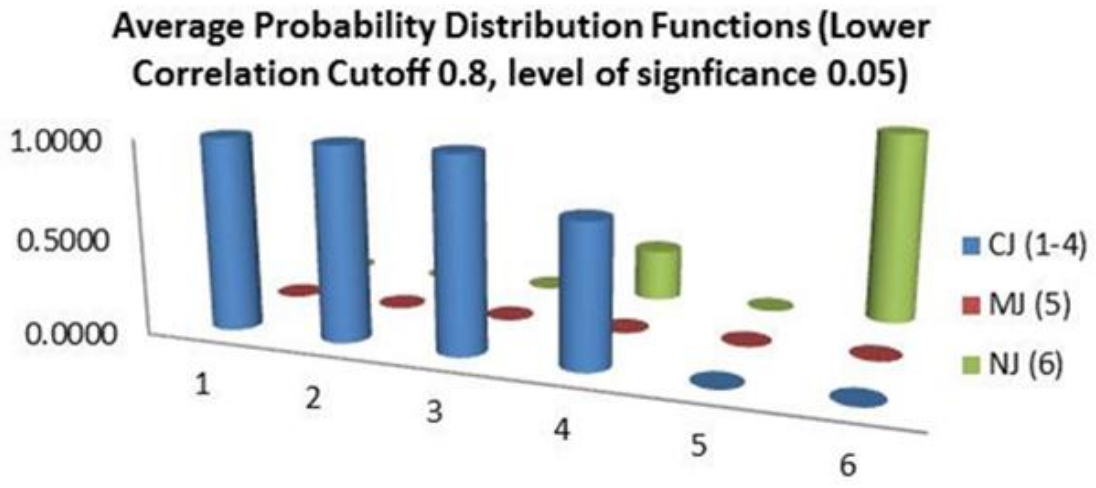

Figure 79: The average probability distribution function plot for classified bullet hole samples at a lower correlation cutoff of 0.8 and classification level of significance of 0.05. Samples 1-3 (CJ) and 6 (NJ) were correctly classified. Sample 4 (CJ) had a small contribution of the sample that classified as NJ, but majority correctly classified. Sample 5 (MJ) was completely unclassified.

Table 49: Results for bullet hole samples with a lower correlation cutoff of 0.8 and classification level of significance of 0.05.

Bullet Hole Transfer Lower Correlation Cutoff 0.8, Classification Level of Significance 0.05												
Sample (Bullet #)	Posterior Probability			Total Number of Transfers	Not Classified	Probability Distribution Function				Average Probability Distribution Function		
	CJ	MJ	NJ			CJ	MJ	NJ	Not Classified	CJ	MJ	NJ
BH1	2	0	0	3	1	0.67	0	0	0.33	1	0	0
BH2	1	0	0	4	3	0.25	0	0	0.75	1	0	0
BH3	1	0	0	4	3	0.25	0	0	0.75	1	0	0
BH4	1.46	0	0.54	4	2	0.36	0	0.14	0.5	0.73	0	0.27
BH5	0	0	0	4	4	0	0	0	1	0	0	0
BH6	0	0	4	4	0	0	0	1	0	0	0	1

6.5 Automobile Paint

For the LIBS analysis of automobile paint samples the original and log intensities were both tested for the full spectral range (200-900 nm). The nonparametric permutation test was used to provide discrimination rates.

The first set of analysis was performed on the spectral intensities using the nonparametric permutation test. The results are shown in Table 50 which is divided into results for each color group and a total summary of the data set at the bottom. Each color group was further subdivided into the number of layers and presence of effect pigment for analysis. For each division of the table the inter-sample and intra-sample comparisons were listed for number of compared, discriminated and percentage of discrimination (or Type I error for intra-samples).

For the inter-sample comparisons, the nonparametric test had 100% discrimination power for the color groups red, blue, tan, green, and silver. The black 4n group had one non-discrimination, which was the result of a comparison between a black 1997 Volkswagen Jetta and a black 2000 Volkswagen Jetta. As these two paints were three years apart from the same make and manufacturer, it is reasonable to assume the formulation of the paint was not altered therefore resulting in the non-discrimination observed. The white color group had non-discriminations for each subdivision, with the lowest discrimination power seen for the white 5n group at 40%. The overall discrimination power for the data set independent of color, layers and effect pigments was 81.93% with a Type II error of 18.07%.

For intra-sample comparisons, the nonparametric permutation test results had a Type I error of 0% for the black, blue, tan, and silver color groups. Of the 90 comparisons there were 4 discriminations: one in the red 5y group, one in the green 3y group, and 2

in the white color group (one in the 4n and one in the 6n groups). The overall Type I error for the data set independent of color, layers, and effect pigments was 4.44%, approximately at the significance level of $\alpha=0.05$.

From these results it was decided to test the data using the log intensities for the nonparametric permutation test. The nonparametric permutation test had a Type I error approximately at the significance level, $\alpha=0.05$, and a Type II error above the significance level.

Table 50: Results from nonparametric permutation test on the spectral intensities for the LIBS spectra of paint samples. Results are displayed by color, number of layers and presence of effect pigments, with summaries for each color group and a total summary at the end of the table. Inter-samples were considered different sample comparisons, and intra-samples were from the same paint.

Color	Layers	Effect Pigments	Inter-sample Comparisons			Intra-sample Comparisons		
			Compared	Discriminated	Power	Compared	Discriminated	Type I error
Red	3	Y	12	12	100	3	0	0
	4	N	24	24	100	4	0	0
	4	Y	4	4	100	2	1	50
	5	Y	4	4	100	2	0	0
Total			**44**	**44**	100	**11**	**1**	**9.09**
Black	3	Y	4	4	100	2	0	0
	3	N	4	4	100	2	0	0
	4	N	12	11	91.67	3	0	0
	5	N	4	4	100	2	0	0
Total			**24**	**23**	**95.83**	**9**	**0**	**0**
Blue	3	Y	40	40	100	5	0	0
	4	Y	12	12	100	3	0	0
Total			**52**	**52**	100	**8**	**0**	**0**
Tan	3	Y	24	24	100	4	0	0
	4	Y	4	4	100	2	0	0
	5	Y	24	24	100	4	0	0
Total			**52**	**52**	100	**10**	**0**	**0**
Green	3	Y	4	4	100	2	1	50
	4	Y	4	4	100	2	0	0
	5	Y	12	12	100	3	0	0
Total			**20**	**20**	100	**7**	**1**	**14.29**
White	3	N	544	428	78.68	17	0	0
	4	N	60	43	71.67	6	1	16.67
	5	N	40	16	40.00	5	0	0

Color	Layers	Effect Pigments	Inter-sample Comparisons			Intra-sample Comparisons		
			Compared	Discriminated	Power	Compared	Discriminated	Type I error
	6	N	24	18	75.00	4	1	25
	7	N	24	21	87.50	4	0	0
Total			**692**	**526**	**76.01**	**36**	2	**5.56**
Silver	3	Y	4	4	100	2	0	0
	4	Y	24	24	100	4	0	0
	5	Y	12	12	100	3	0	0
Total			**40**	**40**	100	**9**	**0**	**0**
Grand Total			**924**	**757**	**81.93**	**90**	**4**	**4.44**

The results from the nonparametric permutation test using the log intensities of the LIBS spectrum are shown in Table 51.

For the inter-samples, the red, blue, tan, green and silver paint samples were 100% discriminated for each subdivision and total color grouping. The black 4n group had one non-discrimination within its inter-samples. Upon looking at the samples it was determined this non-discrimination was a result of the same comparison between a black 1997 Volkswagen Jetta and a black 2000 Volkswagen Jetta seen in the intensity data. For the black color group as a whole there was a 95.83% discrimination power.

The group that presented the greatest difficulty for inter-sample comparisons was the white color group. All of the subdivisions of the white color group had at least one non-discrimination within the inter-samples, with the 3n group having 68 non-discriminations out of 544 comparisons. The lowest discrimination power for the white color group was seen for the 5n subdivision at 70%. For the white color group as a whole there was an 87% discrimination. For the data set independent of color, layers and effect pigments there was 89% discrimination, giving a Type II error of 10.60%.

For the intra-sample comparisons the blue, white and silver color groups were completely non-discriminated, giving a Type I error of 0% for all the subgroups and the total color group. For each of the remaining color groups there was only one discrimination in one of the subdivided groups: red 4y, black 5n, tan 5y, and green 5y.

The Type I error for each of these subgroups appear to be rather high, between 25-50% for the subgroups containing intra-sample discriminations but this was due to the small number of total comparisons. The Type I error for the overall color groups were lower based on the increased number of comparisons considered; the red color group 9.09%, black color group 11.11%, tan color group 10.00%, and the green color group 14.29%. For the data set independent of the color, layers, and effect pigments the Type I error was 3.45%, below the significance level of $\alpha=0.05$.

The nonparametric permutation test results for the overall data set, irrespective of the color, number of layers, or presence of effect pigments, had a total of 924 inter-sample and 90 intra-sample comparisons. The overall discrimination of automobile paints for nonparametric permutation test analysis was 89.83% with a Type I error of 4.44%. At a significance level of $\alpha=0.05$, the Type I error was within a reasonable level. The overall discrimination masked the failure of the white color group to discriminate between inter-samples. The white color group was forty percent of the paint samples with 36 of the 90 automobile samples being white and most of the Type II errors in the analysis were a result of white paint inter-sample comparisons. The individual color groups indicate the applicability of the nonparametric permutation test for automobile paint samples, with caution to be used when analyzing white paint samples. For forensic analysis it is desirable to keep the Type II error low to prevent incorrect association of an individual to a crime, therefore the nonparametric permutation test was preferred as the Type II error was approximately 10%. With caution taken for the

white paint samples, the nonparametric permutation test provides a useful technique for the analysis of LIBS automobile paint spectrum.

Table 51: Results from nonparametric permutation test on the log intensities for the LIBS spectra of paint samples. Results are displayed by color, number of layers and presence of effect pigments, with summaries for each color group and a total summary at the end of the table. Intersamples were considered different sample comparisons, and intrasamples were from the same paint. .

Color	Layers	Effect Pigments	Intersample Comparisons			Intrasample Comparisons		
			Compared	Discriminated	Power	Compared	Discriminated	Type I error
Red	3	Y	12	12	100	3	0	0
	4	N	24	24	100	4	0	0
	4	Y	4	4	100	2	1	50
	5	Y	4	4	100	2	0	0
Total			**44**	**44**	100	**11**	**1**	**9.09**
Black	3	Y	4	4	100	2	0	0
	3	N	4	4	100	2	0	0
	4	N	12	12	91.67	3	0	0
	5	N	4	4	100	2	1	50
Total			**24**	**24**	**95.83**	**9**	**1**	**11.11**
Blue	3	Y	40	40	100	5	0	0
	4	Y	12	12	100	3	0	0
Total			**52**	**52**	100	**8**	**0**	**0**
Tan	3	Y	24	24	100	4	0	0
	4	Y	4	4	100	2	0	0
	5	Y	24	24	100	4	1	25
Total			**52**	**52**	100	**10**	**1**	**10**
Green	3	Y	4	4	100	2	0	0
	4	Y	4	4	100	2	0	0
	5	Y	12	12	100	3	1	33.33
Total			**20**	**20**	100	**7**	**1**	**14.29**
White	3	N	544	476	87.50	17	0	0
	4	N	60	50	83.33	6	0	0

Color	Layers	Effect Pigments	Intersample Comparisons			Intrasample Comparisons		
			Compared	Discriminated	Power	Compared	Discriminated	Type I error
	5	N	40	28	70	5	0	0
	6	N	24	22	91.67	4	0	0
	7	N	24	23	95.83	4	0	0
Total			**692**	**599**	**86.56**	**36**	0	**0**
Silver	3	Y	4	4	100	2	0	0
	4	Y	24	24	100	4	0	0
	5	Y	12	12	100	3	0	0
Total			**40**	**40**	100	**9**	0	**0**
Grand Total			**924**	**830**	**89.83**	**90**	**4**	**4.44**

The nonparametric permutation test analysis of the FTIR data was performed four ways. For each of the tests, the data was performed using the original and the log intensities of the spectra. In addition, two spectral regions were tested: 400-4000 cm^{-1} and 650-2000 cm^{-1}. These four approaches were performed in an attempt to keep the Type I and Type II errors at a minimum. For each approach the results were obtained for the total data set (irrespective of color, number of layers, and presence of effect pigment), color group, and color group subdivisions by layer and presence of effect pigments.

The first analysis used the spectral range of 400-4000 cm^{-1} and the intensities for both nonparametric permutation test results. Table 52 shows the results obtained for nonparametric permutation test. As can be seen high discriminations percentages were obtained by the application of the nonparametric permutation test for each color group and color group subdivision, with the lowest discrimination percentage of 99.82% being observed for the 3n white color group. The overall data discrimination percentage was 99.90%. The issue observed with this data set came for the Type I error, with the smallest Type I error being observed for the white color group of 13.89%. For the remainder of the color groups the Type I error was no lower than 20%, with an overall Type I error of 27.66%. This was high above the significance level. The overall discrimination percentage for nonparametric permutation test was 99.60% and Type I error was again high at 13.83%.

Table 52: Results from nonparametric permutation test on the intensities for the FTIR spectra of paint samples. Results are displayed by color, number of layers and presence of effect pigments, with summaries for each color group and a total summary at the end of the table. Inter-samples were considered different sample comparisons, and intra-samples were from the same paint.

Color	Layers	Effect Pigments	Inter-sample Comparisons			Intra-sample Comparisons		
			Compared	Discriminated	Power	Compared	Discriminated	Type I error
Red	3	Y	12	12	100	3	1	33.33
	4	N	40	40	100	5	3	60
	4	Y	4	4	100	2	1	50
	5	Y	4	4	100	2	1	50
Total			**60**	**60**	100	**12**	**6**	**50**
Black	3	Y	4	4	100	2	0	0
	3	N	4	4	100	2	0	0
	4	N	12	12	100	3	1	33.33
	5	N	12	12	100	3	1	33.33
Total			**32**	**32**	100	**10**	**2**	**20**
Blue	3	Y	40	40	100	5	1	20
	4	Y	12	12	100	3	1	33.33
Total			**52**	**52**	100	**8**	**2**	**25**
Tan	3	Y	24	24	100	4	3	75
	4	Y	12	12	100	3	0	0
	5	Y	24	24	100	4	1	25
Total			**60**	**60**	100	**11**	**4**	**36.36**
Green	3	Y	4	4	100	2	1	50
	4	Y	12	12	100	3	2	66.67
	5	Y	12	12	100	3	1	33.33
Total			**28**	**28**	100	**8**	**4**	**50**
White	3	N	544	543	99.82	17	1	5.88
	4	N	84	84	100	6	2	33.33

Color	Layers	Effect Pigments	Inter-sample Comparisons			Intra-sample Comparisons		
			Compared	Discriminated	Power	Compared	Discriminated	Type I error
	5	N	40	40	100	5	1	20
	6	N	24	24	100	4	1	25
	7	N	24	24	100	4	0	0
Total			**716**	**715**	99.86	**36**	**5**	**13.89**
Silver	3	Y	4	4	100	2	0	0
	4	Y	24	24	100	4	2	50
	5	Y	12	12	100	3	1	33.33
Total			**40**	**40**	100	**9**	**3**	**33.33**
Grand Total			**988**	**987**	**99.90**	**94**	**26**	**27.66**

When the data was analyzed with the spectral intensity for the reduced spectral range (650-2000cm^{-1}), the Type I results improved slightly. Again, all color groups and subgroups had 100% discrimination power except for the 3n white group which had a 99.82% discrimination power for the nonparametric permutation test results. The Type I error for the nonparametric permutation test results decreased slightly but were still above the significance level, α=0.05. The nonparametric permutation test had an overall Type I error of 25.53%, with the lowest Type I error seen for the white color group at 11.11%.

Similar results were observed for the data when the log spectral intensities were obtained. For the spectral range of 400-4000 cm^{-1} the nonparametric permutation test results had an overall discrimination power of 99.90%, with only the 3n white group having a discrimination power below 100% (99.82%). The Type I error was again high at 27.66%.

The final data set tested for FTIR analysis was the log spectral intensities for the spectral range of 650-2000 cm^{-1}. Again the results were similar to the other three data sets. The 3n group was the only group to have below a 100% discrimination power in the nonparametric permutation test results (99.82%), to give an overall discrimination power of 99.90%. The Type I error was again above the significance level cutoff, with an overall Type I error of 25.53%.

The results for the FTIR analysis compared to the LIBS analysis demonstrated an increased Type I error for each set of parameters for nonparametric permutation test. As mentioned previously the FTIR provides molecular information about the sample and works better for the organic components of the samples, which would be seen in the clear polymer top coat of the paint samples. The LIBS, an elemental technique, provides more information on the inorganic portions of the paint samples which would include the pigments, dyes, and fillers seen in the colored layers of the samples. The major difference between the two techniques is the area of analysis of the sample. The LIBS spectra were collected as drill down samples, therefore collecting from multiple layers of the paint sample. Whereas the FTIR spectra were collected using the ATR attachment, therefore limiting the spectral collection to the surface clear coat. Therefore, the higher Type I error in the FTIR analysis is attributed to the limited amount of information provided by the clear top coat.

6.6 Automobile Float Glass

6.6.1 Hypothesis Test

6.6.1.1 Multiple Point Spectral Averaging, 10 Windows 3 Areas

This initial experiment was performed to determine the discrimination percentage using the nonparametric permutation test between different windows. Due to the conditions of a crime scene it is usually unknown what area of a window a piece of glass may originate from, so it was necessary to test multiple areas of a window to ensure the lack of spatial information would not prevent discrimination between windows. Ten full window panes were sectioned into three areas and six LIBS spectra were collected on each area. For each window, the six spectra from each window were considered to be all same window comparisons and nonparametric permutation test was performed to determine the ability to discriminate between same window and different window samples. In-house software [16, 18, 30] was used to perform the nonparametric permutation test, therefore making one comparison per set of spectra. Same window (SW) comparisons resulted in 16 discriminations out of a total of 30 comparisons, which gave a high Type I error of 53%. Of the 405 different window (DW) comparisons, 403 were discriminated, which gave a Type II error of 4.9%.

The boxplot shown in Figure 80 gives the p-value distribution for SW and DW comparisons. The p-value distribution for DW falls compact below the significance level, α=0.05, with very few outliers. The p-value distribution for SW is broad from p-values of 1 to below the significance level, α=0.05, demonstrating a wide range of p-values for SW. From these results it is apparent that the different samples were discriminating well, but same windows were also discriminating at a high percentage. This high same sample discrimination was not observed in initials studies using the same method on a single piece of glass from each window; therefore it was decided that each area of the same window should be considered as a separate sample for comparison purposes.

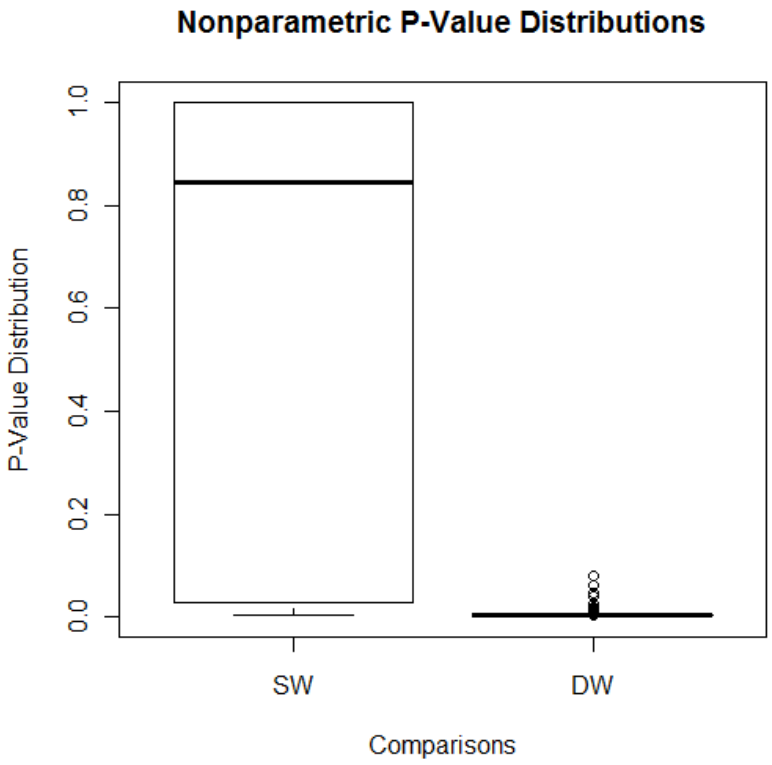

Figure 80: Boxplot demonstrating p-value distributions for nonparametric permutation test results of multiple point 10 window 3 area data.

6.6.1.2 Multiple Point Spectral Averaging, 3 Windows 3 Areas

Due to the high Type I error observed in the 6.6.1.1 experiment, the different areas of the same window were considered as separate samples. As described in the experimental section, three windows (C, D, and J) were selected from the previously sampled ten windows. These three windows were chosen as they had high discrimination rates in the previous experiment. The same three areas (1,2, and 3)

were sampled, though for the nonparametric permutation test there were three groups the comparisons were put into: same window-same area (SWSA), same window-different area (SWDA), and different window (DW). Triplicate sampling (3 sets of 6 spectra) was performed to acquire multiple comparisons for each SWSA samples; this provided a better prediction of the Type I error and also allowed for an overall larger comparison data set. In-house software was used to perform the nonparametric permutation test, therefore making one comparison per set of spectra. The SWSA samples had zero discriminations out of 27 comparisons. DW samples had 219 discriminations out of 243 comparisons, resulting in a Type II error of 10%. While the Type II was slightly over the significance level of $\alpha=0.05$, the DW samples discriminated well. SWDA samples had 45 discriminations out of 81 comparisons, a 56% discrimination rate.

Figure 81 shows the p-value distribution for the three groups of comparisons. Again, the DW distribution is compact below the significance level, $\alpha=0.05$, with few outliers. The SWSA group had a broad uniform distribution between p-values of 1 and the significance level. SWDA also had a broad distribution of p-values, but the median value fell around the significance level. The high discrimination rate of SWDA samples and the low discrimination rate of SWSA indicated spatial variance being observed over different areas of a single window. As the spectra were collected on the surface of the sample, the observed variance could be due to surface contamination or heterogeneity within a single window pane.

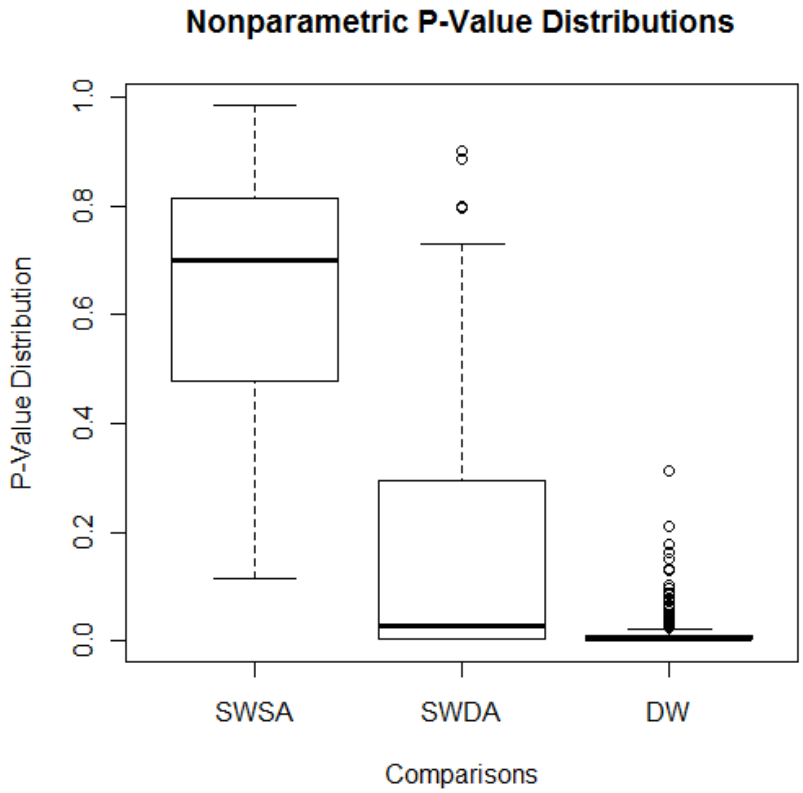

Figure 81: Boxplot demonstrating p-value distribution for nonparametric permutation test results of multiple point 3 windows 3 area data.

6.6.1.3 Multiple Point Spectral Averaging, 2 Windows 5 Areas

The final small scale sampling set collected and analyzed used two of the windows from the first experiment (D and H) and all five areas (1,2,3,4, and 5). All five areas were tested to analyze a larger set of SWDA comparisons. The nonparametric permutation test was performed on the 12 spectra collected on each area of the two windows and comparisons were again grouped as: SWSA, SWDA, and DW. In-house software was used to perform the nonparametric permutation test, therefore making one comparison per set of spectra. SWSA samples had one discrimination out of ten comparisons, a 10% Type I error. While this was above the significance level of α=0.05, the sample size was very small. DW again performed very well with 98 discriminations out of the100 comparisons, giving a Type II error of 2%. SWDA again had a high discrimination rate with 60 discriminations out of 80 comparisons, a 75% discrimination rate. Figure 82 shows a boxplot of p-value distributions for the three groups of comparisons. Again, SWSA had a broad distribution between p-value of 1 and the significance level. The DW distribution was clustered right at or below the significance level with a few outliers. SWDA also had a fairly compact p-value distribution down around the significance level with a few outliers falling at p-values as high as 0.6. Based on these results, in addition to the previous two experimental results, spatial variance was observed between different areas of the same window whether due to surface contamination or sample heterogeneity.

The three experiments discussed to this point have had small sampling sizes and were performed to observe the effect of incorporating known distance changes into the sampling of single window panes. Results have shown that the nonparametric permutation test p-values for SWDA comparisons are sometimes lower than DW comparisons which indicate for some comparisons a greater difference was being observed for SWDA than for DW comparisons. The remaining glass experiments address larger sampling sizes, in addition to comparison of different spectral averaging methods to further investigate the spatial variance being observed.

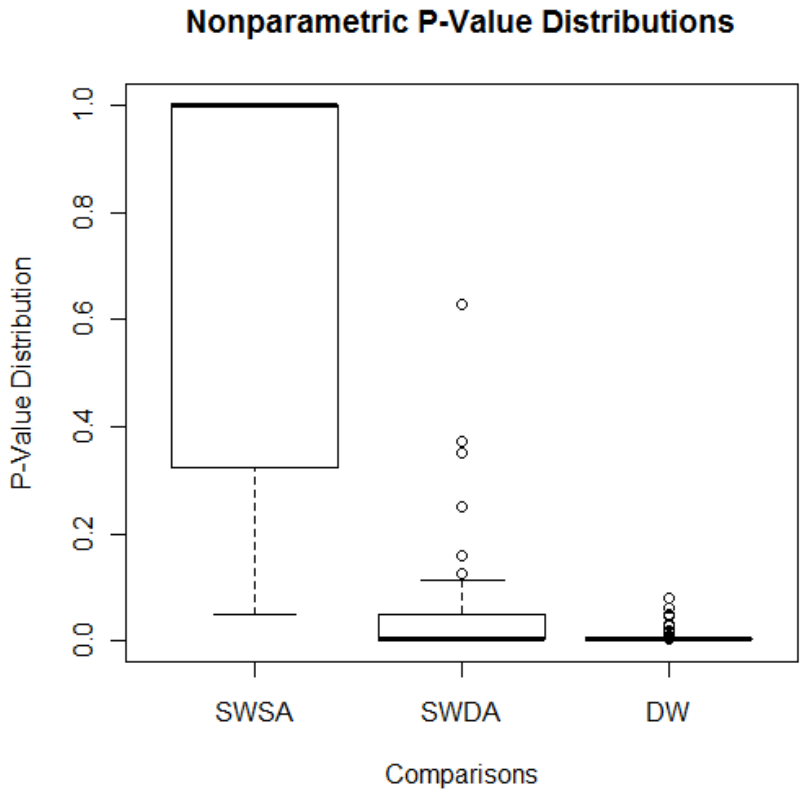

Figure 82: Boxplot demonstrating p-value distribution for nonparametric permutation test results of multiple point 2 windows 5 areas data.

6.6.1.4 Test of Spectral Averaging Method, 10 Windows 5 Areas

After initial tests demonstrated variance in SWDA comparisons using multiple point spectral averaging, it was decided to look further at the spectral averaging methods in a larger scale experiment. All five areas of the ten windows were sampled using each of the three spectral averaging methods discussed in the experimental section (drill down, partial drill down\multiple point, multiple point). The different spectral averaging methods investigated results for purely surface sampling and different extents of drilling into the sample. The results of the different spectral averaging methods should provide additional information on whether the spatial variation was mainly caused by surface contamination or heterogeneity within the glass. The nonparametric permutation test was applied to the three data sets with the calculation of 100 p-values per spectral comparison.

The first set of spectra was collected with the multiple point spectral averaging method used in the glass experiments up to this point. The nonparametric permutation test was performed first with a significance level of $\alpha=0.05$ and then the significance level was varied to determine the ideal significance level, shown in Table 53. As the significance level was reduced the SWDA discriminations were also reduced but SWSA and DW increasingly fell above the significance level. Therefore, a significance level of 0.05 was ideal for the analysis. At a significance level of 0.05 the SWSA comparisons had 243 discriminations out of 5000 comparisons, resulting in a discrimination rate of 5%. DW

performed well with 110279 discriminations out of 112500 comparisons, resulting in a discrimination rate of 98%. SWDA again showed an elevated discrimination rate with 5530 discriminations occurring out of 10000 comparisons, a discrimination rate of 55%. As seen in Figure 83, SWSA p-value distribution was uniform between p-values of 1 to the significance level. DW p-value distributions fell compactly below the significance level with outliers of p-values as high as 0.8. SWDA had a median p-value approximately at the significance level with a small distribution between p-values of 0.4 and 0. SWDA did have outliers that fell almost at a p-value of 1, but the overall distribution fell closer to DW than SWSA.

Table 53: Nonparametric permutation test results from varying significance level for multiple point spectral averaging, 10 window 5 areas.

Alpha	**Negative Log Base 10**	**Discrimination Percentage**		
		SWSA	**SWDA**	**DW**
0.1	1	9.7	66.9	98.9
0.05	1.3	4.9	55.3	98.0
0.01	2	0.9	34.9	94.9
0.003	2.4	0.3	24.3	89.1

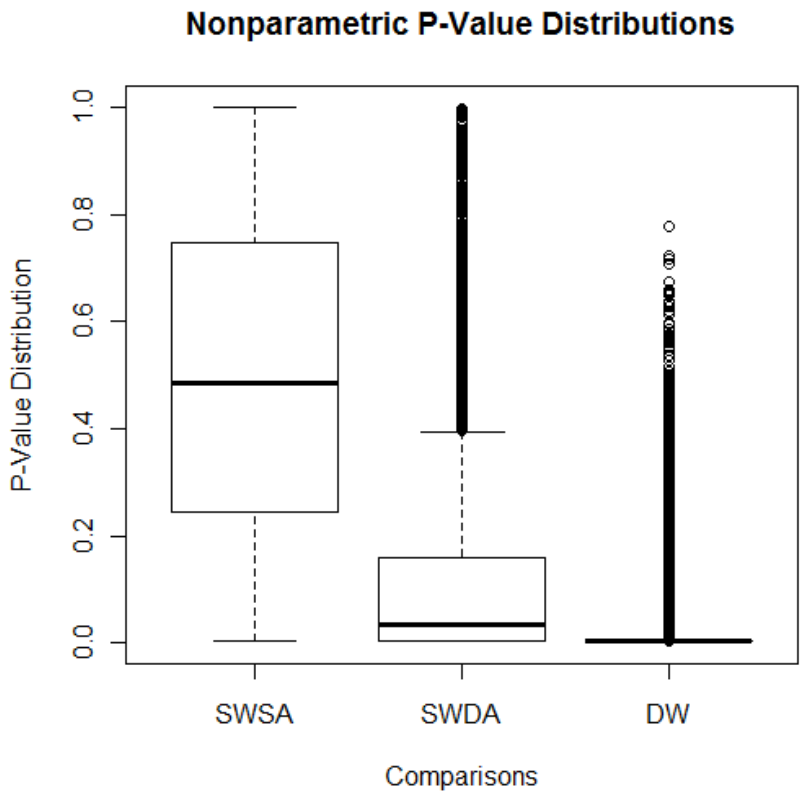

Figure 83: Boxplot demonstrating p-value distribution for nonparametric permutation test results of multiple point 10 windows 5 areas.

The second set of spectra was taken using partial drill down\multiple point spectral averaging, where ten total shots were collected with five shots drilled into two spots. This spectral averaging method had 1/5 of the spectral contribution from the surface of the sample. If the variation being observed in previous experiments between SWDA samples was due to surface contamination then the percent discrimination observed for this spectral averaging method should be reduced. The nonparametric permutation test was again performed first with a significance level of $\alpha=0.05$ and then the significance

level was varied, shown in Table 54. As the significance level was reduced, SWSA remained approximately at the significance level while SWDA and DW decreased in discrimination percentage. The significance level was kept at $\alpha=0.05$ to compare results to the multiple point spectral averaging results. At a significance level of $\alpha=0.05$ SWSA samples had 235 discriminations out of 5000 comparisons, 5%. DW had 82050 discriminations out of 112500 comparisons, a 73% discrimination rate, which was reduced from the multiple point spectral averaging method. The Type II error was 18%. SWDA also had a decreased discrimination rate of 23%, with 2321 discriminations out of 10000 comparisons. While SWDA discriminations decreased, the Type II error was significantly increased. In forensic work, as discussed previously, it is desirable to keep the Type II error at a minimum to prevent false inclusion of samples; therefore this spectral averaging method did not perform as well as the multiple point method. P-value distributions are shown in Figure 84. SWSA and DW comparisons had p-value distributions similar to the multiple point spectral averaging method. DW had outliers that fell at higher p-values, close to 1 and a slightly broader distribution. SWDA had a distribution of p-values similar to SWSA, with a slightly lower median value. These changes in the p-value distributions reflect the discrimination percentages.

Table 54: Nonparametric permutation test results from varying significance level for partial drill down\multiple point spectral averaging, 10 windows 5 areas.

Alpha	Negative Log Base 10	Discrimination Percentage		
		SWSA	SWDA	DW
0.1	1	9.3	30.1	82.1
0.05	1.3	4.7	23.2	72.9
0.01	2	1.0	12.4	51.9
0.003	2.4	2.9	18.8	65.8

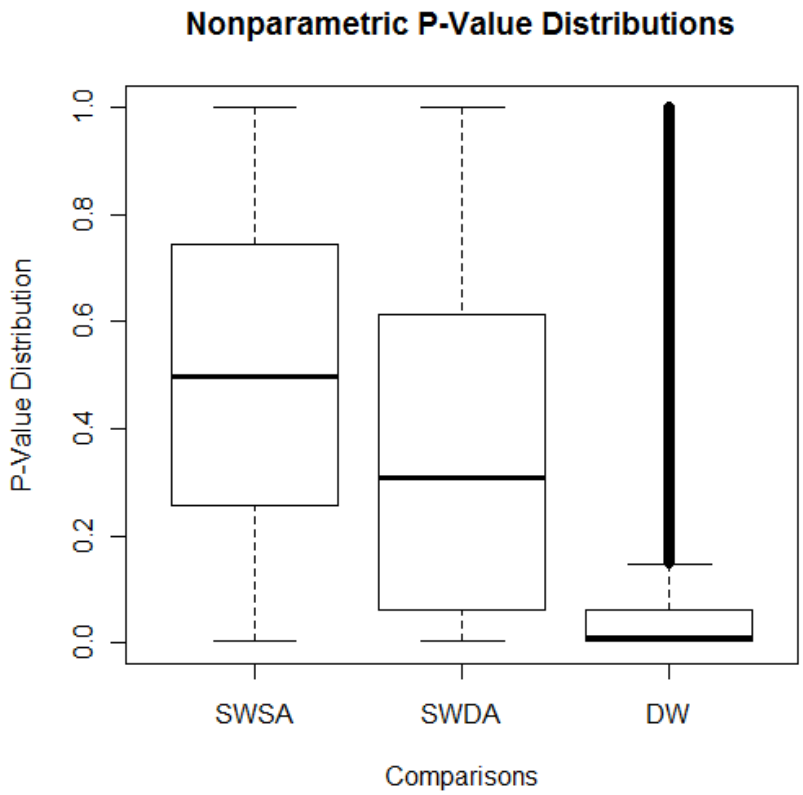

Figure 84: Boxplot demonstrating p-value distribution for nonparametric permutation test results of partial drill down\multiple point 10 windows 5 areas.

The final set of spectra was taken using full drill down spectral averaging, where all ten shots were collected in one spot. This spectral averaging method collected 1/10 of the spectra contribution on the surface. Therefore, this method contained the least amount of surface contribution. The nonparametric permutation test was again performed first with a significance level of $\alpha=0.05$ and then the significance level was varied, shown in Table 55. As the significance level was reduced SWSA remained approximately at the significance level while SWDA and DW decreased in discrimination percentage. The significance level was kept at $\alpha=0.05$ to compare results to the other two spectral averaging method results. For $\alpha=0.05$, SWSA had 273 discriminations out of 5000 comparisons, which was a discrimination rate of 5%. DW had 89775 discriminations out of 112500 comparisons, a discrimination rate of 80%. This resulted in a Type II error of 20%. SWDA had 2526 discriminations out of 10000 comparisons, a discrimination rate of 25%. The boxplot in Figure 85 shows similar distributions to the partial drill down\multiple point data. SWDA had a similar distribution to SWSA, with a slightly lower median value. DW had outliers of p-values around 1, with a small distribution of p-values near the significance level. Results for full drill down did not vary significantly from the partial drill down\multiple point method. The results again demonstrate a decreased amount of discrimination between SWDA while the Type II error increased from the multiple point method.

Table 55: Nonparametric permutation test results from varying significance level for full drill down spectral averaging, 10 windows 5 areas.

Alpha	Negative Log Base 10	Discrimination Percentage		
		SWSA	SWDA	DW
0.1	1	10.0	34.0	86.4
0.05	1.3	5.4	25.3	79.8
0.01	2	0.8	12.6	59.4
0.003	2.4	0.2	6.4	38.6

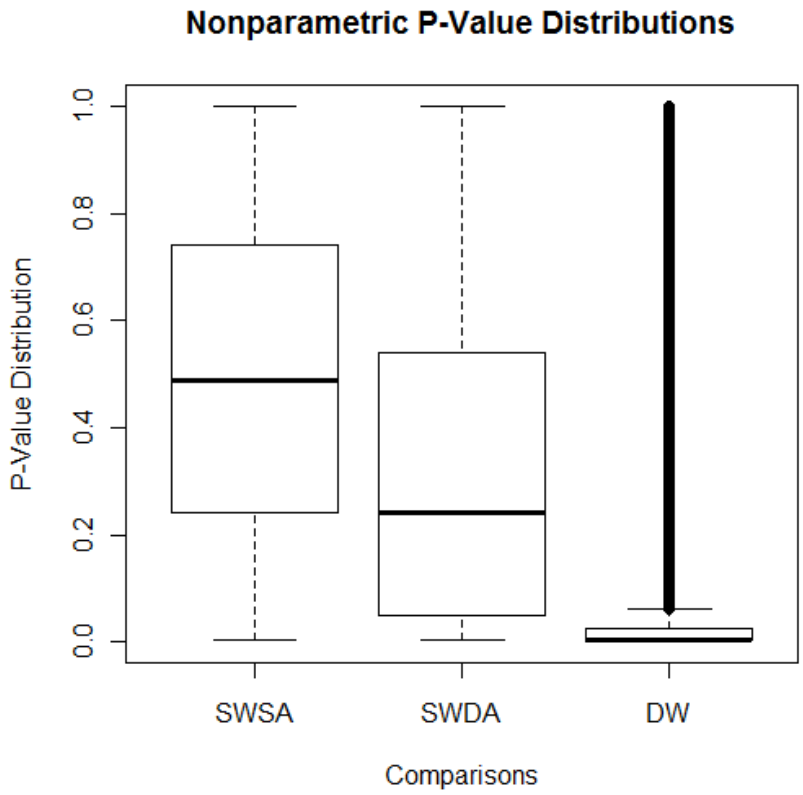

Figure 85: Boxplot demonstrating p-value distribution for nonparametric permutation test results of full drill down 10 windows 5 areas.

For all three methods the SWSA discrimination percentage remained at the significance level. The method that provided the overall best Type II error was the multiple point spectral averaging method. Despite the spectral averaging method, SWDA has a high discrimination rate.

6.6.1.5 Discrimination Versus Inter-Sample Distance Test

Based on the results from the previous glass experiments a known distance experiment was necessary to investigate at what distances discriminations began to be observed. The nonparametric permutation test results of a 3 cm x 1 cm sample are shown in Table 56. All of the same sample comparisons, at a center to center distance of 0 cm, have discrimination percentages at approximately the significance level, $\alpha=0.05$. The comparisons between A2 vs B and A1 vs B fell at higher discrimination percentages then comparisons at further distances, but the remainder of the comparisons increased in discrimination percentage with increased distance. The boxplot shown in Figure 86 shows the p-value distributions for each comparison in order of distance; it shows a general digression of p-values with distance. These results demonstrate an increased discrimination percentage with distance indicating spatial variance being observed within small distance on a single window pane.

Table 56: Nonparametric permutation test results for known distances comparisons.

Comparison	Discriminations	Total Comparisons	Discrimination Percentage	Distance (cm)
A1 vs A1	3	100	3%	0
A2 vs A2	7	100	7%	0
B vs B	3	100	3%	0
C vs C	7	100	7%	0
A1 vs A2	15	100	15%	0.5
A2 vs B	68	100	68%	0.75
B vs C	58	100	42%	1
A1 vs B	100	100	100%	1.25
A2 vs C	39	100	39%	1.75
A1 vs C	79	100	79%	2.25

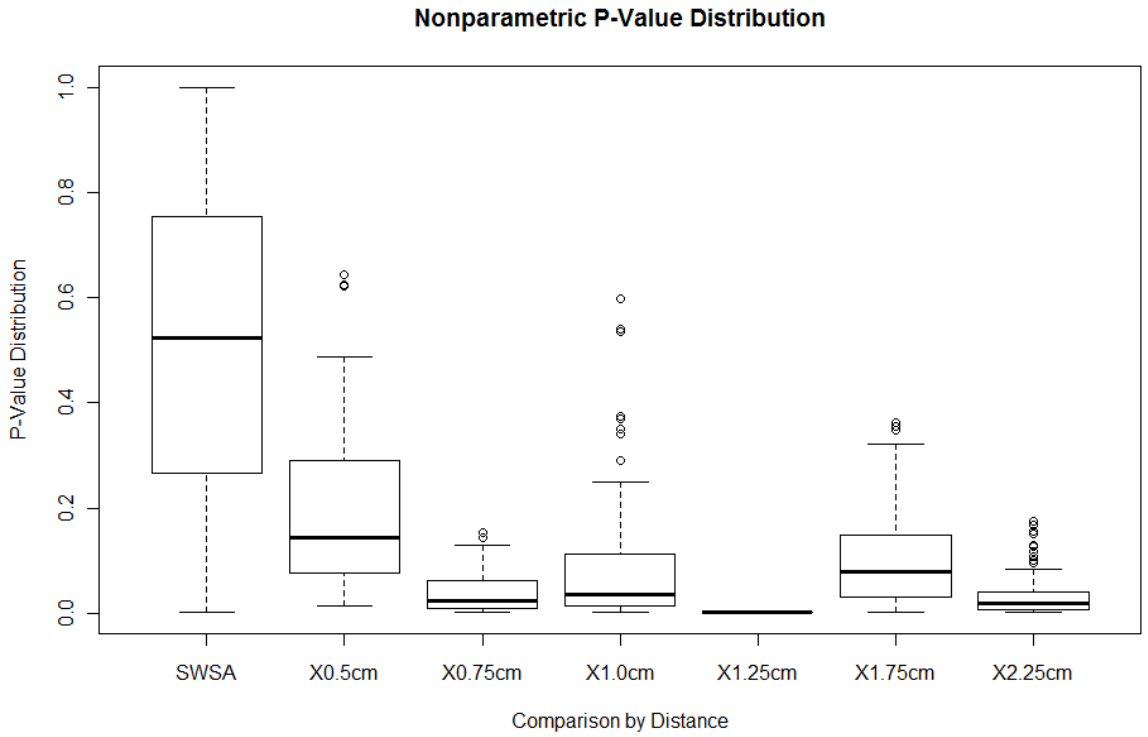

Figure 86: Boxplot of nonparametric permutation test p-values for distance comparison samples.

6.6.1.6 Nonparametric versus Parametric

The comparison of the Wilcoxon Rank Sum test, a nonparametric method, and the Hoteling's t-test, a parametric t-test, was performed to ensure the spatial variation seen within window was not due to our nonparametric method. While the parametric method was not as well suited for our data as it assumed normal distribution of the data, parametric methods are more common data analysis techniques. Therefore, comparisons of the results from the nonparametric method to the parametric method allowed for the determination that the observed spatial variation within a single window pane was not due to the criteria set forth by the nonparametric methods.

Both the Hoteling's T-test and the Wilcoxon Rank Sum test were applied to the data collected for all three spectral averaging methods. The results are shown in Table 57 thru Table 59. For the multiple point spectral averaging method, results shown in Table 57, showed similar results for the Hoteling's t-test and the Wilcoxon Rank Sum test results. The Wilcoxon Rank Sum test discriminated the same number of samples as the Hoteling's t-test, with each discriminating all but one sample. The Wilcoxon Rank Sum test did not discriminate A1 and A4, while the Hoteling's t-test did not discriminate areas A1 and A2. Overall, the two methods demonstrated they were performing similarly and discriminations within a single window pane were being seen for both methods.

Table 57: Results for comparisons of nonparametric versus parametric method for multiple point spectral averaging method. The red numbers represent discriminations while black represents non-discriminations.

Hoteling's T-test					
	A1	A2	A3	A4	A5
A1					
A2	**0.01**				
A3	**21.21**	**12.06**			
A4	**16.83**	**32.41**	**13.31**		
A5	**12.42**	**102.67**	**78.25**	**26.07**	
Wilcoxon Rank Sum Test					
	A1	A2	A3	A4	A5
A1					
A2	**<2.2e-16**				
A3	**<2.2e-16**	**0.01**			
A4	**0.23**	**<2.2e-16**	**0.001**		
A5	**<2.2e-16**	**<2.2e-16**	**<2.2e-16**	**<2.2e-16**	

The results for the partial drill down/multiple point spectral averaging method performed similarly to the multiple point spectral averaging method for the two methods. Again, the Hoteling's t-test and Wilcoxon Rank Sum test discriminated the same areas, with the Wilcoxon Rank Sum test discriminating one additional sample, A1 versus A5. This spectral averaging had less discrimination between the areas within the single window pane, shown in Table 58, for both methods as was seen for the nonparametric permutation results. Again, both statistical methods performed similarly and discriminations were still being observed for the majority of the areas.

Table 58: Results for comparisons of nonparametric versus parametric method for partial drill down/multiple point spectral averaging method. The red numbers represent discriminations while the black represent non-discriminations.

Hoteling's T-test					
	A1	A2	A3	A4	A5
A1					
A2	**0.002**				
A3	**19.37**	**27.79**			
A4	**5.54**	**4.27**	**10.76**		
A5	**2.28**	**9.34**	**8.10**	**2.13**	
Wilcoxon Rank Sum Test					
	A1	A2	A3	A4	A5
A1					
A2	**0.23**				
A3	**<2.2e-16**	**<2.2e-16**			
A4	**0.12**	**0.754**	**<2.2e-16**		
A5	**7.21e-5**	**1.36e-06**	**<2.2e-16**	**0.095**	

The final spectral averaging method tested with both statistical methods was the drill down method. The Hoteling's t-test and the Wilcoxon Rank Sum test differed in results for this spectral averaging method with the results for both shown in Table 59. As can be seen in the table, the Hoteling's T-test discriminated all but one sample. This result resembled the multiple point spectral averaging method as opposed to the partial drill down/multiple point spectral averaging method. This was unexpected as the nonparametric permutation test performed the most similarly for the two drill down methods. The Wilcoxon Rank Sum test, had results more similar to the partial drill down spectral averaging method, with five comparisons discriminating. These results still showed discriminations being observed between the different areas of the same

window pane, they also demonstrated that the Wilcoxon Rank Sum test was more appropriate for our data.

Table 59: Results for comparisons of nonparametric versus parametric method for drill down spectral averaging method. The red numbers represent discriminations while the black represent non-discriminations.

Hoteling's T-test					
	A1	A2	A3	A4	A5
A1					
A2	**0.001**				
A3	**32.26**	**23.24**			
A4	**6.06**	**15.16**	**12.32**		
A5	**5.32**	**4.87**	**17.95**	**8.16**	
Wilcoxon Rank Sum Test					
	A1	A2	A3	A4	A5
A1					
A2	**1.79e-6**				
A3	**2.07e-4**	**2.64e-6**			
A4	**0.71**	**4.52e-8**	**7.07**	**1.98**	
A5	**0.74**	**0.26**	**0.02**	**0.55**	

6.6.1.7 LIBS Imaging

The first set of imaging data analysis was collected on the 1 cm x 1 cm piece of glass. Five layers of the glass was sampled in 16 spots and the PCA scores corresponding to the first three principal components were plotted on an RGB color scale to observe the variance within the small area of the window pane. The loadings for the first three principal components are shown in Figure 87, which demonstrate the elements contributing to each of the colors observed in the plots. The elements contributing to the eigenvector loadings are listed in Table 60.

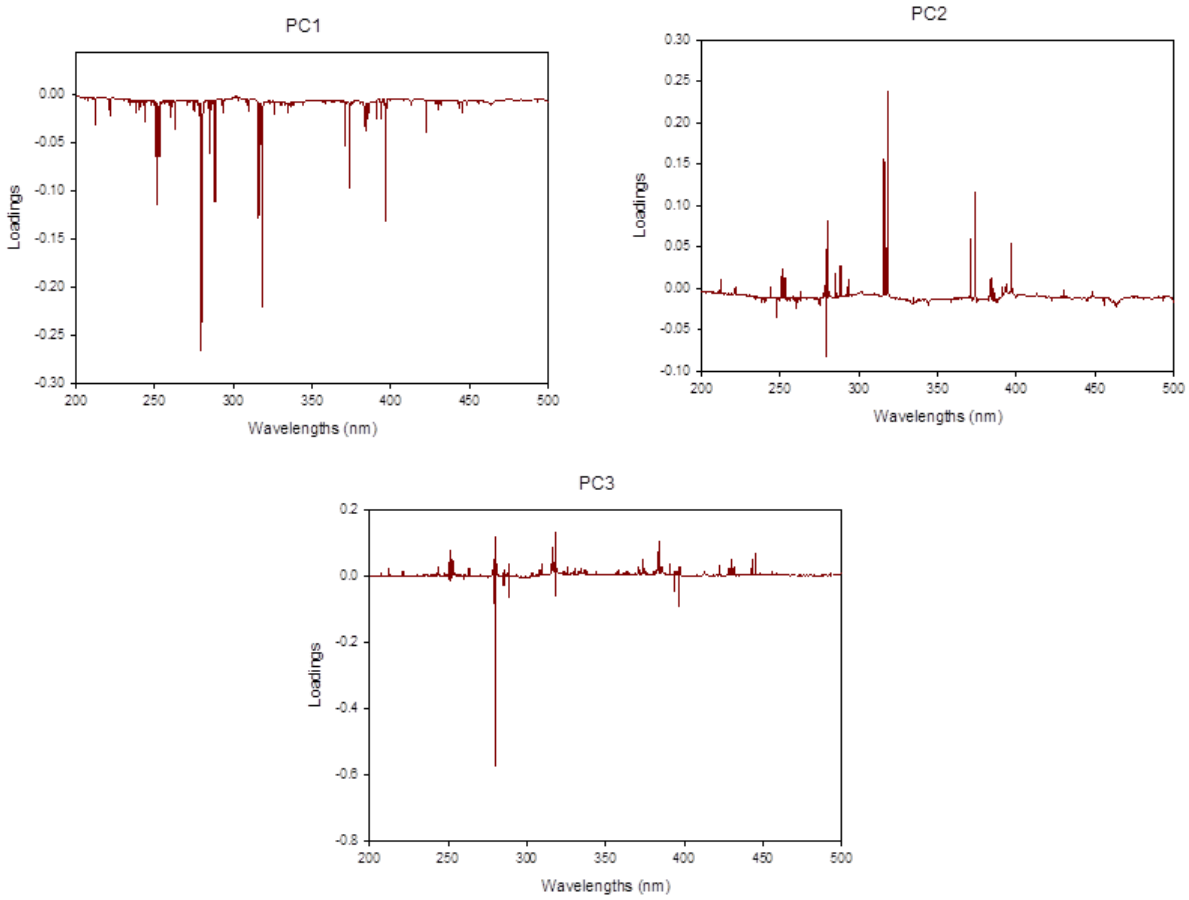

.

Figure 87: Eigenvector plots for the first three principal components for the 1 cm x 1 cm piece of glass.

Table 60: List of elements and wavelengths contributing to the eigenvector loadings for the first three principal components for the 1 cm x 1 cm piece of glass.

Element	Wavelength (nm)
Si	221.67 221.87 250.69 251.61 251.92 252.85 288.16
Mg	383.23 383.83
Mg II	285.28 285.30
Ca	443.50 445.48 445.59
Ca II	315.89 317.93 370.60 373.69
Dy II	396.84
Zr	422.77
Nd II	430.36

Based on these contributions, the normalized scores for the first three principal components were plotted on the RGB color scale for each layer of the 1 cm x 1 cm piece of glass. The plots are shown below in Figure 88. The first layer demonstrates the biggest variation in the areas of the five layers. This increased variation is attributed to surface effects. For the lower layers, there begins to be two domains: the upper left portion of the plots for layer three through five show a greater contribution from the green component while the lower right portion of the plots for those layers show a greater contribution from the blue component. These plots demonstrate variation within this small area of glass within a single window pane and show domains forming within the window areas.

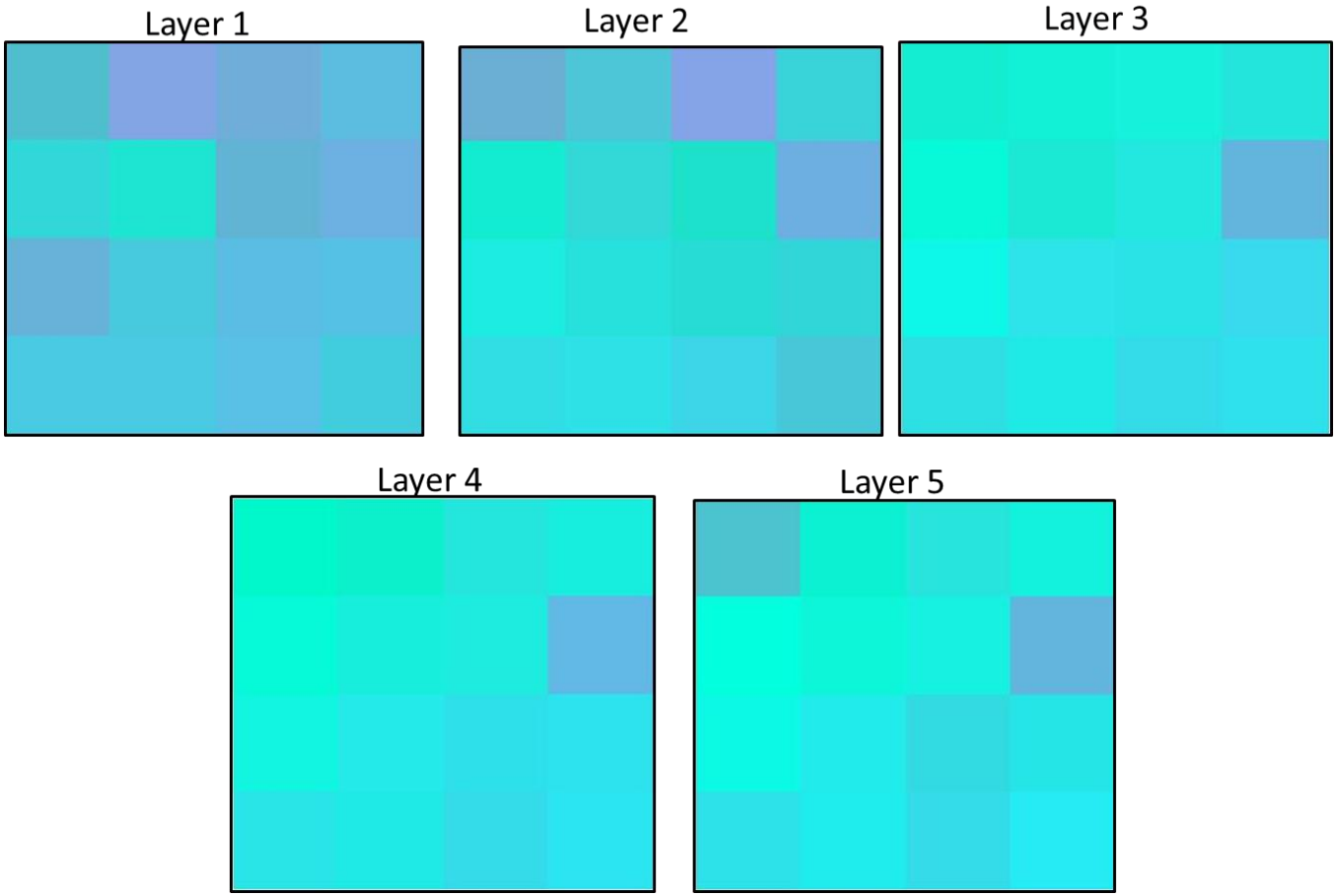

Figure 88: RGB plots of the PCA scores for the five layers of glass from the 1 cm x 1 cm piece of glass.

The 2 cm x 2 cm piece of glass performed similarly. One hundred spots were sampled, and five layers were collected per spot. PCA on the data normalized summed to one was performed to obtain the scores and eigenvectors for plotting. The eigenvectors were plotted, shown in Figure 89, to determine the elements contributing to the variance plotted. Again, the first three principal components were plotted; listed in Table 61 are the elements which contributed to the eigenvector loadings for the three principal components.

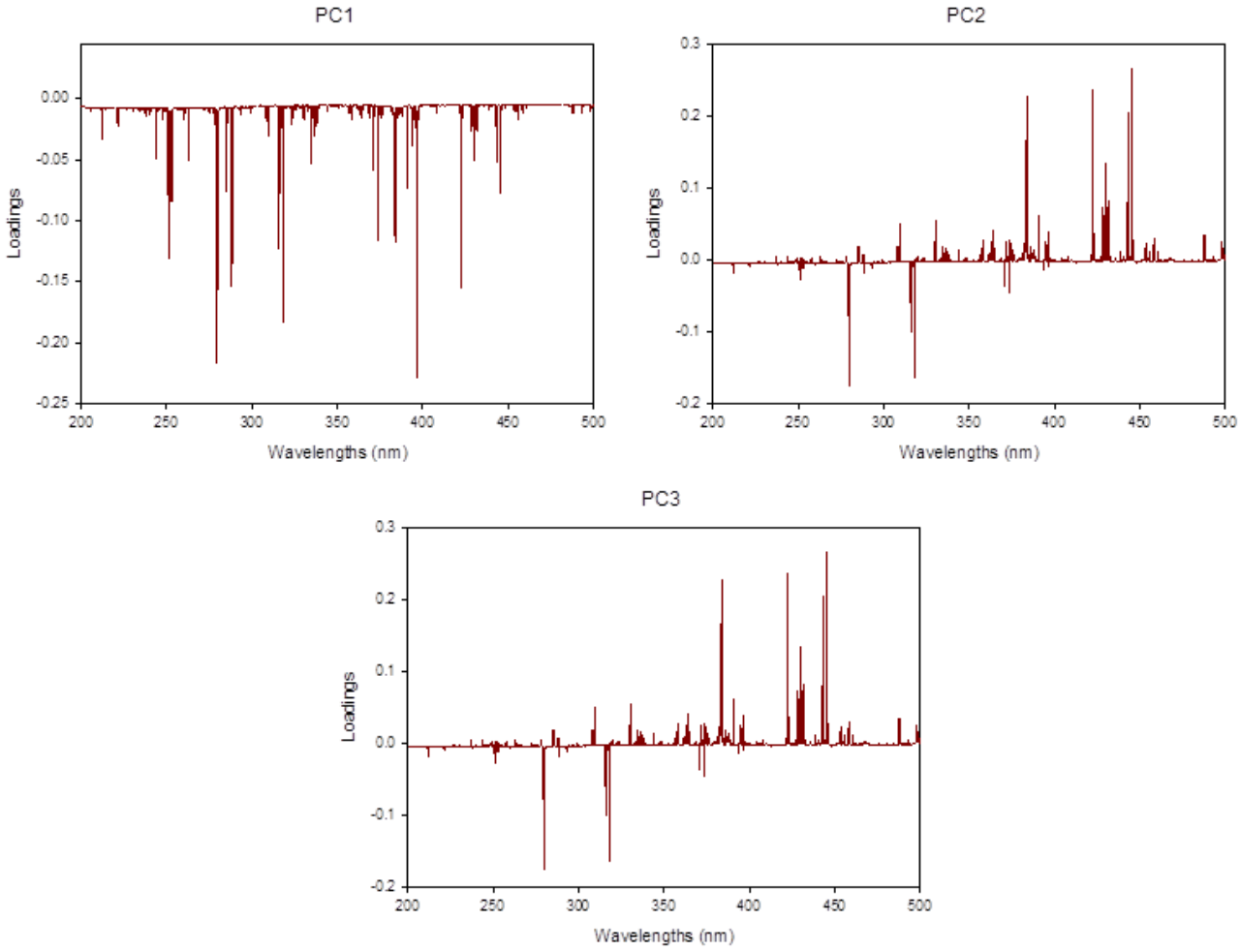

Figure 89: Eigenvector plots for the first three principal components for the 2 cm x 2 cm piece of glass.

Table 61: List of elements and wavelengths contributing to the eigenvector loadings for the first three principal components for the 2 cm x 2 cm piece of glass.

Elements	Wavelengths (nm)
Si	221.81 250.69 251.61 251.92 252.85 288.16
Mg	383.23 383.83
Mg II	279.55 280.27
Na	285.30
Na II	309.27
Ca	315.89 317.93 370.60 443.50 445.48 445.59
Ca II	373.69
Ti II	334.94 336.12 337.28
Dy II	396.84
Zr	422.77
Nd II	430.36
Tb	431.88

The scores corresponding to the first three principal components were plotted on an RGB color scale for each of the five layers of the 2 cm x 2 cm piece of glass. The plots for each layer are shown in Figure 90. For this data set variance can again be seen between the different spots. The first two layers show similar distribution of colors with the greatest contributions coming from the blue and green components. Again, the differences in these layers are attributed to surface effects on the glass. The third and

fourth layers have an overall duller color contribution. These layers have domains beginning to form where the red contribution is strong on the left side and a little bit in the middle. The red contribution begins to be seen in the first and second layer also. The fifth layer is different from the other four layers. This may be due to the beginning of confinement effects of the plasma distorting the results. Overall, this data set also shows variance within the small area of a single window pane. The domains are not as easily detected but there do appear to be domains based on the third and fourth layer.

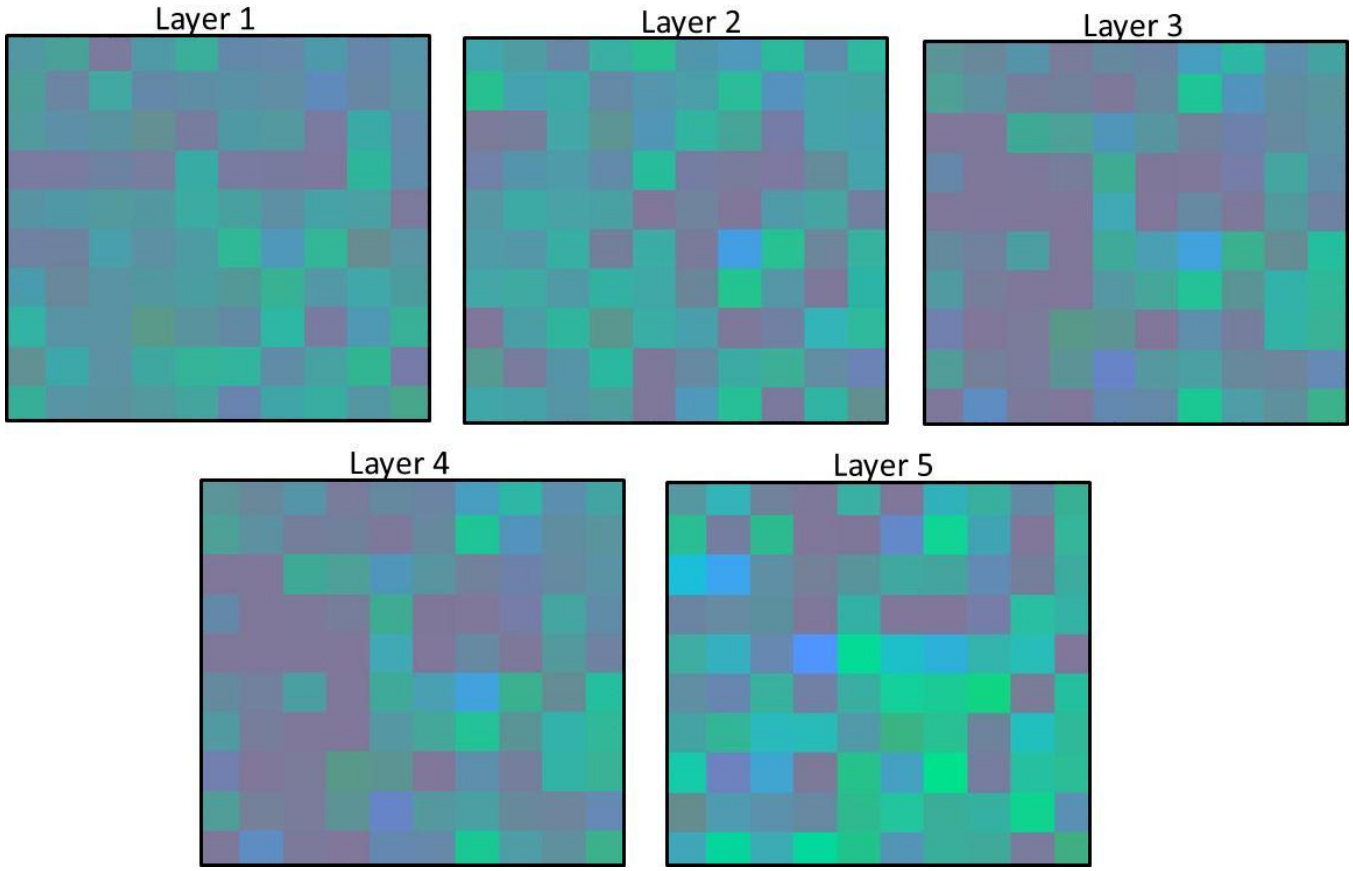

Figure 90: RGB plots of the PCA scores for the five layers of glass from the 2 cm x 2 cm piece of glass.

6.6.2 Wilcoxon Rank Sum Test

The Wilcoxon rank sum test was performed on the data to reduce this method to practice within the forensic community. The data was analyzed for all three spectral averaging methods for the ten windows, five areas. As described in the experimental section, three groups of nonparametric permutation test p-values were set up: known vs. known (KK), known vs. questioned 1 (Q1K) and known vs. questioned 2 (Q2K). The known versus known comparisons included all possible comparisons of four pieces from a single window pane. The known versus questioned 1 consisted of all of the comparisons for the four pieces of the known to a single piece from a different area of the same window. The known versus questioned 2 consisted of all of the comparisons for the four pieces of the known compared to a single piece from a different window. Calculations were performed for each of the ten windows so that each of the five areas was considered questioned 1.

6.6.2.1 Multiple Point Spectral Averaging, 10 Windows 5 Areas

For the multiple point spectral averaging method, 50 calculations were performed for K vs. Q1 and 50 calculations were performed for K vs. Q2. Table 62 provides a summary of the results obtained for the Wilcoxon Rank Sum test. Of the 50 calculations performed for K vs. Q1 37, or 74%, were found to be statistically different. Only 13, or

26%, were calculated to be statistically the same. These results indicate despite the incorporation of some of the spatial variance within a single window pane a statistical difference was observed which resulted in the discrimination of Q1 from K. The variance may be due to surface variation as these results were acquired based on multiple point collection, but the differences observed between different areas of a single window pane were statistically significant. The 50 calculations performed for K vs. Q2 resulted in 43, or 86%, found to be statistically different and 7, or 14%, being statistically the same. The different windows discrimination rate for statistically the same was slightly higher than the significance level, but overall the results for different windows demonstrated the ability to discriminate between them.

Table 62: Wilcoxon Rank Sum test results for the multiple point spectral averaging for questioned versus known.

	KQ1	**KQ2**
Statistically the Same	13	7
Statistically Different	37	43
Total Comparisons	50	50
% Statistically the Same	26%	14%
% Statistically Different	74%	86%

6.6.2.2 Partial Drill Down\Multiple Point Spectral Averaging, 10 Windows 5 Areas

The Wilcoxon Rank Sum test was performed on 50 K vs. Q1 comparisons and 50 K vs. Q2 comparisons for the partial drill down\multiple point spectral averaging method. The

results are shown in Table 63. For the K vs. Q1 comparisons only 15 out of the 50 total comparisons were found to be statistically the same, 30%. The remaining 35 K vs. Q1comparisons were statistically different, 70%. The high percentage of statistically different comparisons for the K vs. Q1 comparisons again indicates that the full extent of spatial variation within a single window pane was not incorporated in the known sample to prevent discrimination of Q1. One fifth of the spectra for each of the samples originated from the surface of the sample, therefore surface contamination may still be contributing to the variance. The 50 K vs. Q2, or different window comparisons, had only two comparisons which were found to be statistically the same, or 4%, which was approximately at the significance level. The remaining 48 comparisons of K vs. Q2 were found to be statistically different which gave a 96% discrimination rate. Therefore, these results were similar to the multiple point spectral averaging method where different windows were successfully discriminated between but samples from different windows were also discriminated between.

Table 63: Wilcoxon Rank Sum test results for the partial drill down\multiple point spectral averaging method for questioned versus known.

	KQ1	**KQ2**
Statistically the Same	15	2
Statistically Different	35	48
Total Comparisons	50	50
% Statistically the Same	30%	4%
% Statistically Different	70%	96%

6.6.2.3 Drill Down Spectral Averaging, 10 Windows 5 Areas

For the drill down spectral averaging method, 50 calculations were performed for K vs. Q1 and 50 calculations were performed for K vs. Q2. A summary of the results obtained for the Wilcoxon Rank Sum test for this data is given in Table 64. For the 50 calculations of Q1 vs. K there were 35, or 70%, statistically different comparisons. Only 15, or 30%, were calculated to be statistically the same. Again, statistical differences were observed for K vs. Q1 comparisons which again indicate that the spatial variance incorporated into the known by the multiple pieces of glass did not account for all the variance within a single window pane. Due to only one of the ten shots being collected on the surface, the variance may be due to variance in the amount of trace elements present in the different areas of a single window pane. This could be due to the manufacturing process or environmental exposure. For the 50 different window comparisons, 48 were found to be statistically different, 96%, and 2 were found to be statistically the same (4%). These results demonstrate the ability to successfully discriminate between different window panes as was seen with multiple point spectral averaging.

Table 64: Wilcoxon Rank Sum test results for the drill down spectral averaging method for questioned versus known.

	KQ1	**KQ2**
Statistically the Same	13	3
Statistically Different	37	47
Total Comparisons	50	50
% Statistically the Same	26%	6%
% Statistically Different	74%	94%

CHAPTER 7: CONCLUSIONS AND FUTURE WORK

The statistical data analysis techniques discussed in this work have shown promise for application to the analysis of forensic samples. The research demonstrated the successfully application of the statistical methods to forensic data acquired by multiple instrumental techniques. The statistical methods were shown to provide desired error rates for classification or discrimination of forensic samples to provide additional backing to conclusions reached by forensic analysts. The results demonstrated the decision to apply a classification method or a discrimination method was determined based on the desired goals of the analysis of specific samples. The classification methods provided in this research were best applied when a library can be compiled of the representative population of the samples to be tested, such as the bullet jackets and organic compounds; while the discrimination methods were best for forensic applications that have populations that change over time, such as the automobile paint and glass samples. Overall, successful results were obtained using all of the applied statistical methods to improve analysis of forensic samples.

7.1 Fire Debris

Results discussed previously indicate the ability of discriminant analysis in the classification of fire debris samples. The results showed the ability to discriminate

between pure ignitable liquid and substrates easily and further classify ignitable liquids into the ASTM classes. While the ignitable liquids were not as easily classified into their ASTM classes, the results of this technique provided statistical backing that did not previously exist. This method begins to move fire debris analysis from a pattern recognition technique to a statistically backed forensic discipline. Data sets not containing the MISC and OXY group provided higher percentages of correct classification then classification of samples when these two classes were included in the analysis. As expected, the MISC and OXY classes encompassed a broad range of samples, therefore samples in these groups and the other ASTM classes have similarities that make classifying more difficult.

Future steps to improve this approach to fire debris classification should investigate ways to deal with the MISC and OXY classes. Methods that may be applied to this issue could include the reclassification of these classes by functional groups present in the samples or a step wise analysis of the samples starting with broad classification and ending with ASTM classifications. In addition to addressing the MISC and OXY classes, the application of this method to mixtures should be addressed, as most if not all fire debris cases will involve samples containing multiple ignitable liquids and/or substrates. Initial investigation into mixtures was performed and difficulty was encountered due to the nature of LDA and QDA as hard classifier methods. The combination of this method with a soft classification method such as the soft classification method described may provide a technique for classifying fire debris mixture samples.

7.2 Bone

7.2.1 Discriminant Analysis

The bone research discussed was preliminary work and should be expanded on further based on the results seen. While the data sets were small, results showed promise for both discriminant analysis for the classification of bones by species and the application of the nonparametric permutation test for the discrimination between different bones from different species.

The bone data was in its initial testing stage and the results showed promise for the discrimination between bones of different species. A small data set was tested in this research to determine the best means for classification or discrimination of bone samples. The nonparametric permutation test results indicate the successful discrimination of the individual bones. Further work needs to be done on larger data set; additional comparisons should be made to obtain more accurate Type I and Type II errors. Additional tests could also be performed with the data grouped by different means; instead of by individual bones, the nonparametric permutation test could be performed to determine the discrimination between species or exposure to specific cleaning or environmental conditions.

Future work should also be performed with increased background knowledge of the samples, i.e. cleaning process and environmental exposure. Additional information about the exposure to environment, cleaning processes, and demographic data could provide useful information in interpreting the results and may explain assumed Type I or Type II errors. Results would be better interpreted with more knowledge of the samples, allowing for a better assessment of the techniques. Also, the data can be grouped into different categories to determine the ability to distinguish between: bone versus non-bone, human versus nonhuman, archeological versus forensic and other potential groupings of interest.

7.3 Organic Compounds and Polymer Mixtures

7.3.1 LIBS

The analysis of the LIBS organic polymers presented a challenge to the soft classification method. As LIBS is an atomic spectroscopy technique the spectral pattern was similar for the organic compounds due to each compound being comprised of the same major elements: C, H, N, and O. Due to the similarity in the spectral pattern, the discrimination between organic compounds was more complicated than analysis with FTIR or Raman. In addition to the similar spectral patterns, sampling in air presented additional complications.

The results from the PCA\TFA analyses showed promise for analyzing multiple spectra from a sample. Results successfully identified the components contributing to the mixture by high correlations in the TFA as long as good separation was observed in the PCA model. The data collected in the argon atmosphere had the best separation of the PCA model and therefore the TFA correlations were the highest. When the compounds in the PCA model were not well separated, only the separated contributor was identified with a high correlation. The remaining compounds resulted in lower TFA correlations, as seen in the air data for nitrocellulose on poly styrene. The application of TFA provided correlation values which could be used to identify a specific class of unique compounds.

The Bayesian decision theory provided results that further backed the TFA analysis. The Bayesian decision theory provided posterior probabilities and kernel distributions based on the TFA correlations which assisted in the identification of the compounds that were present in the mixture. For the LIBS mixture data at least one of the compounds present in the mixture had a posterior probability calculated, resulting in identification of at least one of the components present in each mixture.

While organic compounds were difficult to discriminate between using LIBS spectral data, successful application of the multiple step soft classification method was observed to provide conservative classifications of the polymer mixtures. Future work should be

done to optimize the unique spectral characteristics of different organic compounds in LIBS.

7.3.2 FTIR

The FTIR analysis of the organic compounds provided useful information about the application of PCA\TFA, and Bayesian decision theory on FTIR spectral data. Using a library comprised of eight organic compounds, some having very similar structures, PCA\TFA was successfully applied to complex organic mixtures independent of the background. High correlation values were obtained for the components present in the complex mixtures every time, with separation in correlation values being seen between compounds of similar structure. TFA proved to be useful in identifying the compounds present in complex mixtures with high correlation values.

The Bayesian decision theory results further backed the results from the TFA. In addition to the correlations obtained from the TFA, the Bayesian Decision Theory provided the means to convert the hard classification method of TFA into a soft classification method, which allowed for single, multi, or no classification to be obtained. While it resulted in a slightly more conservative method, the majority of the mixture samples were correctly classified.

As FTIR is a molecular spectroscopy technique, it performed better than LIBS in the identification of the organic compounds in the presence of highly similar structures. The interactions of the functional groups provided additional information not available in the elemental analysis of LIBS which allowed for identification of 2,3-DNT from 3,4-DNT and 2,4-DNT. FTIR was not limited to the identification of just the presence of elements in the compounds, which consisted of carbon, nitrogen and oxygen in all of the organic compounds, allowing it to provide a better method for this analysis.

7.3.3 Raman

The Raman analysis of organic compounds on organic backgrounds provided similar results to the FTIR analysis. As both are molecular spectroscopy techniques they performed similarly for the ability to classify despite the similarity in some of the organic compound structures.

PCA demonstrated separation of the library compounds, while the TFA results showed high correlations for the majority of mixture components to the correct library compound. Theobromine had the lowest correlations observed which was attributed to a poor collection of the organic compound during the Raman analysis. The theobromine results demonstrated the need of good spectral data for application of the statistical methods.

The Bayesian decision theory further supported the results seen in the TFA analysis. The majority of the samples classified correctly, with only two of the mixtures not classifying. There were no incorrect classifications of the mixtures. Overall, the results showed promise for the application of these methods to classify organic compounds within complex mixtures independent of the background. The approach also provides a statistical probability to classifications to assist an analyst in reaching a conclusion.

7.4 Metal Transfers

The TFA results proved to successfully use a library of bullets to identify the class of bullet jacketing used in metal transfer samples independent of the background. For the majority of the samples, the class that had the highest correlation value between the library and sample was the class that was present on the sample. TFA performed best for the single metal transfer with 87% having the highest correlations corresponding to the class present on the sample. As expected the results decreased slightly with the two metals transferred onto the same sample, with 83% correct identification of class based on high correlation. The final method and most complex sampling surface, the bullet holes, also had 83% correct identification of class based on high correlation. The majority of the samples that had the highest correlations corresponding to a different class were MJ samples, or mixtures including MJ. MJ was the hardest metal present in

the experiments and likely the hardest to transfer, therefore making its detection more difficult on the different sample surfaces.

As was shown in the results for the Bayesian decision theory of metal transfer, the combination of TFA/Bayesian decision theory provided the additional statistics needed to give conservative identification of present metals in the sample. The methods demonstrated the best classification ability with a correlation lower cutoff of 0.8 and classification level of significance of 0.05. These parameters set a reasonable expectation for correct classification, and do not assign a sample if insufficient data is available. In that aspect, the method provides for a conservative approach to the classification of metal transfer. The method allows for samples to be unclassified which prevents a high percentage of misclassifications.

The single metal transfer onto two substrates demonstrated the ability of the mathematical technique for the problem at hand, with a high percentage of correct classifications. When the complexity of the issue was increased by transferring two metals to the same spot on the two substrates the number of classifications decreased, but the majority of the samples had correct classification for at least one of the metals present. A small number of the samples correctly classified both components present. In both the single and multiple transfer samples more non-classifications occurred than misclassifications. Again, this represents the conservative nature of the test, with a non-classification being a preferred result over misclassifications. The results of the

multiple transfer samples depended on the transfer order, ability to transfer the bullets so the two lines overlapped, and the transfer ability to the substrate. Variation is expected to occur in the amount of both bullets being observed from each spectrum of the multiple transfer samples, with one bullet being more prominent from one spectrum to the next; results would be influenced by the ratio of the two components that would be collected. These considerations demonstrate the increased complexity from the single transfer to the multiple transfers.

The final metal transfer test was designed to resemble a case work sample, where a bullet hole was sampled. While only one metal was transferred to the substrate, the transfer could not be controlled and the sample surface was irregularly shaped. The number of classifications was much lower for these samples, but when posterior probabilities were calculated, all but one sample was correctly classified. The reduced classification of this data set could be due to LIBS issue with the irregular sample surfaces. Additional efforts should be made to perform this analysis with an instrument with autofocusing capabilities. Autofocusing would eliminate the human error associated with optimizing the sampling height of irregular sample surface.
While this method is conservative in its ability, it has a very low percentage of misclassifications. A non-classification in forensic science is more desirable than a misclassification when it comes to deciding the fate of a person accused of a crime. There are a few suggestions given above that may improve the results of this method. The results do show the ability of combining PCA/TFA/ Bayesian decision theory to

provide statistical backing to background independent classification of metal transfer samples.

7.5 Automobile Paint

The application of the nonparametric permutation test for the analysis of automobile paint spectra collected by both LIBS and FTIR proved to be a useful technique in discriminating paint samples. The nonparametric permutation test was well suited for the application which was attributed to the LIBS data not being guaranteed to follow a normal distribution. Therefore, for LIBS data a technique without the assumption of normality provides a more accurate result.

For the LIBS results the overall discriminating power for nonparametric permutation test was approximately 89% and the Type I error was held below the significance level; the FTIR results for the nonparametric permutation test of the log intensities of the reduced spectral range (650-2000 cm^{-1}) were an overall discriminating power of 99.90% and a Type I error of 25.53%.

The results were improved when the samples were subdivided into groups based on characteristics easily distinguished by visual and microscopic analysis; paint color, number of layers, and presence of effect pigments. The separation of the samples into

subdivisions based on nondestructive methods prior to minimally destructive methods would be the ideal approach for a crime lab to follow in the analysis of evidence. Based on the subdivision, it was apparent that all of the color groups performed well for both inter and intra samples, with the exception of inter-samples within the white color group. Caution should be taken in the comparison of unknown white paint samples until further research is performed to determine the potential cause for lack of discrimination between samples of this color. For the remainder of the color groups, the Type I and Type II errors were kept at nominal levels for the LIBS data.

For the LIBS spectra the nonparametric permutation test provided information about most if not all of the layers of paint in a sample, not just the top layer as seen with the FTIR data. Therefore, the LIBS spectra provided for more individual characteristics for a specific paint to be used during comparison to an unknown paint sample.

The benefit of the nonparametric permutation test in the analysis of automobile paint was that it ensured a fixed Type I error rate described by a significance level, $\alpha=0.05$. This allowed for the Type II rate to be independently determined and in forensic science the Type II error is the one of most importance. This plus the low Type I error showed the success of the nonparametric permutation test for analysis of LIBS data for automobile paint samples.

The difficulty with the FTIR technique as applied in the research was that it only analyzed the top coat of paint, whereas the LIBS analysis sampled and averaged together all of the layers. The LIBS spectra had more unique characteristics making the determination of discrimination/non-discrimination of the comparisons easier. In addition to the limitation to the top coat of paint, the FTIR is a molecular technique which is more informative of the organic components of a sample. Paints are made up of polymers, pigments, dyes and fillers with the majority of the characteristics being inorganic in nature. Again, this is where LIBS provides more characteristic information about the inorganic element components that may provide more unique information about each paint. Based on the results seen, the FTIR would be a good nondestructive screening method for the top coat of a paint sample prior to more in-depth analysis by LIBS of all the layers.

Future work should look to expand the data set and perform more intra-sample comparisons. The addition of more intra-sample comparisons should reduce the individual groups (by color, number of layers, and presence of effect pigments) Type I errors. As was seen in the results, the overall data set had a Type I error below the significance level but the individual groups Type I errors were much higher. This was due to the small number of comparison, as one discrimination out of three would result in a Type I error of 33%. Also, future work should look to expand this method to other areas of physical evidence analysis.

7.6 Automobile Float Glass

The analysis of LIBS automobile float glass spectral data by the nonparametric permutation test and the Wilcoxon Rank Sum test provided valuable information about glass as forensic evidence. The nonparametric permutation test provided a statistical method for discriminating between different automobile window panes. In addition to discriminating between different windows, the nonparametric permutation test presented evidence of spatial variation between different areas of the same window pane. The nonparametric permutation test results were further substantiated with the application of the more stringent Wilcoxon Rank Sum test. In addition to the identification of spatial variation due to the elevated discrimination levels of SWDA comparisons, both methods demonstrated a low discrimination rate for same window-same area comparison and a high discrimination rate for different window comparisons.

The spatial variation was investigated purely in this research to present evidence that it was present. Multiple spectral averaging methods were tested to determine whether the variation being observed was due to the sampling method, surface contamination, or heterogeneity within the glass. All three spectral averaging methods demonstrated elevated levels of discriminations between SWDA comparisons while the SWSA comparisons remained approximately at the significance level. Decreased discriminations of SWDA samples were observed as average spectra were comprised of fewer surface shots, but DW discriminations also decreased. In addition to the

spectral averaging methods, a distance test was set up using the multiple point averaging method. This test demonstrated an increase in discrimination with an increase in distance. While the cause of the spatial variation is currently unknown, it has been shown that special consideration should be taken when comparing samples from the same window without spatial information. The spatial variation could be caused by a number of things including: trace element fluctuation or contamination during manufacturing, environmental effects, or surface contamination. Future work should investigate the cause for observed spatial variation.

Blind tests demonstrated the need for additional investigation into how this method will be applied to forensic casework. The nonparametric permutation test p-values provided the ability to determine whether individual comparisons were discriminated or not. The current limitation is how to deal with same window-different area comparisons. In forensic samples spatial information is rarely obtained, therefore samples from the same window may be discriminated and falsely excluded (Type I error). While this is preferred over false inclusion of evidence (Type II error), the current discrimination levels of same window-different area samples would result in high levels of Type I errors. The issue with forensic application returns to the necessity of further work into determining the cause of spatial variation. Control samples may need to be incorporated into forensic casework to provide a general guideline for acceptable p-value distribution of SWSA, SWDA, and DW comparisons prior to decision of whether or not an unknown piece of evidence originates from a known piece of evidence.

While complications arise for analysis of glass samples due to the observation of spatial variation, the identification of it provides valuable information for forensic analysis. The observation of spatial variation demonstrates the need for multiple pieces of known and questioned samples to be analyzed when possible in case work. Also, the correct sampling parameters should be used for analysis of forensic evidence. Based on the results obtained in this research, multiple point spectral averaging provides the lowest Type II error while keeping SWSA comparisons approximately at the significance level. The other two spectral averaging methods reduced the percentage of SWDA discriminations with the consequence of also increasing the Type II error.

Overall, the analysis of LIBS spectra by nonparametric permutation test and the Wilcoxon Rank Sum test provided the ability to discriminate between different window panes and the identification of spatial variation within a single window pane. While additional work needs to be done to make the methods applicable in forensic casework, both statistical techniques proved to be successful methods for glass analysis.

APPENDIX A:
AUTOMOBILE PAINT SAMPLE LIST

Year	Manufacturer	Make	Color	Effect Pigment	Substrate	Layers
2000	Chrysler	Voyager	White	No	Metal	3
2002	Chrysler	Truck (unknown)	White	No	Metal	3
1990	Dodge Ram	Van B250	White	No	Metal	3
1999	Chrysler	300M	White	No	Metal	3
1996	Dodge	Grand Caravan LE/ES	White	No	Metal	3
1999	Ford	Expedition	White	No	Metal	3
1997	Ford	F150	White	No	Metal	3
1995	Ford	Crown Victoria	White	No	Metal	3
1995	Ford	Mustang	White	No	Metal	3
1998	Oldsmobile	Achieva SL	White	No	Metal	3
1998	Buick	Century Custom	White	No	Metal	3
1997	Oldsmobile	88/LS	White	No	Metal	3
1997	Mercury	Grand Marquis LS	White	No	Metal	3
2000	Chevrolet	Camaro	White	No	Metal	3
2002	Pontiac	Grand Prix SE	White	No	Metal	3
2000	Ford	Focus SE/SE Comfort	White	No	Metal	3
2001	Ford	Ranger	White	No	Metal	3
1998	Dodge	Ram 1500	White	No	Metal	4
1998	Ford	Expedition	White	No	Metal	4
1995	Chevrolet	Caprice Classic	White	No	Metal	4
1998	Isuzu	Rodeo S/LS	White	No	Metal	4
2000	Kia	Sephia	White	No	Unknown	4
2004	Dodge	Grand Caravan	White	No	Unknown	4
1993	Ford	Mustang	White	No	Metal	5
2004	Ford	Econoline E150	White	No	Metal	5
1996	Ford	Mustang	White	No	Metal	5
1997	Buick	Lesabre Limited	White	No	Metal	5
1995	Honda	Civic	White	No	Metal	5
1999	Honda	Civic	White	No	Unknown	6
2002	Buick	Century	White	No	Unknown	6
1997	Mercury	Cougar XR7/30th	White	No	Metal	6
1998	Chevrolet	Blazer	White	No	Metal	6
1995	Acura (Honda)	Integra	White	No	Unknown	7
2002	Dodge	Stratus	White	No	Metal	7
1999	Mitsubishi	Montero Sport LS/XLS	White	No	Metal	7
1997	Ford	Explorer	White	No	Metal	7

Year	Manufacturer	Make	Color	Effect Pigment	Substrate	Layers
2002	Kia	Rio	Blue	Yes	Metal	3
2006	Dodge	Ram	Blue	Yes	Unknown	3
2002	Kia	Optima	Blue	Yes	Unknown	3
2005	Mazda	Tribute	Blue	Yes	Metal	3
2002	Honda	Accord	Blue	Yes	Unknown	3
1987	Dodge	Ram	Blue	Yes	Metal	4
1998	Dodge	Caravan	Blue	Yes	Metal	4
2006	Nissan	Sentra	Blue	Yes	Metal	4
2001	Chrysler	Concorde	Tan	Yes	Metal	3
2002	Chrysler	Sebring	Tan	Yes	Metal	3
2000	Saturn	SC2	Tan	Yes	Metal	3
1988	BMW	325i	Tan	Yes	Metal	3
1993	Toyota	Camry	Tan	Yes	Metal	4
2001	GMC	Safari	Tan	Yes	Unknown	4
2004	Kia	Spectra	Tan	Yes	Unknown	5
2005	Nissan	Maxima	Tan	Yes	Unknown	5
1999	Ford	Taurus	Tan	Yes	Metal	5
2004	Pontiac	Montana	Tan	Yes	Unknown	5
2002	Mazda	B3000	Red	No	Metal	4
2002	Chrysler	Voyager	Red	No	Unknown	4
2004	Chevrolet	Blazer	Red	No	Unknown	4
2002	Pontiac	Grand Am	Red	No	Unknown	4
1995	Chevrolet	S-10	Red	Yes	Metal	3
2006	Honda	Pilot	Red	Yes	Unknown	3
1998	Ford	F150 Lariat	Red	Yes	Unknown	3
1996	Ford	Explorer	Red	Yes	Metal	4
1993	Nissan	Maxima	Red	Yes	Metal	4
1997	Nissan	Sentra	Red	Yes	Metal	5
1998	Infiniti (Nissan)	I30	Red	Yes	Metal	5
2005	BMW	325i	Black	No	Unknown	3
1998	Nissan	Altima	Black	No	Metal	3
2004	Mitsubishi	Lancer	Black	No	Unknown	4
2000	VW	Jetta	Black	No	Metal	4
1997	VW	Jetta	Black	No	Metal	4
1989	Chrysler	New Yorker	Black	No	Metal	5
1997	Honda	Civic	Black	No	Metal	5
2004	Pontiac	Sunfire	Black	Yes	Unknown	3
1999	Honda	Accord	Black	Yes	Metal	3
2004	GMS	Envoy	Green	Yes	Unknown	3

Year	Manufacturer	Make	Color	Effect Pigment	Substrate	Layers
2001	Honda	Accord	Green	Yes	Metal	3
2003	Mazda	Protégé	Green	Yes	Unknown	4
1993	Mitsubishi	3000GT	Green	Yes	Metal	4
2004	Chevrolet	Tahoe	Green	Yes	Metal	5
1995	Volvo	Wagon	Green	Yes	Metal	5
1999	VW	Passat	Green	Yes	Metal	5
2004	Chevrolet	Cavalier	Silver	Yes	Unknown	3
2005	Chrysler	Pacifica	Silver	Yes	Unknown	3
2000	Nissan	Xterra	Silver	Yes	Unknown	5
2006	Suzuki	Forenza	Silver	Yes	Unknown	5
2003	Suzuki	Aerio	Silver	Yes	Unknown	5
2003	Toyota	4Runner	Silver	Yes	Metal	4
2001	Dodge	Dakota	Silver	Yes	Unknown	4
2001	Chrysler	PT Cruiser	Silver	Yes	Metal	4
2003	Acura (Honda)	CL	Silver	Yes	Unknown	4

APPENDIX B:
STANDARD OPERATING PROCEDURE FOR FLOAT GLASS ANALYSIS BY LIBS

STANTDARD OPERATING PROCEDURES:

LIBS FLOAT GLASS ANALYSIS

Laser Induced Breakdown Spectroscopy (LIBS)

Sample Preparation:

1. Select windows and areas need for analysis ensuring they are labeled.
    a. Labeling system:
        i. Capital letter first – corresponds to window sample is from
        ii. Number after capital letter – corresponds to area of window sample is from
            1. (1) – upper left
            2. (2) – center
            3. (3) – lower right
            4. (4) – upper right
            5. (5) – lower left
        iii. Lower case letter after number – corresponds to spectra collected on sample (12 spectra collected per sample – a-l)

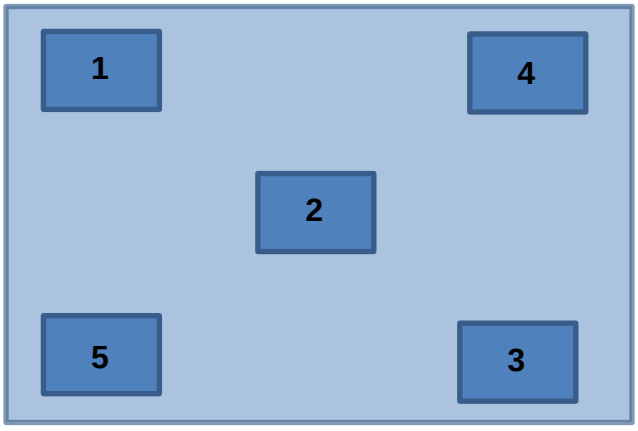

2. Determine float glass side of sample using handheld UV light. It can be difficult to observe at times, so finding darkest place for determination is useful.
3. Cut small sample off of selected area - approximately the width of a standard microscope slide and half the length.
4. Secure sample piece with float glass side down onto glass microscope slide with double sided tape. Label microscope slide with sample label.
5. Remove tinting or tape attached to non-float side of sample.
6. Clean with wipe with cyclohexane to remove any residue of tape or tinting. – Do to all samples even if nothing was adhered to sample to ensure all samples prepared same way. Allow samples to dry.
7. Clean all samples with wipe soaked in DI water. Allow sample to dry
8. Store in enclosed storage case until needed for sampling.

Instrumental Start-up:

1. Remove key from desk drawer under computer and insert into laser power box. Turn into on position
2. Once laser has turned on, beginning running laser.

3. Check energy level is set at desired level for analysis (default at 8.5) and q-switch is on.
4. Allow laser to run for 15-30 minutes to allow it to warm up.

<u>Software start-up:</u>

1. Turn on or wake up computer from sleep mode.
2. Select user profile ‘Student’ for sign in
3. Open from desktop icon LIBS software ‘OOILIBS’ and ‘PLSX’ camera software.
4. In ‘OOILIBS’ software ensure that ‘average’ and ‘shots’ are both set to 1.

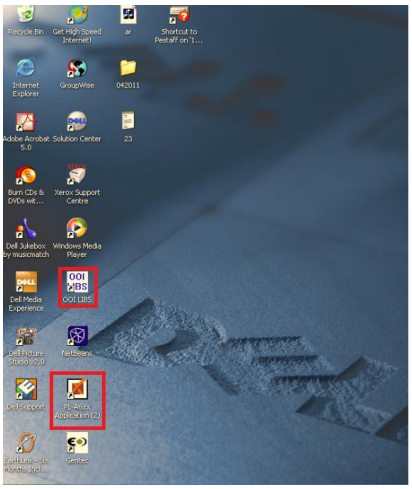

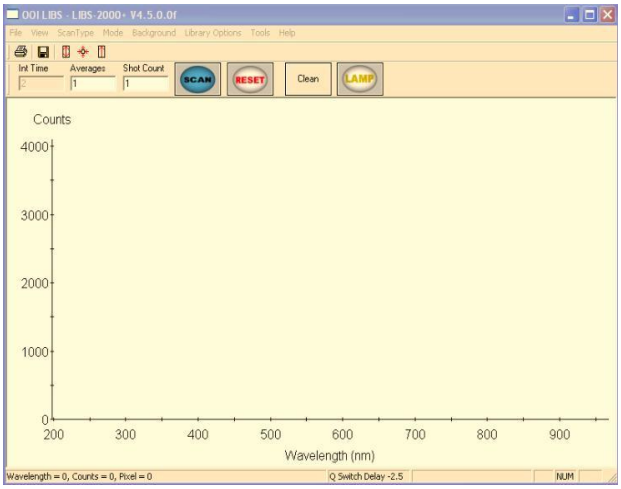

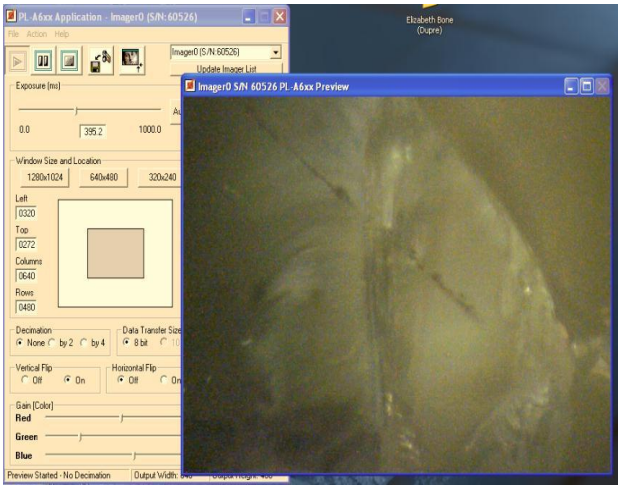

Laser Measurement Test:

1. Ensure sign is displayed outside the laboratory door warning of laser use and eye danger. Place where it is visible to anyone trying to enter laboratory. In addition, place a paper to cover the key code required to enter laboratory as extra precaution in warning to others not to enter laboratory.
2. Ensure everyone in laboratory has correct eye protection on or has left the laboratory.

3. Open sliding compartment door above the LIBS chamber to expose laser beam path.
4. Remove cover on sensor attached to measurement instrument and insert into middle of laser pathway. Sensor should be positioned approximately within box indicated by red tape.

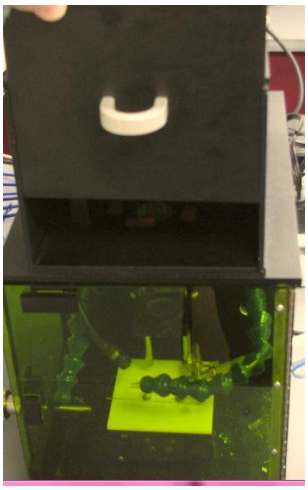

5. Turn on measurement instrument:

a. Use ‘f’ button to pull up drop down menus.
b. Use right arrow to move to ‘scale’ and down arrow to move to ‘300 mJ’. Use middle arrow button to select this scaling.
c. Use ‘f’ button to once again pull up drop down menus.
d. Use down arrow to select ‘statistics’. A new page should appear on the screen.
e. Use down arrow to highlight ‘start’ and middle arrow to select it.
f. Use ‘OOILIBS’ software to perform a single scan by selecting ‘Scan’ button within software.
g. Check statistics – should have a shot value of approximately 175-185.
    i. If statistics are not consistent with expected values, reposition sensor and repeat step f. Select ‘stop’, ‘reset’, and ‘start’ using arrows on measurement instrument.
    ii. If statistics are consistent with expected values, continue to step

h. Select ‘stop’, ‘reset’, and ‘start’ on the measurement instrument and input 50 into ‘average’ box within OOILIBS software. Select ‘Scan’ button and collect the 50 average shots.

i. Record statistics, except ‘current value’, from measurement instrument screen onto sheet in record book.

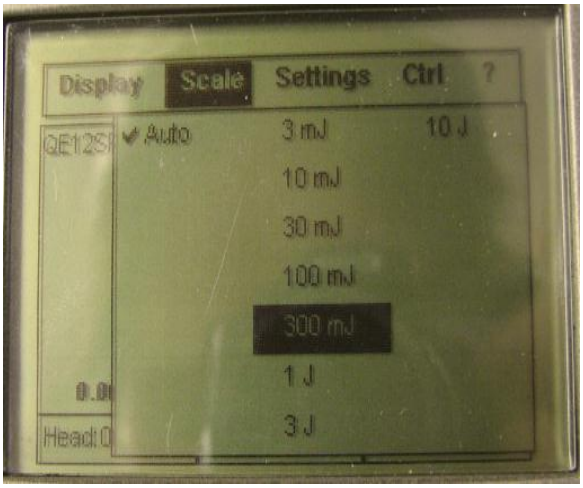

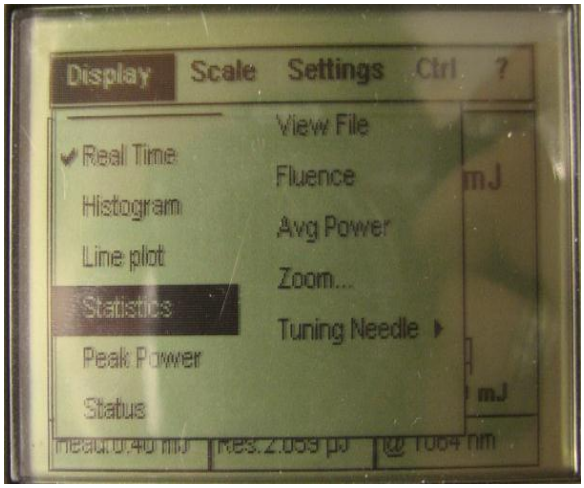

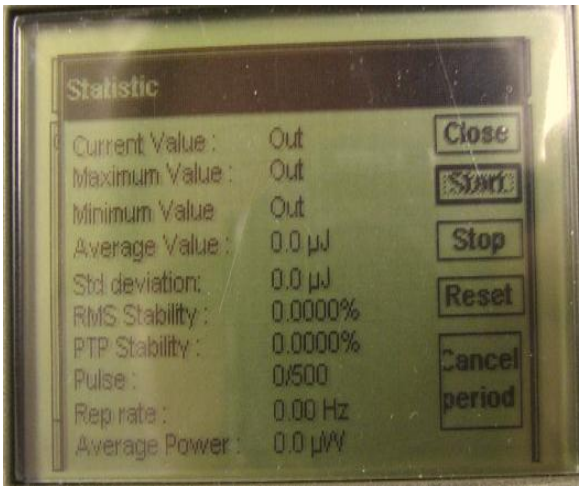

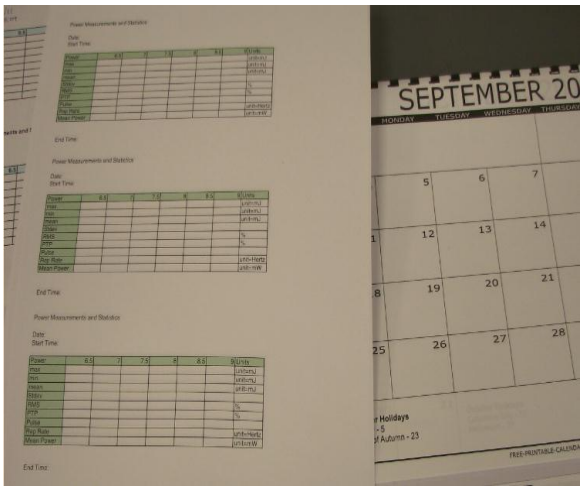

6. Turn off measurement instrument
7. Close sliding compartment door so laser beam is no longer exposed.
8. Remove safety goggles and door signs.

Parameters for spectral collection:

1. Twelve spectra per sample should be collected for data analysis procedures. Two methods to decide between for spectral averaging:
    a. Each spectra will be an average of 10 multiple point shots (address further in sample collection section below).
    b. Each spectra will be an average of 10 shots collected 5 shots in two spots
2. To ensure address shot-to-shot variability and reproducibility issues of LIBS, spectra should be collected in random order
    a. Open excel file
    b. List all sample spectra to be collected in one column
    c. In second column of file use ‘Rand’ function to assign a random number to each spectrum. Type ‘=Rand()’ and press enter. Then pull down so a random number is assigned to each spectrum.

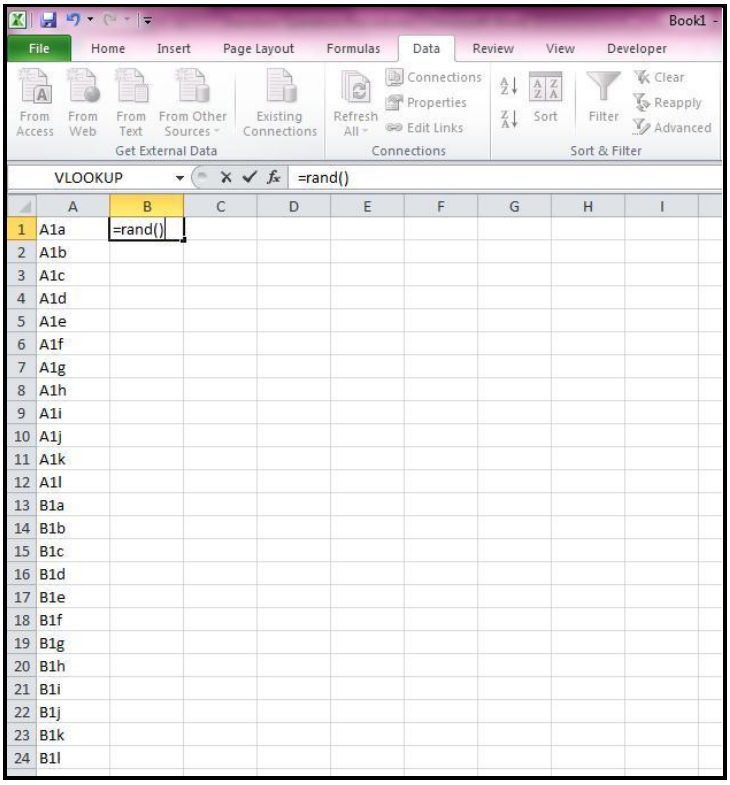

d. Highlight both columns and sort:

   i. Select ‘Data’ on toolbar to give drop down menu

   ii. Select ‘Sort’ in drop down menu

   iii. Pop-up will give you options:

      1. ‘Sort by’ – select column including random numbers
      2. ‘Order’ – select ascending or descending
      3. Press ‘Ok’

   iv. Spectra should be in random order, with random numbers in ascending or descending order.

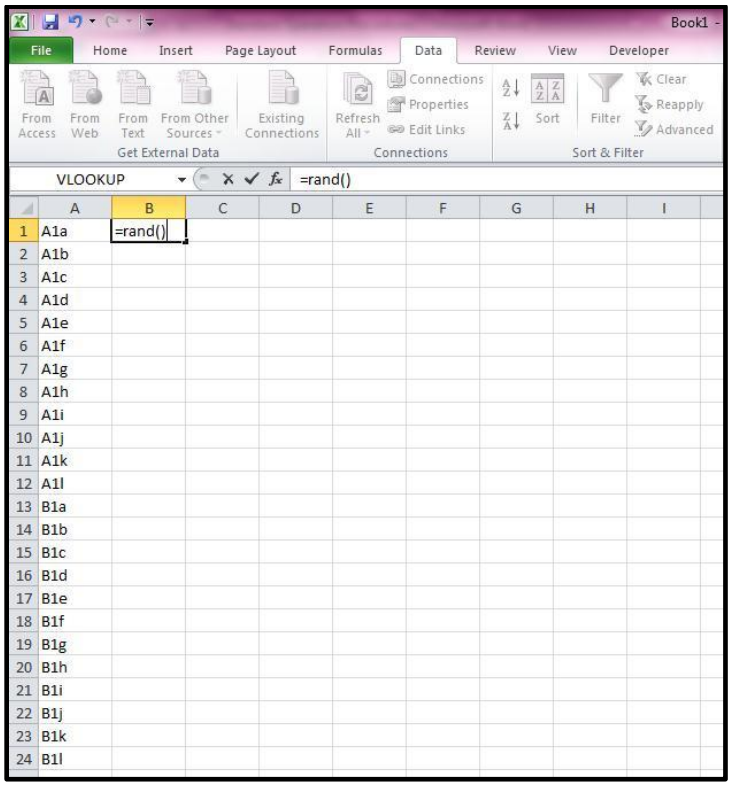

	A	B	C
1	A1a	0.548099	
2	A1b	0.538394	
3	A1c	0.304922	
4	A1d	0.83363	
5	A1e	0.496792	
6	A1f	0.261388	
7	A1g	0.872689	
8	A1h	0.544222	
9	A1i	0.470139	
10	A1j	0.41384	
11	A1k	0.344985	
12	A1l	0.214302	
13	B1a	0.192974	
14	B1b	0.533688	
15	B1c	0.889365	
16	B1d	0.753745	
17	B1e	0.199314	
18	B1f	0.04193	
19	B1g	0.298349	
20	B1h	0.904774	
21	B1i	0.842947	
22	B1j	0.138756	
23	B1k	0.091686	
24	B1l	0.823318	
25			

Sample Collection

1. Place slide with sample into LIBS sample chamber.
2. Turn on light switch on back of LIBS to illuminate sample within sample chamber.
3. Use camera software to locate sample.

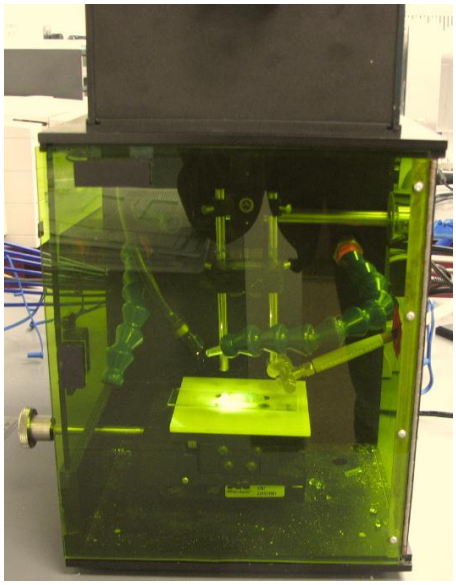

4. Adjust silver knob on right side of the instrument until sample comes into focus on camera software. Depending on sample it may not be an extremely clear focus due to quality of sample and camera, but adjust to best focus possible. This positions the focal lens and fiber optic cable in optimal position for sampling.
5. Select ‘tools’ within OOILIBS software and select ‘Set Q-switch delay’
    a. Adjust Q-switch until spectra in pop-up window has reduced background noise, no apparent jumps between spectrometer collection, and defined spectral lines by moving bar at top of pop-up window. Sample should be moved each time q-switch is changed.
    b. Q-switch should remain in negative values (for collection after plasma is created) and approximately around 5.0. (positive q-switch values begin collection prior to plasma creation).

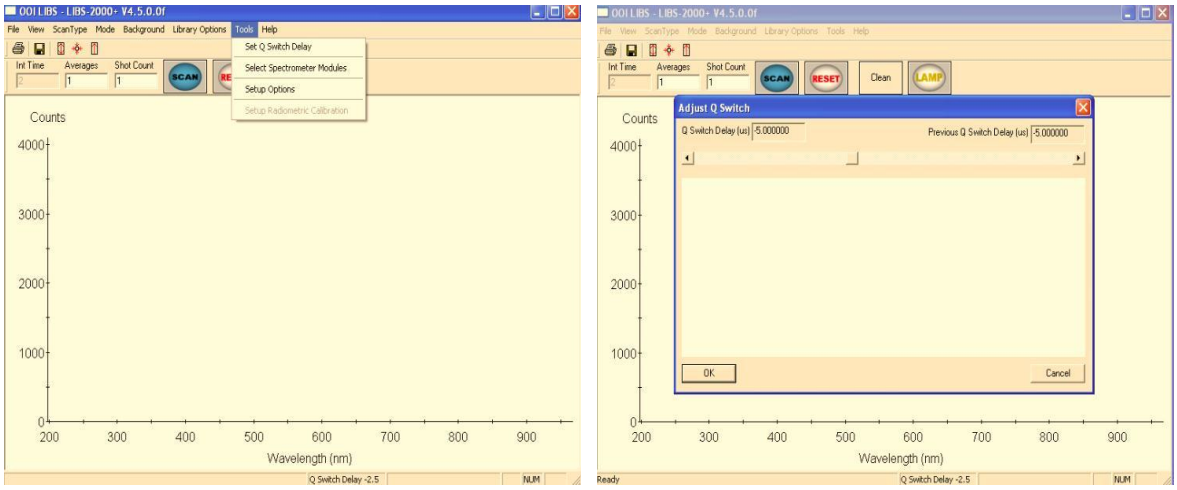

6. Select number of shots to be averaged per spectrum – 10 shots per spectrum – by inputting value in ‘average’ box on toolbar
7. Use ‘Scan’ button to begin spectral collection
    a. After each shot sample must be moved by x-y position knob on left of LIBS sample chamber to perform multiple point averaging of sample spectrum.
8. Use double headed arrow icon on toolbar to normalize the spectrum to the most intense peak.
9. Ensure spectra is acceptable and save to folder in Instrument serve corresponding to date of collection.

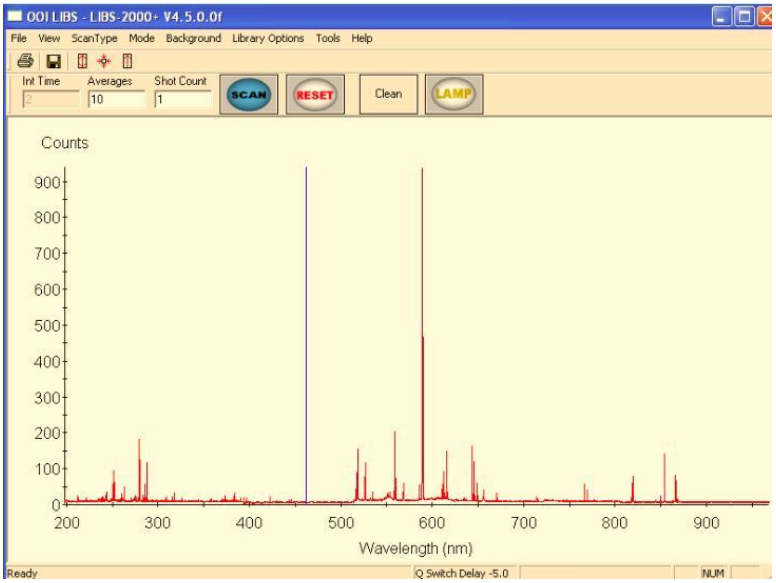

10. Continue steps 1-4 and 7-9 until all sample spectra have been collected.
    a. Exchange samples quickly to keep off time of laser to a minimum (every time the sample chamber door is open the laser is automatically shut off by an interlock).
    b. Do not take extended breaks during sampling, plan to collect all samples in one sitting with minor breaks if absolutely necessary (no longer than 5 minutes). Have everything prepared for sampling prior to beginning analysis.
    c. Check folder containing saved spectra to ensure no spectra were missed, if it is determined only 11 spectra of sample 1 was collected the whole data set is useless.
11. Once sampling is completed, repeat laser measurement steps. Turn off laser and proceed to data processing and analysis.

Additional Software Notes:

On toolbar there are additional tools for analyzing the spectra:

a. In the drop down menu of ‘View’ there are three options
    i. Spectrum
        1. Should always have a black check mark next to it indicating the spectrum should be visible
    ii. Background
        1. Allows for a background spectrum (if collected) to be overlaid on a sample spectrum for comparison
    iii. Overlay
        1. Two overlays can be selected
        2. Choose option ‘Select Overlay 1(or 2)’ to set a previously saved spectrum as an overlay
        3. Return to ‘View’, ‘Overlay’ and select the overlay to be viewed on top of the current spectrum by choosing ‘Overlay 1 (or 2)’.
b. In the drop down menu of ‘ScanType’ default scantype should be set to ‘SingleShot’ with a black check mark next to it
c. In the drop down menu of ‘Mode’ there are two used options:
    i. Normal – the default setting
    ii. Element ID
        1. On selecting this mode a pop-up box will appear

a. Select ‘Analyze’ button to display in left table the lines that have been detected from the sample
b. In the right table will be a list of each element and the number of lines detected for the sample compared to the total number of potential lines that could have been detected for that specific element
c. Adjustment in ‘Peak Height’ box at the bottom will change the number of potential lines that will be considered to be detected based on the counts.
d. This data can be saved by “Save Results’ button at the bottom left of the pop-up box.
e. On completion of using this pop-up box click the red box with the x in the upper right corner
f. Once pop-up box has been removed, left click on spectral box to produce boxes indicating each element and wavelength detected for the spectrum.
    i. To remove these boxes return to ‘Mode’ and select ‘Normal’. Then left click on spectral box.

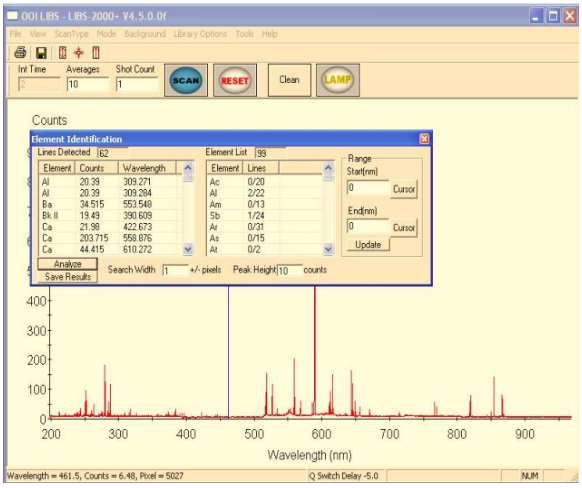

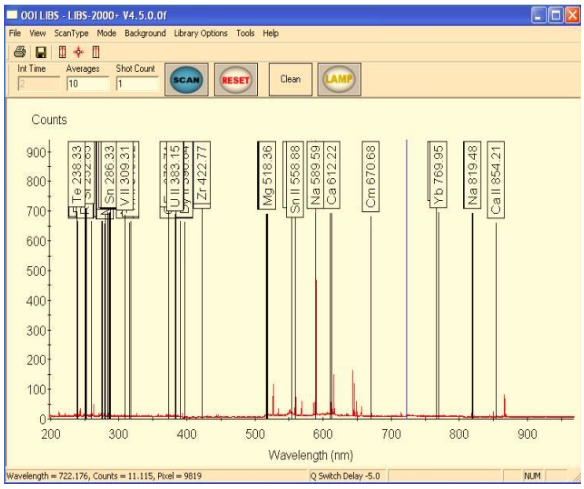

d. Specific areas on spectrum can be zoomed into by holding down ‘shift’ and drawing a box with the mouse with the left button clicked down.

   i. To return from zoomed in double left click on the spectral box

   ii. If ‘control’ is held down instead of ‘shift’ the software will not allow you to back out of the zoomed in view. Whole software will have to be shut down and restarted and all data not saved will be lost.

Data Analysis & Nonparametric Permutation Test

1. Compile spectral data for all windows into one excel file and save it as a compiled data file within pestaff server under your name and a file reflecting date data was collected on.
2. Select wavelength range of 200-500 nm. Resulting in 5636 data points per spectrum. This range was selected because demonstrates all the necessary data while removing atmospheric lines. Save as new file.

3. Compile normalized spectral data for each window area into a csv file. First column, first row will have a title for sample name. First column, second row will have the number of spectral points. First column, third row to end will contain spectral point range. The second column, second row will contain the number of spectrum. The second column to the last filled column, row three through the end will contain the spectral data. Save to a new folder within in the overall data folder, indicating it as MATLAB input files.

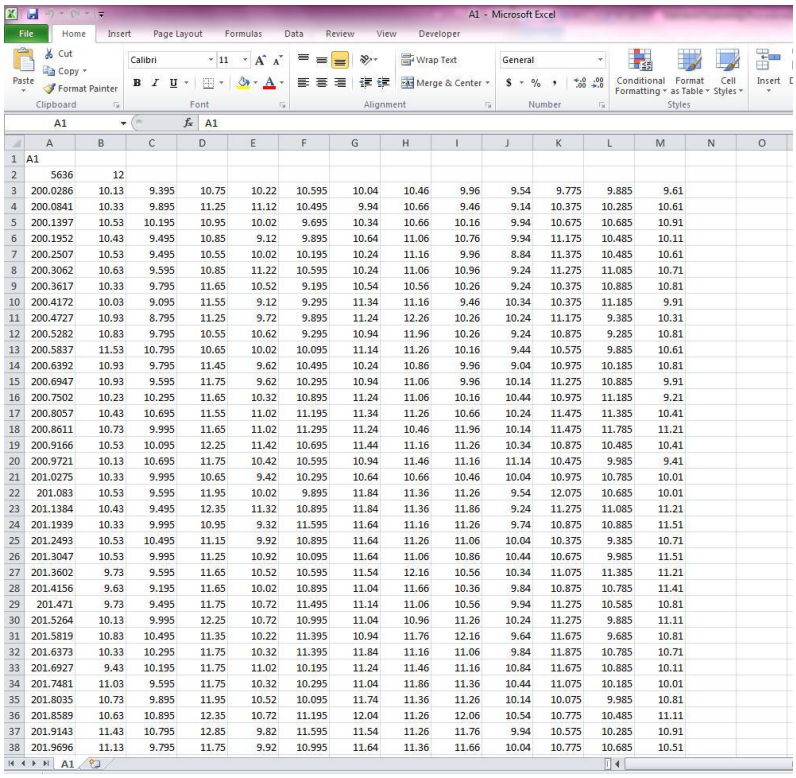

	A	B	C	D	E	F	G	H	I	J	K	L	M	N	O
1	A1														
2	5636	12													
3	200.0286	10.13	9.395	10.75	10.22	10.595	10.04	10.46	9.96	9.54	9.775	9.885	9.61		
4	200.0841	10.33	9.895	11.25	11.12	10.495	9.94	10.66	9.46	9.14	10.375	10.285	10.61		
5	200.1397	10.53	10.195	10.95	10.02	9.695	10.34	10.66	10.16	9.94	10.675	10.685	10.91		
6	200.1952	10.43	9.495	10.85	9.12	9.895	10.64	11.06	10.76	9.94	11.175	10.485	10.11		
7	200.2507	10.53	9.495	10.55	10.02	10.195	10.24	11.16	9.96	8.84	11.375	10.485	10.61		
8	200.3062	10.63	9.595	10.85	11.22	10.595	10.24	11.06	10.96	9.24	11.275	11.085	10.71		
9	200.3617	10.33	9.795	11.65	10.52	9.195	10.54	10.56	10.26	9.24	10.375	10.885	10.81		
10	200.4172	10.03	9.095	11.55	9.12	9.295	11.34	11.16	9.46	10.34	10.375	11.185	9.91		
11	200.4727	10.93	8.795	11.25	9.72	9.895	11.24	12.26	10.26	10.24	11.175	9.385	10.31		
12	200.5282	10.83	9.795	10.55	10.62	9.295	10.94	11.96	10.26	9.24	10.875	9.285	10.81		
13	200.5837	11.53	10.795	10.65	10.02	10.095	11.14	11.26	10.16	9.44	10.575	9.885	10.61		
14	200.6392	10.93	9.795	11.45	9.62	10.495	10.24	10.86	9.96	9.04	10.975	10.185	10.81		
15	200.6947	10.93	9.595	11.75	9.62	10.295	10.94	11.06	9.96	10.14	11.275	10.885	9.91		
16	200.7502	10.23	10.295	11.65	10.32	10.895	11.24	11.06	10.16	10.44	10.975	11.185	9.21		
17	200.8057	10.43	10.695	11.55	11.02	11.195	11.34	11.26	10.66	10.24	11.475	11.385	10.41		
18	200.8611	10.73	9.995	11.65	11.02	11.295	11.24	10.46	11.96	10.14	11.475	11.785	11.21		
19	200.9166	10.53	10.095	12.25	11.42	10.695	11.44	11.16	11.26	10.34	10.875	10.485	10.41		
20	200.9721	10.13	10.695	11.75	10.42	10.595	10.94	11.46	11.16	11.14	10.475	9.985	9.41		
21	201.0275	10.33	9.995	10.65	9.42	10.295	10.64	10.66	10.46	10.04	10.975	10.785	10.01		
22	201.083	10.53	9.595	11.95	10.02	9.895	11.84	11.36	11.26	9.54	12.075	10.685	10.01		
23	201.1384	10.43	9.495	12.35	11.32	10.895	11.84	11.36	11.86	9.24	11.275	11.085	11.21		
24	201.1939	10.33	9.995	10.95	9.32	11.595	11.64	11.16	11.26	9.74	10.875	10.885	11.51		
25	201.2493	10.53	10.495	11.15	9.92	10.895	11.64	11.26	11.06	10.04	10.375	9.385	10.71		
26	201.3047	10.53	9.995	11.25	10.92	10.095	11.64	11.06	10.86	10.44	10.675	9.985	11.51		
27	201.3602	9.73	9.595	11.65	10.52	10.595	11.54	12.16	10.56	10.34	11.075	11.385	11.21		
28	201.4156	9.63	9.195	11.65	10.02	10.895	11.04	11.66	10.36	9.84	10.875	10.785	11.41		
29	201.471	9.73	9.495	11.75	10.72	11.495	11.14	11.06	10.56	9.94	11.275	10.585	10.81		
30	201.5264	10.13	9.995	12.25	10.72	10.995	11.04	10.96	11.26	10.24	11.275	9.885	11.11		
31	201.5819	10.83	10.495	11.35	10.22	11.395	10.94	11.76	12.16	9.64	11.675	9.685	10.81		
32	201.6373	10.33	10.295	11.75	10.32	11.395	11.84	11.16	11.06	9.84	11.875	10.785	10.71		
33	201.6927	9.43	10.195	11.75	11.02	10.195	11.24	11.46	11.16	10.84	11.675	10.885	10.11		
34	201.7481	11.03	9.595	11.75	10.32	10.295	11.04	11.86	11.36	10.44	11.075	10.185	10.01		
35	201.8035	10.73	9.895	11.95	10.52	10.095	11.74	11.36	11.26	10.14	10.075	9.985	10.81		
36	201.8589	10.63	10.895	12.35	10.72	11.195	12.04	11.26	12.06	10.54	10.775	10.485	11.11		
37	201.9143	11.43	10.795	12.85	9.82	11.595	11.54	11.26	11.76	9.94	10.575	10.285	10.91		
38	201.9696	11.13	9.795	11.75	9.92	10.995	11.64	11.36	11.66	10.04	10.775	10.685	10.51		

4. Open NonParametricPermutation v13 GUI on computer where it has been compiled (Multi-processor #3 in NCFS Trace Lab).

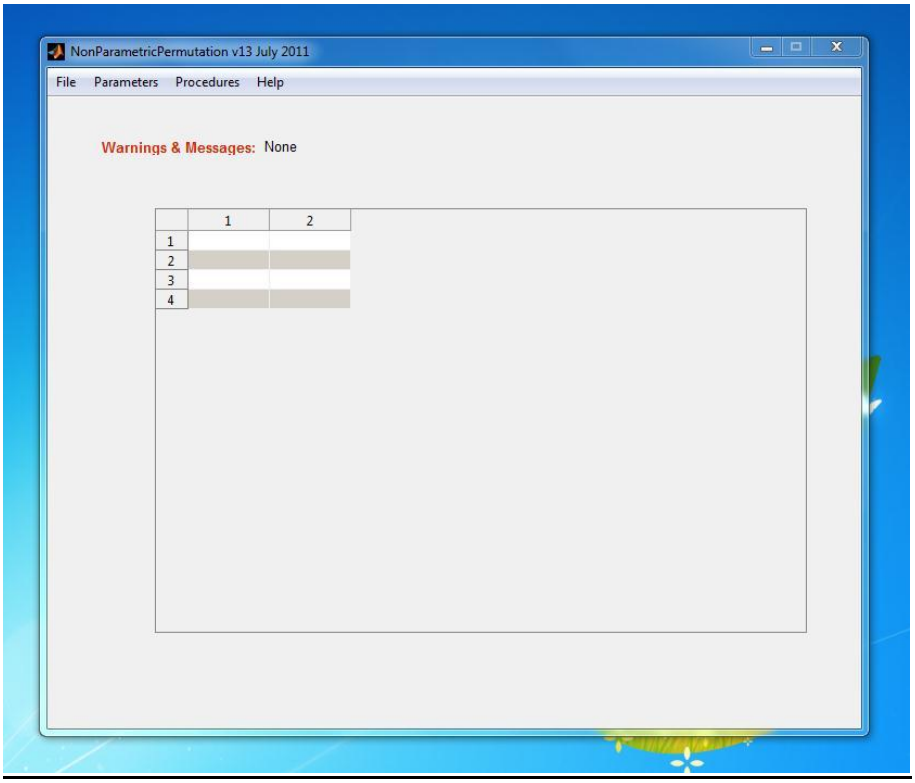

5. In toolbar select ‘Parameters’ for a drop down menu with two options which will be defined prior to analysis:

    a. Choose n – n will be set for 6 to perform 12 choose 6 analysis

    b. Max spectral combinations – will be set based on experiment (at least 20 to ensure the observation of Type I errors)

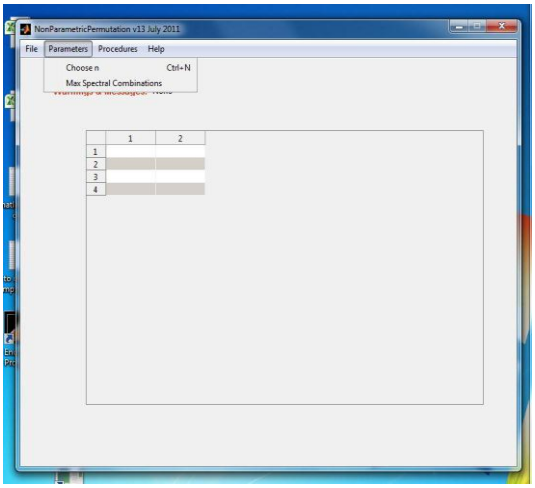

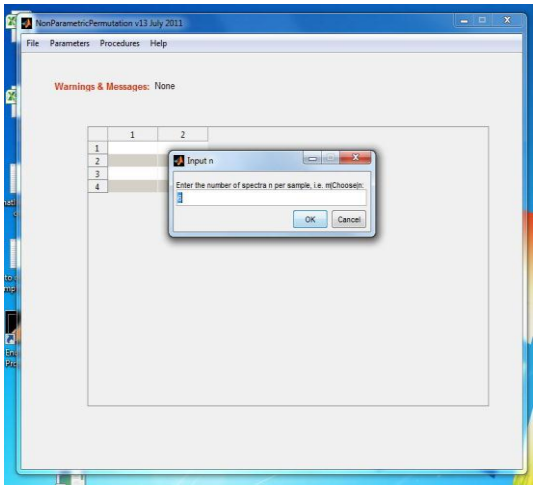

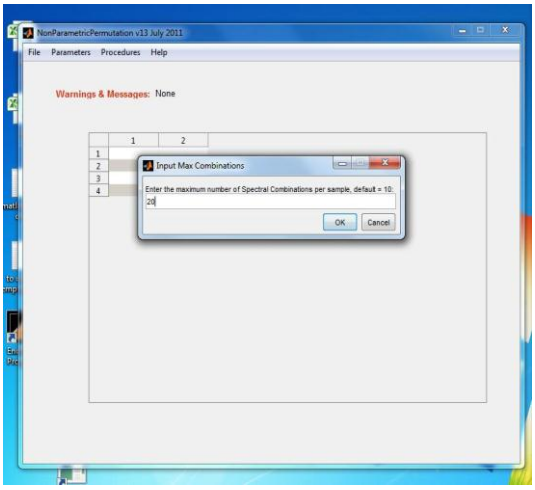

6. Select ‘File’ for a drop down menu where ‘Open’ will be selected
    a. Select folder where data will be analyzed from
    b. Use ‘Control’, ‘Shift’ and left mouse button to select all files and press ok
    c. Give software a minute to load all data, once it is load a list of all samples should appear in software window.

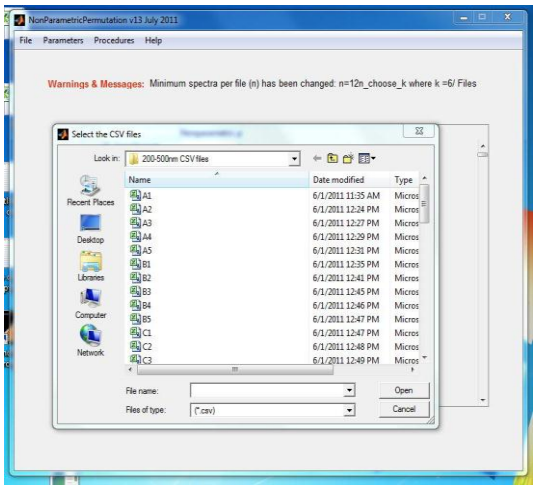

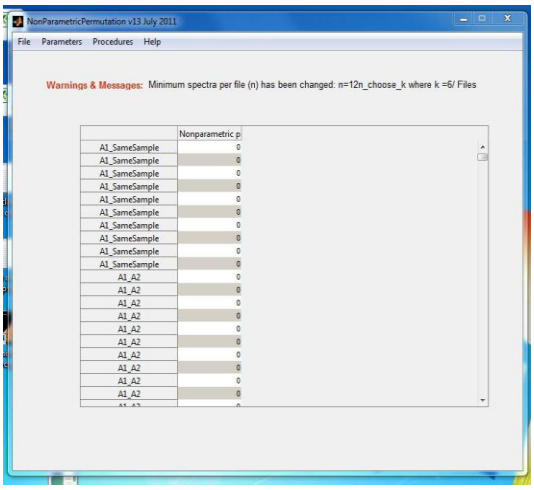

7. After loading data, double check that two Parameters have remained as you set them.
8. Once data has been selected and loaded, select ‘Procedures’ on toolbar to display a drop down menu. Select ‘Calculate Comparisons’.
    a. Once this is selected a new warning message will appear with ‘Calculation in progress, calculations_#% Complete.’
    b. As calculation performs p-values will be displayed for comparisons.
    c. DO NOT minimize or close window during calculation. Calculation will have to be completely restarted if either occurs. Display a sign over computer screen to warn others that a calculation is running.
    d. Calculation may take a while to complete, check occasionally to ensure calculation is still running and progress of calculation.

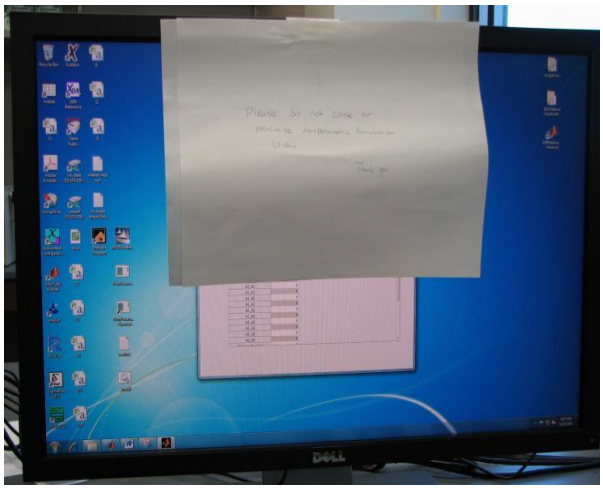

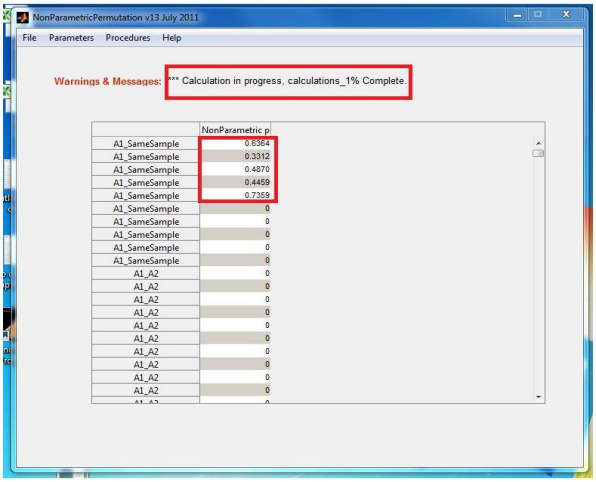

9. Once calculation has completed, new warning message will appear with ‘Calculation Complete’

    a. Select ‘File’ and within the drop down menu select ‘Export Results to Excel’

    b. A pop-up window will appear to prompt you for a file name and destination

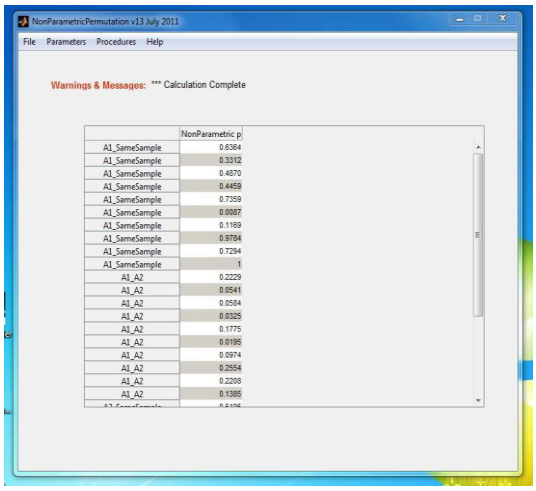

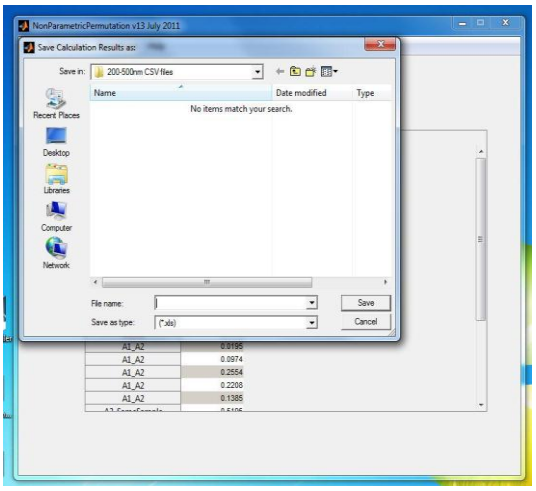

    c. If more calculations are to be performed, select ‘Procedures’ and within the drop down menu select ‘Reset Table’.

        i. Repeat steps 5-9 until all calculations are complete

ii. This can also be done if error occurred in setting up the calculation

10. Select file with exported data from folder it was exported to and open it
    a. Data will be formatted in two columns, sample names and p-values
    b. Highlight in yellow same window same area comparisons with p-values less than 0.05
    c. Highlight in blue different window comparisons with p-values greater than 0.05
    d. Highlight in green same window-different area comparisons with p-values less than 0.05

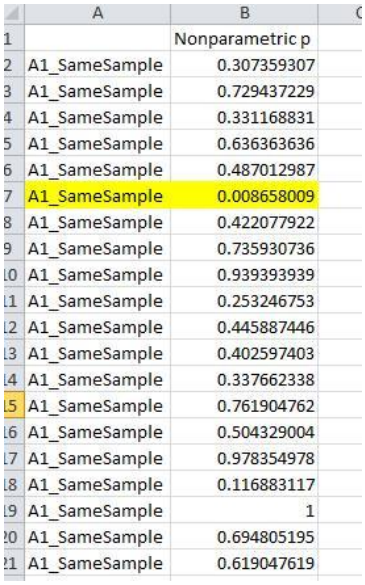

	A	B
1		Nonparametric p
2	A1_SameSample	0.307359307
3	A1_SameSample	0.729437229
4	A1_SameSample	0.331168831
5	A1_SameSample	0.636363636
6	A1_SameSample	0.487012987
7	A1_SameSample	0.008658009
8	A1_SameSample	0.422077922
9	A1_SameSample	0.735930736
10	A1_SameSample	0.939393939
11	A1_SameSample	0.253246753
12	A1_SameSample	0.445887446
13	A1_SameSample	0.402597403
14	A1_SameSample	0.337662338
15	A1_SameSample	0.761904762
16	A1_SameSample	0.504329004
17	A1_SameSample	0.978354978
18	A1_SameSample	0.116883117
19	A1_SameSample	1
20	A1_SameSample	0.694805195
21	A1_SameSample	0.619047619

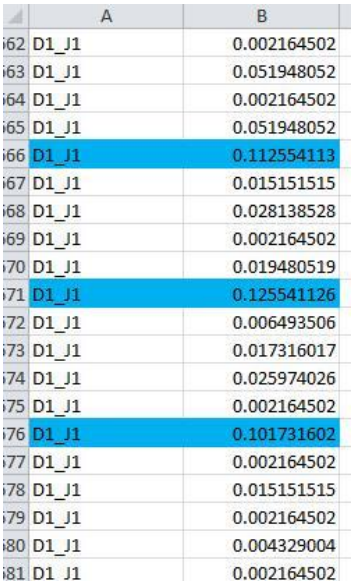

	A	B
62	D1_J1	0.002164502
63	D1_J1	0.051948052
64	D1_J1	0.002164502
65	D1_J1	0.051948052
66	D1_J1	0.112554113
67	D1_J1	0.015151515
68	D1_J1	0.028138528
69	D1_J1	0.002164502
70	D1_J1	0.019480519
71	D1_J1	0.125541126
72	D1_J1	0.006493506
73	D1_J1	0.017316017
74	D1_J1	0.025974026
75	D1_J1	0.002164502
76	D1_J1	0.101731602
77	D1_J1	0.002164502
78	D1_J1	0.015151515
79	D1_J1	0.002164502
80	D1_J1	0.004329004
81	D1_J1	0.002164502

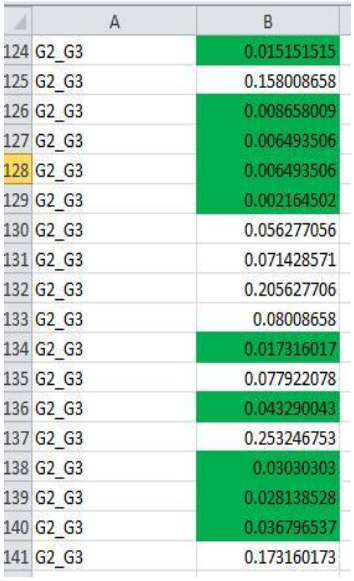

	A	B
124	G2_G3	0.015151515
125	G2_G3	0.158008658
126	G2_G3	0.008658009
127	G2_G3	0.006493506
128	G2_G3	0.006493506
129	G2_G3	0.002164502
130	G2_G3	0.056277056
131	G2_G3	0.071428571
132	G2_G3	0.205627706
133	G2_G3	0.08008658
134	G2_G3	0.017316017
135	G2_G3	0.077922078
136	G2_G3	0.043290043
137	G2_G3	0.253246753
138	G2_G3	0.03030303
139	G2_G3	0.028138528
140	G2_G3	0.036796537
141	G2_G3	0.173160173

11. Create new tab within excel file and begin a comparison table
    a. In first column name cells
        i. Same window same area (SWSA)
        ii. Same window different area (SWDA)
        iii. Different window (DW)

b. In first row name cells

   i. Comparisons

   ii. Non-discriminations

   iii. Discriminations

   iv. Total

   v. D/Total

   vi. ND/Total

c. For each column determine the total number of each have occurred and record

	A	B	C	D	E	F
1	Comparisons	ND	D	Total	D/total	ND/total
2	SWSA	1140	60	1200	0.05	0.95
3	SWDA	904	1096	2000	0.548	0.452
4	DW	12	888	900	0.986667	0.013333
5						
6	20 comparisons for all samples					

Boxplot and Wilcoxon Rank Sum Test

1. Open new csv file

   a. Label first row

      i. SWSA

      ii. SWDA

      iii. DW

   b. Copy all p-values for same window same area comparisons into first column

c. Copy all p-values for same window different area comparisons into second column

d. Copy all p-values for different window comparisons into third column

	A	B	C
1	SWSA	SWDA	DW
2	0.649351	0.309524	0.002165
3	0.116883	0.069264	0.002165
4	0.064935	0.006494	0.002165
5	0.04329	0.025974	0.002165
6	0.361472	0.270563	0.002165
7	0.337662	0.116883	0.002165
8	0.941558	0.047619	0.002165
9	0.95671	0.010823	0.002165
10	0.608225	0.064935	0.002165
11	0.320346	0.075758	0.002165
12	0.164502	0.025974	0.002165
13	0.952381	0.238095	0.002165
14	0.660173	0.101732	0.002165
15	0.422078	0.049784	0.002165
16	0.127706	0.205628	0.002165
17	0.859307	0.103896	0.002165
18	0.4329	0.467532	0.002165
19	0.142857	0.015152	0.002165
20	0.019481	0.025974	0.002165
21	0.725108	0.114719	0.002165
22	0.030303	0.242424	0.004329
23	0.709957	0.383117	0.002165
24	0.244589	0.054113	0.002165
25	0.248918	0.041126	0.004329
26	0.253247	0.054113	0.002165
27	0.151515	0.010823	0.002165
28	0.062771	0.25974	0.006494
29	0.805195	0.168831	0.002165
30	0.950216	0.082251	0.004329
31	0.625541	0.125541	0.002165

2. Open R software (download from internet if necessary. Google R project and follow directions for downloading)

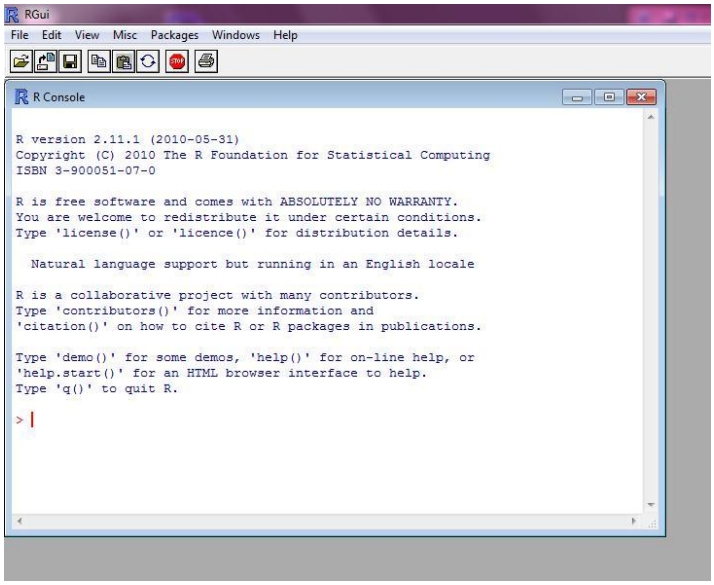

a. Set directory by opening the ‘File’ drop down menu and selecting ‘Change dir…’

    i. Select directory where folder with data file is saved, highlight the folder by clicking on it and pressing ok.

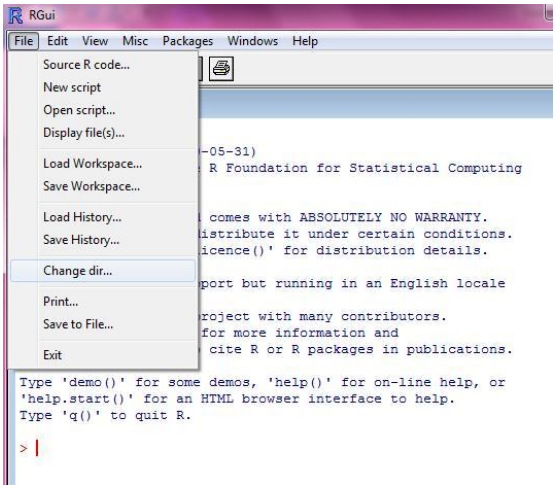

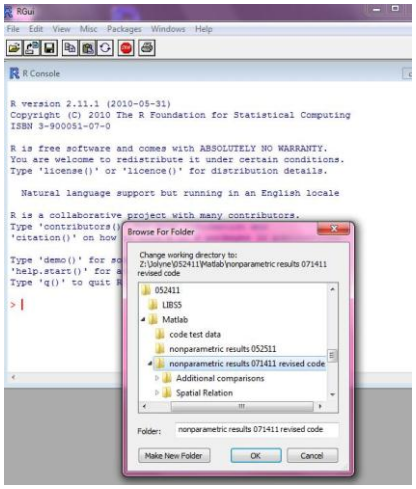

3. Read in data:

    a. R is case sensitive

b. Before arrow is what you are naming the imported data, after the arrow is the command to import the data. Type the file name exactly as it is saved (spaces and capitalization).

c. Command: data <- read.csv('filename.csv')

d. New prompt will appear if entered correctly, otherwise an error has occurred and a message prompting you on what the error was will occur.

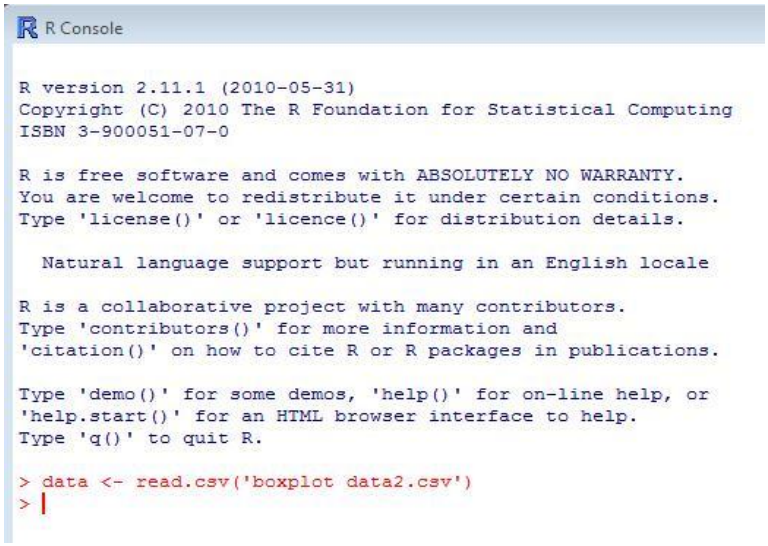

e. Type command for boxplot:

   i. To obtain boxplot of data with just headers from file type: boxplot(data)

   ii. To obtain boxplot of data with x and y labels type: boxplot(data, xlab= 'label', ylab= 'label')

   iii. To obtain boxplot of data with a title, x and y labels type: boxplot(data, xlab= 'label', ylab= 'label', main= 'Title')

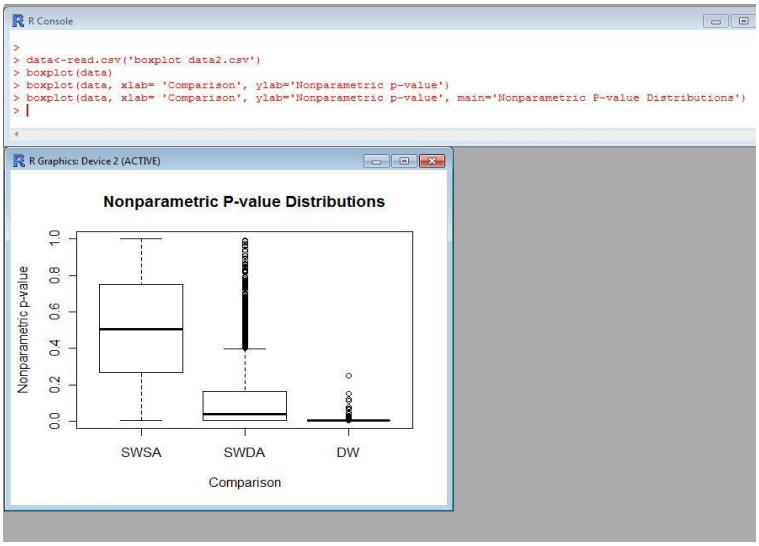

iv. Right click on plot and select ‘Copy as Metafile’

1. Paste to csv file containing p-values and save it as an excel file under same name

4. Compile specific comparisons for Wilcoxon Rank Sum test

a. Select samples to be compared from MATLAB nonparametric results

i. For same window select four of the five areas

1. Ex. A2, A3, A4, A5

ii. For same window different area select the area not used in the same window

1. Ex. A1

iii. For different window select an area from a different window sample

1. Ex. C1

b. Compile all comparisons for each selection into columns

i. All same window same area comparisons

1. Label as KK
2. Ex. A2 vs A3, A2 vs A4, A2 vs A5, A3 vs A4, A3 vs A5, A4 vs A5

ii. All same window different area comparisons

1. Label as KQ1
2. Ex. A1 vs A2, A1 vs A3, A1 vs A4, A1 vs A5

iii. All different window comparisons

1. Label as KQ2
2. Ex. C1 vs A2, C1 vs A3, C1 vs A4, C1 vs A5

c. Save newly compiled data as a csv file with the name of the three groups into desired folder

i. First column should contain KK data, second column KQ1 data, and third column KQ2 data

ii. Ex. A vs A1 vs C1

d. Change R directory to folder containing csv file and import data

i. data <- read.csv('filename.csv')

e. Type command for Wilcoxon Rank Sum test

i. For calculation of KK vs KQ1

1. Wilcox.test(data[,1] , data[,2]) - where 1 data[,1] specifies all rows in column 1 (KK) and data[,2] specifies all rows in column 2 (KQ1)

ii. For calculation of KK vs KQ2

1. Wilcox.test(data[,1] , data[,3]) - where 1 data[,1] specifies all rows in column 1 (KK) and data[,3] specifies all rows in column 3 (KQ2)

iii. Will likely only perform KK vs KQ1 because of the extent of discrimination seen in p-values of different window comparisons.

	A	B	C
1	KK	KQ1	KQ2
2	0.528139	0.164502	0.002165
3	0.322511	0.004329	0.002165
4	0.218615	0.010823	0.002165
5	0.285714	0.017316	0.002165
6	0.430736	0.047619	0.002165
7	0.331169	0.036797	0.002165
8	0.551948	0.212121	0.002165
9	0.508658	0.108225	0.002165
10	0.060606	0.038961	0.002165
11	0.532468	0.004329	0.002165
12	0.606061	0.006494	0.002165
13	0.616883	0.207792	0.002165
14	0.222944	0.25974	0.002165
15	0.082251	0.038961	0.002165
16	0.155844	0.004329	0.002165
17	0.619048	0.285714	0.002165
18	0.571429	0.361472	0.002165
19	0.199134	0.415584	0.002165
20	0.699134	0.311688	0.002165
21	0.714286	0.030303	0.002165
22	0.162338	0.006494	0.002165
23	0.281385	0.017316	0.002165
24	0.108225	0.04329	0.002165
25	0.021645	0.090909	0.002165

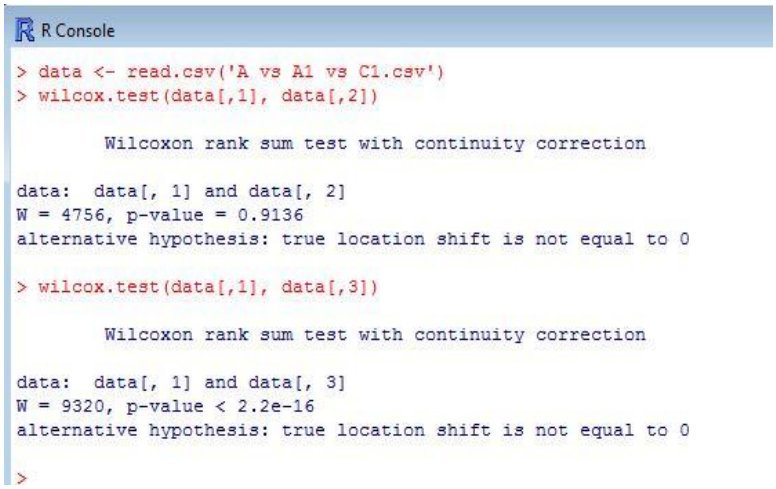

f. Copy read out in command window and paste in csv data file. The save as excel file under the same name.

i. Highlight p-value

1. If it is above 0.05, then samples cannot be statistically discriminated
2. If it below 0.05, then sample can be statistically discriminated

<u>Summarize and Report Data!</u>

APPENDIX C:
FIRE DEBRIS SAMPLES

Sample	ID Number	Class	Sample	ID Number	Class	Sample	ID Number	Class
Exxon Unleaded Premium Gasoling 25% weathered	11625	Gas	Safe Heat	257	OXY	Sunniland Cinch Bug Spray	416	MISC
Exxon Unleaded Premium Gasoline 50% weathered	11650	Gas	Chevron Regular Unleaded Gasoline	258	Gas	Citristrip-Project Afterwash	417	OXY
Exxon Unleaded Premium Gasoline 75% weathered	11675	Gas	Chevron Plus Unleaded Gasoline	259	Gas	Heet Gasoline Antifreeze & Water Remover	418	OXY
Exxon Unleaded Premium Gasoline 90% weathered	11690	Gas	Klean Strip Klean Kutter Remover	25	MISC	Bonide Fruit Tree Spray	419	MISC
BP regular Unleaded Gasoling, 99.1% weathered	100	Gas	Chevron Supreme Unleaded Gasoline	260	Gas	TL-3 Fuel Injector Cleaner	41	MISC
Super G Charcoal Lighter Fluid	101	MPD	Trewax Wood Cleaner	261	ISO	Isoheat Premium Fuel-Line Antifreeze & Water Remover	420	OXY
Lamplight Farms Ultra Pure Smokeless & Odorless Candle & Lamp Oil	102	NA	Bix Tuff-Job Remover	262	OXY	Turtle Wax Bug & Tar Remover	421	MPD
Lamplight Farms Lamp Oil	103	MISC	Bix Stripper	263	OXY	Citristrip Furniture Stripper	422	OXY
Phillips 66 Aviation Gasoline	104	Gas	Flood Penetrol Quality Paint Conditioner	264	MISC	Bardahl-All-U-Need Fuel System Treatment	423	HPD

Sample	ID Number	Class	Sample	ID Number	Class	Sample	ID Number	Class
Phillips 66 Unleaded Regular Gasoline	105	Gas	Klean Strip Japan Drier	265	MPD	Gum Out Mileage Improver	424	HPD
Phillips 66 Low Aromatic Commercial Grade Heptane	106	ISO	Famowood Wood Filler Solvent	266	OXY	TruBurn Kmart Odorless Charcoal Lighter	425	MPD
Phillips 66 PhilJet® A Aviation Fuel	107	HPD	Kiwi Camp Dry Heavy Duty Water Repellent	267	MPD	Citristrip Wipe Away	426	OXY
Phillips 66 0.05% Sulfur Diesel Fuel	108	HPD	Jasco Adhesive Clean-Up	268	MPD	1 Lifter Bug & Tar Remover	427	MISC
Phillips 66 Hexanes	109	MISC	Gold Eagle + 104 Octane Boost	269	HPD	One Shot	428	OXY
Cypar 9	10	MISC	Klean Strip 100% Mineral Spirit Paint Thinner	26	MPD	Dad’s Easy Spray	429	OXY
Phillips 66 Isohexanes	110	ISO	Ace Charcoal Lighter	270	ISO	Chevron Aviation Gasoline 100 Low Lead	42	MISC
Turbo Fuel Jet A Colonial Grade 54 Jet A	111	HPD	Old Masters Paint Remover	271	MISC	Exxon Isopar G	430	ISO
Exxon Jet Fuel Grade JP-8	112	HPD	USA VM&P Naphtha	272	LPD	Wizard Odorless Double Filtered Charcoal Starter	431	MPD
Exxon Aviation Gasoline 100LL	113	MISC	E-Z VM&P Naphtha	273	LPD	Rainbow Odorless Charcoal Lighter Fluid	432	MPD

Sample	ID Number	Class	Sample	ID Number	Class	Sample	ID Number	Class
Exxon Low S #2 Diesel CPL 86 Offroad Diesel	114	HPD	USA Lacquer Thinner	274	OXY	Citronella Oil	433	OXY
Exxon Unleaded Regular Gasoline	115	Gas	Pro Paint Thinner 100% Mineral Spirits	275	MPD	Orange Oil	434	MISC
Exxon Unleaded Premium Gasoline	116	Gas	USA Paint Thinner	276	MPD	Ace Paint Thinner 100% Mineral Spirits	435	MPD
Exxon Mars Crude T0192	117	HPD	Flood Penetrol Quality Paint Conditioner	277	MISC	Diesel Fuel	436	HPD
Sweet South LA Crude T0187	118	HPD	Power Service Diesel Fuel Supplement	278	MISC	Kingsford Odorless Charcoal Lighter Fluid	437	MPD
Exxon Isopar H	119	ISO	Power Service Diesel Kleen Cetane Boost	279	MISC	Klean Strip Odorless Mineral Spirits	438	MPD
SCCC Mineral Spirits 145 EC	11	MPD	Klean Strip VM&P Naphtha	27	LPD	Ace Turpentine (pure gum)	439	MISC
Exxon Isopar C	120	ISO	Shell Rotella DFA Diesel Fuel Additive All Season Formulation	280	OXY	Chevron Techron Concentrate	43	MPD
Exxon Isopar L Fluid	121	ISO	Siloo Heavy Duty Diesel Fuel Conditioner & Injector Cleaner	281	HPD	Ace Odorless Charcoal Lighter	440	MPD
OOPS! The All Purpose Remover	122	MISC	Klean Strip Lacquer Thinner	282	AR	Gunk General Purpose Degreaser	441	OXY

Sample	ID Number	Class	Sample	ID Number	Class	Sample	ID Number	Class
Bruce Clean n' Strip	123	MPD	Kingsford Odorless Charcoal Lighter	283	MPD	Formby's Conditioning Furniture Refinisher	442	OXY
De-Solv-It Citrus Solution	124	MISC	Exxon Aromatic 100	284	AR	BIX Tuff-job Stripper	443	OXY
Goo Gone	125	MISC	Exxon Aromatic 150	285	AR	Gasoline (85 octane)	444	Gas
Coleman Fuel	126	LPD	Exxon Aromatic 200	286	AR	Creosote Coal Tar	445	AR
Gunk Engine Brite	127	MISC	Exxon Isopar E	287	ISO	Pro-Gard Clean Up	44	MPD
Pennzoil Gumout Carb + Choke Cleaner	128	AR	Exxon Isopar K	288	ISO	Pro-Gard Fuel Injector Cleaner	45	MPD
Ace Premium Quality Charcoal Lighter	129	MPD	Exxon Isopar M	289	ISO	Pro-Gard Fuel Injector PLUS Intake Valve Cleaner	46	MPD
Shellsol OMS	12	ISO	Klean Strip Lacquer Thinner	28	MISC	Pro-Gard Gas Treatment	47	MPD
Ace Pure Odorless Mineral Spirits	130	MPD	Exxon Isopar V	290	ISO	Chevron Fuel Oil 6	48	MISC
Ace Pure Gum Turpentine	131	MISC	Prestone Windshield Melt De-Icer Additive	291	OXY	Chevron High Sulfur (HS) Diesel Fuel 2	49	HPD
Ace Odorless, 1-K Grade Kerosene	132	HPD	Klean Strip Automotive Wipe Away	292	MISC	Shellson D43	4	MPD
ZEP Heavy Duty Floor Stripper	133	OXY	ProGard Fuel Injector Cleaner	293	MPD	Chevron Low Sulfur (LS) Diesel Fuel 2	50	HPD
WD-40	134	MPD	Duraflame Fresh Light Charcoal Lighter	294	OXY	Chevron Special LS Diesel Fuel 2	51	HPD

Sample	ID Number	Class	Sample	ID Number	Class	Sample	ID Number	Class
M-1 Remover	135	AR	Zippo Premium Lighter Fluid	295	LPD	Ortho Malathion 50 Plus Insect Spray Concentrate	52	AR
Cutter Citronella Torch Fuel	136	MPD	Tiki Torch Fuel	296	MPD	Ortho Bug B Gon Multi-Purpose Inset Killer Concentrate	53	NP
Klean Strip Roller and Brush Cleaner	137	OXY	Goo Gone	297	MISC	Real Kill Multi-Purpose Insect Killer Concentrate	54	AR
Klean Strip Adhesive Remover	138	OXY	Lamplight Farms Ultra Pure Smokeless & Odorless Candle and Lamp Oil	298	NA	USA Lead Free Japan Drier	55	HPD
Klean Strip Strip-X Stripper	139	AR	Un-Du Candle Wax Remover	299	OXY	SpectracidePRO Diazinon 4E 47.5% Insect Spray Concentrate	56	AR
Shellsol D60	13	MPD	Klean Strip Turpatine	29	MISC	SpectracidePRO Residual Insect Control EC Emulsifable Conc.	57	MISC
Lamplight Farms Citronella Torch Fuel	140	NP	Shell VM&P Naphtha HT	2	LPD	H&C D-100 Solvent	58	AR
LF Citronella Torch Fuel 25% weathered	141	NP	Hess Diesel Fuel	300	HPD	Goof Off the Ultimate Remover	59	AR
LF Citronella Torch Fuel 50% weathered	142	NP	Hess Regular Unleaded Gasoline	301	Gas	Shellsol A100	5	AR

Sample	ID Number	Class	Sample	ID Number	Class	Sample	ID Number	Class
LF Citronella Torch Fuel 75% weathered	143	NP	Hess Regular Unleaded Gasoline 25% weathered	302	Gas	Formby's Lemon Oil Treatment	60	MISC
Parks Liquid Deglosser	144	MISC	Hess Regular Unleaded Gasoline 50% weathered	303	Gas	ZEP Citrus All Purpose Cleaner	61	OXY
Do It Best Liquid Stripper	145	AR	Hess Regular Unleaded Gasoline 75% weathered	304	Gas	Whitaker C-14 Normal Paraffin	62	NA
Sunnyside Brush Cleaner	146	MISC	Good Gone Candle Wax Remover	305	NA	Whitaker Low End Point Mineral Spirits	63	MPD
Sunnyside Odorless Paint Thinner	147	ISO	Lamplight Farms Ultra Pure Smokeless & Odorless Candle and Lamp Oil	306	NA	Whitaker Paint Thinner-Mineral Spirits	64	MPD
Do It Best Quick Stripper	148	AR	Crown Liquid Deglosser	307	OXY	Whitaker Rule 66 Mineral Spirits	65	MPD
Sunnyside Denatured Alcohol Solvent	149	OXY	Crown Brush Cleaner	308	MISC	Whitaker Odorless Mineral Spirits	66	ISO
STP Fuel Injector & Carburetor Cleaner	14	HPD	Piggly Wiggly Odorless Charcoal Lighter Fluid	309	MPD	Whitaker Low Odor Mineral Spirits	67	MISC
Sunnyside Xylol	150	AR	Klean Strip Odorless Mineral Spirits	30	MPD	Whitaker VM&P Naphtha	68	LPD
Sunnyside Naphtha	151	LPD	Klean Strip Turpatine	310	MISC	Whitaker #51 Lacquer Thinner	69	OXY

Sample	ID Number	Class	Sample	ID Number	Class	Sample	ID Number	Class
Sunnyside Lacquer Thinner	152	MISC	Klean Strip Kerosene	311	MISC	Shellsol A150	6	AR
Sunnyside Pure Gum Spirits of Turpentine	153	MISC	Walmart Charcoal Starter	312	MPD	Whitaker #48 Lacquer Thinner	70	OXY
Sunnyside Methyl Ethyl Ketone	154	OXY	Sunnyside Mineral Spirits	313	MPD	Whitaker #11 Lacquer Thinner	71	OXY
Sunnyside t.r.p.s.	155	MISC	Plasti-Kote Liquid Sandpaper	314	OXY	Whitaker Aro-Sol 10 (Aromatic 100)	72	AR
Sunnyside Kerosene	156	HPD	Do It Best Odorless Mineral Spirits	315	MPD	Whitaker Aro-Sol 15 (Aromatic 150)	73	AR
Sunnyside Kerosene, 25% weathered	157	HPD	Laura Lynn Charcoal Starter	316	MPD	Exxon Aromatic 100	74	AR
Sunnyside Kerosene, 50% weathered	158	HPD	Weiman Wax Away	317	ISO	Exxon Aromatic 150	75	AR
Sunnyside Kerosene, 75% weathered	159	HPD	Full Blown Bubble Gum Fuel Fragrance	318	MISC	Exxon Aromatic 200	76	AR
STP Gas Treatment	15	HPD	Wilson's Leather & Suede Protector	319	OXY	Exxon Norpar 12	77	NA
Sunnyside Mineral Spirits	160	MPD	Publix Charcoal Lighter	31	MPD	Exxon Norpar 13	78	NA
Sunnyside Mineral Spirits, 25% weathered	161	MPD	ScotchGard Protector for Leather Upholstery	320	ISO	Exxon Norpar 14	79	NA
Sunnyside Mineral Spirits, 50% weathered	162	MPD	LabChem Kerosene	321	ISO	Shellsol B HT	7	LPD
Sunnyside Mineral Spirits, 75% weathered	163	MPD	Sherwin Williams Ultra Solv 1	322	OXY	Exxon Norpar 15	80	NA

Sample	ID Number	Class	Sample	ID Number	Class	Sample	ID Number	Class
BBQ PRO Charcoal Lighter Fluid	164	MPD	Sherwin Williams Ultra 7000	323	OXY	Exxon Varsol 1	81	MPD
BBQ PRO Charcoal Lighter Fluid 25% weathered	165	MPD	Klean Strip Liquid Sander	324	OXY	Exxsol D 130	82	HPD
BBQ PRO Charcoal Lighter Fluid 50% weathered	166	MPD	Lamplight Famrs Citronella Torch Fuel	325	MPD	Exxsol D 40 Solvent	83	MPD
BBQ PRO Charcoal Lighter Fluid 75% weathered	167	MPD	Coleman Fuel	326	LPD	Exxsol D 60 Solvent	84	MPD
Weiman Wax Away	168	ISO	Ozark Trail Camp Fuel	327	LPD	Exxsol D 80	85	MPD
Goo Gone Candle Wax Lifter	169	NA	Formby's Paint and Poly Remover Wash	328	MISC	Exxsol D 110	86	HPD
STP Octane Booster	16	MISC	Dad's Easy Spray Paint Stain and Varnish Remover	329	OXY	Exxon Isopar E	87	ISO
Guardsman AFTA	170	MISC	Lamplight Farms Lamp Oil	32	MISC	Exxon Isopar K	88	ISO
Goof Off AFTA Stain Lifter	171	MISC	Klean Strip Prep-All	330	MISC	Exxon Isopar M	89	ISO
Orange Clean Super Concentrate	172	MISC	Premium Quality Charcoal Starter	331	ISO	Rubber Solvent 332	8	LPD
Scotch Gard Protector	173	ISO	ArmorAll Waterproofi ng Sealer	332	MPD	Exxon Isopar V	90	ISO
Sanford EXPO White Board Cleaner	174	OXY	Gunk Octane Performanc e Booster	333	HPD	E-Z Paint Thinner	91	MPD

Sample	ID Number	Class	Sample	ID Number	Class	Sample	ID Number	Class
V&O Lanterns Best Quality Lamp Oil	175	HPD	Gunk Liquid Wrench	334	OXY	E-Z VM&P Naphtha	92	LPD
V&O LNPanterns Candle & Lamp Oil	176	NA	Dad's Drip Strip	335	MISC	E-Z Lacquer Thinner	93	MISC
Eliminator Hornet & Wasp Killer	177	NP	King Lighter Fluid	336	MISC	Flood Penetrol Quality Paint Conditioner	94	MPD
ArmorAll Waterproofing Sealer	178	MPD	Jon-e Hand Warmer Fluid	337	MISC	Flood ESP (Easy Surface Prep)	95	MPD
Ozark Trail Camp Fule	179	LPD	Sunnyside Gloss Remover & Pre-paint Cleaner	338	ISO	BP Regular Unleaded Gasoline, 25% weathered	96	Gas
STP Diesel Fuel Treatment	17	HPD	Specs Paint Thinner (low odor mineral spirits)	339	MPD	BP Regular Unleaded Gasoline, 50% weathered	97	Gas
Outers Tri-Lube	180	MPD	Ronsonsol Lighter Fuel	33	LPD	BP Regular Unleaded Gasoline, 75% weathered	98	Gas
Remington Rem Oil	181	MPD	HomeBest Odorless Charcoal Lighter Fluid	340	MPD	BP Regular Unleaded Gasoline, 90% weathered	99	Gas
PRestone Heavy Duty Brake Parts Cleaner	182	MISC	Carbona Stain Devils Candle Wax & Tar Remover	341	OXY	Cypar 7	9	MISC
STP All Season Water Remover	183	HPD	Raid Ant & Roach Killer	342	HPD	Home Depot Paint Thinner From Large Scale Burn 1	MPDb1	MPD

Sample	ID Number	Class	Sample	ID Number	Class	Sample	ID Number	Class
RXP Fuel & Exhaust System Cleaner with Combustion Enhancer	184	MISC	Kilz Upshot Overhead Stain Sealer	343	OXY	Low's Deglosser From Large Scale Burn 1	OXYb1	OXY
Pennzoil Marine Fuel System Cleaner & Stabilizer	185	NP	Klean Strip Paint Clean-Up	344	MISC	Gasoline From Ocala Fire College From Large Scale Burn 1	Gasb1	Gas
ZAP Primer	186	MISC	Qik Joe Charcoal Lighter Fluid	345	ISO	Carpet Padding		SUB
Kilz Original Sealer-Primer-Stainblocker	187	MISC	Ace Premium Quality Charcoal Lighter	346	MPD	Cotton Pajama Pants		SUB
Elmer's Extra Strength Spray Adhesive	188	OXY	Klean Strip VM&P Naphtha	347	LPD	Polyester Quilt Batting		SUB
3M Super 77 Multi-Purpose Adhesive	189	MISC	3M 08984 General Purpose Adhesive Cleaner	348	MISC	Polyurethane Foam Mattress		SUB
STP Super Concentrated Gas Treatment	18	HPD	Ace Pure Odorless Mineral Spirits	349	MPD	100 Olefin		SUB
Folk Art Sanding Sealer	190	OXY	Royal Oak Premium Odorless Charcoal Lighter	34	MPD	Alder		SUB
June Tailer Quilt Basting Spray	191	OXY	Klean Strip Methyl Ethyl Ketone	350	OXY	Aspen		SUB
Northern Lights Lamp Fuel	192	NA	Klean Strip Turpatine	351	MISC	Bamboo Hardwood		SUB
Power Service Diesel Fuel Supplement	193	MISC	Lamplight Farms Lamp Oil	352	NP	Black Leather Swatch		SUB

Sample	ID Number	Class	Sample	ID Number	Class	Sample	ID Number	Class
Power Service Diesel +911	194	OXY	Klean Strip Japan Drier	353	MPD	Cardboard Box		SUB
Howes Lubricator Diesel Treat	195	MISC	Longs Gourmet Grill Charcoal Lighter	354	MPD	Cedar		SUB
Cartel Heavey Duty Fleet Winter Diesel Fuel Conc.	196	OXY	Jasco Adhesive Clean-Up	355	MPD	Character Walnut Laminate		SUB
FPPF Fuel Power Diesel Fuel Treatment	197	OXY	Escort Camp Fuel	356	LPD	Cherry Laminate		SUB
Sea Foam Trans-Tune	198	LPD	Recochem Camping Fuel	357	LPD	Cherry		SUB
Sea Foam Auto Marine Motor Treatment	199	LPD	Mastercraft Varsol	358	MPD	Cinder Blokc		SUB
STP Super Concentrated Fuel Stabilizer	19	HPD	Canadian Northland Charcoal Starter	359	MISC	Clear Hard Maple Laminate		SUB
Shellsol Heptane	1	LPD	Zippo Premium Lighter Fluid	35	LPD	Clear Hickory Sheoga Laminate		SUB
Exxon Clearlite Heater Fuel	200	ISO	Royal Oak Charcoal Lighter	360	MPD	Clear Red Oak Laminate		SUB
Summer Lights Citronella Outdoor Lamp Oil	201	NP	Recochem Fire Starter	361	NP	Clear White Oak Laminate		SUB
Lamplight Farms Lamp Oil	202	HPD	Esso Diesel Fuel	362	HPD	Douglass Fir		SUB
E *Zoil Diesel Aid	203	OXY	Gulf Kerosene	363	HPD	Fiberglass Insulation		SUB
Pennzoil Gumout Xtra Concentrated Carburetor Cleaner	204	MISC	Gulf Diesel Fuel	364	HPD	Finegrain Corktiles		SUB

Sample	ID Number	Class	Sample	ID Number	Class	Sample	ID Number	Class
Pennzoil Gumout Regane Cleaner	205	MISC	Record Kerosene	365	HPD	Foil Insulation		SUB
Gunk Diesel-Tone Diesel Fuel Conditioner	206	HPD	Lamplight Farms Ultra-Pure Smokeless and Odorless Candle & Lamp Oil	366	NA	Hickory Laminate		SUB
Gunk Lead Substitute	207	HPD	OOPS! Multi-Purpose Remover	367	MISC	Hickory		SUB
Gold Eagle +104 Octane Boost	208	MISC	Mr. BarbQ Charcoal Lighter	368	MPD	Industrial Vinyl		SUB
Next Dimension Professional Strength Brake & Parts Cleaner	209	OXY	Gunk Liquid Wrench	369	HPD	Magazines		SUB
Penske Fuel Injector & Carburetor Cleaner	20	HPD	Valvoline SynPower Super Concentrated Fuel Injector Cleaner	36	MISC	Maple		SUB
Gunk Liquid Wrench	210	HPD	Black Magic Tire Wet	370	ISO	Nylon Rope		SUB
3M 06014 Prep and Blend Liquid	211	MISC	Klean Strip Odorless Mineral Spirits	371	MPD	Nylon		SUB
3M 08984 General Purpose Adhesive Cleaner	212	MISC	Parks Epoxy and Lacquer Thinner	372	OXY	Oak		SUB
3M 08892 Rust Fighter	213	MPD	Ace Paint Thinner 100% Mineral Spirits	373	MPD	Old Navy Women's Shoe		SUB

Sample	ID Number	Class	Sample	ID Number	Class	Sample	ID Number	Class
SEM 38354 Plastic Prep	214	LPD	Mobil Kerosene	374	HPD	Olefin Nylon Blend		SUB
Auto Kare SG-7 Tire Dressing	215	MPD	Mobil Gasoline	375	Gas	P.E.T. Polyester		SUB
Klean Strip QAF354 Fiberglass Paint Remover	216	AR	Yaley's Liquid Candle Lamp Oil	376	MISC	Polyester Nylon Blend		SUB
PPG DX330 Wax and Grease Remover	217	MISC	Yaley's Liquid Candle Red Dye	377	MISC	Polyester Rope		SUB
PPG DT870 Reducer	218	OXY	Yaley's Liquid Candle Blue Dye	378	MISC	Polyester		SUB
PPG DT885 Reducer	219	OXY	Yaley's Liquid Candle Green Dye	379	MISC	Poplar		SUB
Parks 100% Mineral Spirit Paint Thinner	21	MPD	VP Racing Fuels Fuel System Cleaner	37	MISC	Roofing Shingles		SUB
PPG DT895 Reducer	220	MISC	Yaley's Liquid Candle Yellow Dye	380	MISC	Roofing Tiles		SUB
Thompson's Waterseal	221	MPD	Marathon 100 Octane Aviation Gasoline	381	MISC	Sketchers Casual Shoes		SUB
Klean Strip 100% Mineral Spirit Paint Thinner	222	MPD	Sunoco 112 Octane Racing Gasoline	382	MISC	Steve Madden Men's Casual Shoe		SUB
Klean Strip Odorless Mineral Spirits	223	MPD	Speedway Gasohol (10%) 87 Octane	383	Gas	Street Smart Boots		SUB
Ace VM&P Naphtha	224	LPD	BP 93 octane Gasoline	384	Gas	Teak Laminate		SUB

Sample	ID Number	Class	Sample	ID Number	Class	Sample	ID Number	Class
Ace Pure Odorless Mineral Spirits	225	MPD	BP 87 Octane Gasoline	385	Gas	Thermal Paper Rolls		SUB
Ace Odorless, 1-K Grade Kerosene	226	HPD	Jon-e Handwarmer Fluid	386	MISC	Trex		SUB
Ace Paint Thinner (100% Mineral Spirits)	227	MPD	Rutland Tank Shield Fuel Oil Additive	387	MPD	Troya Laminate		SUB
Ace Liquid Deglosser	228	MISC	Homebest Odorless Charcoal Lighter Fluid	388	MPD	UV Olefin		SUB
Sunnyside Gloss Remover	229	MISC	Klean Strip Klean Heat Odorless Heater Fuel	389	MPD	Vinyl Floor		SUB
Parks Epoxy and Lacquer Thinner	22	OXY	Power Service Diesel Fuel Supplement	38	MISC	Vinyl Linoleum		SUB
E-Z Low Odor Mineral Spirits	230	MPD	Pro Shop Gas Treatment	390	MISC	Walmart Rain Boot Shoe Coverings		SUB
E-Z Water Wash Brush Cleaner	231	OXY	Pro Sho Super Conc. Fuel Injector Cleaner	391	MISC	White Pine		SUB
Kingsford Odorless Charcoal Lighter (can)	232	MPD	Homestar Citronella Torch Fuel	392	HPD	Yellow Pine		SUB
Kingsford Odorless Charcoal Lighter (bottle)	233	MPD	Mineral Spirits	393	MPD	Office Chair From Large Scale Burn 1		SUB
BBQ PRO Charcoal Lighter Fluid	234	MPD	Speckoz Permethrin TC	394	AR	Mattress From Large Scale Burn 1		SUB
Unifide Gas Line Antifreeze	235	OXY	Condea Vista MR Solvent	395	NP	Pillow From Large Scale Burn 1		SUB

Sample	ID Number	Class	Sample	ID Number	Class	Sample	ID Number	Class
Aura Lamp Oil	236	NA	Condea Vista 47 Solvent	396	MISC	Futon From Large Scale Burn 1		SUB
Tropical Lights Candle and Lamp Oil	237	NA	Condea Vista LPA Solvent	397	NP	Bedspread From Large Scale Burn 1		SUB
Polly S Easy-Lift-Off Paint and Decal Remover	238	OXY	Condea Vista LPA 142 Solvent	398	NP	PET Polyester Carpet and Padding From Large Scale Burn 1		SUB
Model Master Airbrush Thinner	239	OXY	Condea Vista LPA 170 Solvent	399	NP			
Gold Eagle STA-BIL Concentrated Fuel Stabilizer	23	MISC	Pennzoil Roadside Rescue Emergency Fuel Additive	39	MISC			
Top Fuel	240	OXY	Shellsol D38	3	MPD			
Hollowick Liquid Candle Wax	241	NA	Condea Vista LPA 210 Solvent	400	NP			
Aladdin Lamp Oil	242	HPD	Linpar 1416V Normal Paraffin	401	NA			
Crown Odorless Mineral Spirits	243	NP	Exxon Charcoal Lighter 104	402	ISO			
Crown Paint Thinner	244	MISC	Exxon Charcoal Lighter 105	403	MPD			
Crown Turpentine	245	MISC	Exxon Han 906 Solvent	404	AR			
Crown Lacquer Thinner	246	MISC	Exxon Exxate 600 Solvent	405	OXY			
Crown Brush & Roller Cleaner	247	MISC	Exxon Exxate 700 Solvent	406	OXY			
Crown Liquid Deglosser	248	OXY	Exxon Exxate 800 Solvent	407	OXY			

Sample	ID Number	Class	Sample	ID Number	Class	Sample	ID Number	Class
Crown Total Strip Paint Remover	249	OXY	Exxon Exxate 900 Solvent	408	OXY			
Kingsford Odorless Charcoal Lighter	24	MPD	Exxon Exxate 1000 Solvent	409	OXY			
Oatey Purple Primer/Clea ner	250	OXY	Turner Laboratories Octane Booster	40	HPD			
Gel Gloss One Step Cleaner and Polish	251	MISC	Phillips 66 Soltrol 10	410	ISO			
DEFT Clear Wood Finish (Gloss)	252	OXY	Phillips 66 Soltrol 100	411	ISO			
Formby's Build-UP Remover	253	MPD	Phillips 66 Soltrol 130	412	ISO			
Glaze-N-Seal	254	MISC	Phillips 66 Soltrol 170	413	ISO			
H&C De-Greaser	255	OXY	Phillips 66 Soltrol 220	414	ISO			
Ortho Mosquito B Gon	256	AR	Citristrip Wipe Away-All Purpose Remover	415	OXY			

REFERENCES

1. Committee on Identifying the Needs of the Forensic Sciences Community National Research Council, *Strengthening Forensic Science in the United States: A Path Forward*. 2009.
2. Izenman, A.J., *Modern Multivariate Statistical Techniques Regression Classification, and Manifold Learning*. 2008, New York, New York: Springer Science + Business Media LLC.
3. Bottrell, M.C., *Forensic Glass Comparison: Background Information Used in Data Interpretation.* Forensic Science Communications, 2009. **11**(2).
4. Koons, R.D., Buscaglia, J., Bottrell, M., Miller, E.T., *Forensic Glass Comparison*, in *Forensic Science Handbook*, R. Saferstein, Editor. 2002, Prentice Hall: Upper Saddle River, New Jersey.
5. Copley, G.J., *The Composition and Manufacture of Glass and its Domestic and Industrial Applications*, in *Forensic Examination of Glass and Paint*, B. Caddy, Editor. 2001, Taylor & Francis: New York, New York.
6. Hamer, P.S., *Microscopic Techniques for Glass Examination*, in *Forensic Examination of Glass and Paint*, B. Caddy, Editor. 2001, Taylor & Francis: New York, New York.
7. Almirall, J.R., Trejos, T., *Elemental Analysis of Glass Fragments*, in *Forensic Examination of Glass and Paint*, B. Caddy, Editor. 2001, Taylor & Francis: New York, New York.
8. Zadora, G., Ramos, D., *Evaluation of Glass Samples for Forensic Purposes - An Application Likelihood Ratios and Information - Theoretical Approach.* Chemometrics and Intelligent Laboratory Systems, 2010. **102**: p. 63-68.
9. Sjastad, K., Simonsen, S.L., Andersen, T., *Use of Lead Isotopic Ratios to Discriminate Glass Samples in Forensic Science.* Journal of Analytical Atomic Spectrometry, 2011. **26**: p. 325-333.
10. Newton, A.W.M., *An Investigation into the Variability of the Refractive Index of Glass: Part II The Effect of Debris Contaimination.* Forensic Science International, 2001. **204**: p. 182-185.
11. Coumbaros, J., Deman, J., Kirkbridge, K.P., Walker, G.S., Skinner, W., *An Investigation into the Spatial Elemental Distribution Within a Pane of Glass by Time of Flight Secondary Ion Mass Spectrometry.* 53, 2008. **2**(312-320).
12. Zadora, G., *Evaluation of Evidence Value of Glass Fragments by Likelihood Ratio and Bayesian Network Approaches.* Analytica Chimica Acta, 2009. **642**: p. 279-290.
13. Weis, P., Ducking, M., Watzke, P., Menges, S., Becker, S., *Establishing a Match Criterion in Forensic Comparison Analysis of Float Glass Using Laser Ablation Inductively Coupled Plasma Mass Spectrometry.* Journal of Analytical Atomic Spectrometry, 2011. **26**: p. 1273-1284.

14. Bridge, C.M., Powell, J., Steele, K.L., Williams, M., MacInnis, J.M., and Sigman, M.E., *Characterization of Automobile Float Glass with Laser-Induced Breakdown Spectroscopy and Laser Ablation Inductively Coupled Plasma Mass Spectrometry.* Applied Spectroscopy, 2006. **60**(10): p. 1181-1187.
15. Brends-Montero, S., Wiarda, W., De Joode, P., Van Der Pejil, G., *Forensic Analysis of Float Glass Using Laser Ablation Inductively Coupled Plasma Mass Spectrometry (LA-ICP-MS): Validation of a Method.* Journal of Analytical Atomic Spectrometry, 2006. **21**(1185).
16. McIntee, E., et al., *Non-parametric permutation test for the discrimination of float glass samples based on LIBS spectra.* Journal of Chemometrics, 2010. **24**(6): p. 312-319.
17. Bridge, C.M., Powell, J., Steele, K.L, and Sigman, M.E., *Forensic Comparative Glass Analysis by Laser-Induced Breakdown Spectroscopy.* Spectrochimica Acta Part B, 2007. **62**: p. 1419-1425
18. McIntee, E., et al., *Comparative analysis of automotive paints by laser induced breakdown spectroscopy and nonparametric permutation tests.* Spectrochimica Acta Part B: Atomic Spectroscopy, 2010. **65**(7): p. 542-548.
19. Trejos, T., Almirall, J.R., *Sampling Strategies for the Analysis of Glass Fragments by LA-ICP-MS Part I. MIcro-Homogeneity Study of Glass and its Application to the Interpretation of Forensic Evidence.* Talanta, 2005. **67**: p. 388-395.
20. Trejos, T., Almirall, J.R., *Sampling Strategies for the Analysis of Glass Fragments by LA-ICP-MS Part II: Sample SIze and Sample Shape Considerations.* Talanta, 2005. **67**(396-401).
21. Zieba-Palus, J., Michalska, A., and Weselucha-Birczynska, A., *Characterisation of Paint Samples by Infrared and Raman Spectroscopy for Criminalistic Purposes.* Journal of Molecular Structure, 2011. **993**(1-3): p. 134-141.
22. Zieba-Palus, J., Milczarek, J.M., Koscielniak, P., *Working Out Conditions of Identification and Comparative Analysis of Car Paints by Pyrolytic Gas Chromatography Coupled with Mass Spectrometry (PY-GC-MS).* Z Zagednien Nauk Sadowych, 2006. **67**: p. 235-248.
23. Zieba-Palus, J., *Application of Micro-Fourier Transform Infrared Spectroscopy to the Examination of Paint Samples.* Journal of Molecular Structure, 1999. **511-512**: p. 327-335.
24. Wampler, T.P., Bishea, G.A., Simonsick, W.J., *Recent Changes in Automotive Paint Formulation Using Pyrolysis-Gas Chromatography/Mass Spectrometry for Identification.* Journal of Analytical and Applied Pryolysis, 1997. **40-41**: p. 79-89.
25. Szafarska, M., Wozniakiewicz, M., Pilch, M., Zieba-Palus, J., Koscielniak, P., *Computer Analysis of ATR-FTIR Spectra of Paint Samples for Forensic Purposes.* Journal of Molecular Structure, 2009. **924-926**: p. 504-513.
26. Suzuki, E.M., and Carrabba, M., *In situ Identification and Analysis of Automotive Paint Pigments Using Line Segment Excitation Raman Spectroscopy: I. Inorganic Topcoat Pigments.* Journal of Forensic Science, 2001. **46**(5): p. 1053-1069.

27. Muehlethaler, C., Massonnet, G., Esseiva, P., *The Application of Chemometrics of Infrared and Raman Spectra as a Tool for the Forensic Analysis of Paints.* Forensic Science International, 2011. **209**(1-3): p. 173-182.
28. Milczarek, J.M., Dziadosz, M., Zieba-Palus, J., *Way to Distinguish Car Paint Traces Based on Epoxy Primer Layers Analysis by Pyrolysis-Gas Chromatrography-Mass Spectrometry.* Chemia Analityczna, 2009. **54**(2): p. 173-185.
29. McNorton, S.C., Nutter, G.W., Siegel, J.A., *The Characterization of Automobile Body Fillers.* Journal of Forensic Sciences, 2008. **53**(1): p. 116-124.
30. McIntee, E.M., *Forensic Analysis of Automobile Paints by Atomic and Molecular Spectroscopic Methods and Statistical Data Analysis*, in *Chemistry*. 2008, University of Central Florida: Orlando. p. 102.
31. Massonnet, G., and Stoecklein, W., *Identification of Organic Pigments in Coatings: Applications to Red Automotive Topcoats: Part III: Raman spectroscopy (NIR FT-Raman).* Science & Justice, 1999. **39**(3): p. 181-187.
32. LV, J., Feng, J., Liu, Y., Wang, Z., Zhao, M., Shi, R., *Discriminating Amino Resin Paints From Alkyd Resin Paints with Two Kinds of Pigments in Automotive Coatings in Forensic Analysis by FTIR Spectroscopy.* Analytical Letters, In Press.
33. Kochanowski, B.K., Morgan, S.L. , *Forensic Discrimination of Automotive Paint Samples using Pyrolysis-Gas Chromatography-Mass Spectrometry with Multivariate Statistics.* Journal of Chromatographic Science, 2000. **38**(3): p. 100-108.
34. Fido, L.A., *Application of Raman Spectroscopy to Forensic Examination of Paint, Fibres and Documents*. 2006, Queen's University of Belfast: Belfast, UK. p. 229.
35. De Gelder, J., Vandeabelle, P., Govaert, F., Moens, L., *Forensic Analysis of Automotive Paints by Raman Spectroscopy.* Journal of Raman Spectroscopy, 2006. **35**: p. 1059-1067.
36. Gothard, J.A., *Evaluation of Automobile Paint Flakes as Evidence.* Journal of Forensic Science, 1976. **21**(3): p. 636-641.
37. *Standard Guide for Forensic Paint Analysis*. 2002, ASTM International.
38. Caddy, B., ed. *Forensic Examination of Glass and Paint Analysis and Interpretation*. 2001, Taylor & Francis: New York, New York.
39. Saferstein, R., ed. *Forensic Science Handbook*. 2 ed. 2002, Prentice Hall: Upper Saddle River, New Jersey.
40. Streitberger, H.J., Dossel, K.F., ed. *Automotive Paints and Coatings* 2ed. 2008, Wiley-VCH: Munster, Germany.
41. Kuptsov, A.N. *Applications of Fourier Transform Raman and Infrared Spectroscopy in Forensic Sciences*. in *Raman Scattering*. 2000. Moscow, Russia: SPIE.
42. Buzzini, P., and Massonnet, G., *A Market Study of Green Spray Paints by Fourier Transform Infrared (FTIR) and Raman Spectroscopy.* Science & Justice, 2004. **44**(3): p. 123-131.
43. Byers, S.N., *Introduction to Forensic Anthropology* 2nd ed. 2005, Boston: Pearson.

44. Kasem, M.A., Russo, R.E., Harith, M.A., *Influence of Biological Degradation and Environmental Effects on the Interpretation of Archeological Bone Samples with Laser-Induced Breakdown Spectroscopy.* J. Anal. At. Spectrom., 2011. **26**: p. 1722-1739.
45. Samek, O., Beddows, D.C.S., Telle, H.H., Kaiser, J., Liska, M., Caceres, J.O., Gonzales Urena, A., *Quantitative Laser-Induced Breakdown Spectroscopy Analysis of Calcified Tissue Samples.* Spectrochimica Acta Part B, 2001. **56**: p. 865-875.
46. Castro, W., Hoogewerff, J., Latkoczy, C., Almirall, J.R., *Application of Laser Ablation (LA-ICP-SF-MS) for the Elemental Analysis of Bone and Teeth Samples for Discrimination Purposes.* Forensic Science International, 2010. **195**: p. 17-27.
47. Ubelaker, D.H., Ward, D.C., Braz, V.S., Stewart, J., *The Use of SEM/EDS analysis to Distinguish Dental and Osseus Tissue for Other Materials.* Journal of Forensic Sciences, 2002. **47**(5): p. 1-4.
48. Christensen, A.M., Smith, M.A., Thomas, R.M., *Validation of X-ray Fluorescence Spectrometry for Determine Osseous or Dental Origin of Unknown Material.* Journal of Forensic Sciences, 2012. **57**(1): p. 47-51.
49. Ubelaker, D.H., Lowenstien, J.M., Hood, D.G., *Use of Solid-Phase Double-Antibody Radioimmunoassay to Identify Species from Small Skeletal Fragments.* Journal of Forensic Sciences, 2004. **49**(5): p. 1-6.
50. Prieto-Castello, M.J., Hernandez del Rincon, J.P., Perez-Sirvent, C., Alvarez-Jimenez, P., Perez-Carceles, M.D., Osuna, E., Luna, A., *Application of Biochemical and X-ray Diffraction Analyses to Establish the Postmortem Interval.* Forensic Science International, 2007. **172**: p. 112-118.
51. Rusak, D.A., Marsico, R.M., Taroli, B.L., *Using Laser-Induced Breakdown Spectroscopy to Assess Preservation Quality of Archeological Bones by Measurement of Calcium-to-Fluorine Ratios.* Applied Spectroscopy, 2011. **65**(10): p. 1193-1196.
52. Couris, S., Mavromanolakis, A., Fotakis, C., *Laser-Induced Breakdown Spectroscopy (LIBS) A Tool for Rapid In-Situ Elemental Analysis.* SPIE, 2012. **3423**: p. 228-232.
53. DeHaan, J.D., *Kirk's Fire Investigation*. 4th ed. 1997, Upper Saddle River, New Jersey: Prentice-Hall.
54. Midkiff, C.R., *Arson and Explosive Investigation*, in *Forensic Science Handbook*, R. Saferstein, Editor. 2002, Prentice Hall: Upper Saddle River, New Jersey.
55. ASTM, *Standard Test Method for Ignitable Liquid Residues in Extracts from Fire Debris Samples by Gas Chromatography-Mass Spectrometry*. 2010, ASTM: United States. p. 1-11.
56. ASTM, *Standard Practive for Separation of Ignitable Liquid Residues from Fire Debris Samples by Passive Headspace Concentration with Activated Charcoal*. 2005, ASTM: United States. p. 1-3.
57. Tan, B., Hardy, J.K., Snavely, R.E., *Accelerant Classification by Gas Chromatography/Mass Spectrometry and Multivariate Pattern Recognition.* Analytica Chimica Acta, 2000. **422**: p. 37-46.

58. Hupp, A.M., Marshall, L.J., Campbell, D.I., Smith, R.W., McGuffin, V.L., *Chemometric Analysis of Diesel Fuel for Forensic and Environmental Applications.* Analytica Chimica Acta, 2008. **606**(2): p. 159-171.
59. Doble, P., Sandercock, M., Du Pasquier, E., Petocz, P., Roux, C., Dawson, M., *Classification of Premium and Regular Gasoline by Gas Chromatography/Mass Spectrometry, Principal Component Analysis and Artificial Neural Networks.* Forensic Science International, 2007. **132**(1): p. 26-39.
60. Keto, R.O., *GC/MS Data Interpretation for Petroleum Distillate Identification in Contaminated Arson Debris.* Journal of Forensic Sciences, 1994. **40**(3): p. 412-423.
61. Keto, R.O., Wineman, P.L., *Detection of Petroleum-Based Accelerants in Fire Debris by Target Compound Gas Chromatography/Mass Spectrometry.* Analytical Chemistry, 1991. **63**: p. 1964-1971.
62. Kelly, R.L., *Accelerant Identification in Fire Debris by Gas Chromatography/Mass Spectrometry Techniques.* Journal of Forensic Sciences, 1984. **29**(3).
63. Sandercock, P.M.L., Du Pasquier, E., *Chemical Fingerprinting of Unevaporated Automotive Gasoline Samples.* Forensic Science International, 2003. **134**: p. 1-10.
64. Sandercock, P.M.L., Du Pasquier, E., *Chemical Fingerprinting of Gasoline 2. Comparison of Unevaporate and Evaporated Automotive Gasoline Samples.* Forensic Science International, 2004. **140**: p. 43-59.
65. Borusiewicz, R., Zadora, G., Zieba-Palus, J., *Application of Head-Space Analysis with Passive Adsorption for Forensic Purpose in the Automated Thermal Desorption-Gas Chromatography-Mass Spectrometry System.* Chromatographia Supplement, 2004. **60**: p. S133-S141.
66. Williams, M.R., Fernandes, D. Bridge, C., Dorrien, D., Elliott, S., Sigman, M., *Adsorption Saturation and Chromatographic Distortion Effects on Passive Headspace Sampling with Activated Charcoal in Fire Debris Analysis.* Journal of Forensic Sciences, 2005. **50**(2): p. 316-325.
67. Sigman, M.E., Williams, M.R., and Ivy, R.G., *Individualization of Gasoline Samples by Covariance Mapping and Gas Chromatography/Mas Spectrometry.* Analytical Chemistry, 2007. **79**(9): p. 3462-3468.
68. Sigman, M.E., Williams, M.R., Castelbuono, J.A., Colca, J.G., Clark, C.D., *Ignitable Liquid Classification and Identification Using the Summed-Ion Mass Spectrum.* Instrumentation Science & Technology, 2008. **36**(4): p. 375-393.
69. Lazic, V., Palucci, A., Jovicevic, S., Carpanese, M., Poggi, C., Buono, E., *Detection of Explosives at Trace Levels by Laser Induced Breakdown Spectroscopy (LIBS).* Chemical, Biological, Radiological, Nuclear, and Explosives Sensing XI, 2010. **7665**.
70. Agrawal, J.P., Hodgson, R.D., *Organic Chemistry of Explosives*. 2007, West Sussex, England: John Wiley & Sons LTD.
71. Cooper, P.W., Kurowski, S.R., *Introduction to the Technology of Explosives*. 1996, New York, New York: Wiley-VCH.

72. Caygill, J.S., Davis, F., Higson, S.P.J., *Current Trends in Explosive Detection Techniques.* Talanta, 2012. **88**: p. 14-29.
73. Moore, D.S., Scharff, R.J., *Portable Raman Explosives Detection.* Anal Bioanal Chem, 2009. **393**: p. 1571-1578.
74. Skvortsov, L.A., *Laser Methods for Detecting Explosive Residues on Surfaces of Distant Objects.* Quantum Electronics, 2012. **42**(1): p. 1-11.
75. Gottfried, J.L., De Lucia, F.C., Munson, C.A., Miziolek, A.W., *Laser-Induced Breakdown Spectroscopy for Detection of Explosives Residues: A Review of Recent Advances, Challenges, and Future Prospects.* Anal Bioanal Chem, 2009. **395**: p. 283-300.
76. Gottfried, J.L., De Lucia, F.C., Miziolke, A.W., *Discrimination of Explosive Residues on Organic and Inorganic Substrates Using Laser-Induced Breakdown Spectroscopy.* Journal of Analytical Atomic Spectrometry, 2008. **24**: p. 288-296.
77. Brown, C.G., Baudelet, M., Bridge, C., Fisher, M.K., Sigman, M., Dagdigian, P.J., Richardson, M., *Atmosphere Issues in Detection of Explosives and Organic Residues.* Chemical, Biological, Radiological, Nuclear, and Explosives Sensing X, 2009. **7304**.
78. Lazic, V., Palucci, A., Jovicevic, S., Poggi, C., Buono, E., *Analysis of Explosive and Other Organic Residues by Laser Induced Breakdown Spectroscopy.* Spectrochimica Acta Part B, 2009. **64**: p. 1028-1039.
79. Morton, K.D., Torrione, P.A., Collins, L., *Signal Processing for the Detection of Explosive Residues on Varying Substrates Using Laser Induced Breakdown Spectroscopy.* Chemical, Biological, Radiological, Nuclear, and Explosives Sensing X, 2011. **8018**.
80. De Lucia, F.C., Gottfried, J.L., Munson. C.A., Miziolek, A.W., *Multivariate Analysis of Standoff Laser-Induced Breakdown Spectroscopy Spectra for Classification of Explosive-Containing Residues.* Applied Optics, 2008. **47**(31): p. 112-120.
81. Lucena, P., Dona, A., Tobaria, L.M., Laserna, J.J., *New Challenges and Insights in the Detection and Spectral Identification of Organic Explosives by Laser Induced Breakdown Spectroscopy.* Spectrochimica Acta Part B, 2011. **66**: p. 12-20.
82. Lazic, V., Palucci, A., Jovicevic, S., Carpanese, M., *Detection of Explosives in Traces by Laser Induced Breakdown Spectroscopy: Difference from Organic Interferents and Conditions for a Correct Classification.* Spectrochimica Acta Part B, 2011. **66**: p. 644-655.
83. Zachhuber, B., Ramer, G., Hobro, A., Chrysostom, E.T.H., Lendl, B., *Stand-off Raman Spectroscopy: A Powerful Technique for Qualitative and Quantitative Analysis of Inorganic and Organic Compounds Including Explosives.* Anal Bioanal Chem, 2011. **400**: p. 2439-2447.
84. Bremer, M.T., Wrzesinkski, P.J., Butcher, N., Lozovoy, V.V., Dantus, M., *Highly Selective Standoff Detection and Imaging of Tract Chemicals in a Complex Background Using Single-Beam Coherent Anti-Stokes Raman Scattering.* Applied Physics Letters, 2011. **99**(101109).

85. Desilets, S., Ho, N., Mathieu, P., Simard, J.R., Puckrin, E., Theriault, J.M., Lavoie, H., Theberge, F., Babin, F., Gay, D., Forest, R., Maheux, J., Roy, G., Chateauneuf, M., *Standoff Detection of Explosives, A Challenging Approach for Optical Technologies.* Micro- and Nanotechnology Sensors, Systems, and Applications III, 2011. **8031**.
86. Fountain, A.W., Christesen, S.D., Guicheteau, J.A, Pearman, W.F., Chyba, T., *Long Range Standoff Detection of Chemical and Explosive Hazards on Surfaces.* Optically Based Biological and Chemical Detection for Defence V. **7484**.
87. Cremers, D.A., Chinni, R.C., *Laser-Induced Breakdown Spectroscopy-Capabilities and Limitations* Applied Spectroscopy Reviews, 2009. **44**: p. 457-506.
88. Noll, R., Sturm, V., Aydin, U., Eilers, D., Gehlen, C., Hohne, M., Lamott, A., Makowe, J., Vrenegor, J., *Laser-Induced Breakdown Spectroscopy-From Research to Industry, New Frontiers for Process Control.* Spectrochimica Acta Part B, 2008. **63**: p. 1159-1166.
89. Striber, J., Radvan, R., Angheluta, L.M., *Laser Spectroscopy Methods for an 18th Century Grisaille Painting Investigation.* Journal of Optoelectronics and Advanced materials, 2009. **11**(11): p. 1815-1820.
90. Lipscher, J., *True or False? Scientific Methods in the Study of Art Forgeries.* Praxis der Naturwissenschaften, 2004. **53**(5): p. 7-12.
91. Caneve, L., Diamanti, A., Grimaldi, F., Palleschi, G., Spizzichino, V., Valentini, F., *Analysis of Fresco by Laser Induced Breakdown Spectroscopy.* Spectrochimica Acta Part B, 2010. **65B**(8): p. 702-706.
92. Duchene, S., Detalle,V., Bruder,R., Sirven,J.B., *Chemometrics and Laser Induced Breakdown Spectroscopy (LIBS) Analyses for Identification of Wall Paintings Pigments.* Current Analytical Chemistry, 2010. **6**(1): p. 60-65.
93. Schenk, E.R., Almirall, J.R., *Elemental Analysis of Cotton by Laser-Induced Breakdown Spectroscopy.* Applied Optics, 2010. **49**(13): p. C153-C160.
94. Almirall, J.R., Umpierrez, S., Castro, W., Gornushkin, I., Winefordner, J. *Forensic Elemental Analysis of Materials by Laser Induced Breakdown Spectroscopy (LIBS)*. in *Sensors and Command, Control, Communications, and Intelligence (C3I) Technologies for Homeland Security and Homeland Defense IV*. 2005. Orlando, FL USA: SPIE.
95. Rodriguez-Celis, E.M., Gornushkin, I.B., Heitmann, U.M., Almirall, J.R., Smith, B.W., Winefordner, J.D., Omenetoo, N., *Laser Induced Breakdown Spectroscopy as a Tool for Discrimination of Glass for Forensic Applications.* Analytical & Bioanalytical Chemistry, 2008. **391**(5): p. 1961-1968.
96. Naes, B.E., Umpierrez, S., Ryland, S., Barnett, C., Almirall, J.R., *A Comparison of Laser Ablation Inductively Coupled Plasma Mass Spectrometry, Micro X-Ray Fluorescence Spectroscopy, and Laser Induced Breakdown Spectroscopy for the Discrimination of Automotive Glass.* Spectrochimica Acta Part B, 2008. **63**(10): p. 1145-1150.

97. Barnett, C., Cahoon, E., Almirall, J.R., *Wavelength Dependence on the Elemental Analysis of Glass by Laser Induced Breakdown Spectroscopy.* Spectrochimica Acta Part B, 2008. **63**(10): p. 1016-1023.
98. Cahoon, E.M., Almirall, J.R., *Wavelength Dependence on the Forensic Analysis of Glass by Nanosecond 266 nm and 1064 nm Laser Induced Breakdown Spectroscopy.* Applied Optics, 2010. **49**(13): p. C49-C57.
99. Gornushkin, I.B., Panne, U., Winefordner, J.D., *Linear Correlation for Identification of materials by Laser Induced Breakdown Spectroscopy: Improvement Via Spectral Filtering and Masking.* Spectrochimica Acta Part B, 2009. **64**(10): p. 1040-1047.
100. Taschuk, M.T., Tsui, Y.Y, Fedosejevs, R., *Detection and Mapping of Latent Fingerprints by Laser-Induced Breakdown Spectroscopy.* Applied Spectroscopy, 2006. **60**(11): p. 1322-1327.
101. Gottfried, J.L., *Discrimination of Biological and Chemical Threat Simulants in Residue Mixtures on Multiple Substrates.* Analytical and Bioanalytical Chemistry, 2011. **400**(10): p. 3289-3301.
102. Trejos, T., Flores, A., Almirall, J.R., *Micro-Spectrochemical Analysis of Document Paper and Gel Inks by Laser Ablation Inductively Compled Plasma Mass Spectrometry and Laser Induced Breakdown Spectroscopy.* Spectrochimica Acta Part B, 2010. **64**(884-895).
103. Silva, M.J., Cortez, J., Pasquini, C., Honorato, R.S., Paim, A.P.S., Pimentel, M.F., *Gunshot Residues: Screening Analysis by Laser-Induced Breakdown Spectroscopy.* Journal of he Brazilian Chemical Society, 2009. **20**(10): p. 1887-1894.
104. Dockery, C.R., Goode, S.R., *Laser-Induced Breakdown Spectroscopy for the Detection of Gunshot Residues on the Hands of a Shooter.* Applied Optics, 2003. **42**(30): p. 6153-6158.
105. Rosenberg, M.B., Dockery,C.R., *Determining the Lifetime of Detectable Amounts of Gunshot Residue on the Hands of a Shooter Using Laser-Induced Breakdown Spectroscopy.* Applied Spectroscopy, 2008. **62**(11): p. 1238-1241.
106. Sarkar, A., Aggarwal, S.K., Alamelu, D., *Laser Induced Breakdown Spectroscopy for Rapid Identification of Different Types of Paper for Forensic Application.* Analytical Methods, 2010. **2**(1): p. 32-36.
107. Martin, M.Z., Labbe, N., Andre, N., Harris, R., Ebinger, M., Wullschleger, S.D., Vass, A.A., *High Resolution Applications of Laser-Induced Breakdown Spectroscopy for Environmental and Forensic Applications.* Spectrochimica Acta Part B, 2007. **62**(12): p. 1426-1432.
108. Gornushkin, I.B., Ruiz-Medina, A., Anzano, J.M., Smith, B.W., Winefordner, J.D., *Identification of Particulate Materials by Correlation Analysis Using a Microscopic Laser Induced Breakdown Spectrometer.* Journal of Analytical Atomic Spectrometry 2000. **15**(6): p. 581-586.
109. Almirall, J.R., Trejos, T. *Advances in Forensic Chemical Analysis of Materials Using Laser Induced Breakdown Spectroscopy*. in *Pacifichem 2010, International Chemical Congress of Pacific Basin Societies*. 2010. Honolulu, HI.

110. *State of Florida vs Casey Marie Anthony*. 2011, Ninth Judicial Circuit, In and For Orange County Florida.
111. Skoog, D.A., Holler, F.J., and Nieman, T.A., *Principles of Instrumental Analysis*. 5th ed. 1998, South Melbourne, Australia: Brooks/Cole.
112. Subramanian, A., Rodriguez-Saona, L., *Fourier Transform Infrared (FTIR) Spectroscopy*, in *Infrared Spectroscopy For Food Quality Analysis and Control*, D.W. Sun, Editor. 2009, Elsevier, Inc.: New York, NY.
113. Turner, N.W., Cauchi, M., Piletska, E.V., Preston, C., Piletsky, S.A., *Rapid Qualitative and Quantitative Analysis of Opiates in Extract of Poppy Head Via FTIR and Chemometrics: Towards In-Field Sensors.* Biosensors and Bioelectronis, 2009. **24**(11): p. 3322-3328.
114. Kher, A., Stewart, S., Mulholland, M., *Forensic Classification of Paper with Infrared Spectroscopy and Principal Components Analysis.* Journal of Near Infrared Spectroscopy, 2005. **13**(4): p. 225-229.
115. Praisler, M., Dirinck, I., Van Bocxlaer, J., De Leenheer, A., Massart, D.L., *Identification of novel Illicit Amphetamines from Vapor-Phase FTIR Spectra - A Chemometrical Solution.* Talanta, 2000. **53**(1): p. 155-170.
116. Praisler, M., Van Bocxlaer, J., De Leenheer, A., Massart, D.L., *Chemometric Detection of Thermally Degraded Samples in the Analysis of Drugs of Abuse with Gas-Chromatography-Fourier-Transform Infrared Spectroscopy.* Journal of Chromatography A, 2002. **962**(1-2): p. 161-173.
117. Bell, S.E.J., Fido, L. A., Speers, S. J., Armstrong, W. J., and Spratt, S., *Forensic Analysis of Architectural Finishes Using Fourier Transform Infrared and Raman Spectroscopy, Part I: The Resin Bases.* Appl. Spectrosc., 2005. **59**(11): p. 1333-1339.
118. Bell, S.E.J., Fido, L. A., Speers, S. J., Armstrong, W. J., Spratt, S., *Forensic Analysis of Architectural Finishes Using Fourier Transform Infrared and Raman Spectroscopy, Part II: White Paint.* Appl. Spectrosc., 2005. **59**(11): p. 1340-1346.
119. Zieba-Palus, J., and Kunicki, M., *Application of the Micro-FTIR Spectroscopy, Raman Spectroscopy and XRF Method Examination of Inks.* Forensic Science International, 2006. **158**(2-3): p. 164-172.
120. Govaert, F., Bernard, M., *Discriminating Red Spray Paints by Optical Microscopy, Fourier Transform Infrared Spectroscopy and X-Ray Fluorescence.* Forensic Science International, 2004. **140**: p. 61-70.
121. Wang, J., Luo, G., Sun, S., Wang, Z., Wang, Y., *Systematic Analysis of Bulk Blue Ballpoint Pen Ink by FTIR Spectrometry.* Journal of Forensic Sciences, 2001. **46**(5): p. 1093-1097.
122. Wang, J., Sun, S., Zhang, X., Luo, G., *Spectral Analysis and Composition Determination of Blue Ballpoint Writing Inks.* Guangpuxue Yu Gangpu Fenxi, 2000. **20**(2): p. 192-194.
123. Shi, X.F., Wang, Y.J., Wang, W.H., Yao, L.J., Xu, Y.J., *Identification and Differentiation of Gel Pen Ink of Different Categories by FTIR Spectrometry.* Lihua Jianyan, Xuaxue Fence, 2009. **45**(4): p. 394-397.

124. Sarin, R.K., Rasool, S.N., Murty, A.S.R.K., Mehrotra, V.K., *Forensic Examination of Forged Color Xerox Documents by Micro-RAS FTIR Spectroscopy a Simple, Non-Destructive Method to Examine Photocopied Counterfeits.* International Journal of Forensic Document Examiners, 1999. **5**(1-4): p. 265-269.
125. Meng, Z.Y., *Lever-ATR FTIR for Noninvasive Detection of Inkjet Ink in Printing Paper.* Guangpu Shiyanshi, 2009. **26**(6): p. 1583-1586.
126. Fabianska, E., Trzcinska, B.M., *Differentiation of Ball-Point and Liquid Inks - A Comparison of Methods in Use.* Z Zagadnien Nauk Sadowych, 2001. **46**: p. 383-400.
127. Dirwono, W., Park, J.S., Agustin-Camacho, M.R., Kim, J., Park, H.M., Lee, Y., Lee, K.B., *Application of Micro-Attenuated Total Reflectance FTIR Spectroscopy int he Forensic Study of Questioned Documents Involving Red Seal Inks.* Forensic Science International, 2010. **199**: p. 6-8.
128. Causin, V., Casamassima, R., Marega, C., Maida, P., Schiavone, S., Marigo, A., Villari, A., *The Discrimination Potential of Ultraviolet-Visible Spectrophotmetry, Thin Layer Chromatography, and Fourier Transform Infrared Spectroscopy for the Forensic Analysis of Black and Blue Ballpoint Inks.* Journal of Forensic Sciences, 2008. **53**(6): p. 1468-1473.
129. Grieve, M.C., *Another Look at the Classification of Acrylic Fibres, Using FTIR Microscopy.* Science & Justice, 1995. **35**(3): p. 179-190.
130. Grieve, M.C., Griffin, R.M.E., Malone, R., *Characteristic Dye Absorption Peaks Found in the FTIR Spectra of Coloured Acrylic Fibres.* Science & Justice, 1997. **38**(1): p. 27-37
131. West, M.J., and Went, M. J., *The Spectroscopic Detection of Drugs of Abuse in Fingerprints After Development with Powders and Recovery with Adhesive Lifters.* Spectrochimica Acta Part A: Molecular and Biomolecular Spectroscopy, 2009. **71**(5): p. 1984-1988.
132. Ng, P.H.R., Walker, S., Tahtouh, M., Reedy, B., *Detection of Illicit Substances in Fingerprints by Infrared Spectral Imaging.* Anal Bioanal Chem, 2009. **294**: p. 2039-2048.
133. Lanzarotta, A., Gratz, S., Brueggemeyer, T., Witkowski, M., *A Targeted Approach to Detect Controlled Substances in Suspect Tablets Using Attenuated Total Internal Reflection Fourier-Transform Infrared Spectroscopic Imaging.* Spectroscopy, 2011. **26**(2): p. 35-41.
134. Goh, C.Y., Van Bronswijk, W., Priddis, C., *Rapid Nondestructive On-Site Screening of Methylamphetamine Seizures by Attenuated Total Reflection Fourier Transform Infrared Spectroscopy.* Applied Spectroscopy, 2008. **62**(6): p. 640-648.
135. Sharma, S.P., Lahiri, S.C., *Characterization and Identification of Explosives and Explosive Residues Using GC-MS, an FTIR Microscope, and HPTLC.* Energetic Materials, 2005. **23**: p. 239-264.
136. Mou, Y., Rabalais, J.W., *Detection and Identification of Explosive Particles in Fingerprints Using Attenuated Total Reflection-Fourier Transform Infrared Spectromicroscopy.* Journal of Forensic Sciences, 2009. **54**(4): p. 846-850.

137. Banas, K., Banas, A., Moser, H.O., Bahou, M., Li, W., Yang, P., Cholewa, M., Lim, S.K., *multivariate Analysis Techniques in the Forensics Investigation of the Postblast Residues by Means of Fourier Transform-Infrared Spectroscopy.* Anal. Chem., 2010. **82**: p. 3038-3044.
138. Bernhard, W.R., *Paint and Tape: Collection and Storage of Microtraces of Paint in Adhesive Tape.* Journal of Forensic Sciences, 2000. **45**(6): p. 1312-1315.
139. Goodpaster, J. *Applications of Multi-Variate Statistics to Forensic Science*. in *Central Regional Meeting of the American Chemical Society*. 2009. Cleveland, OH.
140. Tahtouh, M., Kalman, J.R., Roux, C., Lennard, C., Reedy, B.J., *The Detection and Enhancement of Latent Fingermarks Using Infrared Chemical Imaging.* Journal of Forensic Sciences, 2005. **50**(1): p. 1-9.
141. Sharma, S.P., Lahiri, S.C., *A Preliminary Investigation into the Use of FTIR Microscopy as a Probe for the Identification of Bullet Entrace Holes and the Distance of Firing.* Science & Justice, 2009. **49**: p. 197-204.
142. Elkins, K.M., *Rapid Presumptive "Fingerprinting" of Body Fluids and Materials by ATR FTIR Spectroscopy.* Journal of Forensic Sciences, 2011. **56**(6): p. 1581-1587.
143. Izake, E.L., *Forensic and Homeland Security Applications of Modern Portable Raman Spectroscopy.* Forensic Science International, 2010. **202**(1-3): p. 1-8.
144. Macleod, N.A., Matousek, P., *Emerging Non-Invasive Raman Methods in Process Control and Forensic Applications.* Pharmaceutical Research, 2008. **25**(10).
145. Urbansky, E.T., *Quantitation of Perchlorate Ion: Practices and Advances Applied to the Analysis of Common Matrices.* Critical Reviews in Analytical Chemistry, 2000. **30**(4): p. 311-343.
146. Shinzawa, H., Awa, K., Kanemastsu, W., Ozaki, Y., *Multivariate Data Analysis for Raman Spectroscopic Imaging.* Journal of Raman Spectroscopy, 2009. **40**: p. 1720-1725.
147. Nafie, L.A., *Recent Advances in Linear and Nonlinear Raman Spectroscopy.* Journal of Raman Spectroscopy, 2010. **41**: p. 1566-1586.
148. Boffard, S.P., Sommer, A.J., Katon, J.E., Godber,S., *Use of Molecular Microspectroscopy to Characterize Pigment-Loaded Polypropylene Single Fibers.* Applied Spectroscopy, 1994. **48**(11): p. 1387-1393.
149. Keen, I., *Characterization of Fibers by Raman Microprobe Spectroscopy.* Journal of Forensic Science, 1998. **43**(1).
150. Massonnet, G., Buzzini, P, Jochem, G., Stauber, M., Coyle, T., Roux, C., Thomas, J., Leijenhorst, H., Van Zanten, Z., Wiggins, K., Russell, C., Chabli, S., and Rosengarten, A., *Evaluation of Raman Spectroscopy for the Analysis of Colored Fibers: A Collaborative Study.* Journal of Forensic Sciences, 2005. **50**(5): p. 1028-1038.
151. Miller, J.V., Bartick, E.G., *Forensic Analysis of Single Fibers by Raman Spectroscopy.* Applied Spectroscopy, 2001. **55**(1792-1732).

152. Lepot, L., De Wael, K., Gason, F., and Gilbert, B., *Application of Raman Spectroscopy to Forensic Fibre Cases.* Science & Justice, 2008. **48**(3): p. 109-117.
153. Lei, S.Y., and Young, R. J., *Deformation of PBO/epoxy Plain Weave Fabric Laminae Followed Using Raman Spectroscopy.* Composites Part A: Applied Science and Manufacturing. **32**(3-4): p. 499-509.
154. Helm, B.N., *State-of-the-Art Technology Behind the Trace Evidence Services of the RCMP Forensic Laboratory Behind Closed Doors.* Candian Chemical News, 2006. **58**(10): p. 10-12.
155. Hayward, I.P., Kirkbride, T.E., Batchelder, D.N., Lacey, R.J., *Use of a Fiber Optice Probe for the Detection and Identification of Explosive Materials by Raman-Spectroscopy.* Journal of Forensic Sciences, 1995. **40**(5): p. 883-884.
156. Cheng, C., Kirkbridge, T.E., Batchelder, D.N., Lacey, R.J., Sheldon, T.G., *In-Situ Detection and Identification of Trace Explosives by Raman Microscopy.* Journal of Forensic Sciences, 1995. **40**(1): p. 31-37.
157. Lewis, I.R., Daniel Jr, N.W., Chaffin, N.C., Griffiths, P.R., Tungol, M.W., *Raman Spectroscopic Studies of Explosive Materials: Towards a Fieldable Explosives Detector.* Spectrochimica Acta Part A, 1995. **51**(12): p. 1985-2000.
158. Sands, H.S., Hayward, I.P., Kirkbride, T.E., Bennett, R., Lacey, R.J., Batchelder, D.N., *UV-Excited Resonance Raman Spectroscopy of Narcotics and Explosives.* Journal of Forensic Sciences, 1998. **43**(3): p. 509-513.
159. Lacey, R.J. *Some Advances in the Use of Raman Spectroscopy in Security Screening Applications*. in *Security and Detection European Conference*. 1997.
160. Moore, D.S., *Instrumentation for Trace Detection of High Explosives.* Review of Scientific Instruments, 2004. **75**(8): p. 2499-2512.
161. Burks, R., and Hage, D., *Current Trends in the Detection of Peroxide-Based Explosives.* Analytical and Bioanalytical Chemistry, 2009. **395**(2): p. 301-313.
162. Harvey, S.D., Vucelick, M. E., Lee, R. N., and Wright, B. W., *Blind Field Test Evaluation of Raman Spectroscopy as a Forensic Tool.* Forensic Science International, 2002. **125**(1): p. 12-21.
163. Tripathi, A., Emmons, E.D., Guicheteau, J.A., Christesen, S.D., Wilcox, P.G., Emge, D.K., and Augustus, W.F. III, *Trace Explosive Detection in Fingerprints with Raman Chemical Imaging*. Vol. 7665. 2010: SPIE. 76650N.
164. Del Río Anaya, M., Garcia-Torales, G., Rodriguez Betancourtt, V., Rodriguez Rojas, R., and Flores Nunez, J., *Analysis of Explosives' Precursors by Means of a Portable Raman Spectrometer*. Vol. 7499. 2009: SPIE. 749902.
165. Stich, S., Bard, D., Gros, L., Wenz, H.W., Yarwood, J., Williams, K., *Raman Microscopic Identification of Gunshot Residues.* Journal of Raman Spectroscopy, 1998. **29**(9): p. 787-790.
166. Claybourn, M., Luget, A., Williams, K.P., *Raman Microscopy and Imaging of Polymers.* Multidimensional Spectroscopy of Polymers: Vibrational, NMR, and Fluorescence Techniques, 1995. **598**(41-60).
167. Pilon, P., Burmeister, S., *Chemistry and Biology Based Technologies for Contraband Detection.* SPIE, 1997. **2937**.

168. Hendra, P.J., *The Industrial Value of Fourier Transform Raman Spectroscopy.* Journal of Molecular Structure, 1992. **266**(97-114).
169. Singh, P., et al., *Raman Spectroscopy in Research and Industrial Applications.* Chemical Industry Digest, 2010. **23**(11): p. 77-83.
170. Frausto-Reyes, C., Ortiz-Morales, M., Bujdud-Pérez, J. M., Magaña-Cota, G. E., and Mejía-Falcón, R., *Raman Spectroscopy for the Identification of Pigments and Color Measurement in Dugès Watercolors.* Spectrochimica Acta Part A: Molecular and Biomolecular Spectroscopy, 2009. **74**(5): p. 1275-1279.
171. Marcolli, C., and Wiedemann, H., *Distinction of Original and Forged Lithographs by Means of Thermogravimetry and Raman Spectroscopy.* Journal of Thermal Analysis and Calorimetry, 2001. **64**(3): p. 987-1000.
172. Edwards, H.G.M., and Munshi, T., *Diagnostic Raman Spectroscopy for the Forensic Detection of Biomaterials and the Preservation of Cultural Heritage.* Analytical and Bioanalytical Chemistry, 2005. **382**(6): p. 1398-1406.
173. Bell, S.E.J., Fido, L. A., Speers, S. J., and Armstrong, W. J., *Rapid Forensic Analysis and Identification of 'Lilac' Architectural Finishes Using Raman Spectroscopy.* Appl. Spectrosc., 2005. **59**(1): p. 100-108.
174. Sikirzhytski, V., Virkler, K., and Lednev, I. K., *Discriminant Analysis of Raman Spectra for Body Fluid Identification for Forensic Purposes.* Sensors, 2010. **10**(Copyright (C) 2011 American Chemical Society (ACS). All Rights Reserved.): p. 2869-2884.
175. Lednev, I.K., and Virkler, K., *Identification of Body Fluids Using Raman Spectroscopy for use in Forensic Analysis*, P.I. Appl., Editor. 2009, The Research Foundation of State University of New York at Albany, USA: United States. p. 33.
176. Virkler, K., and Lednev, I. K., *Raman Spectroscopy Offers Great Potential for the Nondestructive Confirmatory Identification of Body Fluids.* Forensic Science International, 2008. **181**(1-3): p. E1-E5.
177. Virkler, K., and Lednev, I. K., *Analysis of Body Fluids for Forensic Purposes: From Laboratory Testing to Non-Destructive Rapid Confirmatory Identification at a Crime Scene.* Forensic Science International, 2009. **188**(1-3): p. 1-17.
178. Virkler, K., and Lednev, I. K., *Raman Spectroscopic Signature of Semen and its Potential Application to Forensic Body Fluid Identification.* Forensic Science International, 2009. **193**(1-3): p. 56-62.
179. Virkler, K., and Lednev, I.K., *Blood Species Identification for Forensic Purposes Using Raman Spectroscopy Combined with Advanced Statistical Analysis.* Analytical Chemistry, 2009. **81**(18): p. 7773-7777.
180. Virkler, K., and Lednev, I. K., *Forensic Body Fluid Identification: The Raman Spectroscopic Signature of Saliva.* Analyst, 2010. **135**(3): p. 512-517.
181. Virkler, K., and Lednev, I. K., *Raman Spectroscopic Signature of Blood and its Potential Application to Forensic Body Fluid Identification.* Analytical and Bioanalytical Chemistry, 2010. **396**(1): p. 525-534.
182. Claybourn, M., and Ansell, M., *Using Raman Spectroscopy to Solve Crime: Inks, Questioned Documents and Fraud.* Science & Justice, 2000. **40**(4): p. 261-271.

183. White, P.C., *In Situ Surface Enhanced Resonance Raman Scattering (SERRS) Spectroscopy of Biro Inks - Long Term Stability of Colloid Treated Samples.* Science & Justice, 2003. **43**(3): p. 149-152.
184. Mazzella, W.D., and Buzzini, P., *Raman Spectroscopy of Blue Gel Pen Inks.* Forensic Science International, 2005. **152**(2-3): p. 241-247.
185. Mazzella, W.D., and Khanmy-Vital, A., *A Study to Investigate the Evidential Value of Blue Gel Pen Inks.* Journal of Forensic Sciences, 2003. **48**(2): p. 419-424.
186. Udristioiu, E.G., Bunaciu, A. A., Aboul-Enein, H. Y., and Tanase, I. G., *Forensic Analysis of Color Toners by Raman Spectroscopy.* Instrumentation Science & Technology, 2009. **37**(1): p. 23-29.
187. Smith, W.E., White, P.C., Rodger, C., Dent, G., *Raman and Surface Enhanced Resonance Raman Scattering: Applications in Forensic Science.* Handbook of Raman Spectroscopy, 2001. **28**(733-748).
188. McMaster, M.C., *GC/MS A Practical User's Guide*. 2nd ed. 2008, Hoboken, New Jersy: Wiley-Interscience.
189. Hubschmann, H.J., *Handbook of GC/MS Fundamentals and Applications*. 2 ed. 2009, Germany: Wiley-VCH.
190. Watson, J.T., Sparkman, O.D., *Introduction to Mass Spectrometry Instrumentation, Applications and Strategies for Data Interpretation*. 4th ed. 2007, West Sussex, England: John Wiley & Sons, Ltd.
191. McHugh, K.M., *Determining the Presence of An Ignitable Liquid Residue in Fire Debris Samples Utilizing Target Factor Analysis*, in *Chemistry*. 2010, University of Central Florida: Orlando. p. 106.
192. Lewis, J., *The Application of Chemometrics to the Detection and Classification of Ignitable Liquids in Fire Debris Using the Total Ion Spectrum*, in *Chemistry*. 2011, University of Central Florida: Orlando, FL.
193. Hardy, T.B., Snavely, R.E., *Accelerant Classification by Gas Chromatography/Mass Spectrometry and Multivariate Pattern Recognition.* Analytica Chimica Acta, 2000. **422**(1): p. 37-46.
194. Waddell, E.E., Song, E.T., Rinke, C.N., Williams, M.R., Sigman, M.E., *Progress Toward the Determination of Correct Classification Rates in Fire Debris Analysis.* Journal of Forensic Science, In Press.
195. Hoggard, J.C., Wahl, J.H., Synovec, R.E., Mong, G.M., Fraga, C.G., *Impurity Profiling of a Chemical Weapon Precursor for Possible Forensic Signatures by Comprehensive Two-Dimensional Gas Chromatography/Mass Spectrometry and Chemometrics.* Analytical Chemistry, 2010. **82**: p. 689-698.
196. Cone, E.J., Presley, L., Lehrer, M., Seiter, W., Smith, M., Kardos, K.W., Fritch, D., Salamone, S., Niedbala, R.S., *Oral Fluid Testing for Drugs of Abuse: Positive Prevalence Rates by Intercept Immunoassay Screening and GC-MS-MS Confirmation and Suggested Cutoff Concentrations.* Journal of Analytical Toxicology, 2002. **26**(8): p. 541-546.

197. Samyn, N., De Boeck, G., Verstraete, A.G., *The Use of Oral Fluid and Sweat Wipes for the Detection of Drugs of Abuse in Drivers.* Journal of FOrensic Sciences, 2002. **47**(6): p. 1380-1387.
198. Samyn, N., De Boeck, G., Cirimele, V., Verstraete, A., Kintz, P., *Detection of Flunitrazepam and 7-Aminoflunitrazepam in Oral Fluid After Controlled Administration of Rohypnol.* Journal of Analytical Toxicology. **26**(4): p. 211-215.
199. Staack, R.F., Fritschi, G., Maurer, H.H., *Studies on the Metabolism and Toxicological Detection of the New Designer Drug N-Benzylpiperazine in Urine Using Gas Chromatography-Mass Spectrometry.* Journal of Chromatography B, 2002. **773**: p. 35-46.
200. Springer, D., Peters, F.T., Fritschi, G., Maurer, H.H., *New Designer Drug 4'-Methyl-α–Pyrrolidinohexanophenone: Studies on its Metabolism and Toxicological Detection in Urine Using Gas Chromatography-Mass Spectrometry.* Journal of Chromatography B, 2003. **789**: p. 79-91.
201. Schutz, H., Gotta, J.C., Erdmann, F., Ribe, M., Weiler, G., *Simultaneous Screening and Detection of Drugs in Small Blood Samples and Bloodstains.* Forensic Science International, 2002. **126**: p. 191-196.
202. Peters, F.T., Schaefer, S., Staack, R.F., Kraemer, T., Maurer, H.H., *Screening for and Validated Quantification of Amphetamines and of Amphetamine- and Piperazine-Derived Designer Drugs in Human Blood Plasma by Gas Chromatography/Mass Spectrometry.* Journal of Mass Spectrometry, 2003. **38**: p. 659-676.
203. Peters, F.T., Kraemer, T., Maurer, H.H., *Drug Testing in Blood: Validated Negative-Ion Chrmical Ionization Gas Chromatographic-Mass Spectrometric Assay for Determination of Amphetamine and Methamphetamine Enantiomers and Its Application to Toxicology Cases.* Clinical Chemistry, 2002. **48**(9): p. 1472-1485.
204. Paul, L.D., Maurer, H.H., *Studies on the Metabolism and Toxicological Detection of the Eschscholtzia Californica Alkaloids Californine and Protopine in Urine Using Gas Chromatography-Mass Spectrometry.* Journal of Chromatography B, 2003. **780**: p. 43-57.
205. Castlebuono, J.A., *The Identification of Ignitable Liquids in the Presence of Interference Products: Generation of a Pyrolysis Database*, in *Chemistry*. 2008, University of Central Florida: Orlando. p. 122.
206. Sutherland, D., Perr, J., Almirall, J.R. *Identification of Ignitable Liquid Residues in Fire Debris by GC/MS/MS*. in *Advances in Forensic Applications of Mass Spectrometry*. 2004.
207. De Vos, B.J., Froneman, M., Rohwer, E., Sutherland, D.A., *Detection of petrol (gasoline) in Fire Debris by Gas Chromatography/Mass Spectrometry/Mass Spectrometry (GC/MS/MS).* Journal of Forensic Sciences, 2002. **47**(4): p. 736-756.
208. Gilbert, M.W., *The Use of Individual Extracted Ion Profiles Versus Summed Extracted Ion Profiles in Fire Debris Analysis.* Journal of Forensic Sciences, 1998. **43**(4): p. 871-876.

209. Jackowski, J.P., *The Incidence of Ignitable Liquid Residues in Fire Debris as Determined by a Sensitive and Comprehensive Analytical Scheme.* Journal of Forensic Sciences, 1997. **42**(5): p. 828-832.
210. Wallace, J.R., *GC/MS Data from Fire Debris Samples: Interpretation and Applications.* Journal of Forensic Sciences, 1999. **44**(5): p. 996-1012.
211. Stauffer, E., *A Review of the Analysis of Vegetable Oil Residues from Fire Debris Samples: Spontaneous Ignition, Vegetable Oils, and the Forensic Approach.* Journal of Forensic Sciences, 2005. **50**(5): p. 1-10.
212. Borusiewicz, R., Zieba-Palus, J., Zadora, G., *The Influence of the Type of Accelerant, Type of Burned Material, Time of Burning and Availability of Air on the Possibility of Detection of Accelerants Traces.* Forensic Science International, 2005. **160**: p. 115-126.
213. Partouche, F., Espanet, B., Villena, C., Murie, C. *Forensic Analysis of Inkjet Printing by Pyrolysis GC/MS*. in *International Conference on Digital Printing Technologies*. 2005. Baltimore, MD.
214. Aginsky, V.N., *An Application of Chromatographic Methods for Dating Questioned Documents.* Chromatography, 1997: p. 1-6.
215. Aginsky, V.N., *Dating and Characterizing Writing, Stamp Pad, and Jet Printer Inks by Gas Chromatography/Mass Spectrometry.* International Journal of Forensic Document Examiners, 1996. **2**(1): p. 103-116.
216. Weyermann, C., Almog, J., Bugler, J., Cantu, A., , *Minimum Requirements for Application of Ink Dating Methods Based on Solvent Analysis in Casework.* Forensic Science International, 2011. **210**: p. 52-62.
217. Weyermann, C., Kirsch, D., Vera, C.C., Spengler, B., *A GC/MS Study of the Drying of Ballpoint Pen Ink on Paper.* Forensic Science International, 2007. **168**: p. 119-127.
218. LaPorte, G.M., Arredondo, M.D., McConnell, T.S., Stephens, J.C., Cantu, A.A., Shaffer, D.K., *An Evaluation of Matching Unknown Writing Inks with the United States International Ink Library.* Journal of Forensic Sciences, 2006. **51**(3): p. 689-692.
219. LaPorte, G.M., Wilxon, J.D., Cantu, A.A., Mancke, S.A., Fortunato, S.L., *The Identification of 2-Phenoxyethanol in Ballpoint Inks Using Gas Chromatography/Mass Spectrometry-Relevance to Ink Dating.* Journal of Forensic Sciences, 2004. **49**(1): p. 1-5.
220. Berger-Karin, C., Hendriks, U., Geyer-Lippmann, J., *Comparison of Natural and Artificial Aging of Ballpoint Inks.* Journal of Forensic Sciences, 2008. **53**(41): p. 989-992.
221. Milczarek, J.M., Zieba-Palus, J., *Examination of Spray Paints on Plasters by the Use of Pyrolysis-Gas Chromatography/Mass Spectrometry for Forensic Purposes.* Journal of Analytical and Applied Pryolysis, 2009. **86**: p. 252-259.
222. Stephen, M.L. *Fast Gas Chromatography/Mass Spectrometry: Applications in Forensics and Polymer Analysis*. in *56th Southeast Regional Meeting of the American Chemical Society*. 2004. Research Triangle Park, NC.

223. Varmuza, K., and Filzmoser, P., *Introduction To Multivariate Statistical Analysis In Chemometrics*. 2009, New York: CRC Press.
224. Webb, A., *Statistical Pattern Recognition*. 2 ed. 2002, West Sussex, England: John Wiley & Sons, LTD.
225. Malinowski, E.R., and Howery, D.G., *Factor Analysis In Chemistry*. 1980, New York: John Wiley & Sons, Inc. .
226. Malinowski, E.R., *Determination Of Rank By Median Absolute Deviation (DRMAD): A Simple Method For Determining The Number Of Principal Factors Responsible For A Data Matrix.* Journal of Chemometrics, 2009. **23**: p. 1-6.
227. White, K.M., *Statistical Analysis of Visible Absorption Spectra and Mass Spectra Obtained From Dyed Textile Fibers*, in *Chemistry*. 2010, University of Central Florida: Orlando. p. 119.
228. Sachs, L., *Measures of Association: Correlation and Association*, in *Applied Statistics: A Handbook of Statistical Techniques*. 1984, Springer-Verlag: New York.
229. Rinke, C.N., Williams, M., Brown, C., Baudelet, M., Richardson, M., and Sigman, M.E., *Discriminant Analysis in the Presence of Interferences: Combined Application of Target Factor Analysis and a Bayesian Classifier.* Analytica Chemica Acta, in press.
230. Silverman, B.W., *Density Estimation for Statistics and Data Analysis*. 1986, London: Chapman and Hall.
231. Balakrishnama, S., and Ganapathiraju, *Linear Discriminant Analysis-A Brief Tutorial.* Institute For Signal and Information Processing.
232. Engleman, L., *Discriminant Analysis*, in *SYSTAT 13 Manual - Statistics I*. 2009, SYSTAT Software Inc.: Chicago, Il.
233. Morgan, S.L., and Bartick, E.G., *Forensic Analysis On The Cutting Edge: New Methods For Trace Evidence Analysis*. 2007: John Wiley & Sons, Inc.
234. De Maesschalck, R., Jouan-Rimbaud, D., and Massart, D.L., *The Mahalanobis Distance.* Chemometrics and Intelligent Laboratory Systems, 2000. **50**: p. 1-18.
235. Sachs, L., *Statistical Decision Techniques*, in *Applied Statistics: A Handbook of Techniques*. 1984, Springer-Verlag: New York. p. 112-133.
236. Sachs, L., *Applied Statistics: A Handbook of Techniques*. Second ed. 1982, New York: Springer-Verlag.
237. Cremers, D.A., Radziemski, L.J., *Handbook of Laser-Induced Breakdown Spectroscopy*. 2006, West Sussex, England: John Wiley & Sons Ltd.
238. Lee, Y.I., Song, K., Sneddon, J., *Laser-Induced Breakdown Spectrometry*. 2000, Huntington, NY: Nova Science Publishers, Inc.
239. Johnson, R.A., and Bhattacharyya, G.K., *Statistics Principles and Methods*. Fourth ed. 2001, New York: John Wiley & Sons, Inc.
240. Wilcoxon, F., *Individual Comparisons by Ranking Methods.* Biometrics Bulletin, 1945. **1**(5): p. 80-83.
241. Bridge, C.M., *Discrimination of Forensic Trace Evidence Using Laser Induced Breakdown Spectroscopy*, in *Chemistry*. 2007, University of Central Florida: Orlando. p. 181.

242. Miziolek, A.W., Palleschi, V., and Schechter, I., ed. *Laser-Induced Breakdown Spectroscopy (LIBS) Fundamentals and Applications* 2006, Cambridge University Press: New York.
243. Brown, C.G., *Laser Induced Breakdown Spectroscopy for Detection of Organic Residues: Impact of Ambient Atmosphere and Laser Parameters*, in *Physics*. 2011, University of Central Florida: Orlando, Fl.
244. Renard, J.J., and Bolker, H.I., *The Chemistry of Chlorine Monoxide (Dichlorine Monoxide).* Chemical Reviews, 1975. **76**(4): p. 487-508.
245. Coates, J., *Interpretation of Infrared Spectra, A Practical Approach*, ed. R.A. Meyers. 2000, Chichester: John Wiley & Sons Ltd.
246. *Electronic Statistics Textbook*, I. StatSoft, Editor. 2011, Statsoft: Tulsa, OK.